Local and systemic effects of adipocyte-secreted factors in breast cancer

Rebekah Crake

Thesis submitted for the degree of

Doctor of Philosophy

at the

University of Otago Christchurch,

New Zealand

Nov 2019

Abstract

Breast cancer is a complex disease that, once developed, progresses in response to multiple environmental factors, including local microenvironmental factors within the breast and systemic markers in circulation. Obesity affects one third of all New Zealand adults and is known to negatively impact breast cancer outcomes. Epidemiological studies have shown obese women with breast cancer have increased risk of recurrence and metastasis, poorer pathological response rates to chemotherapy, and worse overall survival. The biological mechanisms underlying these associations are complex and not yet completely understood.

Cancer associated adipocytes (CAA) are fat cells located within close proximity to breast tumour cells. *In vitro*, CAA promote breast cancer cell migration, invasion, and resistance to therapy. Analysis of gene expression in breast cancer cells co-cultured with CAA has identified a number of genes which may be supporting disease progression. To further assess the influence of CAA on breast cancer cells, we identified and quantified changes in global protein abundance induced in breast cancer cells co-cultured with human breast adipocytes (CAA), and evaluated these changes by identifying key molecules and pathways that were significantly altered. Global differences in relative protein expression in MCF-7 (ER+, PR+, HER2-) and MDA-MB-231 (ER-, PR-, HER2-) breast cancer cells co-cultured with, or without, mature breast adipocytes in a transwell co-culture system, were measured using isobaric tags for relative and absolute quantification (iTRAQ) labelling and liquid chromatography tandem mass spectrometry (LC-MS/MS). In both control and co-cultured samples, a total of 1,126 proteins and 1,218 proteins were identified in MCF-7 and MDA-MB-231 breast cancer cells, respectively. Relative to controls, 85 proteins in MCF-7 cells (32 upregulated, 53 downregulated) and 63 proteins in MDA-MB-231 cells (51 upregulated, 12 downregulated) were differentially abundant by 1.5-fold or greater in co-cultured cells. Co-culture with CAA caused an enriched upregulation of tricarboxylic acid (TCA) cycle proteins in MCF-7 cells and glycolysis proteins in MDA-MB-231 cells. The glycolytic protein, phosphoglycerate kinase 1 (PGK1), was the only protein that was upregulated by more than 1.5-fold in both MCF-7 and MDA-MB-231 cells co-cultured with CAA.

PGK1 is a kinase enzyme that plays an important role in the glycolytic pathway. In women with breast cancer, increased PGK1 expression in the tumour has been identified as a

predictor of poor patient survival and marker of resistance to paclitaxel. As metabolic co-operation between adipocytes and breast cancer cells is a key mechanism promoting breast tumour progression, we investigated PGK1 overexpression *in vitro*. The transient transfection model for *in vitro* PGK1 overexpression utilised in this study induced differential effects in MCF-7 and MDA-MB-231 breast cancer cells. PGK1 overexpression increased sensitivity to chemotherapy in MCF-7 cells. Whereas, cell proliferation and viability were decreased, and conditioned media lactate concentrations were increased, in *GFP* and *PGK1* expressing plasmid transfected MDA-MB-231 cells. *In silico* analysis showed *PGK1* expression was higher in HER2 enriched compared to triple negative breast cancer cells, and was upregulated in HER2 overexpressing (HER2+) compared to HER2- breast tumours, suggesting that PGK1 expression may be particularly relevant to HER2+ breast cancers.

Obesity is characterised by a state of low-grade chronic systemic inflammation. Breast cancer chemotherapies are predominantly metabolised in liver hepatocytes by cytochrome P450 (CYP) drug metabolising enzymes. Inflammatory cytokines have been shown to downregulate expression and activity of CYP enzymes *in vitro*. Additionally, CYP genotype-phenotype discordance has been observed in patients with advanced cancer. To investigate whether obesity-associated circulating inflammatory cytokines influence *in vivo* activity of CYP enzymes in women receiving chemotherapy for breast cancer, we carried out an exploratory patient study that recruited seven non-obese and five obese women receiving adriamycin-cyclophosphamide (AC) and paclitaxel chemotherapy for stage II or III breast cancer. During chemotherapy, serum levels of B-cell activating factor (BAFF), growth and differentiation factor 15 (GDF-15) and monocyte chemoattractant protein 1 (MCP-1) increased, whereas interleukin 10 (IL-10) levels decreased. Importantly, changes in the levels of circulating inflammatory cytokines during chemotherapy were not associated with differences in body morphometry or voluntary physical activity levels. Activity of the CYP enzymes (CYP2C9, CYP2C19, CYP2D6, and CYP3A4), measured using the 'Inje' probe drug cocktail, were largely unchanged over the course of chemotherapy, although varied between participants. However, increased serum MCP-1 levels correlated with decreased CYP3A4 activity during chemotherapy, and this finding provides preliminary evidence that circulating inflammatory cytokines may negatively influence CYP-mediated chemotherapy metabolism in women undergoing treatment for breast cancer.

This study has provided, for the first time, an extensive list of breast cancer cell protein abundance alterations induced by co-culture with CAA, which can be used as a

comprehensive platform for future investigations. Moreover, this study has validated, for the first time, the feasibility of using the ‘Inje’ cocktail to measure CYP activity in women receiving chemotherapy for breast cancer, and in doing so, has provided preliminary evidence to support the concept that changes in circulating inflammatory cytokines during chemotherapy treatment may impact CYP activity, and thus, chemotherapy metabolism in some patients.

Acknowledgements

Firstly, I would like to express gratitude to my primary supervisor Associate Professor Margaret Currie, for her time, patience and expertise, for her endless encouragement, and for keeping me sane with her wise words of advice throughout this entire PhD- this project would not have been possible without her! I would also like to thank my other supervisors: Dr Elisabeth Phillips, for her hands-on and insightful approach to all my experiments, and for being her down-to-earth, dependable, empathetic, and kind-hearted self from start to finish; Professor Bridget Robinson, for her professional knowledge and advice, and her truly inspiring attitude towards science; and Dr Matthew Strother, for his extensive expertise and his consistent support and guidance.

A massive thank you goes to everyone who is in, or has passed through, the Mackenzie Cancer Research Group over the course of this PhD. Each and every person has touched my life in a uniquely special way. I have thoroughly enjoyed being a part of a group that is SO incredibly talented (in and out of the laboratory), supports each other when needed, and celebrates each other's successes with such passion- it will be hard to beat!!

I would especially like to thank, Professor Mark Hampton, Associate Professor Gabi Dachs, Associate Professor Logan Walker, Helen Morrin, and Lucia Sinclair for their reassurance and guidance, both professionally and personally, over the years, it has been invaluable. I would like to recognise the help and expertise received from Dr Torsten Kleffmann with the mass spectrometry work. Thank you to the Department of Pathology and Biomedical Science for the opportunity and space to work - with particular appreciation going to the administrative team for always being kind, approachable, and willing to help. I am also grateful to the University of Otago for granting me a PhD scholarship.

Thank you to my friends and extended family, who have cheered me on and have gone out of their way to give support whenever and however they could. I am immensely grateful to my parents, David and Julie, and my brother, Matthew - thank you for always nurturing my curiosity, encouraging me to do whatever makes me happy, and providing me with endless amounts of love, I was blessed with the best. Last, but certainly not least, I am deeply grateful to my partner Tian, for not only putting up with the (sometimes daily) PhD mood swings, but for his unwavering love and encouragement every step of the way - I could not have done this without you.

Contents

List of Tables

List of Figures

Abbreviations

Δ	delta ("change in")
®	registered trademark
°C	degrees Celsius
µA	microamperes
µg	microgram
µL	microliter
µM	micrometre
2D	two-dimensional
3D	three-dimensional
A/A	antibiotic-antimycotic
AC	adriamycin (doxorubicin)-cyclophosphamide
ANOVA	analysis of variance
AT	adipose tissue
ATCC	American Type Culture Collection
ATP	adenosine triphosphate
AUC	area under the curve
BCA	bicinchoninic acid
BIA	bioelectrical impedance analysis
BMI	body mass index
bp	base pair
BSA	body surface area
BSA	bovine serum albumin
CAA	cancer associated adipocytes
CAF	cancer associated fibroblasts
CC	co-culture
CCLE	Cancer Cell Line Encyclopedia
CDHB	Christchurch District Health Board
cDNA	complementary deoxyribonucleic acid
CID	collision induced dissociation
CLS	crown-like structure
cm	centimetre
CMV	cytomegalovirus
CO_2	carbon dioxide
CON	control
CORU	Christchurch Oncology Research Unit
CSTBC	Cancer Society Tissue Bank Christchurch
CV	coefficient of variation
CYP	cytochrome P450
DepMap	dependency map
DFS	disease free survival

DME	drug metabolising enzymes
DMEM	Dulbecco's Modified Eagle's Medium
DMSO	dimethyl sulfoxide
DNA	deoxyribonucleic acid
dNTPs	deoxynucleotide triphosphates
DTT	dithiothreitol
E.coli	Escherichia coli
ECM	extra cellular matrix
EDTA	ethylenediaminetetraacetic acid
EGFP	enhanced green fluorescent protein
EGTA	ethylene glycol-bis(β-aminoethyl ether)-N,N,N′,N′-tetraacetic acid
ELISA	enzyme-linked immunosorbent assay
EM	extensive metaboliser
EMT	epithelial to mesenchymal transition
ER(+/-)	oestrogen receptor (positive/negative)
FACS	fluorescence-activated cell sorting
FASP	filter aided sample preparation
FBS	fetal bovine serum
FDA	Food and Drug Administration
FDR	false discovery rate
FFA	free fatty acids
FITC	fluorescein isothiocyanate
For	forward
g	gram
g	relative centrifugal force
GFP	green fluorescent protein
GO	gene ontology
GPS	global positioning satellite
HBSS	hanks balanced salt solution
HCC	hepatocellular carcinoma
HCD	high-energy collision induced dissociation
HDEC	Health and Disability Ethics Committee
HER2/*Erbb2 (+/-)*	human epidermal growth factor receptor 2 (positive/negative)
HRP	horseradish peroxidase
IAA	iodacetamide
IBMX	3-isobutyl-1-methylxanthine
IC50	half maximal inhibitory concentration
IDC	invasive ductal carcinoma
IEF	isoelectric focusing
IM	intermediate metaboliser
IPG	impedance plethysmography
kDa	kilodalton
kg	kilogram
LB	Luria-Bertani

LC-MS/MS	liquid chromatography-coupled tandem mass spectrometry
LDS	lithium dodecyl sulfate
LPS	lipopolysaccharides
LTQ	linear trap quadrupole
M	molar
m/z	mass to charge ratio
M1/M2	pro-inflammatory macrophage/anti-inflammatory macrophage
MES	2-(N-morpholino) ethanesulfonic acid
MET	metabolic equivalent of task
METABRIC	Molecular Taxonomy of Breast Cancer International Consortium
mg	milligram
MgCl2	magnesium chloride
mL	millilitre
mM	millimolar
MOPS	3-(N-morpholino) propanesulfonic acid
mRNA	messenger ribonucleic acid
MTT	3-(4,5-dimethylthiazol-2-yl)-2,5-diphenyltetrazolium bromide
MW	molecular weight
n	sample number
NCBI	National Centre for Biotechnology Information
ng	nanogram
NLR	neutrophil-to-lymphocyte ratio
nm	nanometre
NSCLC	non-small cell lung cancer
NZ	New Zealand
OS	overall survival
PANTHER	protein annotation through evolutionary relationship
PBS	phosphate buffered saline
PCR	polymerase chain reaction
pg	picogram
pH	potential of Hydrogen
PIS/CF	patient information sheet and consent form
PM	poor metaboliser
PR(+/-)	progesterone receptor (positive/negative)
PVDF	polyvinylidene difluoride
R^2	coefficient of determination
RBC	red blood cells
Rev	reverse
RIPA	radioimmunoprecipitation assay
RNA	ribonucleic acid
RNAseq	ribonucleic acid sequencing
RP-HPLC	reversed phase high performance liquid chromatography
rpm	rotations per minute
RSLC	rapid separation liquid chromatography

SDS	sodium dodecyl sulfate
SDS-PAGE	sodium dodecyl sulfate polyacrylamide gel electrophoresis
SEM	standard error of the mean
shRNA	short hairpin RNA
SPE	solid phase extraction
SRB	sulforhodamine B
SVF	stromal vascular fraction
TAE	tris-acetate ethylenediaminetetraacetic acid
TBST	tris-buffered saline and Tween® 20
TCA	tricarboxylic acid
TCEP	tris(2-carboxyethyl)phosphine
TCGA	The Cancer Genome Atlas
TEAB	triethylammonium bicarbonate
Tm	primer melting temperature
TM	Trademark
TNBC	triple negative breast cancer
TPM	transcripts per million
TR	transfection reagent
U	units
UM	ultra-rapid metaboliser
UV	ultraviolet
V	voltage
v/v	volume to volume
WAT	white adipose tissue
WHO	World Health Organisation
WHR	waist to hip ratio

Chapter 1

Introduction

1.1 Obesity

1.1.1 Obesity epidemic

According to the world health organization (WHO) being overweight or obese is defined by abnormal or excessive fat accumulation that poses a risk to health [1]. Alarmingly, the global prevalence of overweight and obesity is increasing at an extraordinary rate in all ages and both sexes, with incidence more than doubling since 1980 in over 70 countries (developing and developed) and increasing in many others [2,3]. In a recent epidemiological study, the global prevalence of the overweight and obesity categories was 39% in adults older than 20 years, and the absolute incidence of obesity was consistently higher in women than men [4]. Furthermore, based on the continuation of the current trends it has been estimated that by 2030, the global prevalence of the overweight and obesity categories will be 57.8% [5]. New Zealand (NZ) is not an exception to the global obesity epidemic, as one in three NZ adults are considered obese, with a further 35% considered overweight [6,7]. Most commonly, obesity is attributed to an imbalance between energy consumption, energy expenditure, and the resultant behavior of the body's weight regulation systems generating a constant positive energy balance [3,8,9].

Clinically, obesity is classified as having a body mass index (BMI) equal to or greater than 30 [1], where BMI is calculated as a person's body weight in kilograms divided by their squared height in meters (kg/m^2). BMI has been employed as the most common and efficient tool for measuring obesity, however, there has been growing interest in the critical differences that exist between BMI and overall body adiposity, as BMI does not distinguish fat mass from fat-free mass, such as muscle and bone [10–13]. General consensus across a number of studies

comparing BMI with measures of body fat percentage suggest that BMI underestimates the prevalence of obesity, although the degree of difference between BMI and body fat percentage was often sex and age-group dependent [12,14–17]. In addition, differences have been reported between ethnicities when comparing body fat percentage across individuals that have the same BMI [18,19], and consequently, it has been suggested that in New Zealand, BMI thresholds separating normal, overweight, and obese groups should be increased for Māori and Pacific Island women, and decreased for Asian women [19].

1.1.2 Obesity and adipose tissue heterogeneity

Obesity is associated with the expansion of adipose tissue depots throughout the body. Adipose tissue, essential for mammalian life, is a highly complex tissue composed mostly of lipid-laden mature adipocytes and pre-adipocytes, but also many stromal vascular fraction (SVF) cells including endothelial cells, blood cells and macrophages [20,21]. Heterogenic qualities of obesity such as the presence and difference between white adipose tissue (WAT) and brown adipose tissue [22], and topographical location of adipose depots throughout the body are now widely recognised [23]. The main WAT depots in the human body are intra-abdominal and subcutaneous fat. Sub-groups identified within these depots, including visceral fat, have differentially expressed genes and specialised roles for controlling metabolism and the immune system [21,24].

WAT is of particular interest in obesity as it has the ability to expand with increasing adiposity, is the body's major supply of FFA (free fatty acids), and represents the largest percentage of total body adipose tissue [21]. Research has shown that WAT acts not only as a lipid storage facility, but it functions as an endocrine system through the release of an assortment of bioactive molecules including chemokines, cytokines and hormone-like factors [25–27]. Through the release of such endocrine molecules, WAT communicates with other adipose depots and organs around the body to maintain energy balance and regulate metabolism, adipocyte differentiation, insulin sensitivity and inflammatory responses, and therefore instigates pathogenesis of metabolic and inflammatory conditions occurring during obesity [20,26,28–30] (Figure 1.1). Visceral fat accumulating within the abdominal cavity is notorious for its association with metabolic syndrome, and for its role in providing increased levels of circulating inflammatory cytokines under obese conditions [31]. Taken together, these findings suggest that adipose tissue heterogeneity has the ability to differentially implicate

obesity in diverse clinical disease outcomes. It is therefore important not only to recognise and measure obesity as a multifactorial pathological condition, but to assess the relevant biological characteristics of excess adiposity when performing research concerned with obesity.

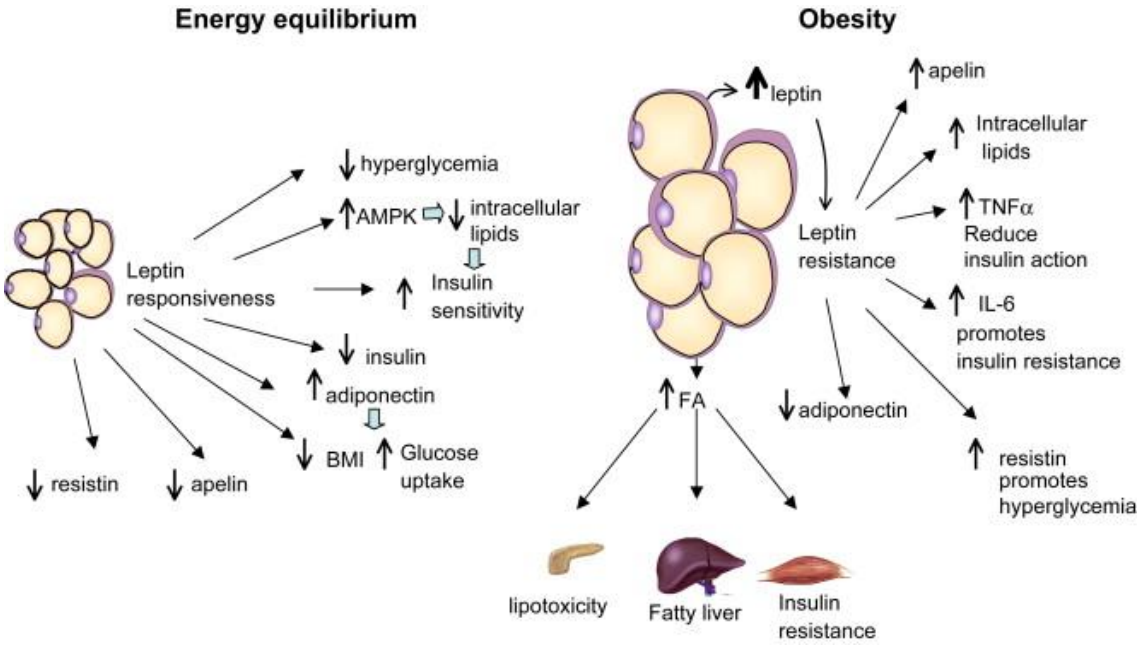

Figure 1.1. White adipose tissue (WAT) in obesity.
Through the release of endocrine acting molecules, WAT communicates with other adipose depots and organs around the body to maintain energy balance and regulate adipose metabolism, adipocyte differentiation, insulin sensitivity and inflammatory responses, and therefore instigates pathogenesis of the myriad metabolic and inflammatory perturbations occurring during obesity. From Vázquez-Vela et al (2008) [32]. Reprinted with permission from Elsevier.

1.1.3 Obesity and inflammation

Obesity is commonly characterised by a state of sub-clinical, chronic inflammation that resembles a low-level version of an acute high-grade inflammatory response such as would normally occur after pathogen infection or tissue damage [33]. A large body of literature describing studies in murine and human adipose tissue agree that major responsibility for the increase in inflammation evident in obesity falls on expanding WAT [20,26,28].

1.1.3.1 Obese adipose tissue and inflammation

Research suggests that inflammatory signalling from adipose tissue originates in enlarged or hypertrophic adipocytes due to the continued oversupply of nutrients in the obese state initiating adipocyte cell stress and damage, and occasionally cell death [33–35]. Although the exact mechanisms triggering inflammatory signalling by hypertrophic adipocytes remain incompletely understood, proposed models include endoplasmic reticulum stress, oxidative damage and tissue hypoxia [34,35]. Initiation of adipocyte endoplasmic reticulum stress is likely due to the substantial quantities of autocrine acting free fatty acids (FFAs) 'spilling out' of hypertrophic adipocytes. In support of this, murine and human studies have shown that adipocyte and macrophage membrane bound toll-like receptor 4 (TLR4) can bind extracellular FFA, inducing a cascade of signalling within the cells, involving NF-κB, that promotes inflammation [36,37]. During obesity, the demand for oxygen in expanding adipose tissue has been shown to exceed supply, inducing hypoxia related changes in adipokine gene expression and secretion, namely an increase in leptin and a decrease in adiponectin [35,38].

Extensive reviews on the role of infiltrating macrophages, and other immune cells, in expanding adipose tissue during obesity, imply that upregulation of pro-inflammatory cytokine and chemokine production occurs in response to a positive feed-forward paracrine interaction between adipocytes and macrophages (Figure 1.2) [20,39,40]. In the mid 1990s, obese adipose tissue from pre-menopausal women was discovered to yield increased levels of the pro-inflammatory cytokine tumour necrosis factor-α (TNF-α) [41]. Since this study, a more recent investigation has reported that stimulation of human adipocytes with TNF-α rapidly and substantially elevates the production of TNF-α and several other pro-inflammatory cytokines and chemokines, such as, monocyte chemoattractant protein-1 (MCP-1 or CCL2), interleukin-6 (IL-6), and vascular endothelial growth factor (VEGF) [42]. MCP-1 is the key chemokine implicated in the recruitment of macrophages, and secretion of MCP-1 from human adipose tissue has been positively correlated with adipocyte size [43,44]. Furthermore, a DNA microarray analysis suggested that interleukin-8 (IL-8), another monocyte chemotactic protein, is expressed at higher levels in larger compared to smaller adipocytes from the same adipose tissue sample [45]. In addition to adipocytes, research suggests that TNF-α is produced by macrophages resident within obese human adipose tissues [46], and that macrophage secreted TNF-α can induce adipocytes to further increase expression of MCP-1 [47]. Taken together, these studies suggest an important role of immune cell recruitment in adipose tissue expansion and local inflammation.

Macrophage infiltration is upregulated in mice adipose tissue during weight gain, with similar increases in macrophage numbers seen in human adipose tissue during obesity [48,49]. Classically, adipose tissue macrophage phenotypes have been defined based on the array of markers they express and inflammatory cytokines they secrete, and are commonly referred to as M2-like and M1-like to describe more anti-inflammatory or pro-inflammatory functions, respectively [50,51]. However, owing to their plasticity, macrophages are now known to express an array of phenotypes that span the M2-like to M1-like spectrum, depending on environmental cues. In addition to the classical M1-like and M2-like divisions, lean and obese adipose tissue macrophages are traditionally referred to as distinct subpopulations, with M1-like or pro-inflammatory phenotypes predominating during obesity [40,52] (Figure 1.2). However, more recently it has been suggested that, during obesity, adipose tissue macrophages express markers that belong to neither the M2-like or M1-like subgroups, but rather are characterised by the simultaneous expression of both M2-like and M1-like markers that are induced in response to metabolic stimuli, rather than cytokine insults [53,54]. Additional evidence also shows that M2-biased $CD206^{+}$ (anti-inflammatory) macrophages dominate the interstitium of obese adipose tissue and, alike M1-like $CD11c^{+}$ (pro-inflammatory) macrophages, are involved in the formation of crown-like structures (CLSs) [55].

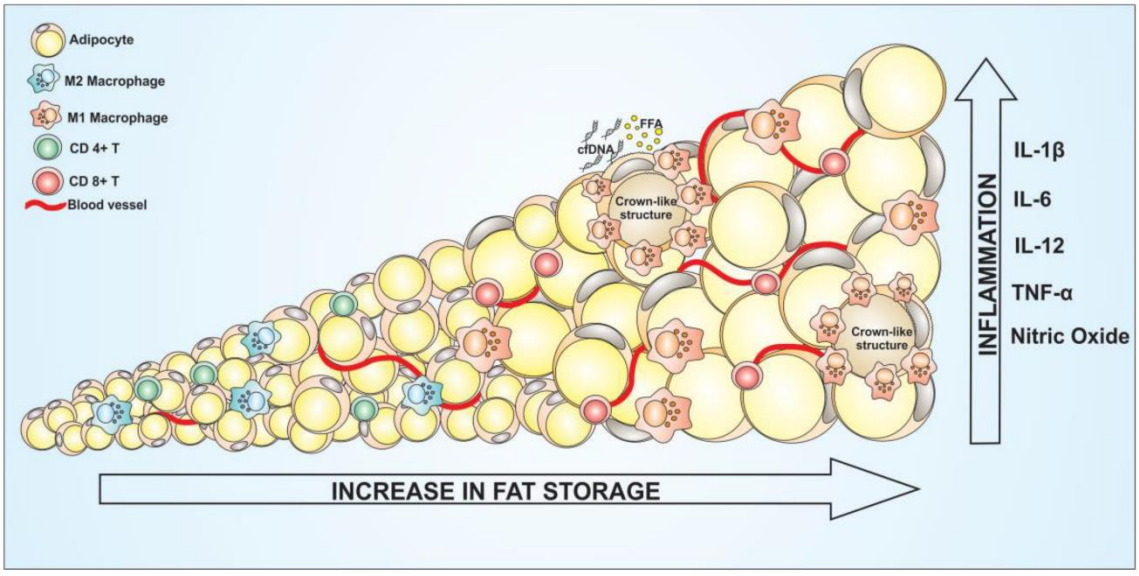

Figure 1.2. Transition of adipose tissue from lean to obese mass.
This schematic highlights the role of adipocyte hypertrophy, macrophage infiltration and the adipocyte-macrophage crosstalk in fostering the development of low-grade chronic inflammation in adipose tissue during obesity. Reprinted from Corrêa *et al* (2019) [56] under the Creative Commons Attribution License.

1.1.3.1.1 Crown-like structures

There are increased numbers of dead adipocytes in obese WAT [57]. Interestingly, events during weight gain that induce adipocyte cell death have been shown to precede increases in adipose tissue macrophage infiltration and pro-inflammatory cytokine expression upregulated during obesity [58]. Research suggests that hypertrophic dead adipocytes are cleared by resident adipose tissue macrophages that form crown-like structures (CLSs) around the dead adipocytes [57,59,60] (Figure 1.3). The frequency of dead adipocytes in adipose tissue of high-fat diet fed mice was positively correlated with an increase in CLS involved macrophages, and an increase in the expression of pro-inflammatory cytokines TNF-α and IL-6 [60]. Furthermore, the presence of CLSs in human mammary adipose tissue has been associated with increasing BMI and adipocyte size [55,61]. This suggests that adipocyte hypertrophy and subsequent death, along with adipose tissue remodelling to form CLSs are important aspects of resident macrophage involvement in the development of inflammation seen in obese WAT(s).

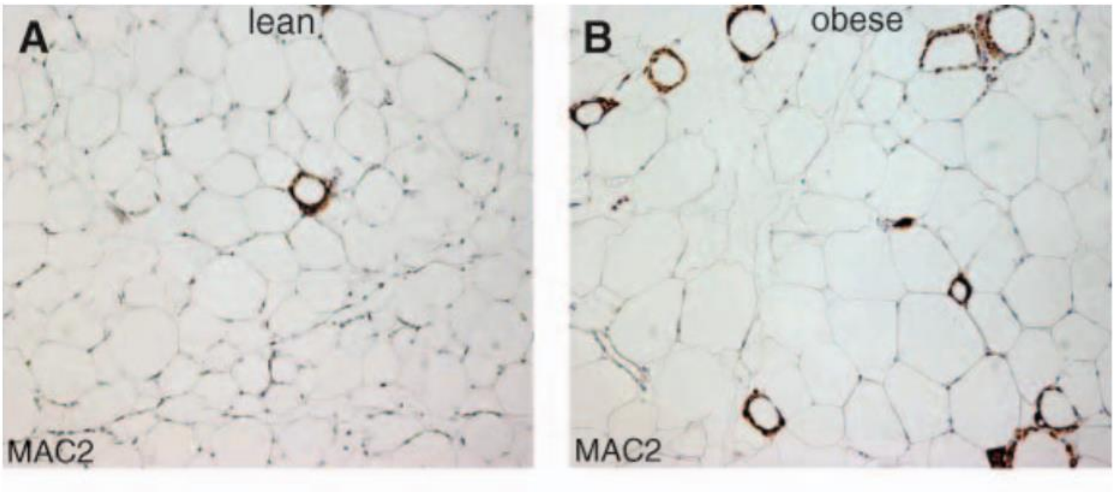

Figure 1.3. Crown-like structures (CLSs) in lean and obese adipose tissue.
Hypertrophic dead adipocytes are cleared by resident adipose tissue macrophages that form CLSs around the dead adipocytes. The presence of CLSs is lower in lean (A) compared to obese (B) WAT. From Cinti *et al* (2005) [57]. Reprinted with permission from American Society for Biochemistry and Molecular Biology.

1.1.3.2 Obesity and low-grade systemic inflammation

Although the extent to which obese adipose tissues are quantitatively contributing to elevations in systemic inflammation are unclear, a well-established hallmark of obesity is the chronically elevated levels of circulating pro-inflammatory adipokines, cytokines and

chemokines, in which key players include leptin, resistin, TNF-α, IL-1β, IL-6, and MCP-1 [28,29,62,63]. In addition, obesity is associated with raised circulating levels of acute-phase proteins, including C-reactive protein (CRP), serum amyloid A (SAA), and alpha 1 acid glycoprotein (AGP) [25,62].

Circulating IL-6 is recognised as one of the primary pro-inflammatory mediators in obesity. Elevated levels of systemic IL-6 can elicit endocrine effects including increased synthesis and secretion of CRP by liver hepatocytes [64], and adipose tissue derived IL-6 can increase systemic CRP in obese humans [31]. In addition to IL-6, adipose tissue levels of TNF-α and leptin are shown to be positively correlated with circulating CRP concentration in obese women [62]. A large meta-analysis of 51 cross-sectional studies measuring obesity by anthropometric measures such as BMI, waist-to-hip ratio and waist circumference, established that obesity was associated with increased levels of serum CRP regardless of age or sex [65]. These studies together provide evidence for the use of CRP as prognostic marker in obesity-associated systemic inflammation.

Taken as a whole, the above findings suggest that pro-inflammatory cytokine production by hypertrophic adipocytes and pro-inflammatory macrophages within obese adipose tissues can act in a paracrine manner to intensify the local inflammatory response, or equally, act systemically in endocrine fashion to stimulate inflammatory cytokine production in other adipose depots or in other organs and cells. Although low-grade chronic systemic inflammation itself is a pathology associated with obesity, it is primarily a condition that leads to secondary pathologies, thus indirectly linking the obese phenotype with a number of inflammation-induced co-morbidities such as diabetes mellitus, insulin resistance, atherosclerosis, psoriasis, renal disease and cancer [28].

1.1.4 Obesity and cancer burden

Excess weight gain and adiposity are associated with an increased risk of developing other health related co-morbidities including but not limited to type II diabetes, cardiovascular diseases, hypertension, stroke, premature death and certain types of cancer [3,66,67]. Evidence suggests that in males and females, 14% and 20% of all cancer associated deaths could be attributable to patients having excess adiposity, respectively [68], and in cancers commonly associated with obesity, including breast, colorectal and prostate, elevated adiposity predicts poorer survival [69]. Moreover, numerous studies have found that BMI is positively correlated

with an increase in cancer risk and mortality, in cancers of the kidney, post-menopausal breast, pancreas, endometrium, liver, and oesophagus [70–74].

In opposition, other studies have found that excess weight, measured as elevated BMI, is associated with better overall cancer survival; notably in colon, kidney and advanced cancer patients [75–82]. Discussion surrounding the discordance in the BMI-cancer survival relationship centres on the crudeness of BMI as a measure of adiposity and physiological variance in the metabolic activity of adipose tissues [83–85], and thus, highlights the importance for obesity-related research to incorporate measures of total body fat mass in conjunction with BMI, ideally accounting for the type, location and amount of adiposity. Regardless of the discordance, obesity remains a modifiable effector of susceptibility and progression in some prevalent cancer types, and therefore provides an advantageous field for cancer research.

The precise mechanisms that are causing increased risk of cancer and worse outcome for cancer patients, during accumulation of excess fat mass, are less well understood. Four distinct mechanisms that have emerged in endeavouring to explain the epidemiological link between obesity and the pathophysiology of cancer include the manifestation of obesity related inflammation, development of insulin resistance and hyperinsulinemia, expression of adipose secreted adipokines such as leptin and adiponectin, and enhanced oestrogen signalling [86–90]. As discussed above, obesity is associated with a condition of low-grade chronic systemic inflammation stemming from the secretion of inflammatory cytokines and chemokines from obese adipose tissue that elicit endocrine effects on other organs and further exacerbate inflammation [91]. Obese adipose tissue has been shown to upregulate the secretion of adipokines such as leptin, cytokines such as IL-6, TNF-α, IL-1β, and chemokines such as MCP-1 and IL-8, that are directly or indirectly involved in cancer pathogenesis [92,93]. Circulating leptin levels are positively correlated with adipose tissue mass, and under such conditions are generally responsible for stimulating inflammatory signalling within adipose tissue, generating a proliferating positive feed-back loop [94]. In addition to inflammation, leptin has been implicated in the regulation of aromatase activity [95] and results in higher concentrations of serum oestrogen levels, where elevated oestrogen signalling is associated with increased cancer risk in certain cancer types, including breast, ovarian and endometrial cancers [96]. Extended periods of excess adiposity can promote a chronic increase in circulating concentrations of insulin, indicating insulin resistance or hyperinsulinemia. During hyperinsulinemia, levels of bioavailable insulin-like growth factor (IGF-1) become elevated in blood due to blocked production of the insulin-like growth factor binding protein (IGFBP),

whereby IGF-1 (a powerful activator of cell mitosis and survival) can favour tumour production and promotion [97,98]. Due to the complex local and systemic effects of obesity, each mechanism is likely playing a role in both tumour initiation and tumour progression, and different cancer types with diverse aetiology are likely influenced by each mechanism in unique ways [91,94].

Understanding the biological underpinnings linking obesity with cancer are important for the development and implementation of future treatment strategies. Currently proposed treatment strategies targeted against adiposity in attempts to negate tumour initiation and metastasis are focused on lifestyle, pharmacological and surgical interventions. Such interventions include improvements in exercise and dietary behaviours, medications that block the inflammatory and hyperinsulinemia signalling pathways (e.g. pioglitazone and metformin), and bariatric surgeries including gastric bypass as a method to rapidly reduce excess adiposity [89,91,99].

1.2 Breast cancer

According to global WHO statistics, 2,088,849 diagnoses of breast cancer were recorded for females and males of all ages in 2018; making up 11.6% of all new cancer cases [100]. Breast cancer is the third most prevalent cancer type in NZ, with 3,294 women being diagnosed in 2017 and more than 600 deaths registered each year [101]. Breast cancer is the aberrant and uncontrolled growth of normal breast cells into a cancerous tumour, that has the potential to spread to lymph nodes and metastasise to form secondary tumours in other locations around the body; reducing survival rates as stages progress [102].

Based on differences in gene expression profiles, breast tumours have been grouped into five main molecular subtypes including luminal A, luminal B, HER2 enriched, claudin-low and basal-like; with a small percentage of 'normal-breast-like' tumours expressing genetic signatures similar to that of breast adipose tissues [103,104] (Figure 1.4). Pathologists currently determine breast tumour subtypes by assessing important clinical biomarkers such as the presence or absence of oestrogen receptor (ER) and progesterone receptor (PR) expression, and the presence or absence of human epidermal growth factor 2 (HER2; *Erbb2*) overexpression. Generally, luminal A and B breast tumours are ER positive (+) and/or PR+ and HER2 negative (-), and luminal B tumours tend to grow slightly faster as they are categorised by their higher levels of the cellular proliferation protein Ki-67 [103–105]. Most HER2 enriched tumours are ER-, PR- and overexpress HER2, whereas, claudin-low and basal-like

breast tumours are ER-, PR- and HER2- (triple negative) but can be distinguished by low expression of claudin-3, -4, and -7 genes in claudin-low tumours [103,104,106].

Clinical management of early stage breast tumours often involves treatments tailored to the molecular subtype of the tumour, for example recombinant antibodies, such as Herceptin (trastuzumab), targeting HER2 in tumours overexpressing HER2 [107,108]. Despite being classed as one of the most significant advancements in the treatment of breast cancer, 70% of patients with HER2+ tumours do not seem to benefit from Herceptin [109]. The causal mechanisms responsible for the both *de novo* and acquired resistance to Herceptin are still unclear [110]. Equally, treatment of basal-like tumours with non-dependence on hormone receptors, or HER2 expression, relies predominantly on carefully devised chemotherapy regimens, as they cannot respond to targeted anti-HER2 or endocrine therapeutics, and unfortunately, despite initial chemo-sensitivity early relapse is common in triple negative breast cancers [111,112]. Taken together, these studies highlight the need for the development of novel therapeutic agents along with better treatment strategies to overcome therapeutic resistance in breast cancer. In addition to clinical approaches, research assessing different lifestyle intervention strategies have become popular in both the prevention and treatment of breast cancer. Such interventions are mainly focused on improving the health consequences of excessive adiposity in women with breast cancer, largely through improving diet and implementing regular physical activity.

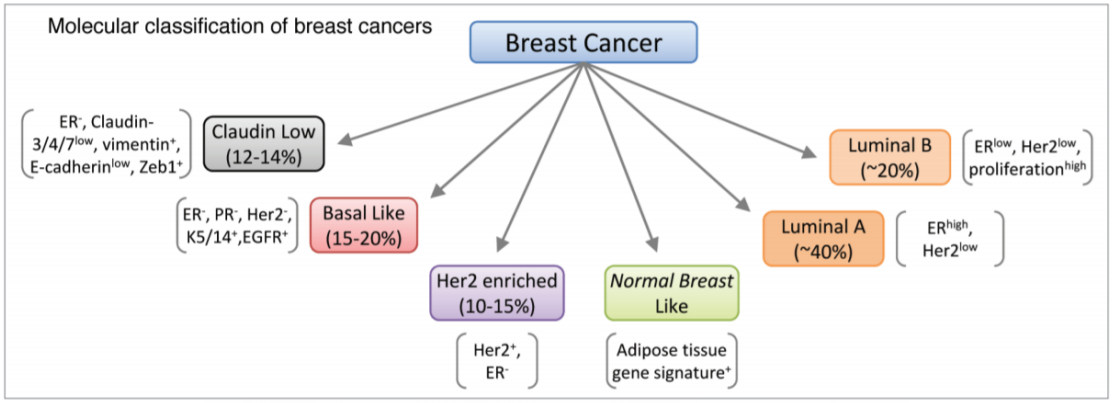

Figure 1.4. Breast cancer molecular subtypes.
Based on differences in gene expression profiles, breast tumours have been grouped into five main molecular subtypes including luminal A, luminal B, HER2 enriched, claudin-low and basal-like; with a small percentage of 'normal-breast-like' tumours expressing genetic signatures similar to that of breast adipose tissues. From Gautam *et al* (2010) [113]. Reprinted with permission from Taylor & Francis.

1.2.1 Breast cancer and obesity

As discussed above, obesity is known to influence the risk and prognosis of a number of cancer types, and this includes breast cancer.

1.2.1.1 Obesity and breast cancer susceptibility

Large epidemiological studies and meta-analyses recognise that obese post-menopausal women have an increased risk of developing breast cancer, whereas high BMI seems to have a protective effect on the risk of developing breast cancer in pre-menopausal women [70,114,115]. In post-menopausal women, susceptibility to breast cancer was shown to increase by approximately 40% for every 10 unit increase in BMI [70], although another study reported breast cancer risk increasing in a non-linear fashion with increasing BMI [114]. A clear inverse relationship was previously determined between obesity and risk of breast cancer in pre-menopausal women [115], however more recent investigations determined that the influence of obesity on breast cancer susceptibility in pre- and post-menopausal women differed depending on breast tumour subtypes [116,117]. In post-menopausal women, obesity was associated with a higher susceptibility to ER positive breast cancer, but had little to no impact on the risk of ER negative breast tumours [116,117]. Whereas, obesity in pre-menopausal women had conflicting effects, showing increased risk of triple negative breast tumours and lowered risk of ER positive breast cancer in one study [116], but no association between BMI and susceptibility to any tumour subtype in the other investigation [117]. It is unclear exactly what biological mechanisms are causing differences in obesity associated pre- and post-menopausal breast cancer risk, but it is likely that metabolic and hormonal changes resulting from menopause dependent differences in total body and visceral adiposity are playing a role [118–120].

1.2.1.2 Obesity and breast cancer outcomes

The association between obesity and breast cancer outcome was first studied in the late 1970's, indicating that obese women had a greater chance of presenting with clinically advanced staged tumours and lymph node metastasis, and had a notably increased likelihood of death over the five year follow up period [121]. These early results are now well supported by more recent and much larger investigations establishing that obesity is related to having more advanced disease at diagnosis, increased risk of recurrence and metastasis, and poorer overall survival in breast cancer patients [122–125]. In support of these studies, two meta-analyses with large populations of breast cancer patients concluded that obesity reduces overall survival rates by 33% and 41% [126,127]. Although prior reporting suggests that reduced overall

survival is likely resulting from co-morbidities arising during obesity [128], opposing data from large meta-analyses have shown similar reductions in both overall and breast cancer specific survival rates in obese women with breast cancer [126,129]; providing evidence for direct effects by obesity-associated factors.

Associations between obesity and poorer survival in ER positive breast tumours [123,125] and pre-menopausal women [125] have been previously reported, yet in contrast, large meta-analyses established that the association between obesity and poorer survival rates is independent of the hormone receptor status of the breast tumour or menopausal status of the patient at diagnosis [116,127,129], indicating that breast cancer susceptibility and breast cancer outcomes are impacted by obesity by different mechanisms.

Individual studies and investigations of pooled data across studies, has revealed that increasing BMI at diagnosis lowers pathological complete response rates in breast cancer patients treated with neoadjuvant chemotherapies [122,130–133]. These findings suggest that the detrimental effects of obesity on breast cancer patient outcome could be preceded by reduced efficacy of chemotherapy on breast tumour regression in obese patients. Hypotheses explaining the causal mechanisms for lesser impact of chemotherapy and reduced survival in obese breast cancer patients are focused on two main propositions: firstly, the under treatment of obese breast cancer patients based on body surface area (BSA) dose-capping [134]; and secondly, the biological interaction of obese adipose tissue with breast tumour cells leading to the development of more aggressive tumours [116].

1.2.1.2.2 Dose-capping chemotherapy in obese patients

Previous findings suggest that overweight and obese women with breast cancer are more likely to receive intentionally reduced doses of chemotherapy [135,136], despite very little evidence for beneficial reductions of chemotherapy related toxicities in obese patients receiving capped doses based on BSA [134,137,138]. Although it has been shown that normal weight breast cancer patients receiving higher doses of chemotherapy had better compliance to chemotherapy, suggestive of a lower frequency of chemotherapy-related toxicities compared to obese patients [122], opposing evidence from a recent investigation of obese breast cancer patients receiving uncapped and no dose reductions of neoadjuvant chemotherapy revealed no difference in treatment related toxicities, and intriguingly, longer progression free survival in obese compared to normal weight patients [139]. Overall, these studies suggest that

the current dose-capping of overweight and obese breast cancer patients is not required, and may even be playing a role in reducing the survival rates of obese breast cancer patients.

1.2.1.2.3 Proposed biological mechanisms

Despite a well-established epidemiological connection between obesity and breast cancer progression, the precise biological mechanisms underlying this relationship are less clear. Proposed explanations for the link between obesity and breast cancer pathogenesis vary from systemic effects such as increased levels of chronic low-grade inflammation (described earlier in Section 1.1.3.2), elevated bioavailable oestrogens, and insulin resistance or hyperinsulinemia, to local in-breast effects including breast adipocyte release of inflammatory adipokines and cytokines, enhanced hormone signalling, and alterations in extracellular matrix (ECM) [91,94,116,140–143] (Figure 1.5).

Obesity is associated with the development of systemic conditions due to the dysfunction of expanding adipose tissues, such as chronic inflammation, insulin resistance, adipokine dysregulation, and elevated bioavailable oestrogens- all of which have been implicated in poorer breast tumour prognosis [144–147]. Several pro-inflammatory cytokines increased in circulation during obesity are overexpressed in primary breast tumours that have poorer outcomes [148]. In particular, IL-6 is shown to stimulate inflammatory signalling in breast cancer cells [149], and increases in levels as tumour size and lymph node involvement increases [150]. Obesity is associated with decreased adiponectin and increased leptin levels in serum, which is a trend similarly measured in breast cancer patients [140,146,151]. The leptin receptor OB-R shows positive expression in 83% of breast tumours, and the upregulated expression of leptin is associated with a greater chance of distant metastasis and poorer survival in breast cancer patients [151]. Leptin is known for its role in upregulating both insulin and oestrogen signalling in patients with breast cancer [152]. Systemic insulin levels remain elevated during obesity, leading to the increased production of the insulin-like growth factor-1 (IGF-1), and during obesity IGF-1 contributes to breast cancer cell growth through binding of its receptor, IGF-1R, that is commonly overexpressed in breast tumours [153–155]. Circulating levels of oestrogens are higher in obese post-menopausal women compared to their normal weight counterparts [156], and due to the expression of oestrogen receptors in many breast cancer cells, elevated bioavailability of oestrogen during obesity is a well-established risk factor for breast tumour development and progression [157,158]. Taken together, the effects of systemic obesity on breast cancer progression are suggested to result from direct endocrine signalling between obese adipose tissues and breast tumour cells. Interestingly, far less attention has

been focused on the possible indirect effects of obesity-associated conditions that may be influencing biological processes in non-tumour organs and tissues. Notably, alterations in liver drug metabolism is likely influenced by higher levels of circulating inflammatory cytokines [159]. This may potentially alter chemotherapy pharmacokinetics, and may explain the poorer pathological response rates to chemotherapy for breast tumours from obese patients. Liver metabolism of breast cancer chemotherapies is discussed later in Section 1.4.

Human breasts are known to harbour relatively large volumes of WAT, and during obesity, dysregulation in local breast WAT is suggested to play a role in breast cancer pathogenesis [91,94]. Levels of breast adipose tissue inflammation, measured as the degree of CLS content in women with breast cancer, is positively correlated with markers of systemic inflammation evident during obesity, such as CRP, IL-6, and leptin [160]. This is suggestive of a convergence between systemic and local breast adipose tissue inflammatory signalling occurring during obesity. IL-6 is shown to stimulate inflammatory signalling between breast cancer cells and nearby adipocytes in the tumour microenvironment, which has been shown to influence breast tumour progression *in vitro* and *in vivo* [150,161]. Moreover, oestrogen synthesis occurs mostly in adipose tissues following menopause, where aromatase converts androgens to bioavailable oestrogens [156]. Increased aromatase expression has been identified in breast adipose tissue of obese post-menopausal women with breast cancer; where aromatase expression is upregulated by pro-inflammatory mediators released by CLSs [160,162–164]. In contrast however, recent findings show expression of breast WAT inflammation (CLS content) in 39% of normal weight women with breast cancer (determined by a BMI < 25 kg/m^2), and inflammation in these women was also associated with more hypertrophic adipocytes, higher systemic inflammation and elevated aromatase expression [165]. Thus, upregulation of breast WAT inflammation, rather than BMI, is a significant determinant of aromatase activity in the breast, and may provide a meaningful target blocking the local effects of breast adipocytes on breast tumour progression. This is just one way in which breast adipose tissue is influencing breast cancer pathogenesis during obesity. The full extent to which biological interactions between breast cancer cells and local stromal adipocytes are influencing breast tumour progression is still unravelling, and is discussed further in Section 1.3 below.

Overall, the relationship between obesity and poor breast cancer prognosis and survival is complex and dynamic, and it is understood that multifaceted interactions between biological systemic and processes localised to the breast are likely influencing obese breast

cancer patient outcomes (Figure 1.5). Further analysis investigating aspects of both the local and systemic effects of obesity on breast cancer progression will hopefully reveal novel mechanistic links and therefore inform rational development of novel treatment strategies.

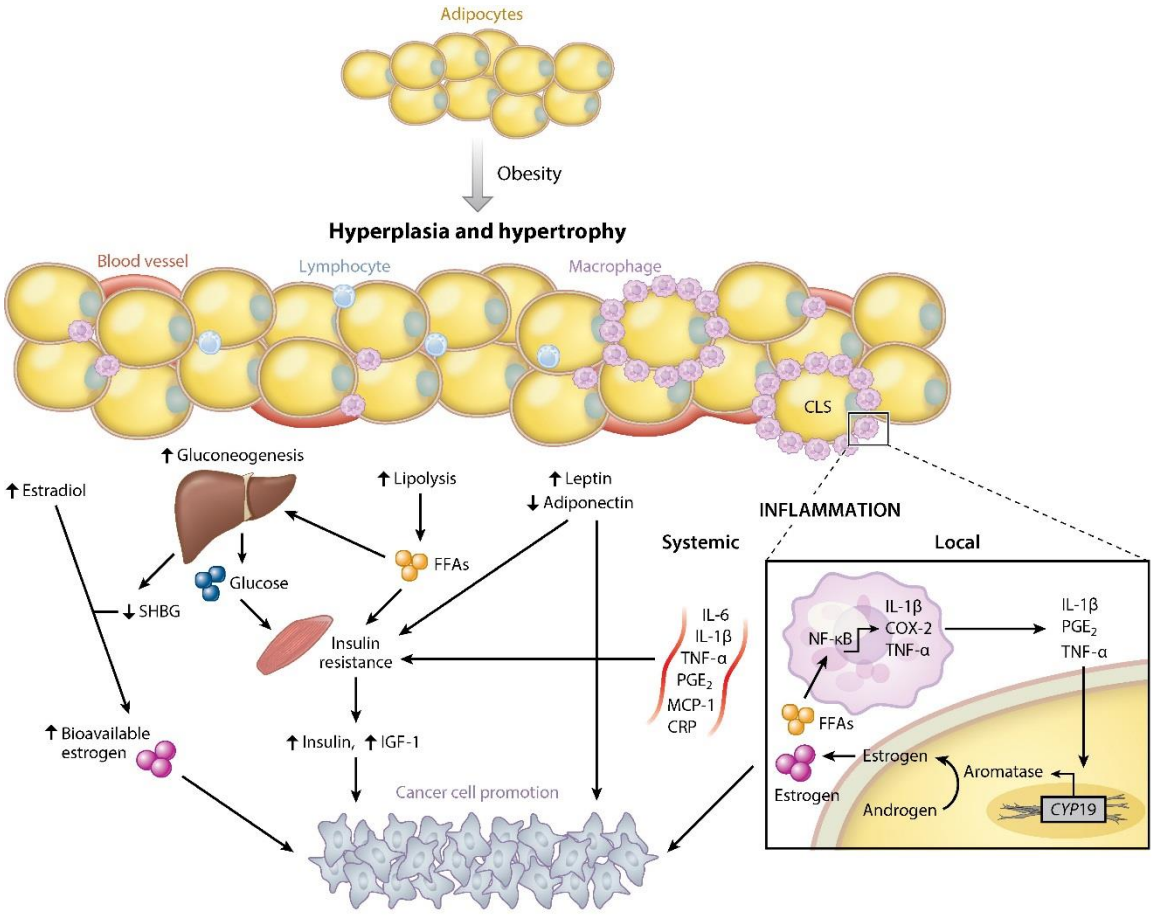

Figure 1.5. Local and systemic effects of adipose tissue on breast cancer progression. Proposed explanations for the link between obesity and breast cancer pathogenesis vary from systemic effects such as increased levels of chronic low-grade inflammation (see Section 1.1.3.2), elevated bioavailable oestrogens, and insulin resistance or hyperinsulinemia, to local effects including release of inflammatory adipokines and cytokines by breast adipocytes, enhanced hormone signalling, and alterations in extra cellular matrix (ECM). From Iyengar *et al* (2015) [94]. Reprinted with permission from ANNUAL REVIEWS.

1.2.2 Breast cancer and physical activity

1.2.2.1 Physical activity and breast cancer susceptibility

The association between physical activity and breast cancer prevention was first acknowledged in 1985 [166], and better understanding of this relationship has developed over the past 30 years. A systematic review of a large number of studies conducted up until 2007 reported a well-established and robust consensus that increased levels of physical activity

reduces the risk of developing breast cancer in a dose-dependent manner [167]. In addition, a more recent meta-analysis comprising over 63,000 cases from 31 studies concluded that the risk of breast cancer declined significantly in a dose-response manner by 5% for every incremental 2 hour per week increase in moderate to vigorous recreational physical activity [168].

1.2.2.2 Physical activity and breast cancer outcomes

A considerable number of studies, including both observational and clinical interventions, have investigated the association of pre- and post-diagnosis physical activity with breast cancer recurrence and survival. Five well designed meta-analyses, all published since 2011, have pooled data across studies to assess the overall effects of physical activity on breast cancer patient outcomes [169–173]. These meta-analyses consistently concluded that breast cancer specific and all-cause mortality were sufficiently reduced by elevated levels of pre-diagnosis and post-diagnosis physical activity, however, the association between increased post-diagnosis physical activity and improved survival was more pronounced than pre-diagnosis physical activity [169–173]. Non-linear dose-response relationships between post-diagnosis physical activity levels and breast cancer survival were reported in two meta-analyses [170,171], whereas, Schmid *et al.* concluded that the risk of mortality in breast cancer survivors decreased in a linear manner, reducing by 24% for every 10 metabolic equivalent of task (MET) hour per week increase in post-diagnosis physical that was performed [172]. In addition to survival outcomes, the meta-analysis by Lahart *et al*. concluded that increased levels of pre-diagnosis and post-diagnosis physical activity were associated with lowered risks of breast tumour-related events such as progression, additional primaries, and recurrences [173]. Although recommendations regarding the optimal type, dose and schedule of physical activity are made difficult by the considerable heterogeneity in the measurement modalities and exercise interventions implemented across previous studies, it was concluded in the most recent meta-analysis by Li *et al.* that a minimum of 2.5 hours per week of moderate intensity recreational physical activity was enough to confer protection against cancer mortality among cancer survivors [171]; a proposal that meets the current WHO recommendations for physical activity in adults [174].

Despite the growing support for exercise-associated improved breast cancer outcomes, the precise biological mechanism responsible for better outcomes in more active breast cancer patients is less understood. A number of possible mechanisms have been

proposed, ranging from intratumoural changes such as enhanced vascularisation (decreasing hypoxia, and increasing blood perfusion and drug delivery) and immune cell infiltrate, to systemic adaptations including decreased levels of circulating sex hormones, leptin, insulin and inflammatory cytokines [116,175–177]. The most studied systemic adaptation of physical activity in breast cancer survivors is the levels of circulating inflammatory cytokines, most probably due to the already existing and robust evidence for physical activity-induced reductions in systemic inflammation in individuals without cancer [178].

1.2.2.2.1 Post-diagnosis physical activity and systemic inflammation

Investigations of the effects of physical activity on systemic markers of inflammation in breast cancer survivors have been conflicting, with some earlier studies suggesting a reduction in circulating CRP levels in exercising breast cancer survivors [145,179], whereas, more recent investigations have suggested that 2 month and 6 month aerobic exercise interventions had no beneficial effect on the levels of circulating inflammatory cytokines such as CRP, TNF-α, and IL-6 [180,181]. Meta-analyses are in support of the former [182–184]. One meta-analysis showed significant decreases in the levels of the pro-inflammatory cytokines IL-6, IL-2, IL-8, and TNF-α in exercising compared to non-exercising breast cancer survivors [182], and another concluded a meaningful reduction in CRP levels for breast cancer survivors participating in greater levels of physical activity [183]. Most recently, a meta-analysis concluded that aerobic plus resistance training was most effective at reducing circulating CRP and TNF-α in breast cancer survivors [184]. In breast cancer survivors, the variation in the duration, dose and type of exercise interventions that have been investigated are likely differentially influencing the inflammatory responses observed, and thus may help explain the discordant results observed in these studies. Evidence for this comes from a recent 16 week aerobic plus resistance exercise study, which reported significantly reduced levels of the systemic pro-inflammatory cytokines CRP, IL-6, IL-8 and leptin, and increased concentrations of the circulating anti-inflammatory marker, adiponectin, in breast cancer survivors [185]; alterations that were not observed in the previous study investigating the shorter duration study with only an aerobic exercise intervention [181]. This suggests that exposures to physical activity, for longer duration, may be required for systemic reductions to materialise in breast cancer survivors, and that aerobic exercise alone may not be enough to decrease markers of systemic inflammation.

Direct biological links between physical activity, regulation of systemic inflammation, and improved breast cancer outcomes have yet to be experimentally demonstrated *in vivo*. However, *in vitro* findings have shown that systemic alterations occurring during acute bouts of physical activity in breast cancer survivors, such as serum increases in muscle secreted cytokines (myokines), were able to inhibit growth of MCF-7 and MDA-MB-231 breast cancer cells [186]. In contrast, systemic changes occurring over time in these patients were not able to inhibit breast cancer cell growth, despite marked reductions in serum cytokine levels of IL-6 and TNF-α [186]. Since these findings, it has been suggested that the control of tumour growth by physical activity in breast cancer patients is effected more by pronounced systemic changes occurring during each bout of acute training, as opposed to less pronounced systemic adaptations in response to training over time [187] (Figure 1.6). This highlights the potential importance that each exercise training session may have on breast tumour progression, even in the short term directly following diagnosis and during chemotherapy treatment.

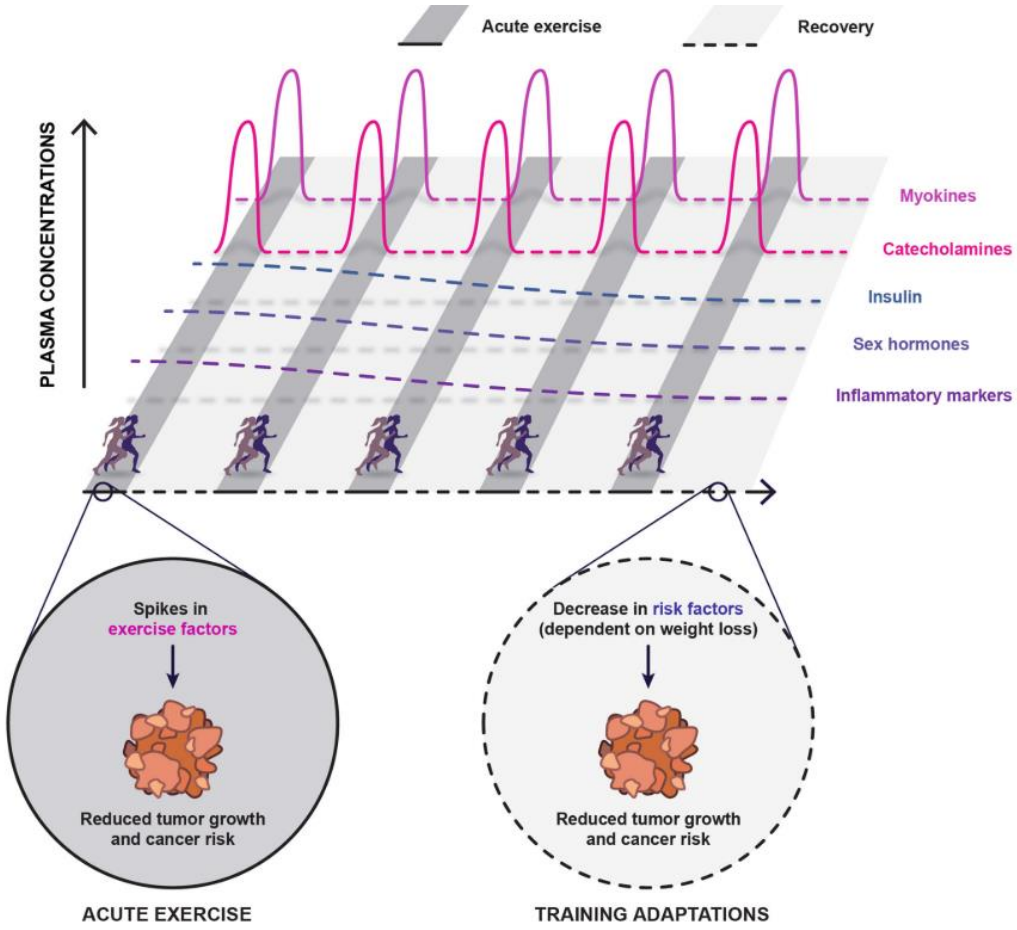

Figure 1.6. Control of tumour growth by physical activity in breast cancer patients.

This schematic shows that tumour growth is affected more by pronounced systemic changes occurring during each bout of acute training, as opposed to less pronounced systemic adaptations in response to training over time. From Dethlefsen *et al* (2017) [187]. Reprinted with permission from Springer Nature.

During Chemotherapy

It has been suggested that aerobic and resistance exercise implemented during adjuvant chemotherapy can improve treatment responses, particularly in women who were overweight or obese [188]. Breast cancer patients performing high doses of approximately 50-60 minutes of combined aerobic and resistance training has been proven to be achievable during treatment, causes no harm to the patient, and does not affect their rate of chemotherapy completion [189,190], although higher-intensity doses of physical activity during chemotherapy was tolerated better by women that were younger, fitter and had a healthy weight BMI (BMI: 18.5 – 24.9) [191]. A recent extensive review has highlighted a number of factors hypothesised to explain how physical activity interacts with chemotherapy to improve treatment efficacy, tolerability and completion without the need for dose-reductions, including stimulation of immune cell signalling, improved drug delivery to the tumour, and regulation of body composition [177]. Yet, despite evidence for beneficial effects of post-diagnosis physical activity on breast cancer outcomes, only a single investigation has assessed the effects of physical activity on markers of systemic inflammation during chemotherapy; reporting no effect of exercise on serum levels of IL-6 or IL-1 [192]. The authors suggested that the inflammatory response associated with chemotherapy was not counteracted by increased levels of combined aerobic and resistance exercise training, although only two markers of inflammation were assessed. Thus, further research assessing the effects of physical activity on circulating inflammatory cytokines during chemotherapy for breast cancer may benefit from measuring cytokine array panels, for example, in order to highlight novel cytokines responsible for the mechanistic link between physical activity, altered systemic inflammation and improved breast cancer outcomes.

1.2.2.2.2 Physical activity, weight change and systemic inflammation

Interestingly, the systemic adaptations that have been proposed to explain the biological link between increased physical activity and improved breast cancer survival, including reductions in circulating levels of sex hormones, leptin, insulin and inflammatory cytokines [140,142], are the same systemic markers that are associated with poorer breast cancer outcomes when circulating levels are increased (see Section 1.2.1.2.3). Thus, it is not

surprising that associations between physical activity and improved breast cancer outcomes are suggested to be driven by reductions in patient adiposity [116,175] (Figure 1.7). In research performed after patients have completed chemotherapy, exercise and calorie restriction in a group of early stage breast cancer survivors resulted in modest body weight and waist-to-hip ratio reductions, and these body compositional changes were positively correlated with markers of inflammation [193]. Moreover, aerobic and resistance exercise training reduced circulating levels of pro-inflammatory cytokines in breast cancer survivors when accompanied by significant decreases in body weight, body fat percentage, waist-to-hip circumference, and adipose tissue IL-6 and anti-inflammatory macrophage concentrations [185]. Conversely, however, another study did not measure the same level of change in circulating inflammatory cytokines in response to a moderate intensity exercise and dietary advice intervention in survivors of triple negative breast cancer, despite a notable decrease in body fat percentage in the intervention group [194]. Therefore, when assessing the impact of post-diagnosis physical activity on systemic adaptations in breast cancer patients it is important that alterations in body composition are also considered.

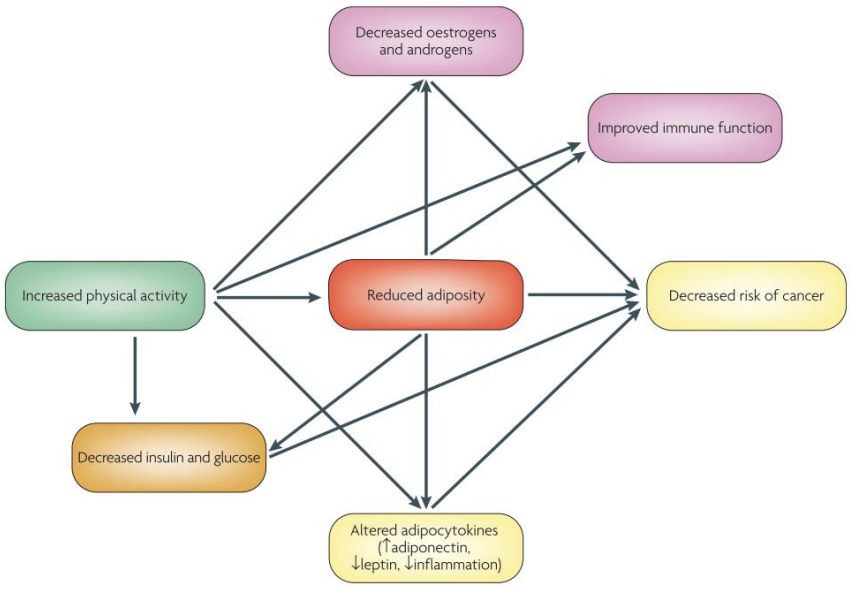

Figure 1.7. Biological mechanisms linking improved breast cancer survival to increased physical activity.
The majority of the systemic adaptations proposed as biological mechanisms for improved breast cancer survival with increased physical activity are systemic markers that are commonly elevated during obesity, such as sex hormones, leptin, insulin and inflammatory cytokines. The associations between increased physical activity and improved breast cancer outcomes are proposed to be driven by reductions in patient adiposity. From McTiernan *et al* (2008) [175]. Reprinted with permission from Springer Nature.

1.2.2.3 Measuring physical activity in cancer patients

When measuring physical activity in cancer patients many studies include survey and/or questionnaire based assessments. However, as more modern technology driven assessments are now more readily available, it is possible to include objective measures of physical activity through the use of pedometers, accelerometers, or global positioning satellite (GPS) data. Objective measures of physical activity offer several advantages over the traditional survey or questionnaire based assessments including reduction of recall bias, continuous physical activity data, and objective measurement of adherence [195], although it has been established that objective measures are best used in combination with self-reported measures of physical activity [196]. Several commercially available accelerometers have been used in clinical studies (RT3, activePAL, Actigraph, Qstartz, Yamax) to determine free range physical activity in both children and adults, with and without the addition of global positioning satellite data [197–199]. Accelerometer data measured using FitBit One® devices, has been validated as a measure of physical activity in studies using questionnaires as well as objective validation against observed activity, such as treadmill walking [200]. Furthermore, a number of studies have validated the use of FitBit™ devices for measuring physical activity in breast cancer patients during chemotherapy treatment [196,201,202], as well as in other solid malignancies [203]. Interestingly, a pilot study in 16 cancer patients provided evidence that showed patients naturally separating themselves into more physically active and less physically active cohorts without any intervention in place (Unpublished Data; Dr Matthew Strother, 2015) (Figure 1.8). Taken together, these studies support the use of FitBit™ devices in both observational and intervention studies for objectively assessing physical activity in participants receiving chemotherapy for cancer.

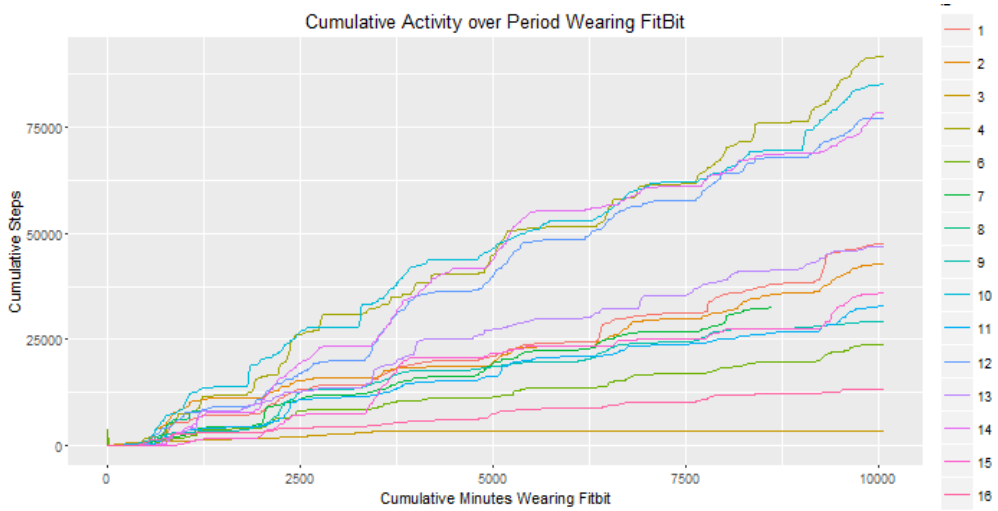

Figure 1.8. Measuring physical activity levels in breast cancer patients during chemotherapy.
A pilot study showed that it is possible to measure physical activity (cumulative steps) in breast cancer patients (n= 16) during chemotherapy using FitBit One® devices, and patients naturally separate into more physically active and less physically active cohorts without any intervention (data unpublished).

1.3 Tumour microenvironment

Tumours predominantly consist of a heterogeneous population of cancer cells, but are also home to an assortment of other residential and invading stromal and immune host cells, vasculature components, extracellular matrix (ECM), and a milieu of secreted factors; collectively referred to as the tumour microenvironment [204,205] (Figure 1.9). Other than cancer cells, cell types commonly found in the tumour microenvironment include fibroblasts, neutrophils, macrophages, endothelial cells, lymphocytes, natural killer cells and adipocytes [204,206]. Interactions between cancer cells and the tumour microenvironment are constantly changing over time, vary between different tumour types, and have been suggested to play a role in all stages of tumourigenesis, including tumour initiation, progression and metastasis [207,208]. Furthermore, the tumour microenvironment has been implicated in modulating responses to chemotherapy, radiotherapy, and other targeted therapies; favouring tumour survival [209].

Foundations for explaining the role of the tumour microenvironment in tumour formation and progression were first laid in the late 1880s by Paget's 'seed and soil' hypothesis, which proposes that for a 'seed' to grow the 'soil' must be liveable and

nurturing; contextually meaning cancer cells need a hospitable environment to grow [210]. Paget's 'seed and soil' theory was initially used as an explanation for why particular organs are more likely to become home to cancer cell metastases, and since then the theory has been expanded to explain not only cancer cell metastasis, but also the importance of the tumour microenvironment in cancer progression prior to metastasis [211].

The crucial role of the ECM modulating gene expression differences between malignant and normal tissues in early microenvironment research highlighted the ability of the cancer cell to continually respond to, and modify, its surrounding microenvironment; a collaboration that was befittingly termed 'dynamic reciprocity' [212]. Since then, it has been debated whether reciprocal interactions between cancer cells and the tumour microenvironment are initiated by alterations to the microenvironment that cause the promotion of carcinogenesis, or by tumours that initially grow independently and eventually signal to the microenvironment to begin supporting its growth [213]. It is likely that both occur, and regardless of how the reciprocal interactions are being initiated, it is clear that co-operation between breast cancer cells and the tumour microenvironment aids breast tumour progression [214,215].

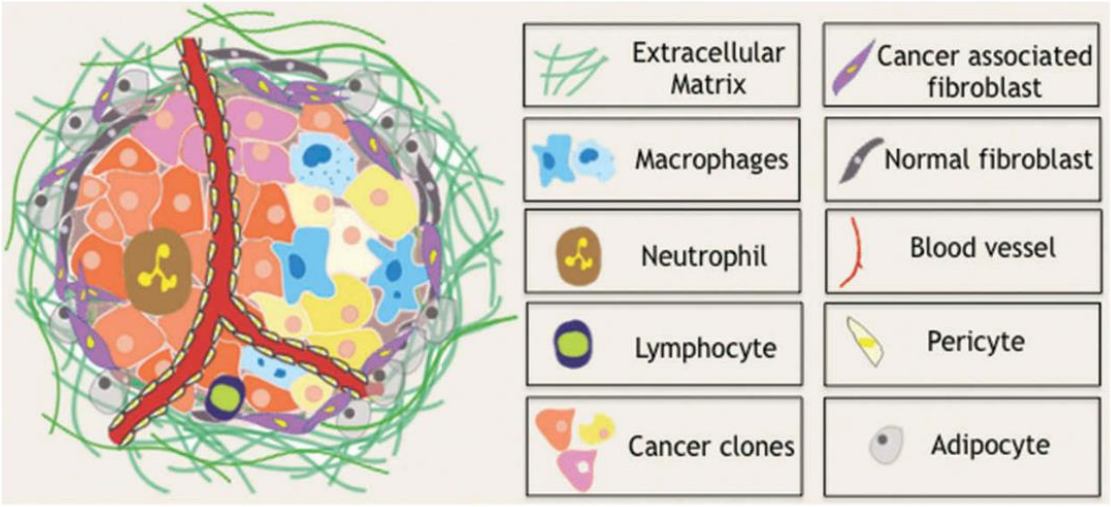

Figure 1.9. Cell types found in the tumour microenvironment.
Tumours predominantly consist of a heterogeneous population of cancer cells, but are also home to an assortment of other residential and invading stromal and immune host cells, vasculature components, extracellular matrix (ECM), and a milieu of secreted factors; collectively referred to as the tumour microenvironment. From Mittal *et al* (2018) [215]. Reprinted with permission from Taylor & Francis.

1.3.1 Breast tumour microenvironment

Development and differentiation of normal mammary glands requires specific communication between stromal and epithelial cells, and pathophysiological alterations in these interactions can enable tumour growth and progression [216]. Although the exact mechanisms behind the tumour microenvironment's role in malignant epithelial activation in the breast are unclear, the transition between normal epithelium to invasive breast carcinoma has been hypothesised to occur through two models - both involving the tumour microenvironment: the 'escape' model by which genetic and epigenetic changes give rise to clonal malignant epithelial and stromal populations that favour tumour proliferation; and the 'release' model where decreased myoepithelial and increased fibroblast populations in the tumour microenvironment disrupt the basement membrane allowing stromal invasion of malignant epithelial cells, enabling further microenvironmental interactions [216]. In 1973, breast carcinoma cells were seen losing their malignant phenotype when grown away from an active tumour microenvironment; providing an early argument for the importance of the tumour microenvironment in breast cancer progression[217]. Since these findings, the breast tumour microenvironment has become the focus of an increasing number of studies, and is now a well appreciated facilitator of the growth, survival and metastasis of breast cancer cells [214,215,218].

Numerous different cell types within the tumour microenvironment have been shown to play a role in breast cancer, including but not limited to, macrophages, neutrophils, fibroblasts and adipocytes [215]. One way in which the tumour microenvironment may be impacting breast cancer progression is through genetic and epigenetic changes in stromal cells [219,220]. Research suggests that breast tumour macrophages are associated with invasion, metastasis, and ultimately poorer patient survival [221]. Tumour associated macrophages have been shown to induce breast cancer cell epithelial to mesenchymal transition (EMT) [222], as well as increase breast cancer metastasis through the secretion of the glycoprotein chitinase-3-like protein 1 (CHI3L1) [223]. Breast cancer progression can be promoted by infiltrating neutrophils secreting factors that stimulate tumour vasculature [224]. Moreover, an important regulator of tumour inflammation is the neutrophil-to-lymphocyte ratio (NLR), where an increased NLR is correlated with adverse survival outcomes in breast cancer patients [225]. Probably the most studied and highly abundant stromal player in the breast tumour microenvironment is the fibroblast. Compared to normal fibroblasts, cancer associated fibroblasts (CAF) from primary breast tumours show differential mRNA and protein

expression profiles despite having similar morphology [226]. CAF have been implicated in the promotion of breast cancer cell EMT, therapy resistance and, through secretion of leptin, breast tumour invasion [227–229].

Until recently, cross-talk between breast tumour related adipocytes, known as cancer associated adipocytes (CAA) and breast cancer cells was largely understudied. In the breast, invading tumours are likely to encounter adipose tissue microenvironments, resulting in direct proximity of breast cancer cells to a milieu of adipocytes and other adipose tissue stromal cells. Thus, as the incidence rates increase and the negative biological consequences of obesity and adipose tissue adipocyte dysfunction become more apparent, attention has become focused on the active role of adipocytes in facilitating breast tumour progression [143,230–232]. It has been suggested that obesity can differentially modulate the microenvironment to favour tumour progression [91,233], and the effects of breast adipocyte dysfunction, such as pro-inflammatory and hormonal signalling, have been associated with breast cancer pathogenesis [150,162]. Therefore, it is likely that reciprocal interactions between CAA and breast cancer cells are influencing obesity-associated poorer breast cancer outcomes.

1.3.1.1 Cancer associated adipocytes (CAA) and breast cancer progression

Recent reviews have emphasised the important actions of proximal adipocytes within and surrounding the breast tumour stroma during disease progression [143,230,232,234]. Breast tissue is particularly rich in WAT adipocytes [91], and these adipocytes can function as autocrine, paracrine and endocrine cells, exerting biological effects through the secretion of cytokines, growth factors, hormones and other adipokines [235]. CAA at the invasive edge of human breast tumours exhibit a modified phenotype, in which they become delipidated with enlarged interstitial spaces, display a decrease in late adipocyte differentiation markers and overexpress inflammatory cytokines including IL-6 and IL-1β [150] (Figure 1.10). This modified CAA phenotype is similarly exhibited by mature adipocytes co-cultured with breast cancer cells *in vitro* [150].

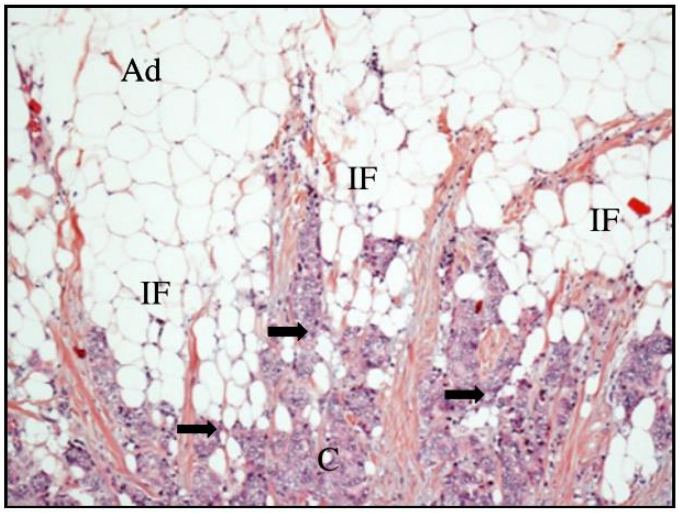

Figure 1.10. Cancer associated adipocytes (CAA) at the invasive margin of a breast tumour.
CAA (black arrows) at the invasive front (IF) of human breast tumours display a modified phenotype, in which they become delipidated with enlarged interstitial spaces, display a decrease in late adipocyte differentiation markers and overexpress inflammatory cytokines including IL-6 and IL-1β. Ad: Adipose; C: tumour centre. From Wang *et al* (2012). Reprinted with permission from Elsevier.

In addition to breast cancer cells promoting the CAA phenotype, it has been shown that direct stimulation of breast cancer cells with factors known to be secreted by mature adipocytes, such as leptin and IL-6, is capable of supporting and promoting breast tumorigenicity in both oestrogen responsive and unresponsive breast cancer cells [161,236]. However, cell-cell interactions *in vivo* are complex, and adipocytes are unlikely to alter breast cancer cell behaviour through a single secreted molecule. *In vitro* studies using conditioned media from 3T3-L1 derived murine adipocytes showed upregulation of anti-apoptotic transcriptional programs in MCF-7 breast cancer cells [237]. Similarly, conditioned media from breast adipocytes induced migration in non-cancerous normal breast epithelial cells [238], and increased migration, proliferation, viability and invasion in a variety of oestrogen receptor (ER) positive and ER negative breast cancer cell lines [239–245].

In vitro studies, using transwell (non-contact) co-culture of CAA with breast cancer cells, have established that CAA promote breast cancer cell proliferation, viability, migration and invasion [150,240,245–250]. In addition, breast cancer cells co-cultured with CAA undergo a partial epithelial to mesenchymal transition (EMT) [150], and become more resistant to radiotherapy [251], chemotherapy [252,253], and other breast cancer therapies [254,255]. During co-

culture, treatment with aspirin, an anti-inflammatory drug, blocked cross-talk between breast cancer cells and adipocytes by inhibiting MCP-1 adipocyte secretion, reducing breast cancer cell proliferation and migration [256]. These *in vitro* findings are further supported by *in vivo* xenograft studies, where human breast cancer cells co-cultured with CAA and subsequently implanted in mice or zebrafish show increased tumour growth and metastasis [248,250,257,258].

Although the precise biological processes responsible for CAA driven breast cancer progression remain unclear, investigations assessing the bidirectional communication between these two cells has recently highlighted the role of altered breast cancer cell and stromal adipocyte metabolism, enhancing breast tumour growth, survival and invasion [259]. Under certain nutrient or growth hormone signals, adipocytes undergo lipolysis, increasing secretion of free fatty acids (FFA) and glycerol [260]. Co-culturing ovarian carcinoma cells with CAA showed enhanced rates of lipolysis in adipocytes, and elevated rates of β-oxidation and cytosolic lipid accumulation in ovarian cancer cells [261]. Although, this study by Nieman *et al.*, mainly focused on ovarian cancer cells, breast cancer cells also showed increased levels of cytosolic lipids following co-culture with CAA [261]. Recent evidence suggests that cross talk with CAA induces breast cancer cell invasiveness, in part, through metabolic remodelling of the breast cancer cell, promoting a shift towards increased mitochondrial fatty acid oxidation [249,262]. Taken together these studies suggest that reciprocal cross-talk between breast cancer cells and CAA induces lipolysis in CAA, which provides lipids as a fuel source for breast cancer cell proliferation and invasion (Figure 1.11).

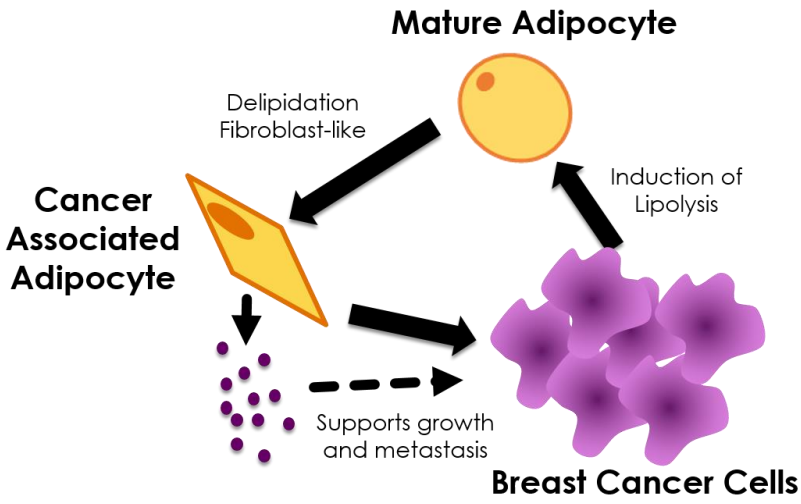

Figure 1.11. Interactions between CAA and breast cancer cells.
Reciprocal cross-talk between breast cancer cells and CAA induces lipolysis in CAA which provides lipids as a fuel source for breast cancer cell proliferation and invasion. CAA release an assortment of other factors such as cytokines, growth factors, hormones and other adipokines, which can influence breast cancer cell behaviour.

The majority of CAA and breast cancer cell co-culture studies have focused on assessing the altered production of specific adipocyte derived factors, such as CCL5, IL-6, IGF-1 and IGFBP-2, that promote breast cancer cell pro-tumour behaviour *via* paracrine actions [150,240,246–248]. In addition to altered expression of adipocyte secreted factors, some of these studies have observed modified expression of targeted genes and proteins in breast cancer cells following co-culture with CAA, including *IL-6*, *IL-8*, *CCL5*, *MCT2*, CPT1A and MMP-2. A number of genes and pathways have been identified by cDNA microarray analysis to be differentially expressed in breast cancer cells after co-culture with CAA [245,250,263] or CAA-conditioned media [237,242].

Despite these studies investigating gene expression changes in breast cancer cells interacting with CAA, the expression of translated proteins is not necessarily predicted by this mRNA expression data, and to date, the global regulation of cell protein abundance in breast cancer cells following co-culture with CAA has not been assessed. Thus, further analysis investigating the local effects of CAA on the proteome expression of human breast cancer cells will identify novel proteins and cellular pathways that are potentially important for breast

cancer progression, and provide an informative platform for future research to develop novel treatment strategies that target CAA-breast cancer cell interactions.

1.4 Breast cancer chemotherapy metabolism

The response of breast cancer patients to chemotherapy treatments is variable and currently largely unpredictable, and it has been suggested that differences in chemotherapy metabolism may play a role in regulating response to chemotherapeutics, both between patients and within an individual over time [264–266]. The majority of chemotherapy drugs used to treat cancer patients are metabolised by cytochrome P (CYP) 450 enzymes in liver cells (hepatocytes) [267]. CYP enzymes are a family of mixed-function oxidases often referred to as drug metabolising enzymes (DME), which modify functional groups and contribute to a significant proportion of all drug metabolism in the human body [268]. CYP enzymes are predominantly localised to the endoplasmic reticulum of hepatocytes, although, they are also found at lower numbers in extrahepatic tissues such as kidney, lung and gut [269]. As a result, chemotherapy drug metabolism in cancer patients, via CYP enzymes, occurs mostly in the liver, although can occur to a lesser extent in these extra-hepatic tissues, including tumours [265]. An important quality of CYP enzymes is that they are substrate selective, for example, CYP1A2, CYP2C9, CYP2C19, CYP2D6 and CYP3A4/5 make major contributions to the metabolism of breast cancer therapeutics, including tamoxifen, cyclophosphamide, docetaxel, doxorubicin and paclitaxel [265,266]. Breast cancer chemotherapies and hormone therapies (in common with drugs used to treat other cancers), have specific properties such as sharp dose-toxicity curves and narrow therapeutic indexes, such that even minor alterations in the expression or activity of CYP DME(s) may affect anti-cancer efficacy, or toxicity to the host [264].

CYP bio-activated prodrugs used to treat breast cancer patients, such as tamoxifen [270] or cyclophosphamide [271], would likely exhibit reduced efficacy under conditions where CYP activity is down-regulated, due to an unexpected decrease in exposure of the tumour to the active metabolite [265,266]. Alternatively, pharmacologically active breast cancer drugs that become deactivated after CYP metabolism, such as doxorubicin [272] or paclitaxel [273], may induce increased toxicity when CYP activity is reduced, due to an unexpected increase in the patient's exposure to the active chemotherapeutic compound [265,266]. In response to chemotherapy related toxicities, treatments are usually dose-reduced or even ceased, and what

we have learnt from the dose-capping of obese cancer patients is that chemotherapy dose-intensities are a critical determinant of tumour response rates and patient outcomes, both of which seem to be negatively affected by reducing dose intensity (see Section 1.2.1.2.2). Therefore, regardless of whether a breast cancer drug is delivered as a pharmacologically active compound or not, reduced CYP activity may participate in the manifestation of chemotherapy resistance (poorer response to chemotherapy and worse patient outcomes following chemotherapy treatment) by slowing down hepatic cancer chemotherapy metabolism.

1.4.1 CYP genotypes

Multiple factors may influence the expression, and thus, activity of hepatic CYP enzymes, including age, sex, environmental exposures, epigenetic events, co-morbid diseases and use of concurrent medications, but most widely studied are genetic polymorphisms within the CYP genes [274]. Many genetic polymorphisms have been identified across different CYP enzymes, providing a source of inter-individual pharmacokinetic variability [275]. The observation that clinical phenotypes (or patient responses) are associated with the presence or absence of particular genetic polymorphisms has led to a number of large scale association studies classifying CYP genotypes into one of three distinct functional subpopulations, including the extensive metabolisers (EMs), poor metabolisers (PMs) or intermediate metabolizers (IMs) [274,276]. A fourth unique genotypic subgroup of ultra-rapid drug metabolisers (UM) has also been classified for CYP2C19 and CYP2D6 [276–278]. Breast cancer patients with a particular variant in the CYP3A4 metabolising gene showed higher blood concentrations of non-metabolised cyclophosphamide, and this was associated with a median survival rate of 1.3 years in comparison to 2.7 years for those patients without the CYP3A4 variant [279]. These studies suggest that inter-patient differences in CYP genotypes could be used to dictate individualised dosing schedules specific to a cancer patient's metabolic genotype. However, upon review, results from large genotype-association studies classifying CYP alleles into distinct genotypic groups based on patient responses, were often found to be inconsistent, and at times conflicting [280,281]. In the pharmacokinetics landscape, this discordance between CYP genotypes and phenotypes is often referred to as 'phenoconversion', and is of particular concern in the current pursuit for personalised medicine [280,281].

1.4.2 Phenotyping CYP enzymes *in vivo*

Clinical outcomes following drug administration may be better predicted by combining CYP genotyping with metabolic phenotyping. Therefore, to complement the wealth of genotype data that is available for human CYP enzymes, metabolic phenotyping approaches have been developed to measure the activity of CYP enzymes *in vivo.* Whether in whole animal models or human subjects, CYP activity can be studied through use of probe drugs. Probe drugs are medications determined to be predominantly metabolised by a single CYP enzyme, thus, by administering the probe drug and then sampling and measuring the concentration of that probe drug and its metabolites, investigators are able to gain insight into the activity of the studied CYP enzyme *in vivo* [282]. An example of this is use of omeprazole, a proton pump inhibitor, to study CYP2C19 activity. By administering omeprazole and subsequently sampling the systemic circulation (plasma) to measure the parent compound (omeprazole) and metabolite (5-hydroxyomeprazole), it is possible to phenotype the activity of CYP2C19 by analysing the parent to metabolite ratio [283]. This probe drug methodology can be used to study specific CYP enzymes in relative isolation, or through combinations of multiple probe drugs (frequently called "cocktails") to phenotype multiple CYP enzymes concurrently [284,285].

The cocktail approach to CYP phenotyping was first proposed by in the late 1980s by Schellens *et al*. [286], and later became revitalised by Frye *et al*. in 1997 [287]. Now used in both academia and the pharmaceutical industry, phenotyping cocktails are designed to limit the potential for interactions between the components, exhibit adequate specificity of agents to allow accurate CYP phenotyping, and minimize observable clinical effects [288]. Specifically, with regards to the latter point, many probe drugs have either been selected because of limited potential for harm at standard dosing (even in the setting of intentional increased exposure such as in CYP-inhibition studies), or reduction in dosing to sub-therapeutic ranges (micro-dosing). Examples of CYP phenotyping cocktails include the "Pittsburgh" cocktail [287], the "Basel" cocktail [289], and the "Inje" cocktail [290]; their respective constituent components and sampling schedules are presented in Table 1.1.

Table 1.1. Examples of phenotyping cocktails.

Cocktail	Components (Enzymes/Transporters Assessed)	Sampling Schedule
Pittsburgh	Caffeine (CYP1A2) Chlorzoxazone (CYP2E1) Phenytoin (CYP2C19) Debrisoquin (CYP2D6) Dapsone (CYP3A4)	Plasma sample at baseline, 4 and 8 hours Urine sample 0-8 hours (inclusive)
Basel	Caffeine (CYP1A2) Efavirenz (CYP2B6) Omeprazole (CYP2C19) Metoprolol (CYP2D6) Losartan (CYP2C9) Midazolam (CYP3A4)	Plasma samples at 0.25, 0.5, 0.75, 1, 2,3, 4, 6, 8, 12, 24, 48, and 72 hours
Inje	Caffeine (CYP1A2) Omeprazole (CYP2C19) Dextromethorphan (CYP2D6) Losartan (CYP2C9) Midazolam (CYP3A4)	Plasma sample at 4 hours Urine sample at 8 hours

1.4.3 CYP phenoconversion

Although an individual may be classed as an EM or IM, based on their CYP genotype, this genotype does not always reflect or accurately predict the observed drug metabolising phenotype (or patient response) [291,292]. This phenomenon has been recently been termed 'phenoconversion', describing the conversion of a drug metabolising enzyme from a genotypic IM or EM, to a phenotypic PM, and therefore, individuals with PM genotypes are largely immune to the possibility of phenoconversion [281]. Consequently, phenoconversion has the potential to alter drug pharmacokinetics in ways that are unexpected when accounting for CYP genotype alone [280,281].

Although the exact biological mechanisms responsible for phenoconversion are yet to be elucidated, two main hypotheses have emerged to explain the CYP genotype-phenotype discordance. The proposed biological mechanisms include drug-drug interactions inhibiting the functional capacity of a particular CYP enzyme [293], and circulating inflammatory cytokines down-regulating hepatocyte gene expression of CYP enzymes [159,281].

Drug-drug interactions can affect the efficacy of the drugs, as some drugs can induce or inhibit particular CYP enzymes [293]. During co-administration of a drug that inhibits the activity of a CYP enzyme, the metabolising phenotype of that enzyme would mimic that of a

genotypic poor metaboliser [293]. When interactions between drugs are well understood they can also become advantageous, as they can be used in combinations to purposefully achieve interactions that induce or inhibit a metabolising enzyme [264,293]. An example of this is dosing with cyclosporine to enhance the oral bioavailability of paclitaxel [294]. Although research has extensively investigated an array of drug-drug interactions in cancer patients, drug interactions causing phenoconversion in oncology are an ongoing concern [264,295]. Data describing the extent of the clinical implications for drug interactions in cancer patients is limited, however, a systematic review was able to conclude that approximately 33% of cancer patients visited by ambulances are recorded to be at risk of effects from drug-drug interactions [296].

In comparison to drug interactions, much less is known about the effects of systemic inflammation on phenoconversion in cancer patients. Non-clinical and clinical findings have pointed towards an association between inflammatory cytokines and reduced CYP expression and activity [159], however, the biological mechanisms for the concentration-inhibition relationship between inflammatory cytokines and CYP activity is incompletely understood. Amongst proposed explanations, the predominant mechanism is the hepatocyte cell surface binding action of pro-inflammatory cytokines causing intracellular signalling events that suppress transcription of CYP coding genes [297]. *In vitro* evidence has been presented for IL-6 mediated downregulation of CYP3A4 activity in hepatocytes, as IL-6 induces translation of the CCAAT-enhancer-binding protein β (C/EBPβ) isoform LIP, an antagonist of C/EBP transcription factors that constitutively promote the expression of CYP3A4 [298,299] (Figure 1.12).

In addition to biological mechanisms, limitations associated with genotyping studies have also been highlighted for their role in phenoconversion [280,281]. In most cases, genotype-association studies have only interrogated the known and generally most prevalent alleles when assigning CYP genotypes to particular patient response. Furthermore, one allele often displays an array of different patient responses making it difficult to genotype that allele into a single discrete group, and therefore, there are a number of identified single nucleotide polymorphisms that have not been assigned to a functional genotypic group, which may account for a portion of the phenoconversion that is being reported.

Further analysis assessing both the presence of CYP phenoconversion and the factors causing it, would help in the development of newer treatment strategies that can negate inter-

patient variability and better regulate patient response. Although the biological mechanisms are still under investigation, associations between inflammatory cytokines and CYP phenoconversion have been documented in human hepatocytes and in patients with inflammatory diseases [159].

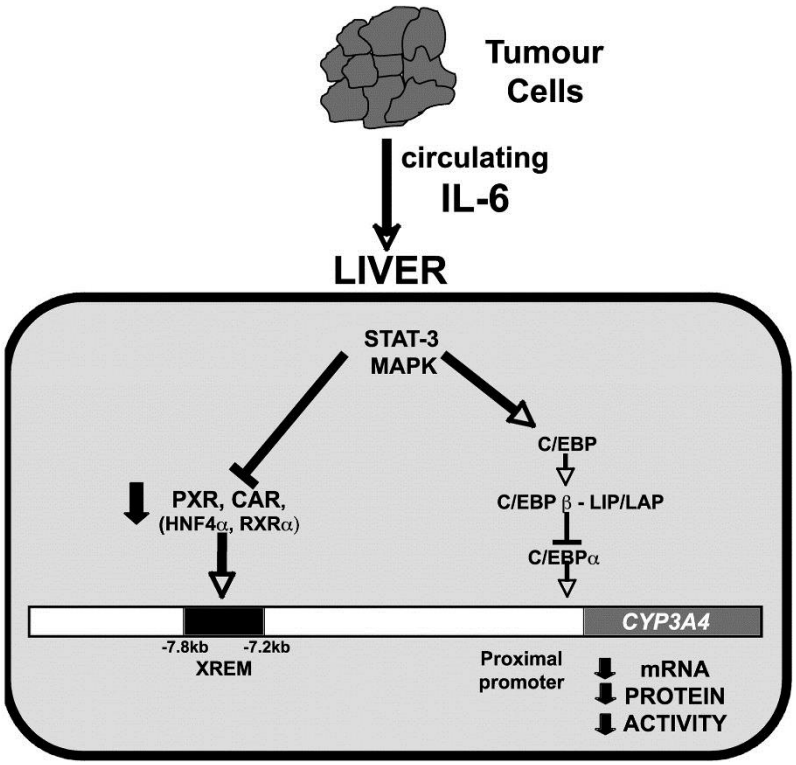

Figure 1.12. IL-6 mediated downregulation of CYP3A4 in the liver.
Schematic showing the proposed mechanism by which IL-6 induces translation of C/EBPβ-LIP in hepatocytes, an antagonist of C/EBP transcription factors that constitutively promote the expression of CYP3A4. From Aitken *et al* (2006) [297]. Reprinted with permission from ANNUAL REVIEWS.

1.4.4 Inflammation induced CYP phenoconversion

There have been a number of studies that have investigated the influence of inflammatory markers on the expression and activity of CYP enzymes *in vitro* and *in vivo*, with the intention of increasing our understanding of the influence of inflammation induced phenoconversion in the treatment of subjects presenting with inflammatory diseases.

1.4.4.1 *In vitro* evidence of human hepatocyte CYP phenoconversion

There are a few prominent *in vitro* studies that have investigated the effects of pro-inflammatory cytokines on the expression of different CYP genes using human hepatocytes.

Human hepatocytes dosed with physiologically relevant concentrations of IL-1, TNF-α and IL-6 were assessed for CYP2B6, CYP2C8, CYP2C9, CYP2C18, CYP2C19 and CYP3A4 mRNA expression. IL-1 mediated a reduction in CYP2C8 and CYP3A4 gene expression by 75% and 95%, respectively, TNF-α suppressed the transcription of CYP2C8 and CYP3A4, and IL-6 reduced mRNA levels of all CYPs studied expect CYP2C18 [300]. Analysis of CYP protein expression supported mRNA results, although translation was not identical [300]. In support of these findings, further investigations with human hepatocytes have identified an IL-6 and IL-1β mediated downregulation of CYP1A2 and CYP3A4 [301,302], with anti-IL-6 monoclonal antibody at least partially blocking the IL-6 mediated suppression [301]. This investigation was not able to identify a synergistic effect of combining IL-6 and IL-1β treatment on suppression of human hepatocyte CYP gene expression, however, they did conclude that IL-6 delivers a more potent effect on transcriptional repression [302]. Lastly, human hepatocytes co-cultured alongside Kupffer cells, treated with either IL-6 or IL-1β, upregulated expression of pro-inflammatory cytokines and acute phase proteins, and intensified the suppression of CYP3A4 transcription [303]. IL-1β lowered CYP3A4 mRNA levels more in hepatocytes that were co-culture with Kupffer cells compared to hepatocytes grown alone, however, the transcriptional suppression of CYP3A4 after IL-6 treatment remained consistent regardless of co-culture [303].

Taken together, these studies show that suppression of CYP genes by pro-inflammatory cytokines in hepatocytes *in vitro* is largely gene specific, with different cytokines influencing CYP gene expression in a unique manner. Moreover, IL-6 is likely a predominant inflammatory cytokine involved in regulating CYP gene expression in humans. It could be argued that these *in vitro* investigations of the effects of a small number of individual inflammatory cytokines on CYP expression and activity is not physiologically relevant, and rather the combined influence of a panel of inflammatory cytokines would better represent the effects of inflammatory diseased states on liver CYP metabolism. This has yet to be investigated *in vitro,* however, clinical studies have investigated *in vivo* CYP activity in patients experiencing conditions of systemic inflammation.

1.4.4.2 Clinical evidence of inflammation induced CYP phenoconversion

In the mid-1990's, a cohort of 12 healthy male volunteers had significantly reduced CYP1A2 and CYP2C19 mediated clearance of probe drugs, theophylline and hexobarbital, after receiving low doses of intravenous lipopolysaccharides (LPS) over two consecutive

mornings [304]; where LPS stimulates secretion of pro-inflammatory cytokines by various cell types. The reduction in CYP1A2 and CYP2C19 mediated drug clearance was paralleled with increases in the circulating inflammatory cytokines, IL-6 and TNF-α, and serum acute phase response proteins, CRP and AGP; however, this correlation was not significant [304]. Shortly after, in 1997, the same effect was established in a population of healthy female participants [305]. Subsequent clinical studies have continued to support these earlier findings, however, instead of LPS induced inflammation, more recent investigations have assessed effects of inflammatory states associated with clinical diseases. Direct evidence of CYP phenoconversion occurring in inflammatory-related diseases including HIV and hepatitis C infection, liver disease and cancer have been published for CYP2C19 and CYP2D6 [283,306–310]. However, no comparable clinical investigations of phenoconversion have been carried out for other important CYP enzymes such as CYP2C9 or CYP3A4, or in different prevalent inflammatory diseases including rheumatoid arthritis, diabetes, chronic kidney diseases, other cancer types and obesity.

1.4.5 Cancer and inflammation induced CYP phenoconversion

Increased levels of systemic inflammation have become a well-recognised hallmark of cancer progression [311]. The initiation and development of elevated peripheral inflammation is consistently associated with poorer patient prognosis and outcome in both early and late stage cancer patients, and is associated with poorer patient responses to chemotherapy treatment [312,313]. Cancer-associated systemic inflammation has been suggested to interact with hepatocytes in the liver, downregulating expression and activity of CYP enzymes important for chemotherapy metabolism and clearance (Figure 1.13).

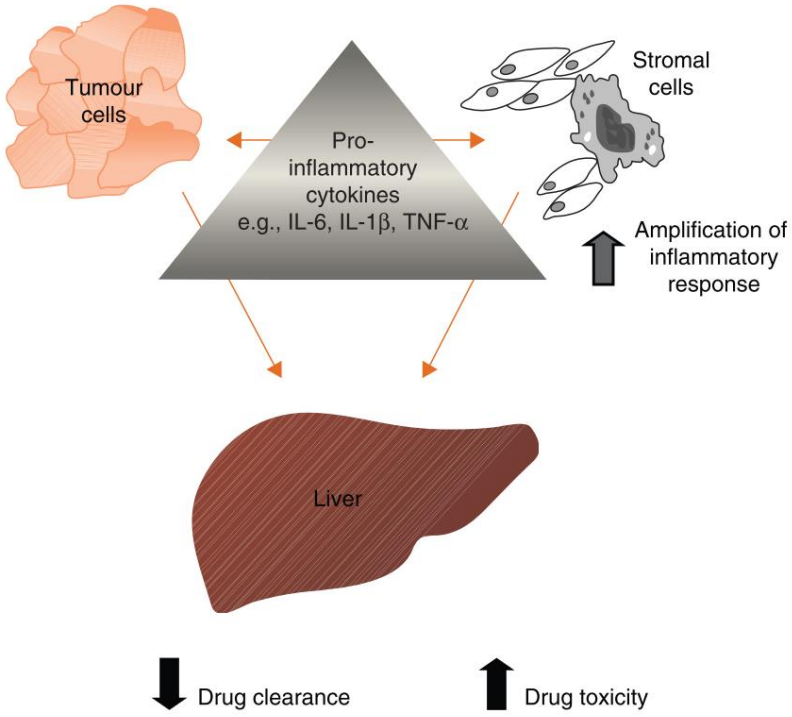

Figure 1.13. Systemic inflammation may influence liver drug metabolism during cancer. This schematic shows cancer-associated systemic inflammation interacting with the liver, downregulating expression and activity of CYP enzymes important for chemotherapy metabolism and clearance, and potentially causing reductions in chemotherapy efficacy and increases in chemotherapy related toxicities. From Kacevska *et al* (2008) [314]. Reprinted with permission from Taylor & Francis.

Phenoconversion has been suggested to occur in breast cancer patients. A study of 80 breast cancer patients observed large inter-patient variability in circulating endoxifen (tamoxifen metabolite) concentrations that were not explained by four *CYP2D6* null alleles, nor by the concomitant administration of medications known to inhibit or induce CYP2D6 activity [315]. Similarly, a more recent study has reported a CYP2D6 genotype and phenotype discordance in a number of breast cancer patients, where low or absent formation of the dextromethorphan metabolite (inferring poor metabolism by CYP2D6), was not explained by CYP2D6 null activity genotypes [316]. In conjunction with the fact that circulating inflammatory cytokine levels were not assessed in either of these investigations, results from these studies are only suggestive of phenoconversion, as other known, but not yet, genotyped polymorphisms of CYP2D6 were not investigated.

In patients with advanced cancers, the acute phase inflammatory response has been associated with reduced CYP activity, but not phenoconversion directly. Specifically,

decreased CYP3A4 dependent metabolism of erythromycin, measured by breath testing, was correlated with increased levels of circulating CRP, and CRP levels were significantly positively correlated with plasma IL-6 levels [317]. However, this study did not address the potential effect of drug-drug interactions which could be influencing CYP3A4 metabolism. In contrast to CYP3A4, mismatch between CYP2C19 genotype and phenotype, and thus phenoconversion, has been documented in a number of advanced cancer patients [283,309,310]. Although the levels of systemic inflammatory cytokines were measured in two out of three of these investigations, concentrations of IL-6, TNF-a, IL-1, TGF-β and CRP were not significantly associated with CYP2C19 phenoconversion [283,310].

Variation in the results across *in vivo* studies assessing CYP activity in inflammatory conditions is postulated to be influenced by the relatively small study numbers restricting statistical power, but also the consequence of different types and concentrations of inflammatory cytokines occurring across a variety of acute and chronic inflammatory responses and pathologies [318]. Differences in levels of circulating inflammatory cytokines between advanced and early stage breast cancer patients is likely to exhibit differential effects on CYP activity, but in addition to cancer-associated inflammation, obesity-associated inflammation may be influencing CYP mediated chemotherapy metabolism in these patients. Obesity is a co-occurring pathology that is strongly associated with poorer outcomes in a number of different cancers including breast cancer [69,126], and thus, it could be speculated that obesity-related systemic inflammation is influencing CYP mediated chemotherapy metabolism, contributing to the poorer pathological response rates to chemotherapy seen in obese women with breast cancer.

1.4.5.1 Obesity, inflammation and CYP activity

Despite obesity being a well-established condition of chronic low-grade systemic inflammation, very little research has investigated the effects of obesity-associated inflammation on CYP activity *in vivo* in humans. In 1999, a review was published that assessed the differences in pharmacokinetics of a number of drugs between non-obese and obese subjects, in which CYP3A4 activity was found to be decreased, and CYP2E1 exhibited increased activity during obesity; yet, the association between obesity and other CYP enzymes remained inconclusive [319]. The majority of the research since this review has been performed in animal models of obesity, and an extensive review of these studies concludes that aside from CYP2C and CYP2E1, obesity is associated with reduced CYP activity [320].

Thus, obesity may play a role in regulating CYP activity (and phenoconversion) in obese breast cancer patients.

Further clinical trials assessing CYP activity and its association with systemic inflammation in breast cancer patients receiving chemotherapy will hopefully highlight key inflammatory markers influencing CYP activity in these patients, and thus, provide targets for future interventions. These studies would benefit from considering the influence of other co-occurring inflammatory conditions known to influence breast cancer patient response to chemotherapy, such as obesity.

1.5 Hypotheses and aims

Cancer associated adipocytes (CAA) within the breast tumour microenvironment and obese white adipose tissue depots throughout the body have both been associated with breast tumour progression [116,150]. Although previous research has attempted to assess the mechanisms by which local CAA and systemic obesity influences breast cancer progression, the precise local and systemic mechanistic properties that are supporting breast cancer development during obesity, are still under investigation.

1.5.1 Local effects of CAA on breast cancer cells

In the same way that past explorations have used transwell co-culture and microarray analysis to identify CAA-induced alterations in breast cancer cell gene expression [250,263], it could be postulated that research investigating regulation of global breast cancer cell protein abundance caused by proximal CAA may reveal novel mechanistic links relevant to breast cancer cell phenotypes. Thus, the first hypothesis for this thesis was that *in vitro* co-culture with CAA differentially regulates protein abundance in breast cancer cells, and consequent alterations in key molecules and pathways are responsible for promoting a progressive breast cancer cell phenotype. To investigate this, the aims were to:

1) Perform proteomic profiling on ER positive (MCF-7) and hormone receptor negative (MDA-MB-231) human breast cancer cells cultured alone or co-cultured with CAA isolated from human breast adipose tissue.
2) Identify differentially regulated molecules and enriched pathways potentially playing an important role in CAA-induced breast cancer cell growth, survival and metastasis that can inform further investigations.

1.5.2 Systemic effects of obesity on breast cancer chemotherapy metabolism

Elevated BMI is associated with the presence of low-grade chronic systemic inflammation, and lower pathological complete response rates to neoadjuvant chemotherapy in breast cancer patients [63,122]. Breast cancer chemotherapy drugs are mostly metabolised by CYP enzymes whose expression in the liver are susceptible to regulation by inflammatory cytokines [159,317], and in breast cancer survivors levels of inflammatory cytokines can be decreased by increased levels of physical activity [182,183]. Based on these associations, it could be speculated that unexpected alterations in the metabolism of chemotherapies could be playing a role in the poorer pathological response to treatment in obese breast cancer patients. Furthermore, the systemic effects of inflammation on the metabolism of clinically important breast cancer chemotherapy agents that operate under very narrow therapeutic windows, is largely overlooked in breast cancer patients. Therefore, the hypotheses for this part of the thesis were, firstly, that circulating inflammatory cytokines in obese breast cancer patients alter CYP enzyme activity in women receiving chemotherapy for breast cancer, and secondly, that concentrations of circulating inflammatory markers in these same women are influenced by levels of physical activity. To investigate these hypotheses an exploratory clinical study was carried out recruiting non-obese (BMI<30) and obese (BMI≥30) women being treated with chemotherapy for stage II or III breast cancer, with the aims to:

1) Assess whether differences in body morphometry and levels of physical activity are associated with concentrations of circulating inflammatory cytokines throughout chemotherapy.
2) Explore the relationship between *in vivo* activity of CYP enzymes important in the metabolism of breast cancer chemotherapy and the concentrations of circulating inflammatory cytokines, throughout chemotherapy.
3) Assess whether such studies are feasible in patients undergoing chemotherapy treatment for stage II and III breast cancer.

Chapter 2

Methods and Materials

2.1 Breast adipocyte collection, isolation and culture

Ethics and sample collection

Breast adipose tissue samples were collected by the Cancer Society Tissue Bank Christchurch (CSTBC), using standard operating procedures [321]. Ethical approval for the study was obtained from the University of Otago Human Ethics Committee (Health) (reference number 12/319). All patients gave informed written consent for the use of their samples for research purposes and access to their medical records. Māori consultation was completed with Elizabeth Cunningham, the Māori Research Advisor of the University of Otago Christchurch. This study is of particular interest and potential benefit to Māori.

2.1.1 Breast adipose tissue samples

All breast adipose tissue samples used in this study were donated by female patients undergoing surgery at Christchurch Hospital for therapeutic or prophylactic mastectomy between March 2016 and March 2017. Adipose tissue was sampled by a pathologist from macroscopically normal breast tissue with maximal margins to any tumour deposit. Patient characteristics and breast cancer pathology were assembled from pathology reports and medical records by the CSTBC.

2.1.2 Isolation of pre-adipocytes

Pre-adipocytes were isolated from breast adipose tissue within 1 hour of surgical resection. The pre-adipocyte isolation protocol was adapted from Lee *et al*. (2012) and is described in detail below [322]. All breast adipose cells used for this study were adherent and maintained in a 37 °C incubator with 95% oxygen and 5% CO_2 atmospheric conditions.

At collection, breast adipose tissue samples were de-identified and given an adipose tissue (AT) sample number (eg. AT 076) before being weighed. Surgical and pathological dyes were washed from the sample using serum free media (Table 2.1) and preheated to 37 °C. Fibrous and vascular areas were excised from the adipose tissue and discarded. The refined sample was minced and digested using 1 mg/mL collagenase type I enzyme in Hanks' Balanced Salt Solution (HBSS; Life Technologies, Carlsbad, CA, USA) by incubation for 2 hours at 37 °C with regular agitation. 2 mL of collagenase was used for every 1 gram of adipose tissue. Collagenase was stored at -80 °C and defrosted immediately before use in a 37 °C water bath. The digested adipose tissue was diluted with 10 mL growth media (Table 2.1). Samples were passed through a metal 250 µM mesh sieve to remove remaining fibrous tissue, transferred to a fresh 50 mL tube (BD Falcon^{TM}), and centrifuged at room temperature for 10 minutes at 2500 x g. Fibrous tissue collected during filtering was combined with the initial discarded vasculature and fibrous waste tissue, and weighed. The total weight (grams) of waste tissue removed was subtracted from the weight of the original breast adipose tissue (grams) specimen, in order to calculate the weight of adipose tissue from which pre-adipocytes were extracted. Following centrifugation, all fractions apart from the cell pellet were discarded, the pellet was resuspended in 10 mL of growth media, and the sample was filtered through a sterile 70 µM cell sieve (In Vitro Technologies, Melbourne, Australia). Samples were re-pelleted by centrifugation for 10 minutes at 25000 x g, and the supernatant was discarded. The pellet (containing the stromal vascular fraction, enriched for pre-adipocytes and red blood cells (RBC)) was resuspended in 1 mL of normal adipose growth medium per 0.6 grams adipose tissue. 1 mL of the cell suspension was plated into each well of a 12 well cellBIND® plate (In Vitro Technologies, Melbourne, Australia), and incubated at 37 °C. Approximately 24 hours after plating, medium was removed from each well of adherent pre-adipocytes and was replaced with 1 mL of sterile 1X Phosphate Buffered Saline (PBS). Non-adherent red blood cells were gently washed away from the adherent pre-adipocytes using the PBS. The PBS wash step was repeated at least 2 times until complete removal of RBC, and replaced with 1 mL per well of growth media.

2.1.3 Culturing of pre-adipocytes

The pre-adipocytes were cultured in normal adipose growth medium, replaced every 2-3 days, until they were observed under light microscopy to reach 100% confluency. Treatment for pre-adipocyte differentiation was performed two days after the pre-adipocytes reached confluency.

2.1.4 Differentiation of pre-adipocytes into mature adipocytes

Pre-adipocytes were supplemented with 1 mL per well of differentiation media (Table 2.1) for 5 days. Then differentiation media was replaced with 1 mL per well of fresh differentiation media minus IBMX supplementation, and incubated for a further 5 days. Differentiation media was replaced with maintenance media (Table 2.1), and maintenance media was replaced every 3-4 days until adipocyte maturation (approximately 14-21 days). Light microscopy was used to determine the differentiation of pre-adipocytes to mature adipocytes, as measured by the accumulation of lipid droplets filling the adipocytes (Figure 2.1). Differentiated adipocytes were considered ready for use in experiments when mature adipocytes covered ≥ 70% confluence. Differentiation and maintenance media were made fresh and sterile filtered through Millex-GV 0.22 µM PVDF syringe filter units (Sigma-Aldrich, St. Louis, MA, USA) immediately before use.

Table 2.1. Adipocyte culture media used in this study.

Name	Media	Supplements
Serum free media	DMEM/F12 medium [+] L-Glutamine [+] 2.438 g/L sodium bicarbonate (Life Technologies, Carlsbad, CA, USA)	1% A/A (Life Technologies, Carlsbad, CA, USA)
Growth media	DMEM/F12 medium [+] L-Glutamine [+] 2.438 g/L sodium bicarbonate	10% FBS (Life Technologies, Carlsbad, CA, USA), 1% A/A
Differentiation media	DMEM/F12 medium [+] L-Glutamine [+] 2.438 g/L sodium bicarbonate	1% A/A, 0.5 mM IBMX (Sapphire Biosciences, Redfern, NSW, Australia), 100 nM insulin (Life Technologies, Carlsbad, CA, USA), 100 nM dexamethasone (Sapphire Biosciences, Redfern, NSW, Australia), 2 nM triiodothyronine (Sigma-Aldrich, St. Louis, MA, USA), 10 µg/mL transferrin (Sigma-Aldrich, St. Louis, MA, USA), 1 µM rosiglitazone (Sapphire Biosciences, Redfern, NSW, Australia), 33 µM biotin (Sigma-Aldrich, St. Louis, MA, USA), and 17 µM pantothenic acid (Sigma-Aldrich, St. Louis, MA, USA)
Maintenance media	DMEM/F12 medium [+] L-Glutamine [+] 2.438 g/L sodium bicarbonate	10% FBS, 1% A/A, 10 nM insulin, and 10 nM dexamethasone

A/A: antibiotic-antimycotic (containing amphotericin B, streptomycin and penicillin); **FBS:** foetal bovine serum; **DMEM/F12:** Dulbecco's Modified Eagle's Medium Nutrient Mixture F-12; **IBMX:** 3-isobutyl-1-methylxanthine

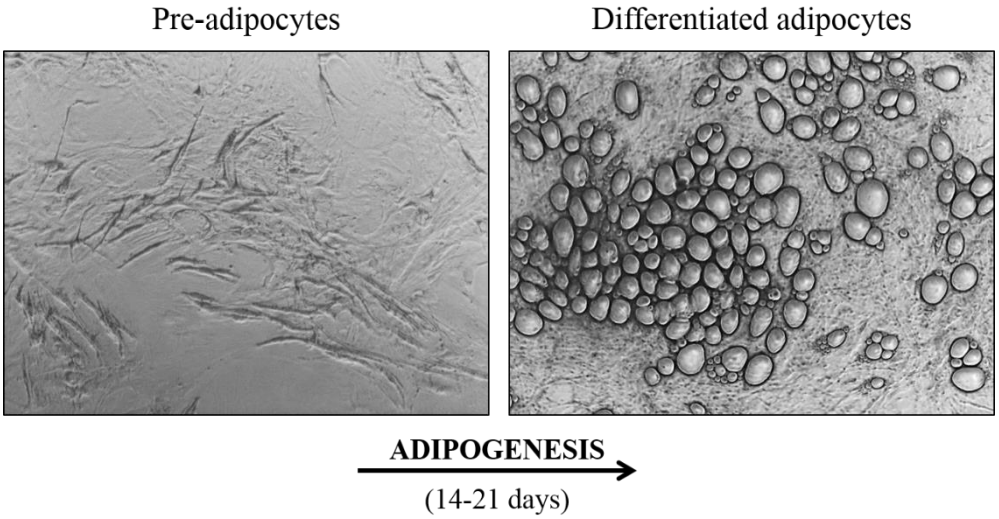

Figure 2.1. Adipocyte differentiation *in vitro*.
Representative image of adipocytes before (pre-adipocytes) and after (differentiated adipocytes) the differentiation procedure (adipogenesis). Images are 10X magnification.

2.2 Breast cancer cell culture

2.2.1 Cell lines

Human breast cancer cell lines HCC70, HCC83, HCC1954, MCF-7, MDA-MB-231, MDA-MB-468, and SKBR3 were purchased from American Tissue Culture Collection (ATCC; Manassas, VA, USA). BT20 and T47D human breast cancer cell lines were obtained as historical specimens. All cell lines were adherent and maintained in a 37°C incubator with 95% oxygen and 5% CO_2 atmospheric conditions. BT20, MCF-7, MDA-MB-231, and MDA-MB-468 cell lines were grown in high glucose Dulbecco's Modified Eagle Medium (GlutaMAX™ DMEM) with 10% foetal bovine serum (FBS) and 1% antibiotic-antimycotic (A/A; containing amphotericin B, streptomycin and penicillin) solution (all from Life Technologies, Carlsbad, CA, USA). HCC70, HCC83, HCC1954, and T47D cell lines were grown in high glucose Roswell Park Memorial Institute (GlutaMAX™ RPMI) 1640 Medium (Life Technologies, Carlsbad, CA, USA) with 10% FBS and 1% A/A solution. SKBR3 cells were grown in McCoy's 5A (modified) Medium (Life Technologies, Carlsbad, CA, USA) supplemented with 10% FBS and 1% A/A solution.

MCF10A wild type breast cell line was purchased from Horizon (Horizon^{TM} Inspired Cell Solutions, Cambridge, UK), and grown in DMEM/F12 medium [+] L-glutamine [+] 15

mM 4-(2-hydroxyethyl)-1-piperazineethanesulfonic acid (HEPES; Life Technologies, Carlsbad, CA, USA) supplemented with 5% horse serum (Life Technologies, Carlsbad, CA, USA), 10 µg/mL insulin (Life Technologies, Carlsbad, CA, USA), 20 ng/mL EGF, 100 ng/mL cholera toxin, and 500 ng/mL hydrocortisone (all from Sigma-Aldrich, St. Louis, MA, USA), and was used as a non-cancer control.

Human breast cancer cell lines were routinely tested for mycoplasma following the polymerase chain reaction (PCR) protocol previously described by Timenetsky *et al*. (2006) [323], using a positive control sample and the GPO-3 and MGSO primers for the generic detection of Mollicutes (type of bacteria lacking a cell wall). Cell lines were free of contamination (Supplementary Figure A.1).

2.2.1.1 Cell line storage and maintenance

All cell line experiments were performed within the first 30 passages. For passaging cells were detached from flasks using TrypLE dissociation reagent (TrypLE™ Express; Life Technologies, Carlsbad, CA, USA), diluted with fresh culturing media and re-seeded into new flasks. For long term cell storage, breast cancer cells were frozen to -80°C in media containing 20% FBS and 10% dimethyl sulfoxide (DMSO; Sigma-Aldrich, St. Louis, MA, USA), and MCF-10A cells were frozen to -80°C in complete culturing media also containing 7.5% DMSO, before being transferred to the liquid nitrogen phase. For cell recovery from liquid nitrogen, cells were rapidly thawed in a 37 °C water bath and immediately transferred to flasks containing culturing media. DMSO containing media was replaced with fresh media following cell adherence to the flask.

2.2.2 Cell counting

All cell concentrations were determined using the Countess™ Automated Cell Counter (Life Technologies, Carlsbad, CA, USA). 10 µL of cells suspended in media were combined at a 1:1 ratio with 0.4% trypan blue stain (Life Technologies, Carlsbad, CA, USA), mixed, and incubated at room temperature for 2 minutes. After staining, 10 µL of cells were pipetted into a disposable Countess™ cell counter chamber slide (Life Technologies, Carlsbad, CA, USA) and inserted into the Countess™ Automated Cell Counter instrument for cell number assessment. Countess™ parameters were set at cell size of 5-60 µM, and cell circularly of 95% roundness.

2.2.3 Basal expression of PGK1 in a panel of breast cancer cell lines

To assess the basal expression of PGK1 in a panel of human breast cancer cell lines, cells were seeded into 6 well plates at 2 x 10^5 cells/well in triplicate wells, and incubated for 48 hours until 70-90% confluency. Protein was extracted from adherent cells following the protocol outlined in Section 2.2.4.2, and the protein supernatant was stored at -80°C until use in Western Blot (Section 2.8).

Breast cancer cell lines included human epidermal growth factor receptor 2 enriched (HER2+; SKBR3 and HCC1954), oestrogen receptor positive (ER+; MCF-7 and T47D), and triple negative/ basal-like (TNBC; MDA-MB-231, MDA-MB-468, HCC70, BT20 and HC38) cell lines. PGK1 expression levels in the MCF-10A breast cell line (a non-tumorigenic mammary epithelial cell line) served as a non-cancer control, and was used to standardise expression across blots.

2.2.4 Cell lysis for Western blot analysis

2.2.4.1 Protein extraction from cell pellets

Protein was extracted from breast cancer cell pellets by lysis on ice using RIPA buffer (50 mM Tris (pH 8.0), 150 mM NaCl, 1 % NP-40, 0.5% sodium deoxycholate, 0.1% SDS; all from Sigma-Aldrich, St Louis, MO, USA) with 1X cOmplete Protease Inhibitor Cocktail (Roche, Basel, Switzerland) added fresh on the day of lysis. Cell lysates were then transferred to pre-cooled microtubes, incubated on ice for 5 minutes, and centrifuged at 12,000 x g for 10 minutes at 4 °C to pellet any insoluble cell debris. Supernatants were collected in pre-cooled microtubes and stored at -80 °C until use.

2.2.4.2 Protein extraction from adherent cells

Protein was extracted from breast cancer cells cultured in 6 well plates by lysing the cells on the plate. Cells were washed with cold PBS, lysed by adding RIPA buffer with 1X cOmplete Protease Inhibitor Cocktail added fresh on the day of lysis, and collected using a cell scraper before transfer into pre-cooled microtubes. Cell lysates were incubated on ice for 5 minutes, and centrifuged at 12,000 x g for 10 minutes at 4 °C to pellet any insoluble cell debris. Supernatants were collected in pre-cooled microtubes and stored at -80 °C until use.

2.2.5 Protein quantification

2.2.5.1 BCA assay

Total protein concentration of cell lysates prepared for Western blot analysis (Section 2.2.4) were determined using the Pierce™ BCA (bicinchoninic acid) Protein Assay Kit

(Thermo Fisher Scientific, Rockford, IL, USA). Briefly, a bovine serum albumin (BSA: Life Technologies, Carlsbad, CA, USA) standard curve (0-2000 µg/mL) was constructed following the microplate procedure, and 200 µL of BCA assay reagent (50:1 ratio of BCA Reagent A to BCA Reagent B) was added to 25 µL of standard or cell lysate, and incubated for 30 minutes at 37 °C protected from light. Absorbance was measured at 565 nm on the Multiskan GO plate reader (Thermo Fisher Scientific, Rockford, IL, USA), and protein concentrations were calculated by extrapolation from the standard curve.

2.2.5.2 Bradford assay

Total protein concentrations were measured in breast cancer cell lysates prepared by filter aided sample preparation (FASP) prior to digestion into peptides (Section 2.4.1). Total protein concentration of cell lysates were determined using a Bradford Protein Assay (BioRad, Hercules, CA, USA) following the manufacturer's instructions. A bovine serum albumin (BSA) standard curve (0-1000 µg/mL) was constructed. 1 µL of protein sample or standard, diluted in 799 µL of Milli-Q water, was combined with 200 µL of Protein Assay Dye Reagent and incubated at room temperature for 5 minutes. Solutions were then transferred to cuvettes and absorbance was read at 595 nm using the Ultrospec 2000 Spectrophotometer (Amersham, Little Chalfont, UK). Protein concentrations were calculated by extrapolation from the standard curve. All protein standards and samples were measured in duplicate.

2.3 Transwell co-culture of mature adipocytes with human breast cancer cell lines

2.3.1 Setting up of transwell co-culture

Transwell co-culture of mature breast adipocytes and human breast cancer cells was performed using 12 mm transwell® permeable support inserts with 0.4 µm polyester membranes (In Vitro Technologies, Melbourne, Australia) pre-soaked in DMEM/F12 medium with 10% FBS, at 37 °C for a minimum of 1 hour. Adipocytes were gently washed with PBS, and maintenance media was replaced with 1 mL per well of normal growth media on the mature adipocytes. Breast cancer cells were detached using TrypLE dissociation reagent and counted using The Countess™ Automated Cell Counter (Life Technologies, Carlsbad, CA, USA) (Section 2.2.2). Transwell inserts were gently transferred into the mature

adipocyte wells. 500 µL per insert of breast cancer cells were added at a final concentration of $1.2x10^5$ cells per insert for MCF-7 and $1x10^5$ cells per insert for MDA-MB-231, and incubated at 37 °C for 72 hours. Control breast cancer cells (MCF-7 and MDA-MB-231) were cultured without mature adipocytes in adipocyte growth media (Table 2.1).

2.3.2 Harvesting breast cancer cells from transwell co-culture

Following transwell co-culture, media was aspirated from the inserts containing breast cancer cells, inserts were carefully removed and placed in fresh 12 well plates with 1 mL per well of TrypLE dissociation reagent. A further 500 µL per insert of dissociation reagent was added and inserts were incubated at 37 °C for 5 minutes. Dissociated cells were collected and pelleted by centrifugation at 225 x g for 4 minutes. Breast cancer cells co-cultured with mature adipocytes from the same breast adipose donor were combined together prior to centrifugation. The pellets were washed by adding 1X ice cold PBS and centrifugation at 507 x g for 4 minutes. After removing the supernatant the breast cancer cell pellets (co-culture and control) were either frozen at -80 °C until protein preparation for discovery mass spectrometry by filter aided sample preparation (FASP; Section 2.4.1), or immediately treated with RIPA buffer to lyse cells and extract protein for Western blotting (Section 2.8).

2.4 Discovery mass spectrometry of breast cancer cells

Discovery mass spectrometry analysis was completed at the Centre for Protein Research (Department of Biochemistry, University of Otago, NZ) under guidance from Dr Torsten Kleffmann.

2.4.1 Filter Aided Sample Preparation (FASP) and enzymatic digestion

Filter aided sample preparation (FASP) with in solution enzymatic digestion was used to prepare breast cancer cells for mass spectrometry. Cell pellets were lysed in a buffer including, 20 mM HEPES pH 7.5, 1 mM ethylenediaminetetraacetic acid (EDTA), 1 mM Triethylene glycol diamine tetraacetic acid (EGTA), 0.2 % sodium dodecyl sulfate (SDS), 5 mM tris(2-carboxyethyl)phosphine (TCEP) and protease inhibitor (complete mini EDTA free; Roche, Basel, Switzerland), and sonicated for short intervals totalling a period of 2 minutes. The insoluble fraction was pelleted by centrifugation at 16,000 x g for 60 minutes. For detergent depletion, the supernatant was loaded onto Amicon Ultra-0.5 mL Centrifugal Filter Units with a membrane molecular weight cut off of 3 kDa (Merck Millipore, Billerica,

MA, USA) at a 1:1 ratio with 0.2 M triethylammonium bicarbonate (TEAB) containing 8 M urea, and centrifuged for 15 minutes at 14,000 x g. Two repetitions of 400 µL 0.2 M TEAB were loaded and centrifuged at 14,000 x g for 15 minutes to exchange urea containing buffer. Proteins were then reduced using 10 mM triethylammonium bicarbonate (TCEP) for 30 minutes at room temperature, followed by alkylation of reduced cysteines by incubation with 30 mM iodacetamide (IAA) (Sigma Aldrich, St. Louis, MA, USA) for10 minutes at room temperature in the dark. Samples were buffer exchanged into 0.5 M TEAB by two consecutive centrifugation steps, and recovered in new collection tubes by inverting the filter and briefly spinning the sample. Total protein concentrations were normalised using a Bradford assay (Section 2.2.5.2) and proteins were digested overnight at 37 °C using 1 µg of mass spectrometry grade trypsin (Promega Corporation, Madison, WI, USA) that was reconstituted in Milli-Q water immediately prior to use. All chemicals used in this section are from Sigma-Aldrich (St. Louis, MA, USA) unless otherwise stated.

2.4.2 ITRAQ labelling and solid phase extraction (SPE)

Peptides were labelled with isobaric tags for relative and absolute quantification (iTRAQ) labels from the iTRAQ® Reagents 8-plex Kit (Sciex, Framingham, MA USA), following manufacturer's instructions. Peptides from MCF-7 and MDA-MB-231 breast cancer cells were analysed in separate 4-plex experiments. iTRAQ reagents were activated with 50 µL of room temperature isopropanol and combined with the peptide samples according to the labelling schedule in Table 2.2, and incubated at room temperature for 2 hours. For each cell line, a test sample of pooled aliquots containing 2 µL of each labelled peptide digest, was dried using the Savant SpeedVac SC100 with a -100°C refrigerated vaper trap (Thermo Fisher Scientific, Waltham, MA, USA), reconstituted in 10 µL of 5% acetonitrile and 0.2% formic acid, and analysed by LC-coupled LTQ-Orbitrap tandem MS (as outlined in Section 2.4.4) to verify the individual reagents labelling efficiency. Samples were normalised according to the total iTRAQ labelling efficiency by dilution with Milli-Q water to quench the labelling reaction. Following normalisation, samples were pooled together, concentrated to an approximate 40 µL final volume using the Savant SpeedVac SC100, and Milli-Q water to a total of 1 mL was added to ensure a final isopropanol concentration ≤ 10%. The pooled sample was desalted by Sep-Pak C-18 (Waters, Milford, MA, USA) solid phase extraction (SPE) with 2% and 80% acetonitrile eluting the salts and peptides, respectively. Cartridges were washed three times with 1 mL of 80% acetonitrile, followed by equilibration three times with 1 mL of 2% acetonitrile before the sample was loaded. Following peptide

binding, cartridges were washed a further two times with 1 mL of 2% acetonitrile. The sample was eluted in 1 mL 80% acetonitrile, split into two 500 µL aliquots, and concentrated to an approximate 100 µL final volume using the Savant SpeedVac SC100.

Table 2.2. Scheme of the isobaric tags for relative and absolute quantification (iTRAQ) labelling.

Cell Line	Sample	iTRAQ Label
MCF-7	Control 1	117
MCF-7	Control 2	118
MCF-7	Co-culture 1	119
MCF-7	Co-culture 2	121
MDA-MB-231	Control 1	114
MDA-MB-231	Control 2	115
MDA-MB-231	Co-culture 1	116
MDA-MB-231	Co-culture 2	117

2.4.3 OFFGEL Isoelectrical Focusing (OFFGEL IEF)

Prior to mass spectrometry analysis, iTRAQ labelled peptides were pre-fractionated by OFFGEL isoelectric focusing (OFFGEL IEF) to reduce sample complexity and improve peptide identification. OFFGEL IEF was performed over the pH gradient (pH 3-10) into 12 individual fractions, using the OFFGEL fractionator (Agilent Technologies, Santa Clara, CA, USA), following the manufacturer's instructions. 1.44 mL of prepared 1.25X Peptide OFFGEL Stock Solution, including thiourea, dithiothreitol (DTT), glycerol and OFFGEL buffer, was combined with the peptide samples (approximately 100 µL) and volume adjusted to 1.8 mL with Milli-Q water. The impedance plethysmography (IPG) strip was set flat in the groove of the tray and covered in Peptide IPG Strip Rehydration Solution to swell the gel. Electrode pads submerged in Peptide IPG Strip Rehydration Solution were placed at either end of the IPG strip before 75 µL of prepared peptide OFFGEL sample was loaded into each of the 24 wells. The IPG strip was submerged in Cover Fluid, electrodes were locked in place at either end of the IPG strip and the fractionation was run at 4500 V until the current reduced from 50 µA to approximately 30 µA. Electrode pads were replaced and Cover Fluid reapplied after 24 hours. The sample was collected as 12 liquid fractions by pooling together every second fraction from the 24 well IPG strip. Each fraction was desalted following the C-18 SPE protocol previously described in Section 2.4.2, evaporated to dryness using the Savant SpeedVac SC100, and reconstituted in 20 µL of mass spectrometry loading buffer (5% acetonitrile and 0.2% formic acid).

2.4.4 Mass spectrometry

Each fraction was subjected to liquid chromatography coupled tandem mass spectrometry (LC-MS/MS) using the Ultimate 3000 RSLC-system fitted inline to the nanospray ionisation source of a LTQ-Orbitrap XL Mass Spectrometer (Thermo Fisher Scientific, Waltham, MA, USA). Separation of peptides was achieved by reversed phase high performance liquid chromatography (RP-HPLC) on an in-house fused silica emitter tip column (15 cm in length with 75 µm inner diameter) packed with C-18 beads (3 µm diameter, 100 Å pore size), under a flow rate of 400 nL per minute. Technical triplicates were measured for each sample over three distinct RP-HPLC gradients established in three linear stages from 5-25 %, 25-45 % and 45-99 % acetonitrile in aqueous 0.2 % formic acid. The timing of each gradient run differed across sample triplicates between 40, 65, and 90 minutes for stage one, 9, 10, and 9 minutes for stage two, and 6, 5, and 6 minutes for the stage three. The column was washed and re-equilibrated between each sample. The orbitrap analyser recorded full precursor ion scans in a mass range of m/z (mass to charge ratio) 400-2000, and at a resolution of 60,000 at m/z 400. The highest four peptide signals for replicate one, and highest five peptide signals for replicate two and three, were selected for both collision induced dissociation (CID) at a normalised collision energy of 35% in the LTQ ion trap for protein identification. The same precursors selected for CID were selected again for high-energy collision induced dissociation (HCD) at a normalised collision energy of 55% for reporter ion detection and quantification in the Orbitrap at a resolution of 15,000 at m/z 400. For replicate one, dynamic exclusion allowed for two repeated MS/MS measurements of the same precursor ion before a 90 second exclusion duration, and for replicate two and three, dynamic exclusion allowed for two repeated measurements before a 150 second exclusion duration.

2.4.5 Data analysis and calculation of relative expression

For peptide identification, the raw spectra were handled under default peak processing settings by Proteome Discoverer 1.4 (Thermo Fisher Scientific, Waltham, MA, USA) by searching the lists of peaks against the human reference amino acid sequence with the Sequest HT (Thermo Fisher Scientific) search engine. Oxidised methionine, methylthiocysteine, deamidation of asparagine and glutamine, and iTRAQ labelling on lysines, tyrosines and the peptide N-terminus were selected as variable modifications. Using the Percolator node, the score threshold was altered to an estimated false discovery rate (FDR) of <1% to reduce false positive identifications. Only those proteins with two or more significant peptide hits were accepted for quantification. The iTRAQ quantification node was used to determine relative

protein abundances, based on iTRAQ reporter ion intensities (i.e. 116/114, 116/115, 117/114, and 117/115 for the MDA-MB-231 4-plex experiment), and the ratios were normalised against the control/control protein ratio median. Observed co-culture/control ratios were modelled on a log2 scale in order overcome the original lack of symmetry around 1.

2.4.5.1 Analysis of differentially regulated proteins

To be selected for further analysis, proteins had to reach the following criteria; have two or more unique peptide hits, two or more ratio counts, and match against the reviewed Swiss-Prot database. Proteins with control/control ratios greater than 1.3 were disregarded to ensure the list of remaining proteins were identified due to the effect of the co-culture with breast adipocytes.

2.5 Bacterial Cell Culture and Plasmid Preparation

2.5.1 Plasmids

An agar stab of DH5α cells containing the pFRT/TO/HIS/FLAG/HA-PGK1 vector backbone (6765 bp; Figure 2.2), created by Markus Landthaler, was obtained from Addgene (Addgene plasmid # 38071; http://n2t.net/addgene:38071; RRID: Addgene_38071; Watertown, MA, USA). pFRT/TO/HIS/FLAG/HA-PGK1 encodes phosphoglycerate kinase 1 (PGK1; NM_000291.4) tagged at the N-terminus with the HIS/FLAG/HA, under the control of a human cytomegalovirus (CMV) immediate early promoter. The PGK1 vector also contains the *bla* (β-lactamase) and *aph(4)-Ia* (aminoglycoside phosphotransferase from E. coli) genes conferring resistance to ampicillin (bacterial) and hygromycin (mammalian), respectively.

A 1 µg/µL solution of pEGFP-n1 (GenBank accession: U55762; Figure 2.2), encoding GFPmut1, an enhanced green fluorescent protein under the control of a CMV promoter, and the *neo* gene allowing selection under kanamycin (bacterial) and G418 (mammalian), was kindly gifted by Associate Professor Gabi Dachs (Mackenzie Cancer Research Group, University of Otago Christchurch), and used as control for optimising and observing breast cancer cell transfection efficiency. The pEGFP-n1 plasmid was originally obtained from ClonTech (Palo Alto, CA, USA), but is now discontinued.

The inducible Dharmacon™ TRIPZ™ Lentiviral vector (pTRIPZ; Horizon™ Inspired Cell Solutions, Cambridge, UK, Figure 2.2) was obtained from Dr Paul Pace (Centre for Free

Radical Research, University of Otago Christchurch) as a 2 µg/µL solution with the 259 bp shRNAmir insertion site replaced with a ~30 bp non-sense DNA sequence. pTRIPZ tightly regulates the expression of a target gene in response to doxycycline treatment. In this study pTRIPZ was used as a backbone for the insertion of the *HIS/FLAG/HA/PGK1* amplicon in an attempt to create breast cancer cell lines that stably overexpress the PGK1 enzyme.

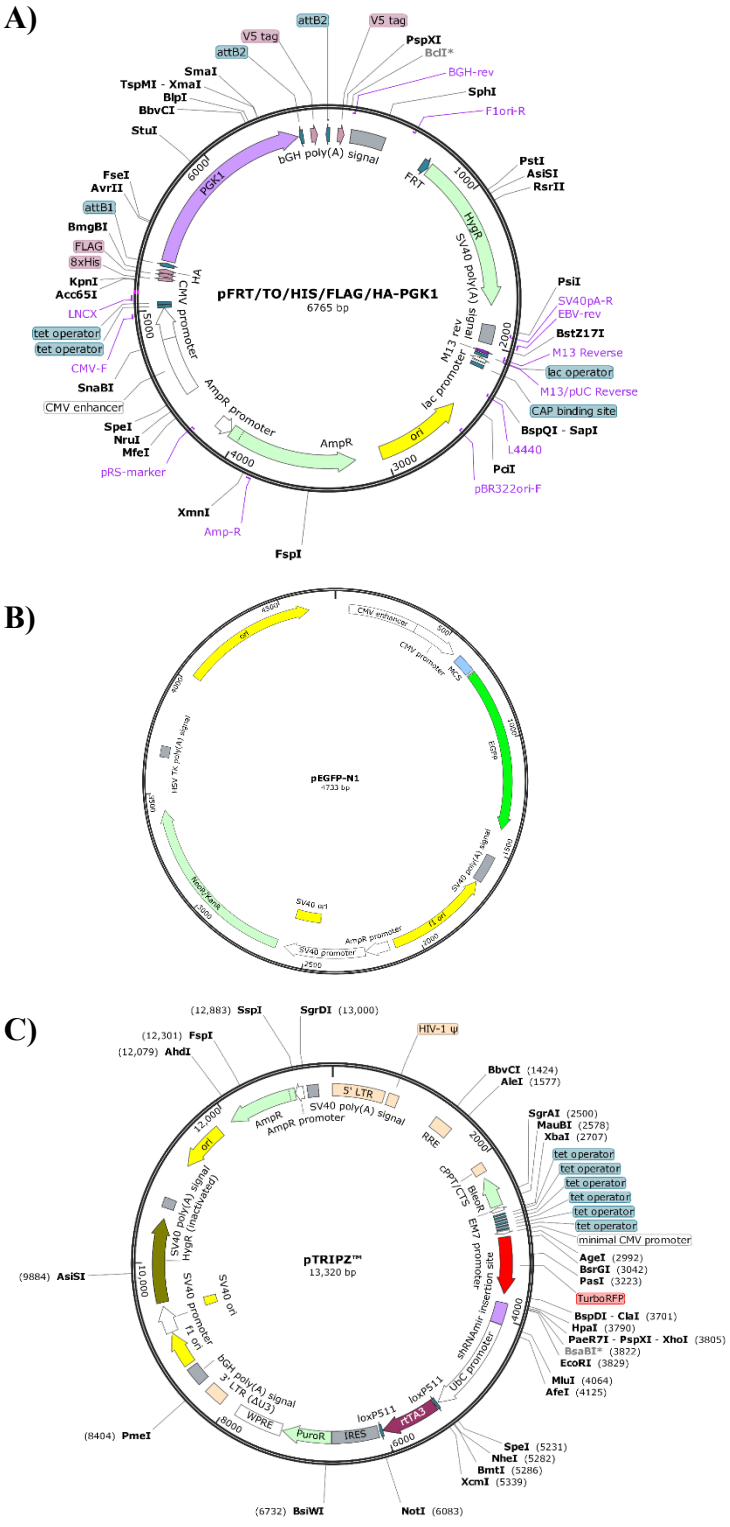

Figure 2.2. Plasmid maps.
A) pFRT/TO/HIS/FLAG/HA-PGK1 (Addgene plasmid #38071), B) pEGFP-n1 (*discontinued* ClonTech plasmid) and C) pTRIPZ (Dharmacon™ Lentiviral vector). Unique cutting restriction enzymes are shown for pFRT/TO/HIS/FLAG/HA-PGK1 and pTRIPZ. The maps were downloaded and modified using SnapGene Version 4.3.6.

2.5.2 Bacterial streaking and inoculation

All bacterial cell handling was performed under standard microbiological aseptic techniques. For plating, an agar stab of DH5α cells containing the pFRT/TO/HIS/FLAG/HA-PGK1 vector backbone was streaked onto Luria-Bertani (LB) agar plates containing 100 µg/mL ampicillin and incubated overnight at 37 °C. For inoculation, single LB agar colonies were transferred to inoculation tubes containing 5 mL of antibiotic LB and incubated overnight with sufficient aeration at 37 °C in an orbital shaker at 200 rpm. Negative controls were antibiotic LB without bacterial cells. For storage, 500 µL of the cell inoculation culture was combined with 500 µL of 50% sterile glycerol in a cryovial, and cells were frozen for long term storage at -80 °C. Streaking directly from frozen glycerol stock was performed when further plasmid was required.

2.5.3 Plasmid extraction

Plasmids were isolated from bacterial cells using the NucleoSpin® Plasmid kit (Macherey-Nagel, Bethleham, PA, USA) for mini preparations of 5 mL LB cultures, and the NucleoBond® Xtra Midi kit (Macherey-Nagel, Bethleham, PA, USA) for midi preparations of 100 mL LB cultures. Mini preparations, used for molecular cloning experiments (Section 2.6), were performed on DH5α and Stbl3 bacterial cells, isolating the pFRT/TO/HIS/FLAG/HA-PGK1 and the pTRIPZ-pFRT/TO/HIS/FLAG/HA-PGK1 plasmids, respectively. Midi preparations isolating the pFRT/TO/HIS/FLAG/HA-PGK1 plasmid, used for transfecting breast cancer cell lines (Section 2.7), was performed on DH5α bacterial cells.

To grow a 100 mL LB culture, 100 µL of the 5 mL LB culture was added to 100 mL of LB media containing the equivalent antibiotic, and incubated overnight at 37 °C in an orbital shaker at 200 rpm. Bacterial cells were pelleted by centrifugation at 5,000 x g for 10 minutes. Kit protocols were followed for plasmid extraction from cell pellets.

2.5.3.1 NucleoSpin® Plasmid Mini Preparations

Cell pellets were resuspended in 250 µL of refrigerated Buffer A1 (containing RNase A), lysed with 250 µL of Buffer A2, and neutralised with 300 µL of Buffer A3. Precipitated protein, genomic DNA, and cell debris were pelleted by centrifugation for 5 minutes at 11,000 x g, and the pellet discarded. The supernatant was spun through NucleoSpin® Plasmid column by centrifugation at 11,000 x g for 1 minute. Columns were washed with 2 x 600 µL of Buffer A4. Pure plasmid DNA was eluted under low ionic strength conditions using 2 x 15 µL of 5

mM tris hydrochloride (Buffer AE, pH 8.5), incubated on the column for 2 minutes at 70 °C before centrifugation at 11,000 x g for 1 minute. Plasmid DNA was stored at -20 °C until use.

2.5.3.2 NucleoBond® Xtra Midi Preparations

Cell pellets were resuspended in 8 mL of 4 °C RES Buffer (with RNase A) and lysed with 8 mL of LYS Buffer by gentle inversion of the tube and incubation at room temperature for 5 minutes. NucleoBond® Xtra Columns were equilibrated by wetting the entire filter with 12 mL of EQU Buffer. Cell lysates were neutralised with 8 mL of NEU Buffer and filtered through the column by gravity flow. 5 mL of EQU Buffer was filtered by gravity flow to wash the filter and the filter was removed. 8 mL of Buffer WASH was filtered through the column by gravity flow. Pure plasmid DNA was eluted under high salt concentrations, and a shift of pH from 7.0 to 9.0, using 5 mL of pre-heated (50 °C) ELU Buffer filtered through the column by gravity flow. Plasmids were precipitated to remove excess salt contaminants by adding 3.5 mL of room temperature isopropanol to the eluted plasmid DNA, vortexing thoroughly, and centrifuging at 5,000 x g for 20 minutes at room temperature. The pellet was washed using 2 mL of room temperature 70% ethanol, centrifuged again at 5,000 x g for 5 minutes, air-dried at room temperature for 15 minutes and reconstituted in 100 µL of Milli-Q water. Plasmid DNA was stored at -20 °C until use.

2.5.3.3 DNA quantification

The yield and purity of the plasmid extractions was determined by measuring the A260/A280 absorbance ratio on a NanoDrop ND-8000 spectrophotometer (NanoDrop Technologies, Rockland, DE, USA).

2.5.4 Transformation

A strain of competent *E.coli* (Stbl3) used for transformation of foreign plasmids and ligation products was kindly gifted by Associate Professor Logan Walker (Mackenzie Cancer Research Group, University of Otago Christchurch). To maintain competence *E.coli* (Stbl3) cells were stored at -80 °C.

Competent Stbl3 bacterial cells were thawed on wet ice for 25-30 minutes. 100 µL of the cells were mixed with 5 µL of ligation reaction product (generated in Section 2.6.3), gently mixed, and incubated on ice for 30 minutes. Samples were heat shocked for 1 minute at 42 °C and immediately placed back on ice for 2 minutes. 1 mL of room temperature LB media was added to the transformed cells and incubated at 37 °C for 1 hour in an orbital shaker at 200 rpm. Transformed cells were pelleted by centrifugation at 50 x g for 90 seconds, the

supernatant was decanted, and residual media was used for cell pellet resuspension. 100 µL of the cell suspension was spread evenly across pre-heated (37 °C) LB agar plates containing appropriate antibiotics. Plates were inverted and incubated overnight at 37 °C for colony formation. Negative control plates were Stbl3 cells after heat shock, with no additional DNA.

2.6 Molecular cloning of *PGK1* into the pTRIPZ vector

2.6.1 Polymerase chain reaction (PCR) and sequencing

PCR was used to amplify the full length *PGK1* gene from the pFRT/TO/HIS/FLAG/HA-PGK1 plasmid isolated from DH5α bacterial cells.

2.6.1.1 Primer Design

Primers were designed using Primer3web version 4.1.0. The National Centre for Biotechnology Information (NCBI) Primer-BLAST tool was used to assess the specificity of the primer sets. Primers were synthesised by Integrated DNA Technologies (IDT; Singapore), reconstituted in Milli-Q water to a concentration of 100 µM, and stored at -20 °C until use.

Primer pairs designed for the amplification of *PGK1* from the pFRT/TO/HIS/FLAG/HA-PGK1 plasmid included homology with the plasmid sequence (17 bp), *Xho*I or *Mlu*I restriction enzyme cut sites (6 bp), and a 5' overhang (4 bp) (Table 2.3). An overhang with ≥ 4 bp was required for optimal restriction enzyme binding and cleavage.

Primer pairs designed for the amplification of the *PGK1* insert from the pTRIPZ-HIS/FLAG/HA/PGK1 ligated plasmid included 17 bp homology with the plasmid sequence.

Primers designed to sequence the pTRIPZ-HIS/FLAG/HA/PGK1 ligated plasmid over the insertion sites and result in sequences spanning the full length of the *PGK1* gene, had complete homology to the binding sequence (17 bp) (Table 2.4).

Table 2.3. PCR primers.

Name	Sequence (5' to 3')	Tm (°C)	Amplicon Length (bp)
PGK1.For	GCAA**CTCGAG**ACCATGCACCACCACCA	70.73	1403
PGK1.Rev	GCGC**ACGCGT**GGGTCTAGATCCTAAAT	68.63	
TRIPZ.Seq*	GGAAAGAATCAAGGAGG	48.5	1758
TRIPZ.Seq.Rev*	TCTTATGAGCAGCGGGC	56.0	

Tm: primer melting temperature; **bp:** base pairs. **Bold***:* Restriction enzyme cut site sequence. Underline: Overhang sequence. *Primers were also used for sequencing.

Table 2.4. Sequencing primers.

Name	Sequence (5' to 3')	Tm (°C)
TRIPZ.Seq*	GGAAAGAATCAAGGAGG	48.5
PGK1.Seq	GACCTAATGTCCAAAGC	47.4
TRIPZ.Seq.Rev*	TCTTATGAGCAGCGGGC	56.0

Tm: primer melting temperature. *Primers were also used as a primer pair for PCR.

2.6.1.2 PCR and agarose gel visualisation

PCR amplification was carried out using the Taq-Ti Heat-activated DNA Polymerase (Fisher Biotec, Wembley, WA, Australia) in a final reaction volume of 25 µL including, 2.5 µL of 10X PCR buffer, 2 µL of 25 mM $MgCl_2$, 1 µL of 10 mM deoxynucleotide triphosphates (dNTPs), 1 µL of each primer (PGK1.For and PGK1.Rev) at 10 µM, 0.25 µL of Taq DNA polymerase enzyme, 2 µL of 25 ng/µL plasmid DNA and 15.25 µL of Milli-Q water. For negative control reactions plasmid DNA was replaced with an equal volume of Milli-Q water. Thermal cycling conditions, performed by the Mastercycler pro PCR system (Eppendorf, Hamburg, Germany), included an initial denaturation step at 95°C for 2 minutes, followed by 35 cycles of denaturation (95°C, 15 seconds), annealing (60°C, 15 seconds) and extension (72°C, 30 seconds). The size of the amplicon was determined according to the Kapa Universal DNA ladder (Kapa Biosystems, Boston, MA, USA) by combining 2.5 µL of PCR product with 1 µL of DNA loading dye. Products were loaded on to a 1.5% agarose gel (0.75 g agarose, 50 mL 1X TAE buffer and 1.5 µL of SYBR™ Safe DNA Gel stain (Life Technologies, Carlsbad, CA, USA)), and run for 45 minutes at 90 V. Visualisation of the gel was performed under UV light on the Alliance 4.7 imaging system (Uvitec Cambridge, Cambridge, UK).

If the PCR was successful, the remaining PCR product was purified using the NucleoSpin® PCR and Gel Clean-up kit (Macherey-Nagel, Bethleham, PA, USA), following kit protocol. Briefly, reaction volumes were increased to 50 µL with Milli-Q water, mixed

with 50 µL of Buffer NTI and bound to the silica membrane of the NucleoSpin® PCR and Gel Clean-up Column by centrifugation at 11,000 x g for 30 seconds. For washing, 2 x 700 µL of Buffer NT3 were centrifuged at 11,000 x g for 30 seconds through the column, and DNA was eluted under low salt conditions in 2 x 15 µL 5 mM tris hydrochloride (Buffer NE, pH 8.5), incubated on the column for 5 minutes at 70 °C, and centrifuged at 11,000 x g for 1 minute. Purified DNA was immediately digested as described in Section 2.6.2.

2.6.1.3 Sequencing

To confirm successful ligation of the pTRIPZ plasmid vector with the *HIS/FLAG/HA/PGK1* insert sequence the pTRIPZ-HIS/FLAG/HA/PGK1 plasmids were sequenced. pTRIPZ-HIS/FLAG/HA/PGK1 plasmid was purified from Stbl3 cultures using the NucleoSpin® Plasmid mini preparation spin columns (Macherey-Nagel, Bethleham, PA, USA) (Section 2.5.3.1). 5 µL sequencing reactions were prepared with 1 µL of primer (TRIPZ.Seq or PGK1.Seq) at 3.2 µM, 1 µL plasmid DNA (approximately 300 ng total DNA) and 3 µL Milli-Q water. Sequencing was completed by the Genetic Analysis Service (University of Otago, Dunedin) on the ABI 3730xl DNA Analyser. Sequences were assessed on SnapGene Viewer 4.3.6 for alignment with the predicted pTRIPZ-HIS/FLAG/HA/PGK1 sequence.

2.6.2 Restriction digestion

PCR amplification of the *HIS/FLAG/HA/PGK1* sequence was performed using a specifically designed primer set with *Xho*I and *Mlu*I restriction enzyme cut sites positioned 4 bp from each 5' end (Table 2.3). All *Xho*I and *Mlu*I restriction sites within the *HIS/FLAG/HA/PGK1* PCR product and pTRIPZ plasmid were resolved using SnapGene Version 4.3.6 (Figure 2.2). The *Xho*I and *Mlu*I restriction enzymes were chosen because they do not cleave elsewhere within the *HIS/FLAG/HA/PGK1* PCR product. Each enzyme cleaves the pTRIPZ plasmid at a single site in order to linearize the vector, and are compatible for simultaneous digestion.

The *Xho*I enzyme (20,000 U/mL; New England BioLabs®, Ipswich, MA, USA) cuts at 5'- C|TCGAG -3', and the *Mlu*I enzyme (10,000 U/mL; New England BioLabs®, Ipswich, MA, USA) cuts at 5'- A|CGCGT -3'. Digests were performed in 40 µL reaction volumes with NEBuffer™ 3.1 (New England BioLabs®, Ipswich, MA, USA). Components of each reaction are listed in Table 2.5. DNA digests were incubated for 2 hours at 37 °C. To dephosphorylate the 5' end of the plasmid preventing religation of the DNA, 2 µL of calf intestinal phosphatase

(CIP) and 3.5 µL of 10X CutSmart® Buffer (both from New England BioLabs®, Ipswich, MA, USA) were added directly into the pTRIPZ digest reaction, and incubated at 37 °C for 30 minutes. Finally, the temperature was increased to 80 °C for 20 minutes to denature enzymes.

Table 2.5. Reaction conditions for DNA digests with *Xho*I and *Mlu*I restriction enzymes.

Reagents	PCR Product (µL)	pTRIPZ (µL)	Uncut pTRIPZ (µL)
Milli-Q Water	4	31	34
10X NEBuffer™ 3.1	4	4	4
PCR Product	29	-	-
pTRIPZ DNA	-	2	2
XhoI Enzyme	1	1	-
MluI Enzyme	2	2	-

2.6.2.1 Gel Purification

For visualisation and purification, DNA digests were mixed with 10% (v/v) DNA loading dye and separated on a 0.8% agarose gel (0.4 g agarose, 50 mL 1X TAE buffer, and 1.5 µL of SYBR™ Safe DNA Gel stain) for 90 minutes at 70 V. Under UV illumination, DNA bands were excised with a scalpel blade. DNA was purified from the agarose gel using the NucleoSpin® Gel and PCR Clean-up kit (Macherey-Nagel, Bethleham, PA, USA), following the recommended protocol. Briefly, the agarose gel was band weighted and dissolved by adding 200 µL of Buffer NTI per 100 mg of agarose and incubated 50 °C for 10 minutes. The dissolved gel was bound to the silica membrane of the NucleoSpin® Gel and PCR Clean-up Column by centrifugation at 11,000 x g for 30 seconds. Contaminants were removed by centrifugation at 11,000 x g for 30 seconds with 2 x 700 µL of Buffer NT3 washes. Pure DNA was eluted under low salt conditions in 2 x 15 µL 5 mM tris hydrochloride (Buffer NE, pH 8.5), incubated on the column for 5 minutes at 70 °C before a 1 minute centrifugation at 11,000 x g. DNA concentration and purity was determined using the NanoDrop ND-8000 spectrophotometer as described in Section 2.5.3.3. Purified DNA was stored at 4 °C until use.

2.6.3 Ligation

Ligation of the *HIS/FLAG/HA/PGK1* insert containing the full length *PGK1* gene with the linearised pTRIPz lentiviral vector was performed in 25 µL reaction volumes using T4 DNA ligase (New England BioLabs®, Ipswich, MA, USA) and a 1:3 ratio of pTRIPZ (vector) to PGK1 (insert), calculated using the Promega Biomath Calculator, determining the molar

ratio of insert to vector (https://worldwide.promega.com/resources/tools/biomath/). Reactions contained 10X ligase buffer (with 10 mM ATP; New England BioLabs®, Ipswich, MA, USA), T4 DNA ligase enzyme, pTRIPz plasmid (~200 ng total DNA), *HIS/FLAG/HA/PGK1* amplicon (~65 ng total DNA), and Milli-Q water. Negative control reactions replaced *HIS/FLAG/HA/PGK1* DNA with equivalent volume of Milli-Q water. An uncut (circular) pTRIPZ vector reaction, excluding *HIS/FLAG/HA/PGK1* DNA, was performed as a positive control for transformation. Ligation reactions were gently mixed, spun and incubated overnight at 16 °C. Reactions were stored at 4 °C until transformation into competent Stbl3 (*E.coli*) bacterial cells.

2.7 Transfection of human breast cancer cells

Oestrogen receptor positive MCF-7 and oestrogen receptor negative MDA-MB-231 breast cancer cells were transfected with full length *PGK1* to characterise the effect of PGK1 overexpression on chemotherapy response and lactate production.

2.7.1 Verification of plasmid DNA

The identity and purity of the pFRT/TO/HIS/FLAG/HA-PGK1 and pEGFP-n1 plasmids were validated by separation on a 1% agarose gel (0.5 g agarose, 50 mL 1X TAE buffer, and 1.5 µL of SYBR™ Safe DNA gel stain) according to the HighRanger Plus 100 bp DNA Ladder (Norgen Biotek, Thorold, ON, Canada). 8 µL of 10 ng/µL plasmid DNA was mixed with 1 µL of DNA loading dye and run for 45 minutes at 90 V. Visualisation of the gel was performed under UV light on the Alliance 4.7 imaging system (Uvitec Cambridge, Cambridge, UK).

2.7.2 Transient transfection of MCF-7 and MDA-MB-231 cells

To assess transfection efficiency, MCF-7 and MDA-MB-231 breast cancer cells were transfected with the pEGFP-n1 plasmid (containing the gene for enhanced green fluorescent protein (GFP); Figure 2.2B), using the jetPRIME® (Polyplus-transfection, Illkirch, France) reagent. MCF-7 and MDA-MB-231 cells were seeded into 6-well plates at a density of 1.6 x 10^5 cells/well and grown until they reached 60-70% confluence. Media was replaced (GlutaMAX™ DMEM with 10% FBS, without A/A), and a 1:2 ratio of plasmid DNA (2 µg) to reagent (4 µL) was added to the cells. After 6 hours, cells were washed with GlutaMAX™ DMEM with 10% FBS, without A/A. Transfection efficiency was determined 54 hours post

transfection using fluorescence-activated cell sorting (FACS; Cytomics FC500 MPL Flow Cytomter, Beckham Coulter, Brea, CA, USA; data analysis with the CXP software) and visualisation with live-cell microscopy (Olympus IX-81, Tokyo, Japan) to quantify cells expressing EGFP.

For transfection experiments, MCF-7 and MDA-MB-231 breast cancer cells were seeded in 6 well plates at 2.4 x 10^5 cells/well for PGK1 transfection, 2 x 10^5 cells/well for GFP transfection, and 1.6 x 10^5 cells/well for the transfection reagent only and cell only controls. Media was replaced 24 hours after seeding, and MCF-7 and MDA-MB-231 breast cancer cells were transfected with the pFRT/TO/HIS/FLAG/HA-PGK1 plasmid at a ratio of 1:2 plasmid (2 µg) to jetPRIME® reagent (4 µL). DNA was excluded from negative controls, and the pEGFP-n1 plasmid at a ratio of 1:2 plasmid (2 µg) to jetPRIME® reagent (4 µL) was used as a vehicle control. Transfection media was replaced with GlutaMAX™ DMEM with 10% FBS after 6 hours. The expression of PGK1 in the cells after 54 hours was assessed using Western blot (Section 2.8).

If the transfection was successful (EGFP expression visualised by live-cell microscopy), the effect of PGK1 overexpression was assessed using the experimental schema depicted in Figure 2.3, and the assays described below.

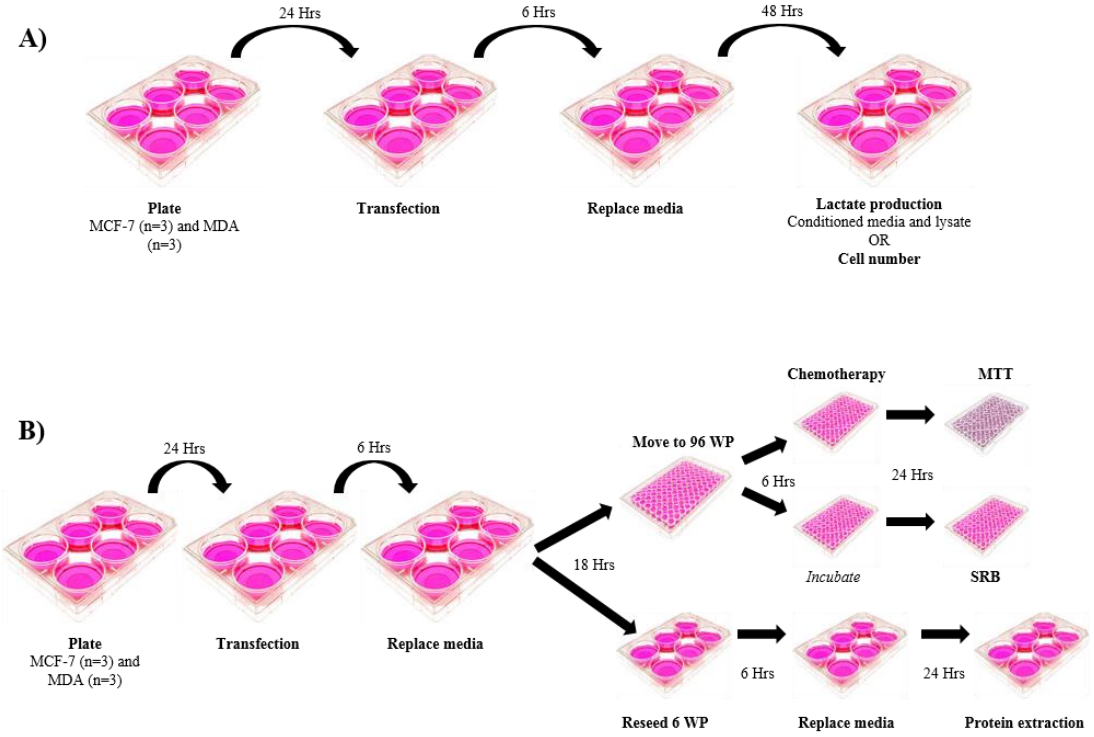

Figure 2.3. Experimental schema for transfection of MCF-7 and MDA-MB-231 breast cancer cells with pFRT/TO/HIS/FLAG/HA-PGK1.
A) Protocol for lactate production and live cell number analysis, and B) analysis of cell proliferation, PGK1 overexpression, and cell viability in response to breast cancer chemotherapies.

2.7.2.1 Lactate quantification

The effect of PGK1 protein overexpression on lactate production by breast cancer cells after 48 hours was measured using the colourimetric L-Lactate Assay Kit (Abcam, Cambridge, MA, USA), following manufacturers guidelines. Sample preparation was performed on ice. Briefly, conditioned media was transferred into microtubes and cells were washed with 1 mL of cold PBS. 100 µL of Lactate Assay Buffer was added per well and cells were lysed and harvested into microtubes by scraping. Conditioned media and lysates were centrifuged at 11,000 x g for 5 minutes at 4 °C, and the supernatant collected into pre-cooled microtubes. Cell lysates, and 150 µL of conditioned media samples, was deproteinised with the Deproteinizing Sample Preparation Kit- TCA (Abcam, Cambridge, MA, USA), following manufacturer's instructions, to remove lactate dehydrogenase and limit the degradation of lactate. In 96 well plates, total reaction volumes were 100 µL per well comprising, 50 µL of standard, lysate or conditioned media, 46 µL of Lactate Assay Buffer, 2 µL of Lactate

Substrate Mix and 2 µL of Lactate Enzyme Mix. Lactate Enzyme Mix was replaced with Lactate Assay Buffer for background control. Sample controls included deproteinised Lactate Assay Buffer and media (GlutaMAX™ DMEM with 10% FBS) cultured without cells. Reactions were mixed and incubated at room temperature for 30 minutes. Absorbance was measured at 450 nm on the Multiskan GO plate reader (Thermo Fisher Scientific, Rockford, IL, USA). L-lactate concentration was calculated by extrapolation from the standard curve (ranging from 0 µM to 2000 µM using the L-Lactate Standard supplied with the kit) and normalisation to live cell number. Live cell number was determined using the Countess™ Automated Cell Counter (Section 2.2.2).

2.7.2.2 Chemotherapy response

Breast cancer cells transfected with PGK1 in 6 well plates, were moved to 96 well plates 24 hours after transfection (Figure 2.3). Cells were collected in 500 µL of TrypLE dissociation reagent, centrifuged at 610 x g for 4 minutes, and resuspended in 200 µL of GlutaMAX™ DMEM with 10% FBS for counting (Section 2.2.2). Cells were plated in 96 well plates (100 µL/well) at 1.1 x 10^4 cells/well for MCF-7 and 1 x 10^4 cells/well for MDA-MB-231, and incubated for 6 hours until cell adhesion occurred. Remaining cells were plated back into 6 well plates for protein extraction and validation of PGK1 transfection using Western blot (Section 2.8; Figure 2.3).

Cell proliferation and viability assays were performed in parallel. For cell proliferation, the 96 well plate was supplemented with another 100 µL per well of GlutaMAX™ DMEM with 10% FBS (no A/A), and incubated at 37 °C for 24 hours until sulforhodamine B (SRB) analysis (Section 2.7.2.2.1). For cell viability, the 96 well plate was treated for 24 hours with previously determined IC50 concentrations of paclitaxel (SANDOZ, Princeton, NJ, USA) and 4-hydroperoxycyclophosphamide (Cayman Chemical, Ann Arbor, MI, USA) (Table 2.6). The paclitaxel used was a clinical grade paclitaxel solubilised in ethanol to 6 mg/mL, and stored at room temperature. 4-hydroperoxycyclophosphamide was a crystalline solid that was stored at -80 °C until solubilisation with dimethyl sulfoxide (DMSO) prior to use. Paclitaxel (in ethanol) and 4-hydroperoxycyclophosphamide (in DMSO) were diluted in GlutaMAX™ DMEM with 10% FBS (no A/A) for use in viability assays. 4-hydroperoxycyclophosphamide is spontaneously converted in aqueous solution to 4-hydroxycyclophosphamide, the latter of which is believed to be the active metabolite of cyclophosphamide *in vivo.* Cell viability was measured using an 3-(4,5-dimethylthiazol-2-yl)-2,5-diphenyltetrazolium bromide (MTT) assay (Section 2.7.2.2.2).

Table 2.6. IC50 concentrations of breast cancer chemotherapies. IC50 concentrations of paclitaxel and 4-hydroperoxycyclophosphamide were used to treat control and transfected MCF-7 and MDA-MB-231 human breast cancer cells.

	Paclitaxel	4-hydroperoxycyclophosphamide
MCF-7	62 µM	25 µM
MDA-MB-231	20 µM	23 µM

2.7.2.2.1 SRB

The sulforhodamine B (SRB) assay is a colourimetric assay which can assess cell proliferation based on the binding of SRB to cell proteins allowing measurements of protein content [324]. Breast cancer cell proliferation was measured in 96 well plates using the Sulforhodamine B Cell Cytotoxicty Assay Kit (Abcam, Cambridge, MA, USA), following kit protocol. Briefly, cells were fixed adding 50 µL per well of Fixative Solution for 1 hour at 4 °C. After fixation, cells were gently washed three times with Milli-Q water, dried at 50 °C for 30 minutes, and stained with 50 µL per well of SRB Solution for 15 minutes in the dark at room temperature. SRB Solution was removed by washing four times 1X Washing Solution. Cells were dried at 50 °C for 30 minutes and solubilised with 200 µL of 1X Solubilisation Solution per well. Absorbance was measured at 565 nm using the Multiskan GO plate reader (Thermo Fisher Scientific, Rockford, IL, USA). Each assay was performed with blank wells containing medium without cells, for background correction.

2.7.2.2.2 MTT

The conversion of 3-(4,5-dimethylthiazol-2-yl)-2,5-diphenyltetrazolium bromide (MTT) to purple formazan crystals by mitochondrial dehydrogenases is a colourimetric assay used to quantify cell viability as a function of mitochondrial activity in metabolically active cells [325]. The effect of PGK1 transfection on the viability of chemotherapy treated breast cancer cells was measured in 96 well plates using an MTT assay. MTT was reconstituted in 1X PBS at 5 mg/mL, sterile filtered through a Millex-GV 0.22 µM PVDF syringe filter unit, and diluted to 0.5 mg/mL in RPMI 1640 Medium without phenol red (Life Technologies, Carlsbad, CA, USA). Media was aspirated, and the cells were incubated with 100 µL of 0.5 mg/mL MTT per well for 3 hours at 37 °C. Formazan crystals were dissolved by adding 100 µL of solubilisation solution (89% isopropanol, 10% Triton-X and 1% hydrochloric acid (1M)) per well and pipetting up and down. Absorbance was measured at 540 and 690 nm on

the Multiskan GO plate reader. Each assay was performed with blank wells containing medium without cells, for background correction.

2.8 Western blotting

2.8.1 SDS-PAGE

Protein extracted from cell lysates was prepared for sodium dodecyl sulfate polyacrylamide gel electrophoresis (SDS-PAGE) under reducing conditions; including final concentrations of 100 mM dithiothreitol (DTT; Sigma-Aldrich, St. Louis, MA, USA), 1X Blot™ LDS sample buffer (Life Technologies, Carlsbad, CA, USA), and Milli-Q water. Proteins were denatured by heating at 70 °C for 10 minutes. 5 µg of total protein was loaded per well.

Depending on the molecular weight (MW) of the target protein, proteins were either resolved on Bolt™ 4-12% Bis-Tris Plus or 12% Bis-Tris Plus SDS gels for 75 minutes at 125 V in a Bolt Mini Gel Tank using Blot™ 3-(N-morpholino) propanesulfonic acid (MOPS) and 2-(N-morpholino) ethanesulfonic acid (MES) SDS Running Buffers, respectively (all from Life Technologies, Carlsbad, CA, USA). Molecular mass of proteins was estimated using 4 µL of the SeeBlue™ Plus2 Pre-stained Protein Standard (Life Technologies, Carlsbad, CA, USA).

2.8.2 Transfer

0.45 µm polyvinylidene difluoride (PVDF) membranes were activated in 100% methanol for 30 seconds and equilibrated in Milli-Q water prior to use. Separated proteins were transferred to the activated PVDF membranes using the Bolt Mini Blot Module in 1X Bolt™ Transfer Buffer (Life Technologies, Carlsbad, CA, USA) with 10% methanol for 60 minutes at 20 V. Following transfer, membranes were blocked with 5% skimmed milk powder in Tris-buffered saline with 0.1% Tween®20 (TBST) for 60 minutes at room temperature.

2.8.3 Antibodies

PVDF membranes were incubated with primary antibodies in 5% skimmed milk in TBST at 4 °C overnight. Primary antibodies were optimised to the concentrations specified in Table 2.7.

Table 2.7. Antibodies for Western blotting.

Primary Antibody	Predicted band (kDa)	Source, dilution	Company (product code)
FLAG	48	Monoclonal mouse, 1/1000	Sigma-Aldrich, St Louis, MO, USA (F1804)
NDRG1	43	Monoclonal rabbit, 1/5000	Abcam, Cambridge, MA, USA (ab124689)
PGK1	44	Polyclonal rabbit, 1/1000	Abcam, Cambridge, MA, USA (ab38007)
TFF1	14	Monoclonal rabbit, 1/1000	Abcam, Cambridge, MA, USA (ab92377)
β-actin	42	Monoclonal mouse, 1/10000	Sigma-Aldrich, St Louis, MO, USA (A5316)

kDa: kilodaltons

Membranes blotted for NDRG1, PGK1 and FLAG were stripped with mild stripping buffer (1.5 g glycine, 1 mL 10% SDS and 1 mL Tween20; made up to 100 μL and adjusted to pH 2.2), washed 3 times with TBST for 5 minutes each, blocked with 5% skimmed milk powder in TBST for 60 minutes at room temperature, and re-probed for β-actin. Membranes probed for TFF1 were cut to separate the TFF1 and β-actin bands before probing with primary antibodies.

Membranes were washed with TBST 3 times for 5 minutes each and incubated for 60 minutes at room temperature with suitable horseradish peroxidase (HRP) conjugated secondary antibodies diluted in TBST. Secondary antibodies included polyclonal goat anti-rabbit immunoglobulins/HRP (Dako, Glostrup, Copenhagen, Denmark) at 1/5000 for NDRG1, PGK1 and TFF1, and goat anti-mouse polyclonal immunoglobulins/HRP (Dako, Glostrup, Copenhagen, Denmark) at 1/5000 for FLAG and β-actin. Membranes were washed with TBST 3 times for 5 minutes each, and incubated with Amersham ECL primer Western blotting detection reagents (GE Healthcare, Little Chalfont, Buckinghamshire, UK) for 3 minutes at room temperature before being imaged by chemiluminesence on the Alliance 4.7 (Uvitec Cambridge, Cambridge, UK). The same samples were measured on multiple membranes from different SDS-PAGE gels (n= 3) to ensure reproducibility of the Western blot assay.

2.8.4 Relative expression

Membranes were quantified using ImageJ software (Version 1.49). The NDRG1, PGK1, and TFF1 densitometry values were compared to their respective β-actin bands to calculate relative protein expression values. A control sample was run on each gel to normalise relative protein expression across repeated gels.

2.9 Bioinformatics

2.9.1 Overrepresented cellular components and pathways in breast cancer cell proteomes

The iTRAQ ratios, generated in Section 2.4, were averaged and log transformed for each identified protein. Two different lists of proteins for each cell line were uploaded into the protein annotation through evolutionary relationship (PANTHER) classification system (Version 12.0; http://www.pantherdb.org/) for cellular component and pathway analysis using gene list analysis [326,327]. The first list was analysed for overrepresented cellular components (PANTHER GO-Slim cellular components) [328], and included all the proteins that were identified by proteomic profiling in MCF-7 (n= 1126) and MDA-MB-231 (n= 1218) breast cancer cells. The second list was analysed for over-represented PANTHER pathways [329], and included only those proteins that had an average fold change ≥ 1.1 compared to controls, to indicate potentially meaningful pathways enriched in CAA-MCF-7 (n= 576) and CAA-MDA-MB-231 (n= 554). Statistical over-representation testing by PANTHER was performed using the human genome as the reference list, and the binomial statistic p-values were corrected for multiple testing using the Bonferroni correction method.

2.9.2 *In vitro PGK1* expression in breast cancer cell lines

PGK1 expression data (RNAseq) was retrieved from the Broad Institutes' Cancer Cell Line Encyclopedia (CCLE; https://portals.broadinstitute.org/ccle) for 57 different breast cancer cell lines and was utilised to assess the association between *PGK1* expression and breast cancer molecular subtypes. Transcriptional characteristics of 48 breast cancer cell lines, including the presence or absence of the oestrogen receptor (ER), progesterone receptor (PR) and *ERBB2* overexpression (human epidermal growth factor receptor 2; HER2) status were used to categorise the breast cancer cell lines into molecular subtypes, including luminal (ER+ and/or PR+, HER2+/-), HER2 enriched (ER-, PR-, HER2+) and triple negative (ER-, PR-, HER2-), and the difference in *PGK1* mRNA levels was compared between the breast cancer cell line subtypes.

Furthermore, utilising the Broad Institute's Cancer Dependency Map (DepMap; https://depmap.org/portal/depmap/), the CCLE gene expression data was used to correlate *PGK1* expression in different breast cancer cell lines with sensitivity (AUC) to paclitaxel and cyclophosphamide (breast cancer chemotherapies).

2.9.3 *In vivo PGK1* expression in breast tumours

Data from The Cancer Genome Atlas (TCGA)[104] and Molecular Taxonomy of Breast Cancer International Consortium (METABRIC)[330] retrieved from cBioPortal (http://www.cbioportal.org/) was utilised to assess gene expression of PGK1 and its association with clinicopathological features, including ER, PR and *ERBB2* (HER2) expression status, of the 825 and 2,000 breast tumours in these cohorts, respectively. The difference in *PGK1* mRNA expression (microarray z-scores) was compared between the breast tumours based on presence or absence of the clinical biomarkers ER, PR and HER2. In addition, the METABRIC study has reported molecular subtypes of the breast tumours including luminal A, luminal B, HER2 enriched, basal, and claudin-low, and therefore, difference in *PGK1* gene expression between different subtypes was evaluated. Gene expression data for hypoxia inducible factor 1 (*HIF-1*) and solute carrier family 16 member 3 (*SLC16A3;* protein name monocarboxylate transport 4 [MCT4]) (microarray z-scores) were also retrieved from METABRIC and correlated with *PGK1* expression. TCGA and METABRIC do not have BMI data associated with the patient tumours, and therefore differences in PGK1 (mRNA or protein) expression between obese and normal weight were not assessed.

2.10 Patient study

2.10.1 Ethics and participant recruitment

Ethical approval for the 'Clinical Protocol' (Appendix B) and 'Participant Information Sheet and Consent Form' (PIS/CF; Appendix C) was obtained on 2/9/2016 through the Health and Disability Ethics Committees (HDEC) Full Review Pathway by the Central Committee (reference number 16/CEN/116/AM01) under the study title 'An Exploratory Study to Assess the Impact of Obesity-Related Inflammatory Markers on Breast Cancer Drug Metabolism in Response to Regular Moderate Exercise during Chemotherapy'. Locality was approved for Christchurch Hospital by the CDHB Research Office, and recruitment began on 1/3/2017. A post-approval amendment to the original 'Clinical Protocol' to recruit both neoadjuvant and adjuvant breast cancer patients receiving chemotherapy at Christchurch Hospital was accepted on 7/6/2017. On 1/3/18 an application to extend recruitment until 31/12/2018 was submitted and approved. The study was closed to recruitment on 25/12/18. All patients gave

informed written consent for their participation in the study, the use of their samples for research purposes, and access to their medical records.

Māori consultation was completed with Karen Keelan, the Māori Research Advisor of the University of Otago Christchurch. This study is of particular interest and potential benefit to Māori.

2.10.2 Participant selection

Full inclusion and exclusion criteria are listed in Appendix B, and the following is a brief description. Eligible participants were women aged 18 or over, with clinically defined stage II or III breast cancer receiving neoadjuvant or adjuvant combined Adriamycin (doxorubicin)-cyclophosphamide (AC) and paclitaxel chemotherapy as treatment. Further inclusion criteria were: ability and willingness to take oral medications; willingness to wear a FitBit One® device periodically throughout chemotherapy; adequate end-organ function (see Appendix B; 'Clinical Protocol' Inclusion Criteria); no known sensitivity or contraindications to any of the cocktail components. Relevant exclusion criteria included: urinary incontinence or current use of a urinary catheter; impaired mobility due to disability or medical illness; known cirrhosis of the liver or active infection with viral hepatitis, currently taking medications known to be strong inhibitors or inducers of the cytochrome P450 (CYP) enzymes being studied (see Appendix B; 'Clinical Protocol' Exclusion Criteria). Weak CYP inducers or inhibitors were accepted (see Appendix B). Patients matching the above criteria that were not already enrolled in a conflicting trial, were identified and approached by CDHB medical oncologists, and were required to understand and give informed written consent for their participation in the study.

2.10.3 Basic study design

The design of the study is comprehensively outlined in the 'Clinical Protocol' available as Appendix B, and depicted here in Figure 2.4. In brief, a medical oncologist presented the study and informed consent document during an initial appointment, and then performed informed consent following the participant's chemotherapy education session, which typically was within 2 weeks of the initial appointment with no additional delay to treatment initiation. Participants received planned standard of care chemotherapy including four 21-day cycles of AC, followed by administration of paclitaxel for twelve 7-day cycles (weekly). All chemotherapy was administered intravenously as per standard-of-care, with

standard pre-medication, and adjunctive medications as clinically indicated. Dose delays, reductions, and modifications were made as per routine care indicators.

In the 2 weeks leading up to cycle 1 day 1 of AC, participants had body morphometry measured (including body mass index (BMI), waist to hip ratio (WHR) and body fat percentage using bioelectrical impedance analysis (BIA); Section 2.10.4)), and were given the probe drug cocktail with subsequent pharmacokinetic sampling of blood (4 hour post-administration) and urine (0-8 hour post-administration collection) (Section 2.10.8). FitBit One® devices were worn (unless specified in a device removal journal) following cycle 1 day 1 AC for 21 days, dose 1 day 1 of paclitaxel for 7 days, and dose 6 day 1 of paclitaxel for 7 days. Blood samples were taken at the end of each FitBit cycle, and were processed to collect serum (Section 2.10.6) for inflammatory cytokine analysis (Section 2.10.7). Following dose 6 day 7 of paclitaxel, participants had body morphometry re-measured and were given the second probe drug cocktail with subsequent blood (4 hour) and urine (0-8 hour) sample collection.

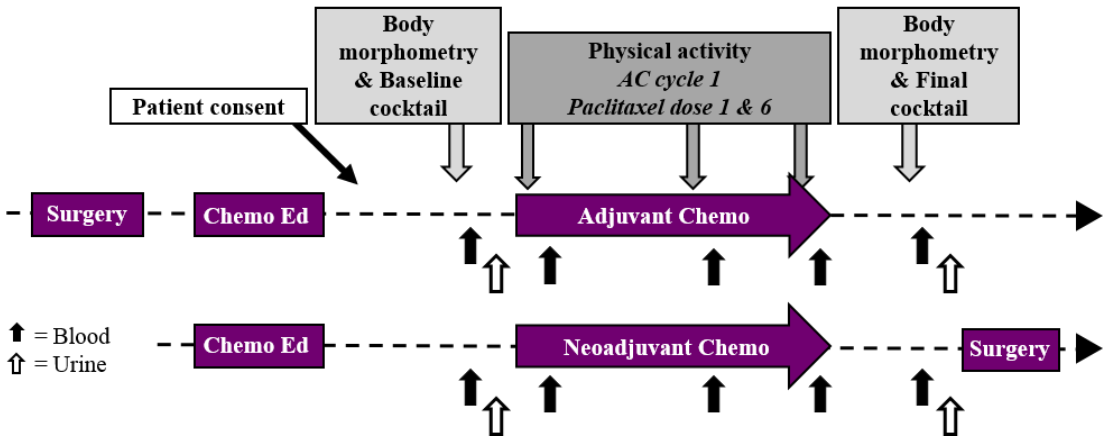

Figure 2.4. Schedule for the patient study.
Neoadjuvant and adjuvant chemotherapy patients are outlined by separate timelines (purple horizontal arrows). Body morphometry and cocktail administration are indicated by light grey vertical arrows, and physical activity monitoring periods are shown by dark grey vertical arrows. Blood and urine sampling are represented by vertical black and white arrows, respectively.

2.10.4 Body morphometry measurements

Body morphometry measurements were recorded by the study nurse prior to the participants starting chemotherapy, and the same measurements were repeated following dose

6 of weekly paclitaxel, as outline in Figure 2.4. Measurements included height (cm), weight (kg), waist and hip circumference (cm), and fat, muscle and bone composition (%) using the Tanita Body Composition Analyser (Wedderburn, Hornby, Christchurch, NZ). Intra-patient differences were calculated by comparison to pre-chemotherapy measurements. Body mass index (BMI) was calculated from height and weight, by dividing a participant's weight in kilograms by their height in meters squared (BMI= kg/m^2). Waist to hip ratio (WHR) was calculated as the waist circumference divided by the hip circumference.

2.10.5 Physical activity monitoring

Participants wore FitBit One® devices for a total of 35 days during their chemotherapy treatment, including 21 days following cycle 1 day 1of AC, and 7 days following paclitaxel dose 1 and dose 6. Participants were required to record a daily journal documenting when they removed the FitBit One® device, for how long the device was removed and what activity was performed during this time. Each time the participant returned to clinic after wearing the FitBit One®, physical activity data, including daily step count was retrieved from the device.

2.10.6 Patient blood samples

All blood samples were collected from study participants by Christchurch Oncology Research Unit (CORU) research nurses (CDHB staff) in the oncology day ward. Blood was collected in red top plain tubes (BD CAT coagulation) for serum, and lavender top EDTA tubes (lavender top; K2E 7.2 mg) for plasma. Lavender top EDTA tubes were centrifuged within 30 minutes of collection, and red top plain tubes were incubated at room temperature for 30 minutes before centrifugation; centrifugation was 1000 x g for 15 minutes at 4 °C. Supernatant was collected in cyrovials and stored at -80 °C until use.

Plasma and serum purity was validated using serum protein electrophoresis on all collected samples prior to use. Serum protein electrophoresis is a common diagnostic procedure and was performed by Catherine Rollo (and team) at the Protein Chemistry Laboratory (Canterbury Health Laboratories). The complete absence of a fibrinogen band between the beta and gamma globulins indicates a pure serum sample (Supplementary Figure A.2).

2.10.7 Serum concentrations of inflammatory cytokines

2.10.7.1 Human cytokine array

The relative expression of 105 human cytokines were measured in patient serum taken at baseline and following paclitaxel dose 6, using the Human XL Cytokine Array Kit (R&D

Systems, Minneapolis, MN, USA) following manufacturer's instructions. Briefly, 4 x 25 µL aliquots of serum were pooled together from non-obese patients, and obese patients, taken at baseline and again following dose 6 of paclitaxel, yielding 4 x 100 µL samples (Samples 1-4; Table 2.8). Nitrocellulose membranes with duplicate antibody spots were blocked with 2 mL of Array Buffer 6 for 1 hour at room temperature. Samples were diluted in 1400 µL of Array Buffer 6 and incubated with membranes at 4°C with gentle rocking overnight. Membranes were washed with 1X Wash Buffer 3 times for 10 minutes each and incubated individually with 1500 µL of Detection Antibody Cocktail (30 µL of Detection Antibody diluted in 1470 µL of 1X Array Buffer 4/6) for 1 hour at room temperature. Using 1X Wash Buffer as before, the membranes were washed and incubated with 2 mL of 1X Streptavidin-HRP for 30 minutes at room temperature with gentle shaking. Membranes were washed again with 1X Wash Buffer 3 times for 10 minutes each and incubated with 1 mL Chemi Reagent Mix (1:1 volume of Chemi Reagents 1 and 2) for 1 minute at room temperature protected from light. The membranes were imaged by chemiluminesence on the Alliance 4.7 (Uvitec Cambridge, Cambridge, UK).

2.10.7.1.1 Relative expression

Membranes were quantified using ImageJ software. The densitometry values on each membrane were averaged across duplicate spots and compared to the average of the negative control spots to remove background. Positive control spots on each membrane were used to normalise across membranes. The relative difference in cytokine expression was determined by comparing signals across membranes.

Table 2.8. Serum samples pooled together for their use in human cytokine array.

Sample	Patient	BMI	Collection time	Obesity status
1	4	20.7	Baseline	Non-obese
	9	22.2	Baseline	Non-obese
	11	25.5	Baseline	Non-obese
	5	26.6	Baseline	Non-obese
2	2	33.1	Baseline	Obese
	6	34	Baseline	Obese
	1	34.1	Baseline	Obese
	7	39.4	Baseline	Obese
3	4	21.8	Paclitaxel dose 6	Non-obese
	9	22.1	Paclitaxel dose 6	Non-obese
	11	26.4	Paclitaxel dose 6	Non-obese
	10	27.9	Paclitaxel dose 6	Non-obese
4	2	33.6	Paclitaxel dose 6	Obese
	5	34	Paclitaxel dose 6	Obese
	1	34.1	Paclitaxel dose 6	Obese
	6	36.5	Paclitaxel dose 6	Obese

2.10.7.2 Enzyme-linked immunosorbent assay (ELISA)

Cytokine concentrations in patient serum were measured using Quantikine® ELISA kits for human angiopoietin-2 (ANG2), B-cell activating factor (BAFF), C-reactive protein (CRP), growth differentiation factor 15 (GDF-15), interleukin 1β (IL-1β), interleukin 4 (IL-4), interleukin 10 (IL-10), monocyte chemoattractant protein 1 (MCP-1) and tumour necrosis factor-α (TNF-α) (R&D Systems, Minneapolis, MN, USA), according to manufacturer's instructions. Specifically, 96 well plates pre-coated with appropriate antibodies were incubated with standards (in duplicate) and samples; as indicated by serum volume and incubation time in Table 2.9. Incubations were at room temperature with gentle shaking, and if required, serum was diluted in Calibrator Diluent provided with the kit (Table 2.9). Wells were then washed 4 times with 1X Wash Buffer. 200 µL of the conjugate antibody was added per well and incubated at room temperature for 1 or 2 hours with gentle shaking (Table 2.9). Next, plates were washed 4 times with 1X Wash Buffer. Colour Reagents A and B were mixed at a 1:1 ratio, and 200 µL of the resulting Substrate Solution was added per well. Plates were incubated at room temperature for 20 or 30 minutes protected from light (Table 2.9). 50 µL of Stop Solution was added per well, and absorbance was measured on the Multiskan GO plate reader at 450 nm and 570 nm to assess the colour change from blue to yellow. Absorbance values at 450 nm were subtracted from background absorbance at 570 nm, and cytokine concentrations were extrapolated from the standard curve using the protein standard supplied with each kit.

Table 2.9. Enzyme-linked immunosorbent assay (ELISA) volumes, dilutions and incubation times. Quantikine® ELISA kits were used to measure the concentrations of different human cytokines in patient serum samples.

Cytokine	Standard and Serum Volumes (µL/well)	Serum Dilution	Serum Incubation (hours)	Conjugate Antibody Incubation (hours)	Substrate Solution Incubation (minutes)
ANG2	50	1:5	2	2	30
BAFF	50	1:2	3	1	30
CRP	50	1:100	2	2	30
GDF-15	50	1:4	2	1	30
IL-1β	200	-	2	2	20
IL-4	50	-	2	2	20
IL-10	200	-	2	2	30
MCP-1	200	1:2	2	2	30
TNF-α	50	-	2	2	30

2.10.8 Liver enzyme activity

2.10.8.1 Cocktail administration

This study utilised a modified 'Inje' probe drug cocktail, adapted from Ryu *et al*. (2007)[290], to assess the *in vivo* function of cytochrome P450 (CYP) liver enzymes. The probe drug cocktail was comprised of the following medications and doses, assessing the following CYPs, respectively: CYP1A2, 100 mg caffeine tablet (Key Pharmaceuticals, Pty Ltd, Port Macquarie, NSW, Australia; Batch: P60064); CYP2C9, 25 mg losartan tablet (Actavis, NJ, USA; Batch: GXM016002); CYP2C19, 20 mg omeprazole tablet (Mylan, PA, USA; Batch: ZC16064B); CYP2D6, 30 mg of dextromethorphan syrup (Pfizer, Sydney, NSW, Australia; Batch: 17RDX10A); and CYP3A4, 1 mg of midazolam syrup (Claris Injectables Ltd, Ahmedabad, India; Batch: B5A0219). Syrups were diluted in 50 mL of plain water, and the used cups were rinsed and rinsing water swallowed to ensure the whole midazolam and dextromethorphan dose was administered. This cocktail was selected because these drugs, at the lower doses, have minimal risk of causing clinical effect, even in the context of significantly delayed clearance of drugs. Study participants were administered with the cocktail medications on two separate occasions, prior to beginning chemotherapy, and again following dose 6 of paclitaxel. Any concomitant medications taken in the 24 hours preceding the cocktail administration were recorded by study nurses.

2.10.8.2 Pharmacokinetic sampling

Study participants fasted from midnight on the study day and were requested to refrain from consuming caffeine containing beverages for 24 hours prior to cocktail administration.

Blood samples were taken at baseline (prior to administration of cocktail) and 4 hours after the administration of the cocktail (Figure 2.4). Blood samples were processed (Section 2.10.6) for the collection of serum and plasma. Up to 50 mL of urine was obtained before the cocktail was administered. Total urine was collected for 8 hours after the cocktail was administered, and following mixing, 50 mL aliquot of this urine was taken. Plasma, serum, and urine samples were stored at -80°C until use in pharmacokinetic analysis.

2.10.8.3 Cocktail drug and metabolite concentrations

Measurements of the phenotyping cocktail drugs and metabolite concentrations in serum and urine samples were performed using two in-house LC-MS/MS methods developed, validated and performed by Mei Zhang and Associate Professor Matthew Doogue from Clinical Pharmacology (Department of Medicine, University of Otago Christchurch) and Toxicology (Department of Specialist Biochemistry, Canterbury Health Laboratories) [331]. Briefly, serum was used to assess the concentrations of caffeine, paraxanthine, omeprazole, 5-hydroxyomeprazole, midazolam and α-hydroxymidazolam, and urine was needed for the measurement of losartan, E-3174, dextromethorphan and dextrorphan concentrations. The measurements were performed by the Agilent 6460 LC-MS/MS system for midazolam and α-hydroxymidazolam, and the API 4000 LC-MS/MS system for dextromethorphan, dextrorphan, caffeine, paraxanthine, losartan, E-3174, omeprazole, 5-hydroxyomeprazole and paracetamol. The limits of the quantification in serum and urine were 0.2 ng/mL for midazolam and α-hydroxymidazolam, 1.25 ng/mL for dextromethorphan, and 5.0 ng/mL for caffeine, paraxanthine, losartan, E-3174, omeprazole, 5-hydroxyomeprazole, dextrorphan and paracetamol. The intra- and inter-day coefficients of variation (CVs) over the analysed concentration ranges for all the compounds were <10%.

2.10.8.4 CYP phenotypic activity

Phenotypic activity was calculated from the probe parent drug to metabolite concentration ratio (metabolic ratio) for each cocktail component administered prior to beginning chemotherapy (‘before chemotherapy’) and again following dose six of paclitaxel (‘after chemotherapy’). The phenotyping indices used in the current study were: 0-8 hour urine concentration ratio of losartan/ E-3174 and dextromethorphan/dextrorphan in order to assess CYP2C9 and CYP2D6 activity, respectively, and the 4 hour serum concentration ratios of omeprazole/5-hydroxyomeprazole and midazolam/α-hydroxymidazolam in order to assess CYP2C19 and CYP3A4 activity, respectively.

Changes in CYP enzyme activity during chemotherapy was assessed by measuring the difference between the metabolic ratios from after chemotherapy to before chemotherapy. Differences greater than 1.25-fold for each individual participant, were categorised as clinically meaningful changes in CYP activity; as guided by the United States (US) Food and Drug Administration (FDA) *in vivo* drug metabolism and drug interaction study recommendations [332].

2.11 Statistical analysis

Data analysis was performed in GraphPad Prism Version 5.01. Normal distribution of data was assumed for cell culture studies (Chapter 3 and Chapter 4), as normality testing is not able to be performed on low replicate numbers. Non-normal distribution of patient study data (Chapter 5) was assumed based on the inherent variability associated with clinical data, and thus, non-parametric testing was performed. Statistical significance was considered as a p-value < 0.05.

2.11.1 Cell culture analysis

Mean and standard error of the mean (SEM) were calculated for data from independent replicate experiments. Statistical significance between control and manipulation experiments were tested by paired and unpaired two-tailed T-testing, One-way ANOVA with Tukey's Multiple Comparison Testing, and Two-way ANOVA with *post-hoc* Bonferroni correction. Correlations were evaluated using the Pearson's correlation coefficient. IC50 concentrations of chemotherapeutic agents were determined from non-linear fit dose-response curves that were fitted using the four parameter variable slope model.

2.11.2 Patient study analysis

Median values were calculated for patient study data. Statistical significance between paired data was determined by Wilcoxon matched-pairs signed rank testing. Mann Whitney U testing was used for the comparison of unpaired data. Serum cytokine concentrations throughout chemotherapy were compared to baseline using the Kruskal-Wallis test. Correlational data was evaluated using the Spearman's correlation coefficient.

Chapter 3

Transwell co-culture with human breast adipocytes alters the proteome of human breast cancer cells

Results presented in this chapter have been published in:

Crake, RLI., Phillips, E., Kleffmann, T., and Currie, MJ. Co-culture with human breast adipocytes differentially regulates protein abundance in breast cancer cells; Cancer Genomics & Proteomics *16*: 319-332, 2019

3.1 Introduction

Cancer associated adipocytes (CAA) within the breast tumour microenvironment have been shown to promote breast cancer cell migration, invasion and resistance to therapy [116,150]. Previous research has assessed potential mechanisms by which local CAA may be influencing breast cancer progression [245,248,250], however, the precise mechanisms by which the CAA-breast cancer cell crosstalk supports breast cancer development has not yet been determined.

Transwell co-culture and microarray analyses assessing CAA-induced alterations in breast cancer cell gene expression have identified a number of important gene alterations [245,263]. Yet, regulation of global breast cancer cell protein abundance caused by proximal CAA remains to be investigated. Assessment of protein abundance changes in breast cancer cells interacting with CAA may introduce novel mechanistic links, not evident in microarray analyses, with more relevance to clinically advancing breast cancer phenotypes. Therefore, it was hypothesised that *in vitro* co-culture with CAA differentially regulates protein abundance

in breast cancer cells, and alterations in key molecules and pathways may highlight mechanisms responsible for the CAA-induced promotion of progressive breast tumours.

Global protein abundance differences have been previously determined in four human breast cancer cell lines grown alone *in vitro*, using isobaric tags for relative and absolute quantification (iTRAQ) labels and tandem mass spectrometry (MS/MS) [333]. Relative expression changes were determined by comparing protein expression to a normal breast cell line, identifying a total of 1,020 proteins from which potential biomarkers and pathways associated with breast cancer were identified [333]. The main advantage for the use of iTRAQ labelling in discovery mass spectrometry is the identification and quantification of cell or tissue lysate proteomes in up to eight samples simultaneously [334].

iTRAQ labelling and tandem mass spectrometry were utilised in the current investigation to identify and quantify differential *global* protein abundance in MCF-7 and MDA-MB-231 breast cancer cells co-cultured with CAA *in vitro*, compared to control breast cancer cells cultured alone. To account for disease heterogeneity associated with breast tumour molecular subtypes, this study utilised breast cancer cell lines from two different molecular subgroups.

3.1.1 Aims

The aim of this chapter was to profile global protein abundance differences in ER positive (MCF-7) and hormone receptor negative (MDA-MB-231) human breast cancer cells cultured alone or co-cultured with CAA isolated from human breast adipose tissues, and identify key molecules and pathways regulated by CAA. This was approached by:

1) Culturing MCF-7 and MDA-MB-231 breast cancer cells in transwell co-culture with or without mature breast adipocytes (CAA) that were differentiated from preadipocytes isolated from human breast adipose tissue samples (Section 3.2.1).
2) Determining CAA-induced protein abundance differences in MCF-7 and MDA-MB-231 breast cancer cells by measuring protein levels using iTRAQ labelling and mass spectrometry in co-cultured and control breast cancer cells (Section 3.2.2).
3) Assessing differentially regulated proteins to identify enrichment of particular cellular components and pathways in MCF-7 and MDA-MB-231 breast cancer cells co-cultured with CAA, using bioinformatic analysis (Section 3.2.3).

4) Validating protein abundance differences quantified by mass spectrometry in selected candidate proteins using Western blotting analysis (Section 3.2.4).

3.1.2 Experimental approach

The isolation and differentiation of human breast adipocytes is shown in Figure 3.1, and the overall experimental workflow for this study chapter is depicted in Figure 3.2.

Effect of CAA co-culture on enrichment of cellular components and pathways in MCF-7 and MDA-MB-231 cells, were assessed using protein annotation through evolutionary relationship (PANTHER) classification systems by gene list analysis of the co-culture/control iTRAQ ratios (Section 3.2.3; detailed methodology described in Chapter 2; Section 2.9.1).

For all Western blotting in this study chapter, samples were normalised to total protein by BCA assay (Chapter 2; Section 2.2.5.1). Relative protein levels were determined by measuring band densities with ImageJ (Version 1.49), normalising the densities to a loading control, and comparing the normalised densities to controls.

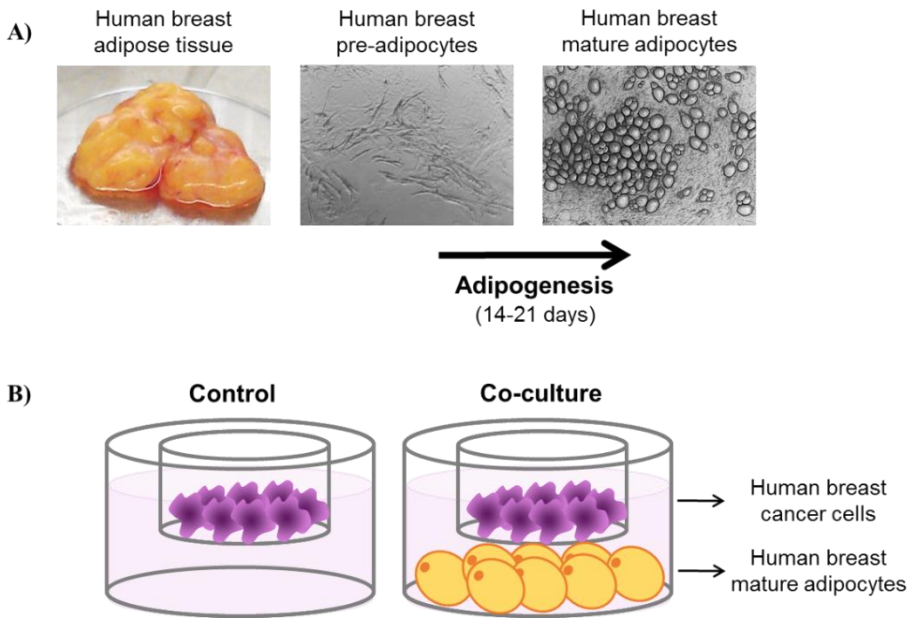

Figure 3.1. Transwell co-culture of human breast cancer cells and human breast adipocytes.
A) Human breast adipose tissue was processed to isolate pre-adipocytes. Specialised media was used to promote adipogenesis (differentiation into mature adipocytes) *in vitro*, over 14-21 days (described in detail in Chapter 2; Section 2.1). B) Schematic of MCF-7 or MDA-MB-231 human breast cancer cells (purple; inside insert) that were either cultured alone (control) or with mature breast adipocytes (yellow; bottom well; co-culture) for 72 hours, then breast cancer cells were isolated for analysis using LC/MS/MS and Western blotting.

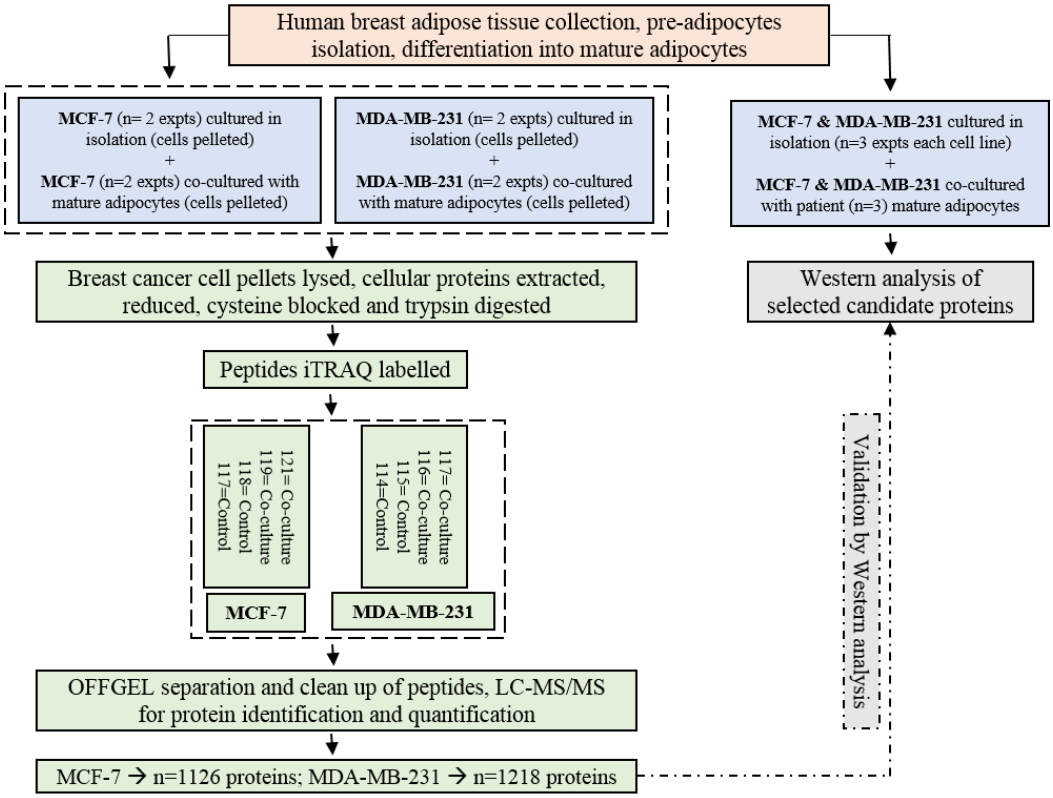

Figure 3.2. Workflow used to assess global protein abundance in MCF-7 and MDA-MB-231 breast cancer cells cultured alone or in co-culture with mature breast adipocytes (cancer associated adipocytes [CAA]).
Initially, human breast adipose tissues were processed to isolate pre-adipocytes, and pre-adipocytes were differentiated *in vitro* to mature adipocytes (orange boxes). Mature breast adipocytes were used in transwell co-culture with MCF-7 and MDA-MB-231 breast cancer cells (depicted here by blue boxes, and described in detail in Chapter 2; Section 2.3). Protein was extracted from breast cancer cells from two separate experiments; one experiment assessed global protein abundance using iTRAQ labelling and mass spectrometry (depicted here by green boxes, and described in detail in Chapter 2; Section 2.4), and the second used Western blotting analysis to validate candidate proteins (depicted here by grey boxes, and described in detail in Chapter 2; Section 2.8).

3.1.3 Acknowledgments

I would like to thank Dr Torsten Kleffmann, and other members of the Centre for Protein Research laboratory (University of Otago), for their help and expertise in developing the protein sample preparation protocol for iTRAQ mass spectrometry, performing mass spectrometry analysis, and their guidance with analysing the mass spectrometry data. Breast adipose tissue samples and matching clinicopathological data were provided by the Cancer Society Tissue Bank Christchurch (CSTBC).

3.2 Results

3.2.1 Clinicopathological data associated with human breast adipose tissue samples used in this study

Overall, this study used breast adipose tissue isolated from seven donors (Table 3.1). The donors ranged in age from 35-81 years, ranged in BMI from 23.3-41.4, and stated their ethnicity as NZ European (n= 5), Māori (n= 1), or Russian (n= 1) (Table 3.1). All seven donors had a mastectomy for breast cancer (Table 3.1). All donors were diagnosed with stage II or III invasive ductal carcinoma (IDC), and two received neoadjuvant chemotherapy prior to surgery (Table 3.1). All breast adipose tissues were sampled from the same breast as the tumour (Table 3.1).

For assessment of global protein abundance by mass spectrometry, mature adipocytes from four separate breast adipose tissue samples were co-cultured with human breast cancer cells (n= 2 with MCF-7 cells, and n= 2 with MDA-MB-231 cells) (Table 3.1). The remaining three breast adipose tissue samples had mature adipocytes co-cultured with both breast cancer cell lines (n= 3 with MCF-7, and n= 3 with MDA-MB-231 cells), and relative expression of candidate proteins were measured by Western blotting analysis (Table 3.1).

Mature adipocytes differentiated from breast adipose tissue samples are depicted in Figure 3.3. Microscopic examination of these adipocytes showed that the mature adipocytes used in the co-culture experiments were mostly multilocular, containing multiple lipid vacuoles per cell (Figure 3.3). A number of unilocular (cells with a single lipid vacuole) mature adipocytes were present in breast adipose tissue samples from donors 076 and 078 (Figure 3.3).

Table 3.1. Clinicopathological data for the donors and breast adipose tissue samples used for co-culture with human breast cancer cells.

Sample	Age	Ethnicity	BMI	Surgery	Previous Treatment	Breast Cancer*	Histological Type	Stage	Experiment (Cell line**)
AT 076	61	Russian	27.8	Mastectomy	None	Yes	IDC NST	IIB	Mass spectrometry (MDA-MB-231)
AT 078	35	Maori	41.4	Mastectomy	None	Yes	IDC NST	IIB	Mass spectrometry (MDA-MB-231)
AT 079	76	NZ European	28.8	Mastectomy	None	Yes	IDC NST	IIIC	Mass spectrometry (MCF-7)
AT 080	75	NZ European	31.8	Mastectomy	Neoadj chemo	Yes	IDC NST	IIIC	Mass spectrometry (MCF-7)
AT 086	43	NZ European	23.3	Mastectomy	Neoadj chemo	Yes	IDC NST	IIB	Western validation (MCF-7 & MDA-MB-231)
AT 087	72	NZ European	25	Mastectomy	None	Yes	IDC Basal-like	IIA	Western validation (MCF-7 & MDA-MB-231)
AT 089	81	NZ European	25.8	Mastectomy	None	Yes	IDC NST	IIIA	Western validation (MCF-7 & MDA-MB-231)

AT: adipose tissue; **BMI**: body mass index; **DCIS**: ductal carcinoma in situ; **IDC**: invasive ductal carcinoma; **NST**: no special type; **Neoadj chemo**: Neoadjuvant chemotherapy (chemotherapy given before breast cancer surgery).
*Breast tumour was located in the same breast as the adipose tissue was sampled from (Yes/No).
**Human breast cancer cell line used for co-culture with the breast adipose tissue sample.

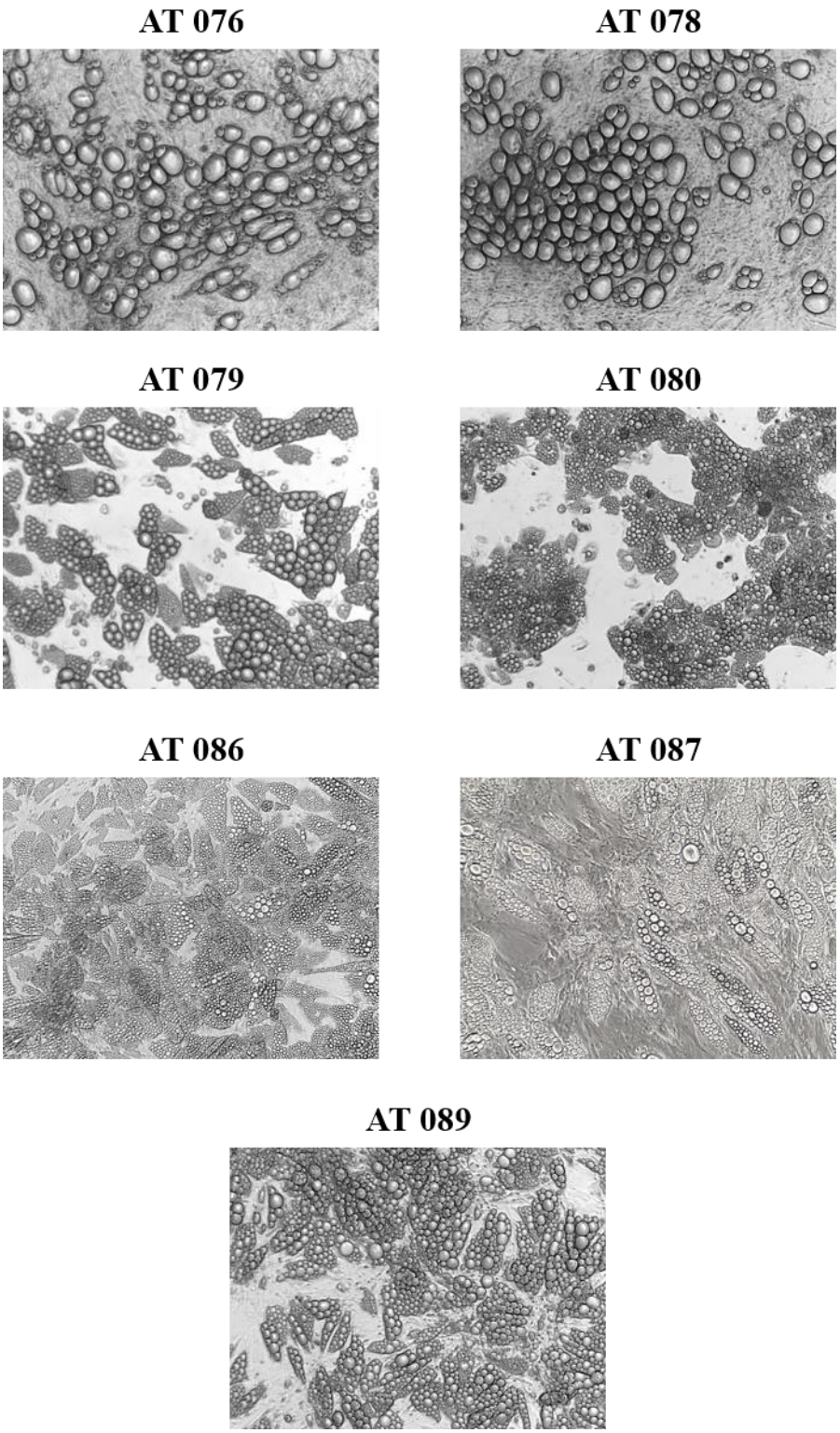

Figure 3.3. Mature breast adipocytes used for co-culture experiments.
Representative images of mature adipocytes differentiated from human breast adipose tissue pre-adipocytes (10X magnification) from each of the breast adipose tissue (AT) samples used. Images were taken prior to transwell co-culture with MCF-7 and/or MDA-MB-231 human breast cancer cell lines.

3.2.2 Effect of co-culture with CAA on MCF-7 and MDA-MB-231 breast cancer cell protein abundance

For the MCF-7 mass spectrometry experiment, the 118 iTRAQ label signal (control MCF-7 cells) was much higher than the 117 (control MCF-7 cells), 119 (co-cultured MCF-7 cells), and 121 (co-cultured MCF-7 cells) label signals. In addition, searching peak lists on Sequest HT observed similar co-culture/control ratios for 119 and 121 (co-culture) against 117 (control), whether or not the 118 label peaks were considered in the search (data not shown). As a consequence, the 118 tag signals were removed from the analysis to avoid interference with data normalisation.

3.2.2.1 Distribution of protein abundance changes for all identified proteins

In total, 1,126 proteins and 1,218 proteins were identified in both control and co-cultured MCF-7 and MDA-MB-231 breast cancer cells respectively, by using iTRAQ labelling and discovery mass spectrometry (Supplementary data provided at https://www.otago.ac.nz/mackenzie-cancer/research/otago715163.html).

Relative protein abundance differences or fold change values between co-cultured and control cells for each identified protein were quantified by assessing all of the co-culture/control iTRAQ ratio combinations for each cell line, including 119/117 and 121/117 for MCF-7 cells, and 116/114, 116/115, 117/114, and 117/115 for MDA-MB-231 cells.

Comparing the distribution of the average fold change for each identified protein showed that the majority of the identified proteins were similarly expressed in CAA co-cultured MCF-7 and MDA-MB-231 cells compared with controls (Figure 3.4). The median of the average fold change values for all proteins identified in MCF-7 and MDA-MB-231 cells were -0.029 and -0.003, respectively (data not shown). Similar fold changes between co-culture and control were reported for MCF-7 and MDA-MB-231 co-culture experiments using adipocytes isolated from individual breast adipose tissue samples ($p>0.05$; Figure 3.5), suggesting that the effects of CAA activity on protein abundance was not likely to be adipose tissue/patient specific.

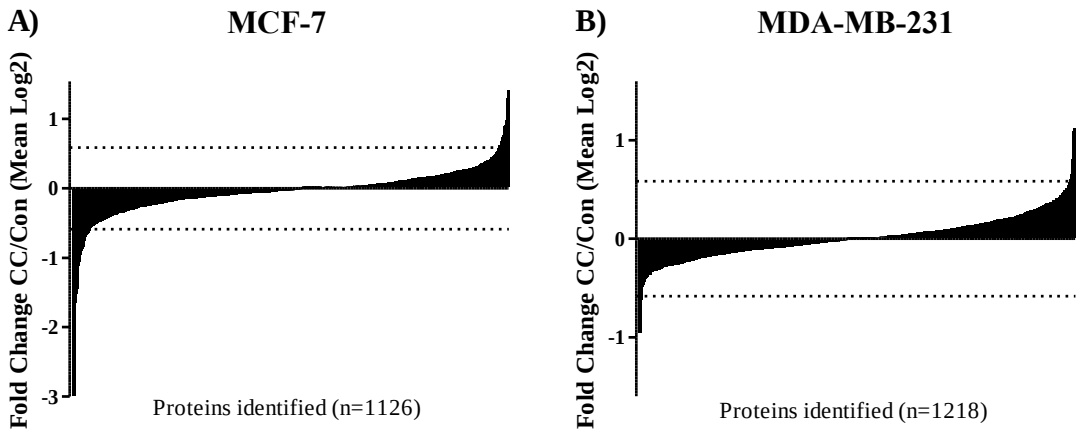

Figure 3.4. Distribution of the iTRAQ ratios identified and quantified by mass spectrometry in co-cultured compared to control MCF-7 and MDA-MB-231 breast cancer cells.

The average co-culture (CC; co-cultured with CAA for 72 hours) versus control (Con; cultured alone for 72 hours) ratios (log2) for all the proteins identified in A) MCF-7 cells (1,126 proteins) and B) MDA-MB-231 cells (1,218 proteins) with each black vertical bar representing an identified protein, and horizontal dotted lines representing fold change (FC) values of 1.5 (log2).

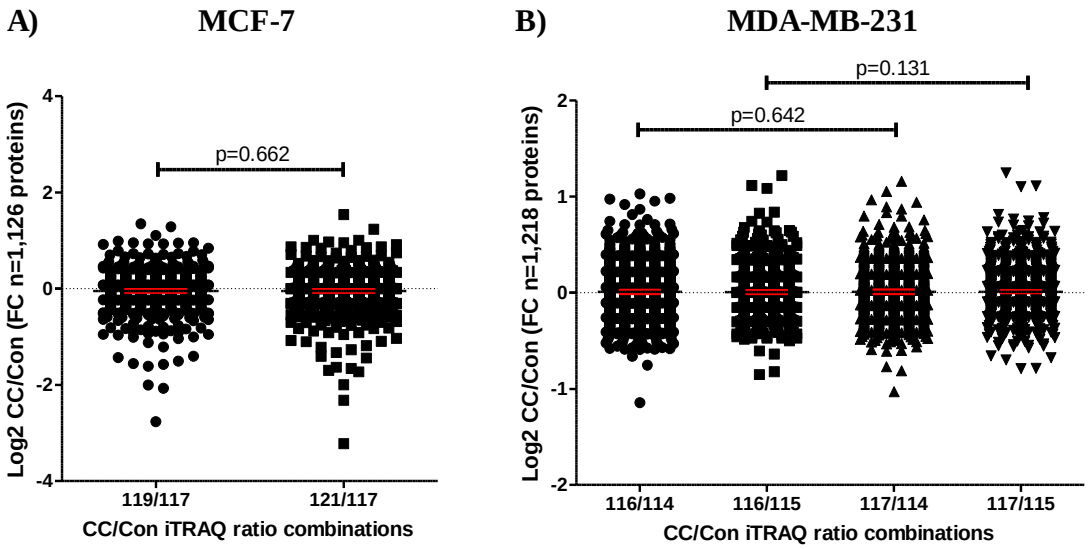

Figure 3.5. Fold change values for each protein identified by iTRAQ mass spectrometry in co-cultured compared to control breast cancer cells.

Fold change values were the change in protein abundance between CAA co-cultured and control A) MCF-7 and B) MDA-MB-231 breast cancer cells (log2), for the 1,126 and 1,218 proteins that were identified, respectively. Horizontal black dotted line represents no difference in protein abundance between co-culture and control. Red error bars represent mean ± SEM. Statistical significance was evaluated by paired t-tests; p-values < 0.05 were considered statistically significant.

3.2.2.2 Differentially abundant proteins

To determine the proteins that were differentially regulated by co-culture with CAA in MCF-7 and MDA-MB-231 breast cancer cells this study selected those proteins that had at least one iTRAQ ratio that was 1.5-fold or greater (upregulated or downregulated) in co-cultured compared to control cells; co-culture/control ratios are presented as the log base 2 (log2) of the fold change.

Eighty five out of 1,126 (7.55%) proteins in MCF-7, and 63 out of 1,218 (5.17%) proteins in MDA-MB-231, were differentially expressed in co-cultured compared to control cells (Figure 3.6). Of these differentially expressed proteins, more were downregulated (n= 53) than upregulated (n= 32) in MCF-7 cells (Figure 3.6A), whereas more were upregulated (n= 51) than downregulated (n= 12) in MDA-MB-231 cells (Figure 3.6B).

Three proteins, phosphoglycerate kinase 1 (PGK1), lysosomal protective protein (PPGB), and vacuolar protein sorting-associated protein 35 (VPS35) were differentially regulated in co-cultured versus control cells by 1.5-fold or greater in both MCF-7 and MDA-MB-231 cell lines (Table 3.2). However, PGK1 was the only upregulated protein in both cell lines, whereas PPGB and VPS35 were downregulated in MCF-7 cells but upregulated in MDA-MB-231 cells (Table 3.2).

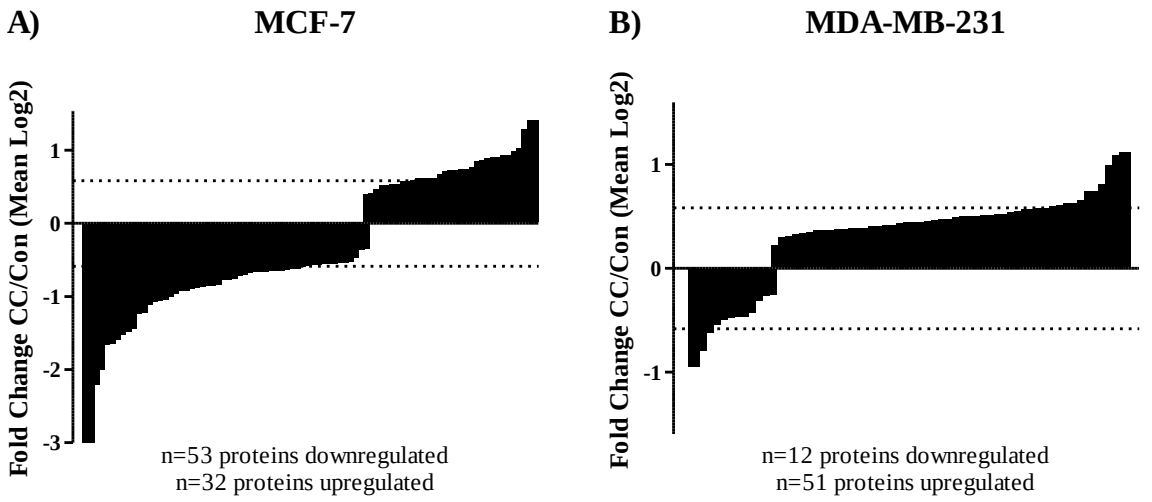

Figure 3.6. Distribution of differentially regulated proteins identified and quantified in co-cultured compared to control MCF-7 and MDA-MB-231 breast cancer cells.
The average co-culture (CC; co-cultured with CAA for 72 hours) versus control (Con; cultured alone for 72 hours) ratios (log2) for all the proteins quantified as having at least one CC/Con ratio greater than 1.5-fold (either upregulated or downregulated) in A) MCF-7 cells (85 proteins) and B) MDA-MB-231 cells (63 proteins). Of the differentially expressed proteins, n= 53/85 were downregulated in MCF-7, whereas n= 51/63 proteins were upregulated by more than 1.5-fold in MDA-MB-231 cells. Vertical black bars represent different proteins and horizontal dotted lines represent fold change values of 1.5 (log2).

Table 3.2. Proteins with an abundance difference of 1.5-fold or greater in both MCF-7 and MDA-MB-231 cells after co-culture with CAA.

UniProt ID	Protein Name	MCF-7 CC/Con (FC log2)*	MDA-MB-231 CC/Con (FC log2)*
P00558	Phosphoglycerate Kinase 1 (PGK1)	0.532	0.565
P10619	Lysosomal Protective Protein (PPGB)	-0.662	0.466
Q96QK1	Vacuolar protein sorting-associated protein 35 (VPS35)	-0.344	0.365

CC: Co-culture, **Con:** Control; **FC:** Fold change.
*Average difference in relative protein abundance (log2) between co-culture and control MCF-7 and MDA-MB-231 breast cancer cells.

3.2.2.3 Top 20 most differentially abundant proteins

Lists of the top 20 most differentially regulated proteins (excluding keratin proteins) in MCF-7 and MDA-MB-231 cells following transwell co-culture with CAA are presented in Table 3.3 and Table 3.4. Of the 20 most differentially regulated proteins, 17 were downregulated in MCF-7 cells (Table 3.3), whereas 16 were upregulated in MDA-MB-231 cells (Table 3.4).

In MCF-7 cells, trefoil factor 1 (TFF1) exhibited the largest increase of all the identified proteins (log2 fold change= 1.410), and the S100 calcium-binding proteins A4 and A6 (S100-A4 and S100-A6) were the two most downregulated proteins (log2 fold change= -2.199 and -2.995, respectively) (Table 3.3). Three of the top 20 most differentially regulated proteins in MCF-7 cells were annexin proteins, including annexin A2 (ANXA2; log2 FC= -1.041), annexin A5 (ANXA5; log2 FC= -1.218), and annexin A6 (ANXA6; log2 FC= -1.054); all downregulated by co-culture with CAA (Table 3.3).

The most upregulated and downregulated proteins in MDA-MB-231 cells co-cultured with CAA were myeloid-associated differentiation marker (MYADM; log2 fold change= 1.118) and 4F2 cell-surface antigen heavy chain (4F2; log2 fold change= -0.952), respectively (Table 3.4). PGK1, upregulated in both MCF-7 and MDA-MB-231 cells (Section 3.2.2.2), was one of the top 20 differentially regulated proteins in MDA-MB-231 cells, upregulated on average by 1.48-fold (log2 fold change: 0.565) (Table 3.4).

Table 3.3. The top 20 proteins organised from most upregulated to most downregulated based on fold change (FC) in MCF-7 cells co-cultured with mature breast adipocytes.

UniProt ID	Protein	Protein Description	Length[a]	Unique Peptides[b]	logFC[c]	Abundance Variability[d]
P04155	TFF1	Trefoil factor 1 (Breast cancer oestrogen-inducible protein)	84	2	1.410	30.8
P16615	AT2A2	Sarcoplasmic/endoplasmic reticulum calcium ATPase 2	1042	2	1.291	100.35
Q5JPE7	NOMO2	Nodal modulator 2	1267	3	0.980	18.4
Q03135	CAV1	Caveolin-1	178	4	-0.962	33.2
Q99439	CNN2	Calponin-2	309	3	-1.008	85.45
P07355	ANXA2	Annexin A2	339	19	-1.041	9.95
P08133	ANXA6	Annexin A6	673	17	-1.054	37
Q15417	CNN3	Calponin-3	329	2	-1.071	95.4
P09211	GSTP1	Glutathione S-transferase P	210	5	-1.108	54.1
P08758	ANXA5	Annexin A5	320	15	-1.218	3.3
P48509	CD151	CD151 antigen (Membrane glycoprotein SFA-1)	253	2	-1.23	24.6
Q9H299	SH3L3	SH3 domain-binding glutamic acid-rich-like protein 3	93	5	-1.438	34.7
P84074	HPCA	Neuron-specific calcium-binding protein hippocalcin	193	2	-1.48	28.75
P21980	TGM2	Protein-glutamine gamma-glutamyltransferase 2	687	10	-1.519	40.35
P50453	SPB9	Serpin B9 (Cytoplasmic antiproteinase 3)	376	2	-1.586	47.4
P16070	CD44	CD44 antigen (Extracellular matrix receptor III)	742	4	-1.653	44.8
P09382	LEG1	Galectin-1	135	7	-1.656	22.15
P08670	VIME	Vimentin	466	22	-2.003	60.7
P26447	S10A4	Protein S100-A4 (Calvasculin) (Metastasin)	101	4	-2.199	109.15
P06703	S10A6	Protein S100-A6	90	3	-2.995	26.5

[a] Amino acid residues; [b] Number of unique peptides identified based on a FDR of < 1%; [c] Log of the average co-culture / control ratios (fold change); [d] Variability of the peptide ratios as a percentage (normalised measure of the peptide ratio spread).

Table 3.4. The top 20 proteins organised from most upregulated to most downregulated based on fold change (FC) in MDA-MB-231 cells co-cultured with mature breast adipocytes.

UniProt ID	Protein	Protein Description	Length[a]	Unique Peptides[b]	logFC[c]	Abundance Variability[d]
Q96S97	MYADM	Myeloid-associated differentiation marker	322	3	1.118	6.33
Q92597	NDRG1	Protein NDRG1 (Differentiation-related gene 1 protein)	394	5	1.093	9.87
Q04941	PLP2	Proteolipid protein 2	152	2	0.996	16.95
O15427	MOT4	Monocarboxylate transporter 4	465	3	0.804	19.47
O75976	CBPD	Carboxypeptidase D	1380	6	0.74	16.21
P48651	PTSS1	Phosphatidylserine synthase 1	473	2	0.739	22.57
O95479	G6PE	GDH/6PGL endoplasmic bifunctional protein	791	2	0.656	9.28
P04233	HG2A	HLA class II histocompatibility antigen gamma chain (CD74)	296	3	0.628	9.43
P40261	NNMT	Nicotinamide N-methyltransferase	264	5	0.624	29.75
Q99961	SH3G1	Endophilin-A2	368	3	0.604	17.95
Q8IV08	PLD3	Phospholipase D3	490	5	0.59	24.16
P13674	P4HA1	Prolyl 4-hydroxylase subunit alpha-1	534	7	0.576	21.21
P14854	CX6B1	Cytochrome c oxidase subunit 6B1	86	2	0.573	5.07
Q9Y237	PIN4	Peptidyl-prolyl cis-trans isomerase NIMA-interacting 4	131	2	0.567	35.36
P00558	PGK1	Phosphoglycerate kinase 1	417	24	0.565	4.25
P26885	FKBP2	Peptidyl-prolyl cis-trans isomerase FKBP2	142	3	0.546	7.41
Q15003	CND2	Condensin complex subunit 2	741	2	-0.544	15.76
Q9Y570	PPME1	Protein phosphatase methylesterase 1	386	6	-0.62	12.6
O00622	CYR61	Protein CYR61 (Cysteine-rich angiogenic inducer 61)	381	3	-0.795	28.47
P08195	4F2	4F2 cell-surface antigen heavy chain	630	6	-0.952	13.22

[a] Amino acid residues; [b] Number of unique peptides identified based on a FDR of < 1%; [c] Log of the average co-culture / control ratios (fold change); [d] Variability of the peptide ratios as a percentage (normalised measure of the peptide ratio spread).

3.2.3 Effects of CAA on pathway and cellular component enrichment in MCF-7 and MDA-MB-231 breast cancer cells

3.2.3.1 Enriched pathways

There were 584 proteins (from 1,126 proteins in total) and 554 proteins (from 1,218 proteins in total) differentially regulated by 1.1-fold or greater in MCF-7 and MDA-MB-231 cells co-cultured with CAA compared to controls, respectively (data not shown). The enrichment of pathways relating to proteins that were differentially regulated by 1.1-fold or greater, the direction of regulation (upregulated or downregulated), and the corresponding proteins associated with these pathways, are presented for MCF-7 and MDA-MB-231 cells in Table 3.5 and Table 3.6, respectively.

Three pathways were significantly enriched for differential regulation in MCF-7 cells including tricarboxylic acid (TCA) cycle, ubiquitin proteasome, and Huntington Disease (Table 3.5). MDA-MB-231 cells exhibited significant enrichment of four pathways, including glycolysis, *de novo* purine biosynthesis, ubiquitin proteasome, and Parkinson Disease (Table 3.6).

The enriched TCA cycle in MCF-7 cells, and glycolysis pathway in MDA-MB-231 cells, were the only pathways with all associated proteins upregulated by co-culture with CAA (Table 3.5 and Table 3.6). Abundance of glycolytic and TCA cycle proteins in CAA co-cultured MCF-7 and MDA-MB-231 cells are depicted in Figure 3.7; determined from full protein identification and quantification lists (Supplementary data provided at https://www.otago.ac.nz/mackenzie-cancer/research/otago715163.html). Increased expression of TCA cycle proteins in MCF-7 cells co-cultured with CAA included citrate synthase (CS), isocitrate dehydrogenase 2 and 3G (IDH2, IDH3G), 2-oxoglutarate dehydrogenase (OGDH), dihydrolipoyllysine-residue succinyltransferase component of 2-oxoglutarate dehydrogenase complex (DLST), succinate dehydrogenase B (SDHB), fumarate hydratase (FH) and malate dehydrogenase (MDH2) (Figure 3.7). Upregulated expression of glycolytic proteins in MDA-MB-231 cells co-cultured CAA included ATP-dependent 6-phosphofructokinase liver type (PFKL), ATP-dependent 6-phosphofructokinase platelet type (PFKP), fructose-bisphosphate aldolase A (ALDOA), triosephosphate isomerase (TPI1), phosphoglycerate kinase 1 (PGK1) and enolase 2 (ENO2) (Figure 3.7).

The ubiquitin proteasome pathway was commonly enriched in both MCF-7 and MDA-MB-231 cells co-cultured with CAA, in which the majority of the associated proteins were

26S proteasome subunit proteins, and were downregulated during co-culture. The component of the eukaryotic translation initiation factor 3 complex (EIF3F) required for initiation of protein synthesis was downregulated in both cell lines. MCF-7 cells predominantly downregulated the 19S regulatory particle subunit proteins, whereas MDA-MB-231 decreased expression of both 19S and 20S subunit proteins. Proteins involved in *de novo* purine biosynthesis were differentially regulated in MDA-MB-231 cells co-cultured with CAA, with upregulation and downregulation occurring within this pathway.

Table 3.5. Enriched cellular pathways in the complement of proteins that were found differentially regulated in MCF-7 cells co-cultured with CAA.

PANTHER Pathway*	Upregulated Proteins[a**]	Downregulated Proteins[b**]
TCA Cycle	FH, OGDH, CS, DHTKD1	-
Ubiquitin Proteasome	PSMD14, UCHL5	EIF3F, PSMC4, PSMD8, PSMD1, PSMD6, PSMD12, PSMD9, UBE2D3, UBE2N
Huntington Disease	ARF5, CYC1, GAPDH, CLTB	DCTN1, CLTA, BAX, ARF6, ARPC5, CAPN1, CAPN2, VAT1, TUBB6

[a] Proteins increased by 1.1-fold or greater in MCF-7 and MDA-MB-231 cells following transwell co-culture with mature adipocytes; [b] Proteins decreased by 1.1-fold or greater in MCF-7 and MDA-MB-231 cells following transwell co-culture with mature adipocytes; *PANTHER pathways recognised as significantly enriched ($p<0.05$). **Proteins are represented by gene names as reported by UniProtKB.

Table 3.6. Enriched cellular pathways in the complement of proteins that were found differentially regulated in MDA-MB-231 co-cultured with CAA.

PANTHER Pathway*	Upregulated Proteins[a**]	Downregulated Proteins[b**]
Glycolysis	ALDOA, PGK1, ENO2, TPI1, PFKL	-
De novo purine biosynthesis	AK4, AK2, CMPK1	ADSL, PPAT, GART, NME2, IMPDH2
Ubiquitin proteasome	UBE2L3	EIF3F, PSMC1, PSMC4, PSMC3, PSMD11, PSMD13, PSMD7
Parkinson disease	YWHAG, NDUFV2, UBE2L3, YWHAZ, GRP78, PSMB10, YWHAB, SFN	MAPK1, PSMA5, PSMD13, PSMB3, CSNK2A1, FYN, PSMA3, PSMA6, HSPA8, PSMB7

[a] Proteins increased by 1.1-fold or greater in MCF-7 and MDA-MB-231 cells following transwell co-culture with mature adipocytes; [b] Proteins decreased by 1.1-fold or greater in MCF-7 and MDA-MB-231 cells following transwell co-culture with mature adipocytes; *PANTHER pathways recognised as significantly enriched ($p<0.05$). **Proteins are represented by gene names as reported by UniProtKB.

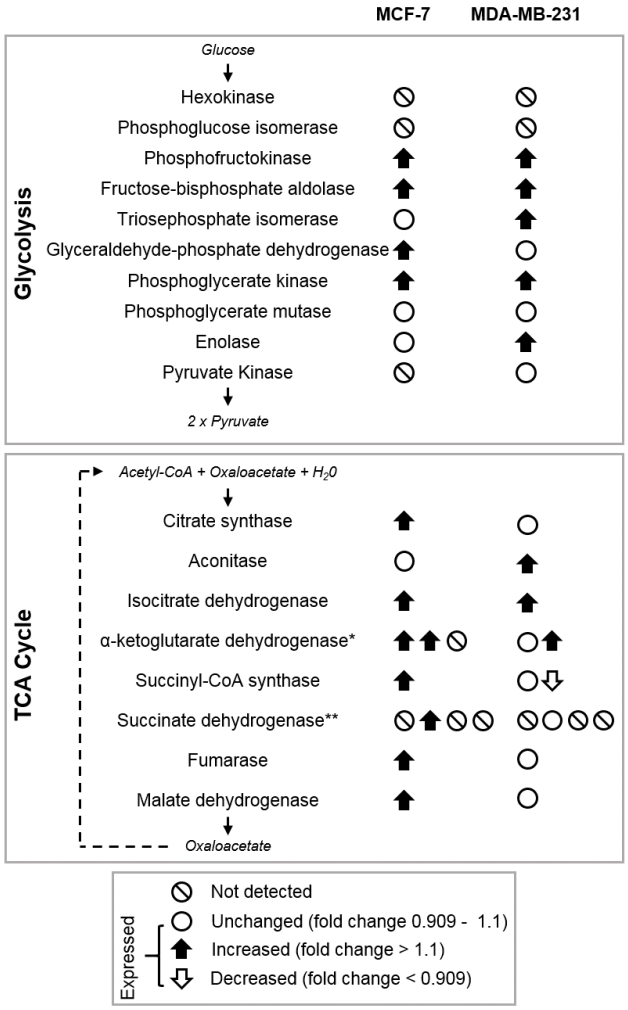

Figure 3.7. Schematic showing that MCF-7 and MDA-MB-231 breast cancer cells upregulate enzymes of glycolysis and TCA cycle after co-culture with CAA.
iTRAQ LC-MS/MS protein abundance data and bioinformatic analysis indicated an enriched upregulation of TCA cycle and glycolysis pathway proteins in MCF-7 and MDA-MB-231 breast cancer cells after co-culture with CAA. Up and down arrows represent enzymes with abundance changes greater than 10%, and the direction of regulation (increased or decreased) compared to control breast cancer cells. White circles show enzymes that were detected but not differentially regulated following co-culture. White circles with black lines are enzymes undetected in this study. *Complex comprising three subunits: *OGDH, DLST* and *DLD,* respectively. **Complex comprising four subunits*: SDHAF2, SDHB, SDHC* and *SDHD,* respectively. Complex subunits are gene names as reported by UniProtKB.

3.2.3.2 Cellular components

To assess cellular components from which proteins were enriched, this study included all proteins identified in CAA co-cultured and control MCF-7 (n= 1,126 proteins) and MDA-MB-231 (n= 1,218 proteins) cells.

Similar cellular components were enriched in both MCF-7 and MDA-MB-231 cells co-cultured alone or with CAA, mostly pertaining to intracellular cytoplasmic, organelle and macromolecular complexes (Figure 3.8). Enriched components within these orders were proteins from the nucleus and nuclear structures, as well as cell cytoskeletal, ribosomal and protein complexes.

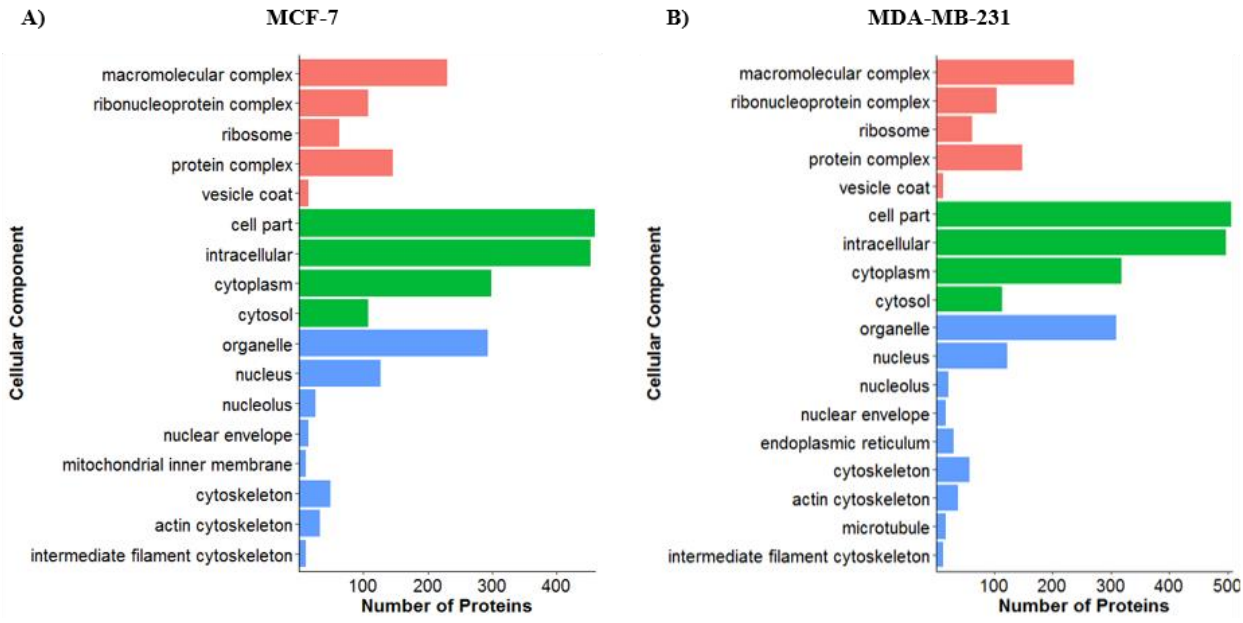

Figure 3.8. Cellular components significantly enriched in breast cancer cells after transwell co-culture with adipocytes.
Cellular components significantly enriched from the lists of identified proteins in A) CAA-MCF-7 and B) CAA-MDA-MB-231 are grouped under the parent classifications; macromolecular complexes (red), cell parts (green), and organelles (blue). Component hierarchy runs from top to bottom within each parent classification. Identification of cellular components using bioinformatic analysis was performed using the PANTHER classification system (Version 12.0) and statistical over-representation testing ($p<0.05$).

3.2.4 Validation of mass spectrometry results by Western blot analysis

To validate mass spectrometry results, Western blot analysis was used to determine the relative protein abundance of n-myc downstream regulated 1 (NDRG1), phosphoglycerate kinase 1 (PGK1) and trefoil factor 1 (TFF1) in CAA co-cultured compared to control MCF-7 and MDA-MB-231 cells. These three candidate proteins were selected based on differential abundance in either or both MCF-7 and MDA-MB-231, their relevance to breast cancer and the availability of well-characterised primary antibodies. In MCF-7 cells co-cultured with CAA, the densitometry for NDRG1 represents the sum of both bands.

In concordance with the iTRAQ quantification, PGK1 and TFF1 showed increased expression in MCF-7 cells, when measured by Western blotting (fold change: PGK1= 1.551 and TFF1= 2.856) (Figure 3.9A and C). Similarly, NDRG1 and PGK1 were increased in CAA-MDA-MB-231 cells, validating the iTRAQ results (fold change: NDRG1= 4.632 and PGK1= 1.547) (Figure 3.9B and D). However, the NDRG1 upregulation was more than 2-fold higher when measured by Western blot analysis compared to the iTRAQ quantification (NDRG1= 2.137) (Figure 3.9B and D). As expected, mass spectrometry did not detect TFF1 expression in hormone receptor negative MDA-MB-231 cells, and this was validated by Western blot analysis (Figure 3.9B and D). The only discordance was NDRG1 fold change measured in MCF-7 cells, showing an upregulation by Western blot analysis (fold change: 2.193), but no change in expression by iTRAQ quantification (fold change: 0.952) (Figure 3.9A and C). Furthermore, in accordance with the findings of the iTRAQ measurements, the fold changes measured by Western blot analysis for PGK1 and TFF1 candidate proteins remained consistent across the replicates, whereas the fold changes for NDRG1 were more variable (Figure 3.9A and B).

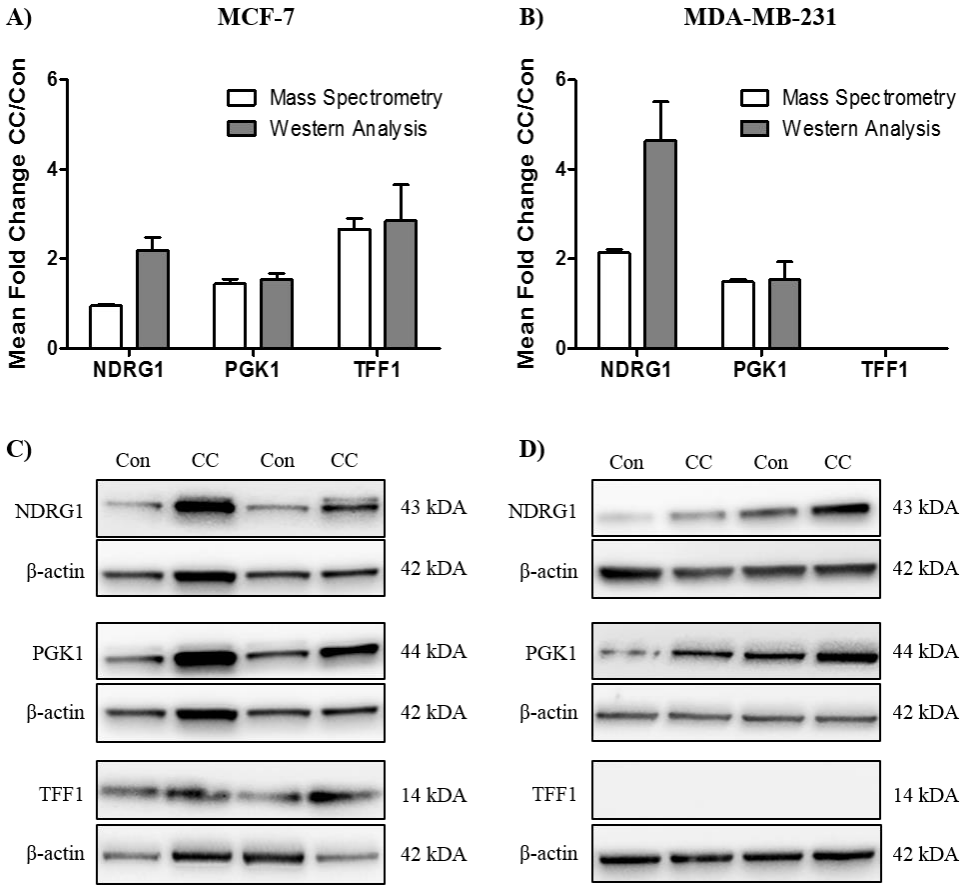

Figure 3.9. Validation of candidate protein abundance by Western blot analysis.
A and B) The average fold change in protein abundance in co-culture (CC) compared to control (Con) MCF-7 and MDA-MB-231 cells, for each candidate protein (NDRG1, PGK1 and TFF1) as measured by iTRAQ LC-MS/MS (white; 4-plex experimental with n= 2 co-culture and n= 2 controls) and Western blot analysis (grey; n= 3 co-culture/control). Data is presented as mean ± SEM. C and D) Representative Western blots for the abundance measurement of PGK1, TFF1 and NDRG1 in MCF-7 and MDA-MB-231 cells grown alone or in co-culture with CAA for 72 hours.

3.3 Discussion

The complex reciprocal communication between breast cancer cells and mature breast adipocytes has pro-tumorigenic consequences [150,251]. However, the processes causing CAA-related breast cancer pathogenesis have not been fully elucidated. Thus, studies investigating proteomic and phenotypic changes in breast cancer cells interacting with CAA are necessary and clinically meaningful.

Differential regulation of rationally targeted proteins following co-culture with CAA has been investigated in previous studies [246,249,250]. As a point of difference, the current study is novel in that it has identified and quantified the changes in *global* protein abundance in two well-characterised breast cancer cell lines, MCF-7 and MDA-MB-231, in response to a 72 hour transwell co-culture with mature human breast adipocytes. Using discovery mass spectrometry, protein abundance changes were identified and quantified for a similar number of proteins in both breast cancer cell lines, however, the proteome distribution profiles were unique to each cell line. Moreover, the majority of the proteins identified in both breast cancer cell lines remain unchanged by cross-talk with CAA.

3.3.1 Differential protein abundance in CAA co-cultured breast cancer cells

Differential protein abundance of 1.5-fold or greater was quantified for a relatively small proportion of the total number of proteins identified in both MCF-7 and MDA-MB-231 breast cancer cell lines following co-culture with mature breast adipocytes.

MCF-7 and MDA-MB-231 breast cancer cell lines represent two distinct molecular subtypes of breast cancer. Oestrogen and progesterone responsive MCF-7 cells, categorised as having luminal A phenotype [335,336], showed predominant downregulation of all the highly differentially regulated proteins during co-culture with CAA. In contrast, MDA-MB-231 hormone receptor negative cells that are categorized as having a claudin-low phenotype [335,336] and are considered to be a more metastatic and invasive breast cancer cell model than MCF-7 cells, mainly demonstrated upregulation of highly differentially regulated proteins in response to CAA co-culture. These trends in protein abundance regulation remained consistent in the top 20 most differentially expressed proteins for each cell line.

Breast cancer cells with distinct molecular subtypes show diverse protein expression profiles [337], and therefore, basal protein expression heterogeneity between MCF-7 and MDA-MB-231 breast cancer cells is a likely explanation for the unique distribution patterns of protein abundance changes occurring in response to interactions with CAA. In addition to protein expression differences, previous studies provide evidence for varying effects of CAA on the pro-tumorigenic behavior of different breast cancer cell lines *in vitro* [249,250]. Increased colony formation of human breast cancer cell lines MCF7, MDA-MB-361, MDA-MB-231 and MDA-MB-157 has been demonstrated after co-culture with CAA, but not for MDA-MB-468 and SK-BR3 cells [250]. In addition, transwell co-culture with mature murine adipocytes significantly increased the proliferation and migration of MCF-7 and MDA-MB-231 cells, however, co-culturing with 'obese' mature adipocytes (that have greater lipid content) further augmented proliferation and migration of MDA-MB-231 cells, but not MCF-7 cells [249]. Therefore, future research utilising differential abundance data from this study should consider the molecular subtype of the breast cancer cells, as cell line specific protein expression profiles may play a role in determining how the carcinoma cells communicate with and gain survival advantage from stromal CAA.

Abundance of the S100 calcium-binding proteins A4 and A6 (S100-A4 and S100-A6), and annexin A2, A5 and A6 (ANXA2, ANXA5 and ANXA6) proteins were notably decreased in MCF-7 cells during co-culture with CAA. S100 proteins bind calcium, and through this interaction sense fluctuations in intracellular and extracellular calcium concentrations and translate this into cellular responses [338]. Annexins bind both calcium and membrane phospholipids, in which phospholipid binding is regulated by calcium binding [339]. It could be speculated that concentrations of calcium are depleted during co-culture with CAA, resulting in downregulated expression of breast cancer cell calcium binding proteins. Interestingly, the intracellular and extracellular concentrations of calcium have not yet been investigated in the context of adipocyte-breast cancer cell crosstalk. Moreover, interactions between S100 and annexin proteins have been previously associated with breast cancer cell-endothelium adhesion and plasma membrane repair [340,341]. Thus, the complex interaction between S100 and annexin proteins, and calcium concentrations in breast cancer cells interacting with nearby CAA may be important regulators of breast tumour progression, and thus require further investigation.

Myeloid-associated differentiation marker (MYADM) was the most upregulated protein in CAA co-cultured MDA-MB-231 cells. Although the function of MYADM is

unknown, it has been suggested to play a role in cell spreading and migration during co-localisation with Ras-related C3 botulinum toxin substrate 1 (Rac1) in cell membrane protrusions [342], and myeloid differentiation [343]. In the current study, Rac1 was similarly expressed in co-cultured and control MDA-MB-231 cells (Supplementary data provided at https://www.otago.ac.nz/mackenzie-cancer/research/otago715163.html). The only association reported for MYADM in cancer, is the upregulation in hepatocellular carcinoma (HCC) compared to adjacent normal liver, measured by iTRAQ quantitative proteomics [344]. MYADM expression levels, its impact on prognosis and its mechanistic function in breast cancer, is yet to be determined.

In response to co-culture with CAA, MDA-MB-231 cells showed the greatest downregulation in 4F2 cell-surface antigen heavy chain (4F2), previously recognised for its role in integrin-dependent cell signalling leading to cell spreading and migration, and apoptotic defence [345]. 4F2, also known as solute carrier family 3 member 2 (SLC3A2) or CD98, was recently associated with the development of resistance to the doxorubicin chemotherapy agent [346]. However, in contrast with the CAA-induced 4F2 reduction measured in the current analysis, SLC3A2 was observed to be dramatically upregulated during the development of doxorubicin resistance; although this was assessed in hormone responsive MCF-7 cells rather than the hormone unresponsive MDA-MB-231 cells [346]. Thus, 4F2 could be involved in chemotherapy resistance pathways in triple negative breast tumours with CAA interactions, but the direction of regulation requires further investigation.

Since the aim of the current study was to obtain proteomic profiles from two disparate breast cancer cell lines after exposure to CAA for lead generation purposes, the subsequent application of additional independent methods to confirm protein fold change values, such as Western blotting, should be considered as the next step in any further investigation of candidate protein(s).

3.3.2 Western blotting validation of mass spectrometry

Three proteins identified by mass spectrometry were selected for validation by Western blot analysis, including n-myc downstream regulated 1 (NDRG1), phosphoglycerate kinase 1 (PGK1) and trefoil factor 1 (TFF1). Western blot analysis validated the iTRAQ results for all but NDRG1 protein abundance in MCF-7 cells.

These three candidate proteins were chosen because they appeared in the top 20 most differentially regulated proteins in either MCF-7 (Table 3.3) or MDA-MB-231 (Table 3.4) cells, all upregulated by co-culture with CAA. In addition, expression of NDRG1, PGK1 and TFF1 has been previously associated with poor breast cancer outcomes and, in some cases, increased resistance to anti-tumour therapeutics [347–349], underlining the clinical relevance of the current study's findings in breast cancer progression.

The NDRG1 gene is upregulated by hypoxia in a number of human tumours [350]. The role of NDRG1 expression in breast cancer remains controversial, most likely due to its pleiotropic functions involving cell growth and differentiation, immune and stress responses, and lipid biosynthesis [351]. Increased expression of NDRG1 has been associated with suppression of breast tumour metastasis [352], yet elevated NDRG1 expression has also been observed in invasive compared to non-invasive breast tumours and in ER+ tumours that were associated with poorer clinical outcomes [353,354]. The functional role of TFF1 in breast cancer has not been fully elucidated. In breast tumours, *TFF1* mRNA levels are positively and linearly correlated with the levels of ER and PR proteins [355]. Moreover, increased TFF1 expression has been associated with chemotherapy resistance and increased cell migration and invasion [348,356], but conversely, has shown inverse associations with tumour development, and tumour size and grade [355,357]. Thus, further research is required to fully elucidate the roles of increased NDRG1 and TFF1 in breast tumours in adipocyte rich environments. PGK1 expression and its association with breast tumour progression and outcome is discussed below (Section 3.3.3).

The potential for iTRAQ measurements to underestimate fold change may explain the smaller fold change values reported here by iTRAQ compared to Western blot analysis, particularly for NDRG1 expression in MCF-7 cells [358]. Additionally, investigation of NDRG1 expression in MCF-7 cells has previously observed double banding at 43 and 44 kDa, which was replicated in the current study by MCF-7 cells co-cultured with CAA [359]. It has been suggested that additional 44 kDa bands represent different isoforms of NDRG1 due to post-translational modifications, such as phosphorylation [351,359]. Therefore, it could be speculated that the smaller fold changes quantified using iTRAQ analysis were due to CAA induced NDRG1 phosphorylation at sites that interfered with the calling of the NDRG1 peptides measured during mass spectrometry, but did not interfere with the recognition sequence for the anti-NDRG1 antibody used for Western blotting. The anti-NDRG1 antibody target sequence is not publicly available, and thus, this theory remains speculative. Further investigation assessing the difference in peptide identification and antibody binding

sequences, as well as the analysis of post-translational NDRG1 phosphorylation may help explain the discordance observed in the current study.

3.3.3 Increase in breast cancer cell PGK1 expression

Phosphoglycerate kinase-1 (PGK1) was the only protein to be similarly differentially upregulated by more than 1.5-fold in both cell lines after adipocyte co-culture with CAA, highlighting a potential mechanism by which CAA may promote breast cancer cell migration, invasion and resistance to therapy in breast cancer cells with different molecular subtypes.

PGK1 is overexpressed in a variety of cancers [349,360–364], and high PGK1 protein expression in tumours is associated with increased metastatic dissemination [365,366], a multidrug resistant phenotype [349,367,368] and poor patient survival outcomes [349,363,364]. In breast cancer, PGK1 mRNA and protein are more highly expressed in breast tumour than in normal breast tissue [349], and elevated tumour PGK1 protein expression is associated with high histologic grade, positive ER, HER2 and p53 status, and poor overall survival in patients treated with paclitaxel [349]. Therefore, it could be speculated that CAA-induced increases in PGK1 protein expression measured in the current study, may be promoting the more aggressive phenotypes evident in breast cancer cells co-cultured with CAA in previous studies [150,245–251,253].

PGK1 is more highly expressed in breast cancer cell lines and human breast tumours with HER2 amplification [369], yet is not significantly associated with any particular breast cancer molecular subtype [349]. The MCF-7 and MDA-MB-231 breast cancer cell lines used in the current co-culture study are known to be negative for HER2 overexpression [335,336]. Thus, it would be interesting for future studies to assess PGK1 expression following transwell co-culture with mature breast adipocytes in HER2 overexpressing breast cancer cells.

PGK1 catalyzes the reversible conversion of 1,3-diphosphoglycerate to 3-phosphoglycerate, and is the first ATP generating enzyme in the glycolytic pathway [370]. Interestingly, knockdown of PGK1 in MCF-7 and MDA-MB-231 breast cancer cells, reduced cell invasiveness, and decreased the expression of proteins associated with the mesenchymal phenotype [371]. Moreover, decreased expression of PGK1 in MCF-7 and MDA-MB-231 cells has been associated with suppressed cell metabolism, measured as a decrease in cytoplasmic and mitochondrial ATP production [372]. In addition to its function as a glycolytic enzyme, recent evidence shows that PGK1 has a number of other mechanistically distinct functions that

are determined by post-translational modification and subcellular localisation [373–376]. For example, PGK1 can function as a protein kinase to reduce mitochondrial pyruvate metabolism and initiate cellular stress-induced autophagy [374–376]. Therefore, based on its different cellular functions, PGK1 has the potential to co-ordinate aerobic glycolysis, mitochondrial metabolism and autophagy, to maintain cellular homeostasis and promote proliferation during tumourigenesis. The current study did not address the metabolic phenotypes of breast cancer cells after transwell co-culture with CAA. Therefore, future studies are required to better understand the subcellular localisation and function of PGK1 in breast cancer cells exposed to CAA, and its role in co-ordinating metabolic pathways with other cellular processes critical to breast cancer cell survival, growth and metastasis.

3.3.4 Pathways regulated in co-cultured breast cancer cells

Pathway analysis showed that transwell co-culture with CAA induced both MCF7 and MDA-MB-231 breast cancer cell lines to upregulate a number of proteins involved in glycolysis and the tricarboxylic acid (TCA) cycle (Figure 3.7). MCF-7 cells co-cultured with CAA upregulated more proteins involved in the tricarboxylic acid (TCA) cycle, whereas, MDA-MB-231 cells co-cultured with CAA primarily upregulated proteins involved in glycolysis.

In line with a metabolic shift towards enhanced glycolysis, MDA-MB-231 cells also showed upregulated abundance of lactate dehydrogenase subunits LDHA and LDHB, and monocarboxylate transporter 4 (MCT4) (Supplementary data provided at https://www.otago.ac.nz/mackenzie-cancer/research/otago715163.html), which are involved in the interconversion of pyruvate and lactate [377,378], and transport of cellular lactate [379], in and from breast tumour cells, respectively.

The ‘Warburg effect’ describes the metabolic shift to aerobic glycolysis cancer cells undergo to fulfil their energetic requirements, even under conditions of adequate oxygen supply [380], and triple negative breast cancer cells and tumours are characterised by elevated glycolysis [381]. More recently, the two-compartment energy model has been proposed to explain the unique metabolic relationships occurring between cancer cells and stromal cells within the tumour microenvironment. According to this model, cancer cells act as metabolic parasites that stimulate catabolic pathways in proximal stromal cells to gain an energetic advantage that fuels cancer cell metabolism and tumour progression [260]. Previous studies have

shown that ovarian, prostate, and breast cancer cells induce lipolysis in stromal adipocytes, and that the resulting metabolites (glycerol, free fatty acids) are secreted and transferred to cancer cells where they induce proliferation, migration and invasion [249,261,262,382]. Furthermore, these studies showed that adipocyte co-culture enhances breast cancer cell progression by stimulating fatty acid uptake, storage and mitochondrial fatty acid oxidation in both MCF7 and MDA-MB-231 breast cancer cells [249,262]. Carnitine palmitoyltransferase 1 (CPT1) is the rate-limiting enzyme in mitochondrial fatty acid oxidation [383], and basal levels of CPT1 and fatty acid oxidation are higher in MCF-7 than MDA-MB-231 breast cancer cells [249]. In the current study, global proteome analysis identified an upregulation of CPT1A in both MCF-7 and MDA-MB-231 breast cancer cells co-cultured with CAA (Supplementary data provided at https://www.otago.ac.nz/mackenzie-cancer/research/otago715163.html). Together with the observed enrichment for increased expression of TCA cycle proteins in MCF-7 breast cancer cells, these results suggest that mitochondrial fatty acid oxidation is likely an important source of metabolites for the TCA cycle in MCF-7 cells within an adipocyte rich environment.

Differences in metabolic responses to CAA may be driven in part by oncogenic mutations characteristic to each breast cancer cell line [384]. For example, MCF-7 cells are *PIK3CA* mutant but carry a wildtype *TP53* gene, whereas, the more invasive MDA-MB-231 cells have a mutant *TP53* gene but are wildtype for *PIK3CA* [384]. Both of these genes are recognized as prognostic markers in breast cancer [385,386], and may also influence the unique protein expression profiles exhibited by MCF-7 and MDA-MB-231 breast cancer cells following co-culture with CAA. It has been shown that by inhibiting PDH kinase 2 (PDK2), functional p53 upregulates the activity of pyruvate dehydrogenase (PDH) [387]. This promotes the conversion of pyruvate to acetyl-CoA, which subsequently enters the TCA cycle, and may contribute to the upregulation of TCA cycle proteins in MCF-7 cells during co-culture.

In addition to metabolic pathways, this study identified downregulation of ubiquitin proteasome pathway proteins in both MCF-7 and MDA-MB-231 breast cancer cells, upregulation of proteins involved in *de novo* purine biosynthesis in MDA-MB-231 cells, and downregulation of a component of the eukaryotic translation initiation factor 3 complex (EIF3F) in both cell types. These adipocyte co-culture induced changes may represent shifts in protein degradation and DNA synthesis that aid in promoting breast cancer cell proliferation and migration. Taken together, these diverse pathway enrichments demonstrate the complex nature of the breast cancer cell proteomic heterogeneity and interplay between breast cancer cells and stromal CAA.

3.3.5 Transwell co-culture model

Similar to previous investigations [150,240,246,249,250,253,255,263], this study used a 2D transwell co-culture model that physically separates CAA and breast cancer cells, yet allows reciprocal cross-talk between the two cell populations via secreted factors. In comparison to previous co-culture studies, a major strength of the current investigation is the use of adipocytes isolated and differentiated from human mammary adipose tissue, whereas, most other studies have used murine pre-adipocyte cell lines or human abdominal adipose tissue pre-adipocytes [150,240,246,249,253,255,263].

Mature breast adipocytes used in the *in vitro* co-culture experiments were mostly multilocular, as they contained multiple lipid vacuoles per cell. In humans, multilocular adipocytes are characteristic of brown adipose tissue *in vivo*, whereas uniloculated adipocytes with singular lipid vacuoles are usually characteristic of white adipose tissue [21] (Figure 3.10). In human breast cancer, the browning of mammary adipose tissues has been observed to be greater in adipocytes surrounding breast tumours compared to adipocytes near benign lesions [388]. Although the diversity between unilocular and multilocular adipocytes was not addressed in the current study, future *in vitro* and *in vivo* investigations might need to consider the difference that lipid vacuole content may be having on nearby breast cancer cell phenotypes.

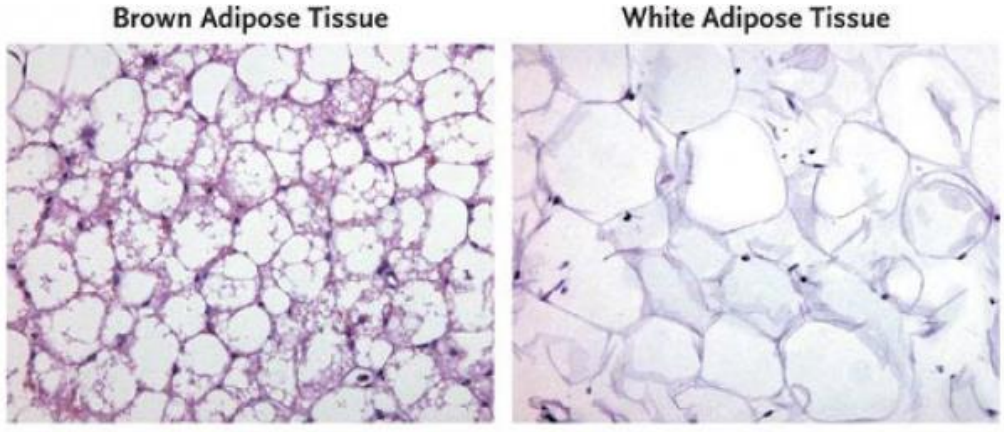

Figure 3.10. Brown *versus* white adipose tissue adipocytes.
Morphological appearance of white (unilocular adipocytes) and brown (multilocular adipocyte) adipose tissue in a 46 year old women. Reproduced with permission from Lichtenbelt *et al* [389], Copyright Massachusetts Medical Society.

The transwell co-culture model used in the current investigation used breast adipocyte and cancer cell monolayers, whereas breast tumours *in vivo* are 3-dimensional (3D) and have potential for direct CAA and breast cancer cell contact [150]. Interestingly, previous studies using 3D collagen gel matrixes allowing direct as well as indirect interactions between CAA and breast cancer cells, have all observed similar, although more pronounced, effects of CAA on breast cancer cell growth, migration and invasion, in comparison to cell monolayer models [241,244,390]. Concordance between previous monolayer and 3D models supports the possible translation of this studies *in vitro* protein abundance results to breast tumours with adipocyte rich environments *in vivo*.

Lastly, this study measured a snapshot of protein expression in a population of breast cancer cells after a 72 hour adipocyte co-culture, whereas the expression of proteins *in vivo* is likely to be dynamic and to fluctuate over time. Thus, further studies are required to better understand how CAA affect breast cancer cell phenotype and function by measuring abundance of proteins and their associated pathways over varying time points.

3.4 Summary

This study has, for the first time, shown global differences in relative protein abundance and identified a number of protein abundance changes in breast cancer cells co-cultured with human mature breast adipocytes in an *in vitro* transwell system. Hormone receptor positive (MCF7) and triple negative (MDA-MB-231) breast cancer cells showed predominant downregulation and upregulation of highly differentially regulated proteins, respectively, supporting the concept that reciprocal communication between breast cancer cells and CAA is heterogeneous, and likely breast cancer cell type specific. Analysis showed that the regulated molecules participate in pathways related to metabolism, protein ubiquitination and purine synthesis, and identified PGK1 as the only commonly up-regulated protein in both cell lines. Overall, by assessing global protein abundance, this investigation aids in better understanding the molecular mechanisms by which CAA regulate breast cancer cell phenotype and function, and provides a platform for future research to explore novel protein targets involved in breast cancer cell-CAA crosstalk.

Chapter 4

Overexpression of PGK1 in breast cancer

4.1 Introduction

Reciprocal interactions between adipocytes and breast cancer cells through soluble factors within the breast tumour microenvironment are known to contribute to breast tumour progression [150,246,391]. Recent discoveries suggest that the key mechanism promoting tumour progression is the metabolic co-operation between adipocytes and breast cancer cells in the tumour microenvironment [249,259,262]. In the previous chapter (Chapter 3), discovery mass spectrometry identified phosphoglycerate kinase 1 (PGK1) to be the only protein upregulated by more than 1.5-fold in both MCF-7 and MDA-MB-231 human breast cancer cells co-cultured with mature breast adipocytes (Chapter 3; Section 3.2.2.2). PGK1 plays an important role in cell metabolism, generating the first ATP molecule at step 7 of the glycolytic pathway by catalysing the reversible conversion of 1,3-diphosphoglycerate to 3-phosphoglycerate [370]. Thus, this finding highlights increased PGK1 expression as a potential regulator through which breast adipocytes in the tumour microenvironment may be promoting breast cancer cell migration, invasion, and resistance to therapy.

PGK1 mRNA expression is regulated by transcription factor hypoxia inducible factor 1α (HIF-1α) [392], the chief regulator of the hypoxic response. HIF-1α has an established role in the reprogramming of cancer cell metabolism, to preferentially perform aerobic glycolysis over oxidative phosphorylation, overcoming fluctuations in oxygen tension and driving tumour growth and invasion [311,393,394]; a phenomenon referred to as the 'Warburg Effect' [380]. Aerobic glycolysis in tumour cells is associated with an increase in glucose consumption, a reliance on glycolysis via the inhibition of oxidative phosphorylation, and an enhanced

production and secretion of lactate that is converted from cytosolic pyruvate, the product of glycolysis [380,395,396].

A variety of cancers exhibit increased mRNA and protein expression of PGK1, including endometrial, pancreatic, prostate, colon, hepatocellular, astrocytoma, and breast [349,360–364,397,398]. Higher PGK1 expression in these cancers is associated with radio-, chemo-, and multidrug resistance phenotypes [349,362,367,368,398], enhanced metastatic spread [365,366,398], and poorer survival outcomes for patients [349,363,364,397]. In breast tumours, elevated PGK1 protein expression is associated with larger and higher stage tumours [371], worse histologic grade, and ER, HER2 and p53 expression [349]. Furthermore, higher expression of PGK1 in breast tumours correlates with poorer overall and disease free survival [371], and worse overall survival in patients treated with paclitaxel [349]. Interestingly, of all the glycolytic proteins, PGK1 was the most upregulated in primary breast tumours from patients with associated metastases when compared to primary breast tumours from patients without metastases [371].

In human breast cancer cells, knockdown of PGK1 reduced cell invasiveness and decreased expression of proteins associated with mesenchymal phenotype [371]. Decreased expression of PGK1 is also associated with suppressed cell metabolism, measured as a decrease in cytoplasmic and mitochondrial ATP production [372]. What has yet to be investigated is whether increased expression of PGK1 promotes breast cancer cell growth and survival through its influence on metabolism.

4.1.1 Aims

The first aim of this chapter was to produce hormone receptor positive MCF-7 and hormone receptor negative MDA-MB-231 human breast cancer cells overexpressing PGK1 protein. This was approached by:

1) Cloning a PGK1 expressing lentiviral vector (Section 4.2.1).
2) Transiently transfecting MCF-7 and MDA-MB-231 breast cancer cell lines with a PGK1 expressing vector (Section 4.2.2 and 4.2.3).

The next aim of this chapter was to investigate the effect of PGK1 overexpression on metabolism, growth, and chemotherapy response in MCF-7, and MDA-MB-231 breast cancer cells. This was done by:

3) Measuring the concentration of lactate produced by MCF-7 and MDA-MB-231 cells in response to increased PGK1 expression (Section 4.2.4).
4) Assessing the rate of cell proliferation in MCF-7 and MDA-MB-231 cells overexpressing PGK1 (Section 4.2.5).
5) Investigating the effect of increased PGK1 levels on the sensitivity of MCF-7 and MDA-MB-231 breast cancer cells to paclitaxel and cyclophosphamide chemotherapies (Section 4.2.6).

Lastly, this chapter aimed to characterise *PGK1* expression in breast cancer cells *in vitro* and breast tumours *in vivo*, and to better understand the regulation of *PGK1* by clinically important breast cancer phenotypes. This was approached by:

6) Measuring basal PGK1 levels in a panel of breast cancer cell lines and relating this to the presence or absence of the clinical biomarkers ER, PR and HER2 (Section 4.2.7).
7) Assessing *PGK1* mRNA expression in breast cancer cell lines and associating this with the presence or absence of the clinical biomarkers ER, PR and HER2, and with sensitivity to breast cancer chemotherapies (Section 4.2.8).
8) Investigating the expression of *PGK1* mRNA in large publicly available breast tumour cohorts and associating this with clinical biomarkers, tumour subtypes, and expression of other regulatory and metabolism related genes (Section 4.2.9).

4.1.2 Experimental approach

4.1.2.1 Overexpressing PGK1 in human breast cancer cells

This study initially planned to use lentiviral transduction to stably overexpress PGK1 in MCF-7 and MDA-MB-231 human breast cancer cells using the Inducible Dharmacon™ TRIPZ™ Lentiviral Collection, and HEK239T cell line for viral packaging. Therefore, molecular cloning experiments were designed to insert the *PGK1* genetic sequence into the pTRIPZ lentiviral vector backbone (detailed methodology described in Chapter 2; Section 2.5 and Section 2.6). Plasmid DNA containing *HIS/FLAG/HA*-tagged *PGK1* was purified from DH5α bacterial cells. The *PGK1* sequence was amplified using PCR, the PCR product digested with restriction enzymes, the digested DNA purified by gel electrophoresis, and the purified DNA sequence ligated into the pTRIPZ vector backbone. The ligation products were transformed into competent Stbl3 bacteria, and colonies growing under ampicillin selection were inoculated. Plasmid DNA was extracted from inoculated bacterial cultures, and

sequencing was performed to validate the insertion of the full *PGK1* gene sequence into the pTRIPz vector backbone. Unfortunately, sequencing could not validate the insertion of the full length *PGK1* gene into the pTRIPZ vector. This necessitated a change in experimental approach, with the new strategy using transient overexpression of PGK1 in MCF-7 and MDA-MB-231 human breast cancer cells.

Transfection efficiency of MCF-7 and MDA-MB-231 breast cancer cells with the commercially available jetPRIME® transfection reagent was determined using a GFP-encoding plasmid. The jetPRIME® transfection reagent was used to transfect MCF-7 and MDA-MB-231 breast cancer cells with the *HIS/FLAG/HA*-tagged *PGK1* expressing plasmid, and overexpression of PGK1 was validated by measuring the relative PGK1 levels using Western blot analysis after 54 hours. Breast cancer cells were lysed with RIPA buffer for protein analysis. Transfection reagent and plasmid DNA were excluded from control cells. Transfection reagent treated cells were used to assess toxicity caused by the transfection reagent, and transfection with the GFP expressing plasmid was used as a vehicle control (detailed methodology described in Chapter 2; Section 2.7).

4.1.2.2 Investigating effects of PGK1 overexpression in human breast cancer cells

The influence of increased PGK1 expression on the production of lactate in MCF-7 and MDA-MB-231 cells was investigated by measuring the intracellular and extracellular concentrations of lactate in cell lysates 54 hours after transfection and in media conditioned for 48 hours by transfected cells, respectively (detailed methodology described in Chapter 2; Section 2.7.2.1). Cell lysates and conditioned media were deproteinised to remove lactate dehydrogenase enzymes that can degrade lactate, and lactate was quantified using an L-lactate assay kit. Lactate concentrations were standardised to the number of live cells present 54 hours after transfection, determined using an automated cell counter.

Effects of PGK1 overexpression on cell proliferation and sensitivity to chemotherapy, 54 hours after transfection, was evaluated in MCF-7 and MDA-MB-231 cells reseeded into 96 well plates 24 hours after transfection. Cell proliferation in PGK1 overexpressing MCF-7 and MDA-MB-231 cells, relative to controls, was measured by SRB assay 30 hours after moving the cells to 96 wells plates. Chemotherapy response was investigated in PGK1 overexpressing MCF-7 and MDA-MB-231 cells by assessing cell viability after a 24 hour treatment with IC50 doses of paclitaxel and 4-hydroperoxycyclophosphamide, using an MTT assay. IC50 doses were determined by dose-response curves evaluating cell viability, using

MTT assay analysis, in response to paclitaxel and 4-hydroperoxycyclophosphamide over a range of concentrations (0-100μM) for 24 hours (detailed methodology described in Chapter 2; Section 2.7.2.2).

4.1.2.3 Regulation of PGK1 expression by breast cancer phenotypes

Western blot analysis was used to identify basal levels of PGK1 protein in a panel of breast cancer cell lines grown under standard cell culturing conditions, including hormone receptor positive (n= 2), HER2 enriched (n= 2), and triple negative (n= 5) cell lines. Breast cancer cells were lysed with RIPA buffer for protein analysis (detailed methodology described in Chapter 2; Section 2.8). The MCF10A (mammary epithelial) breast cell line was used to standardise PGK1 protein expression across blots.

To determine which breast cancer phenotypes are associated with differences in *PGK1* regulation, *PGK1* mRNA expression in breast cancer cell lines and breast tumour datasets was compared between clinically important breast tumour phenotypes (ER+ *vs* ER-; PR+ *vs* PR-; HER+ *vs* HER2-) and molecular subtypes (luminal; HER2 enriched; triple negative/basal) (detailed methodology described in Chapter 2; Section 2.9.2 and Section 2.9.3).

For all Western blotting in this study chapter, samples were normalised to total protein by BCA assay (detailed methodology described in Chapter 2; Section 2.2.5.1). Relative protein levels were determined by measuring band densities with ImageJ (Version 1.49), normalising the densities to a loading control, and comparing the normalised densities to controls.

4.1.3 Acknowledgments

Cell culture and protein extraction of some breast cancer cells was performed by Devon Bull (University of Otago, undergraduate student) under my laboratory supervision as part of her summer studentship. The strain of competent *E.coli* (Stbl3) was created by George Wiggins (Mackenzie Cancer Research Group, University of Otago Christchurch), and kindly gifted by Assoc. Prof. Logan Walker (Mackenzie Cancer Research Group, University of Otago Christchurch) for use in transforming plasmids and ligation products. Sequencing was performed by the Genetic Analysis Service (GAS; University of Otago). I would like to thank Assoc. Prof. Gabi Dachs (Mackenzie Cancer Research Group, University of Otago Christchurch) and Dr Paul Pace (Centre for Free Radical Research, University of Otago

Christchurch) for their advice throughout the molecular cloning experimentation, and the Centre for Free Radical Research Group for donating the pTRIPZ^{TM} lentiviral vector backbone. I also thank Dr Judith McKenzie and Liping Goddard (Haematology Research Group, University of Otago Christchurch) for carrying out the FACS analysis.

4.2 Results

4.2.1 Production of a *PGK1* expressing lentiviral vector

4.2.1.1 Preparation of the *PGK1* insert and pTRIPZ vector for ligation

pFRT/TO/HIS/FLAG/HA-PGK1 plasmid was purified from DH5-α bacteria. To verify the plasmid contained the full length *PGK1* sequence, 1403 bp DNA fragments encoding the *PGK1* sequence and upstream HIS/FLAG/HA tag were amplified from the pFRT/TO/HIS/FLAG/HA-PGK1 plasmid using PCR (Figure 4.1).

*Xho*1 and *Mlu*1 restriction enzymes uniquely cut the pTRIPZ vector, producing an approximate 30 bp non-sense sequence (too small to visualise on an agarose gel), and a linearised 13061 bp vector fragment. To verify the restriction enzymes were optimally cutting, digestion of the pTRIPZ vector with *Xho*1 and *Mlu*1 restriction enzymes was confirmed by showing digested vector (linearised) running further through an agarose gel than uncut (circular) pTRIPZ plasmid (Figure 4.2).

Digesting the PCR amplicon (*PGK1* gene) with *Xho*1 and *Mlu*1 restriction enzymes cleaves off 5 bp DNA fragments from each end of the amplicon generating a 1393 bp insert encoding *PGK1*. The digested *PGK1* insert and linearised pTRIPZ vector were separated on, and purified from, an agarose gel (Figure 4.3).

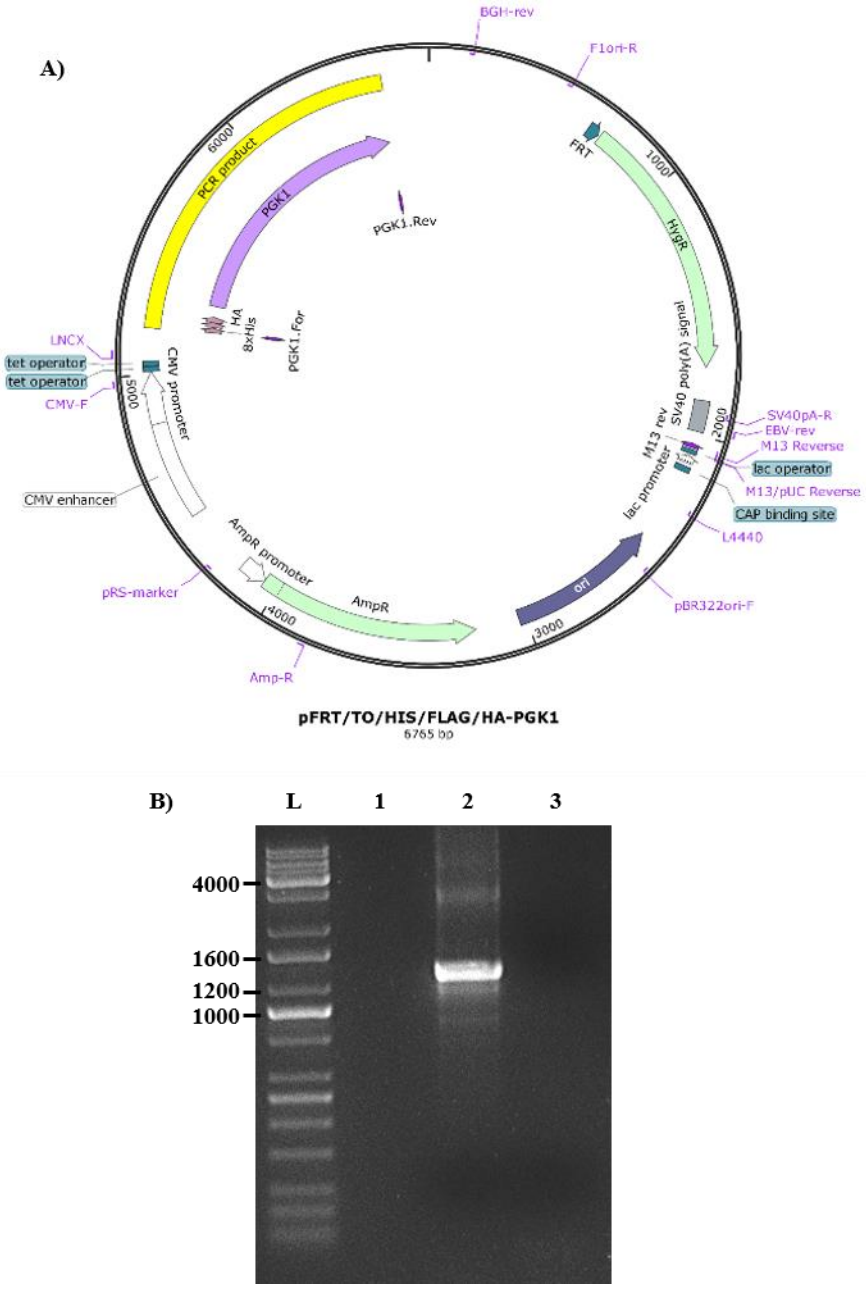

Figure 4.1. Amplification of the *HIS/FLAG/HA-PGK1* sequence from the pFRT/TO/HIS/FLAG/HA-PGK1 plasmid.

A) Plasmid map of the pFRT/TO/HIS/FLAG/HA-PGK1 plasmid (6765 bp) showing the *PGK1* gene (light purple; 1254 bp), PGK1.For and PGK1.Rev primer pair binding sites (dark purple; each 17 bp), and the sequence amplified by PCR (yellow; 1403 bp). The map was downloaded from Addgene and modified with SnapGene. B) DNA gel of *HIS/FLAG/HA-PGK1* PCR products (1403 bp) amplified from the pFRT/TO/HIS/FLAG/HA-PGK1 plasmid. The PCR product (lane 2) was subjected to gel electrophoresis, and the size was confirmed according to a DNA ladder (L). For negative control (lane 3) no DNA was added to the PCR reaction, and a lane gap was left between the ladder and the PCR product (lane 1).

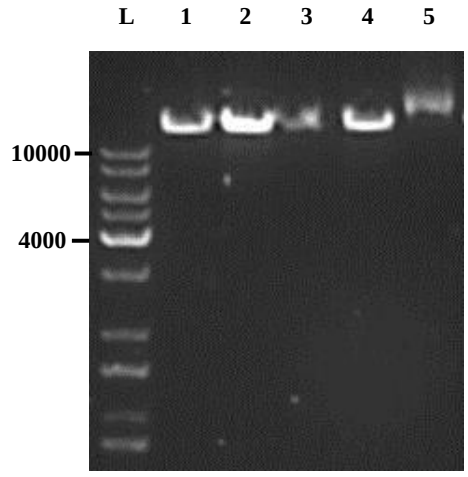

Figure 4.2. DNA gel of the pTRIPZ vector digested with the *Xho*I and *Mlu*I restriction enzymes.
The pTRIPZ vector (13091 bp) was digested with *Xho*I (lane 1) and *Mlu*I (lane 2) separately, and in a double digest with both enzymes (lane 4). For the negative control (lane 5) no restriction enzymes were added to the digestion reaction (uncut pTRIPZ vector). The digests were subjected to gel electrophoresis and their sizes were confirmed according to a DNA ladder (L). A lane gap was used (lane 3) due to spill over during loading of lane 2.

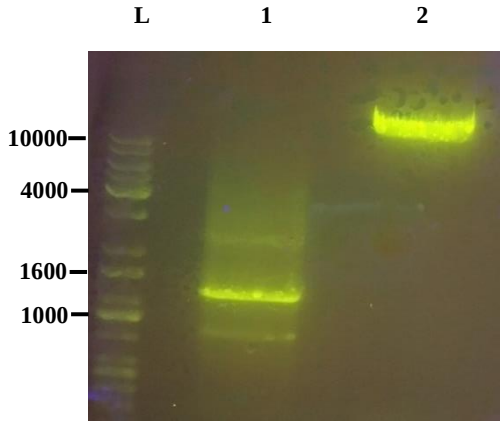

Figure 4.3. DNA gel of the *PGK1* insert and pTRIPZ vector digested with the *Xho*I and *Mlu*I restriction enzymes.
*Xho*I and *Mlu*I restriction enzymes digested the *PGK1* insert (lane 1; 1393 bp) and pTRIPZ vector (lane 2; 13061 bp), and digestion products were subjected to gel electrophoresis and their sizes were confirmed according to a DNA ladder (L).

4.2.1.2 Validating the *PGK1* insert and pTRIPZ vector ligation

The digested and purified *PGK1* insert and linearised pTRIPZ vector were ligated together using the DNA joining enzyme T4 DNA ligase; Figure 4.4 depicts the theoretical ligation of the fragments. Successful ligation was determined as the formation of colonies on ampicillin LB agar of Stbl3 (competent *E.coli* strain) bacteria transformed with the ligation product.

A single colony (Clone 1) grew from an initial ligation experiment, seven colonies (Clone 2-8) grew from a second ligation experiment, and three colonies (Clone 9-11) grew from a third ligation experiment. Clones were inoculated, and plasmid DNA was extracted.

To confirm the insertion of the *PGK1* sequence into the pTRIPZ vector, Sanger sequencing was performed on plasmid DNA extracted from clone 1 using the two sequencing primers, TRIPZ.Seq and PGK1.Seq. Using the TRIPZ.Seq primer, an 1112 bp amplicon was sequenced. Sequencing with the PGK1.Seq primer was unsuccessful. Aligning the TRIPZ.Seq amplicon sequence with the pTRIPZ-HIS/FLAG/HA/PGK1 vector sequence revealed successful ligation of the pTRIPZ vector with the 5' end of the *PGK1* insert. However, only a partial insertion of the *PGK1* gene was observed, as the sequence jumped from site 4548 to site 11024 on the pTRIPZ-HIS/FLAG/HA/PGK1 plasmid (Figure 4.5).

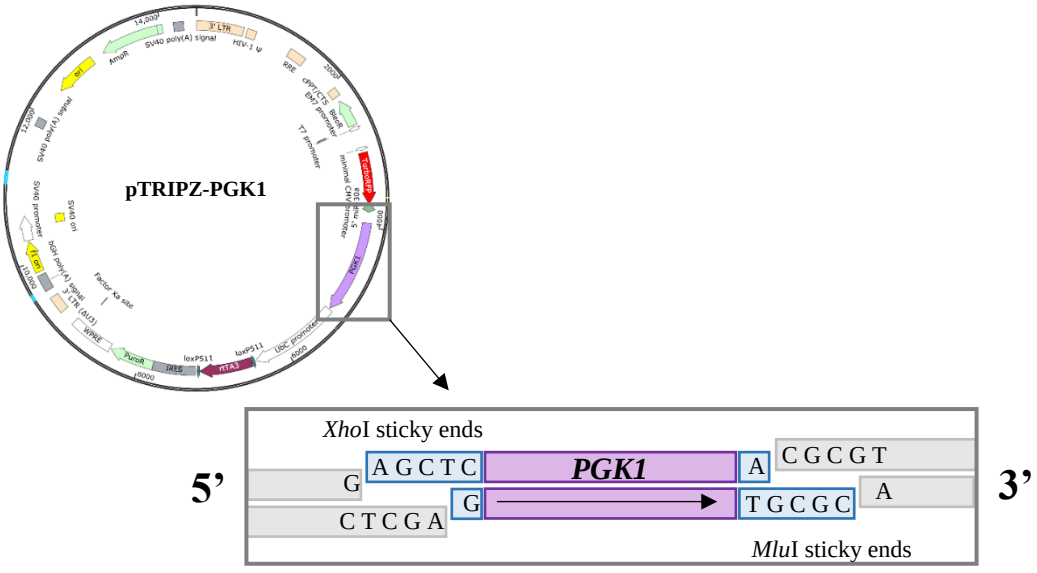

Figure 4.4. Theoretical image of the ligation between the *PGK1* insert with the linearised pTRIPZ vector to generate the pTRIPZ-HIS/FLAG/HA/PGK1 ligated plasmid.
The *PGK1* insert and pTRIPZ vector were digested with the *Xho*I and *Mlu*I restriction enzymes to generate matching sticky ends that were ligated together using the using the T4 DNA ligase enzyme.

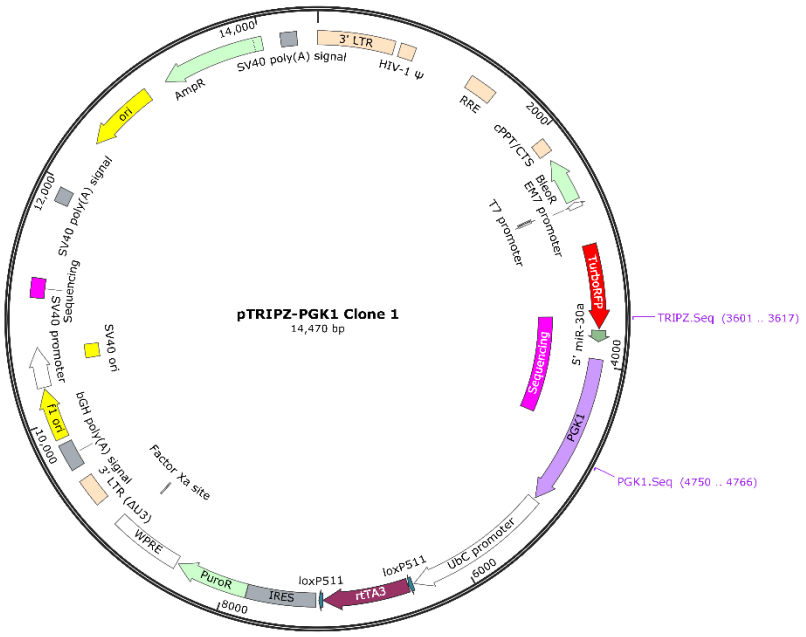

Figure 4.5. Plasmid map showing the primer binding sites and sequencing products of the pTRIPZ-HIS/FLAG/HA-PGK1 plasmid extracted from clone 1.
Binding sites of the TRIPZ-Seq (3601-3617 bp site) and PGK1.Seq (4750-4766 bp site) primers (17 bp annealing; light purple text) are on the forward strand. Sequencing from the TRIPZ-Seq primer was successful, generating an 1112 bp amplicon sequence (pink plasmid feature). The sequence read from site 3601-4548, and then jumped to site 11024 reading for another 164 bp to site 11187; skipping 6475 bp of the plasmid sequence. Sequencing from the PGK1.Seq primer was unsuccessful. The pTRIPZ vector map was downloaded from Addgene and modified with SnapGene to include to *PGK1* insert sequence (purple plasmid feature).

To determine which of the ten remaining clones represent the best candidates for sequencing, the extracted plasmids were subjected to PCR to amplify the *PGK1* insert DNA fragment from the pTRIPZ-HIS/FLAG/HA/PGK1 ligated plasmid. Plasmid extracted from Clone 2 resulted in a PCR product band (Figure 4.6). Amplification of the *PGK1* insert fragment from clones 1 and 3-11 was unsuccessful, and therefore sequencing of these clones was not performed.

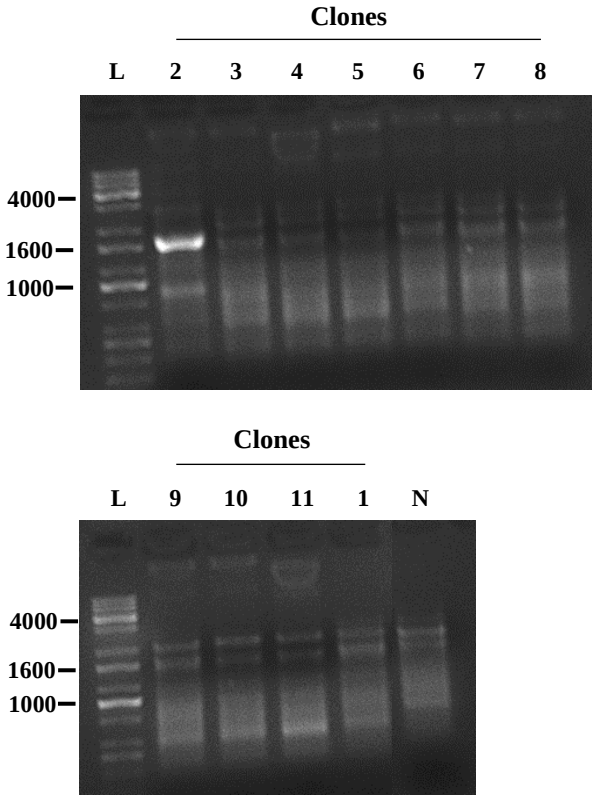

Figure 4.6. DNA gels of *PGK1* PCR products amplified from the plasmid DNA extracted out of eleven different Stbl3 bacterial clones.
The pTRIPZ-HIS/FLAG/HA/PGK1 ligated plasmid extracted from Stbl3 bacterial clones 1-11 was subjected to PCR with the TRIP.Seq and TRIPZ.Seq.Rev primers to amplify the inserted *PGK1* sequence (1758 bp). The PCR products were separated by gel electrophoresis, and the size was confirmed according to a DNA ladder (L). For negative control (N) no DNA was added to the PCR reaction.

To confirm the insertion of the full length *PGK1* sequence in the plasmid extracted from clone 2, Sanger sequencing was performed using the sequencing primers TRIPZ.Seq and TRIPZ.Seq.Rev. An amplicon of 1138 bp read length was sequenced using the TRIPZ.Seq primer, and alignment with the pTRIPZ-HIS/FLAG/HA/PGK1 ligated plasmid vector sequence revealed successful ligation of the pTRIPZ vector with the 5' end of the *PGK1* insert. However, only a partial insertion of the *PGK1* gene was observed, as the sequence jumped from site 3805 to site 9548 on the pTRIPZ-HIS/FLAG/HA/PGK1 plasmid (Figure 4.7). Thus, sequencing of the pTRIPZ-HIS/FLAG/HA/PGK1 plasmids extracted from Clone 1 and 2, could not validate the insertion of the full length *PGK1* gene into the pTRIPz lentiviral vector.

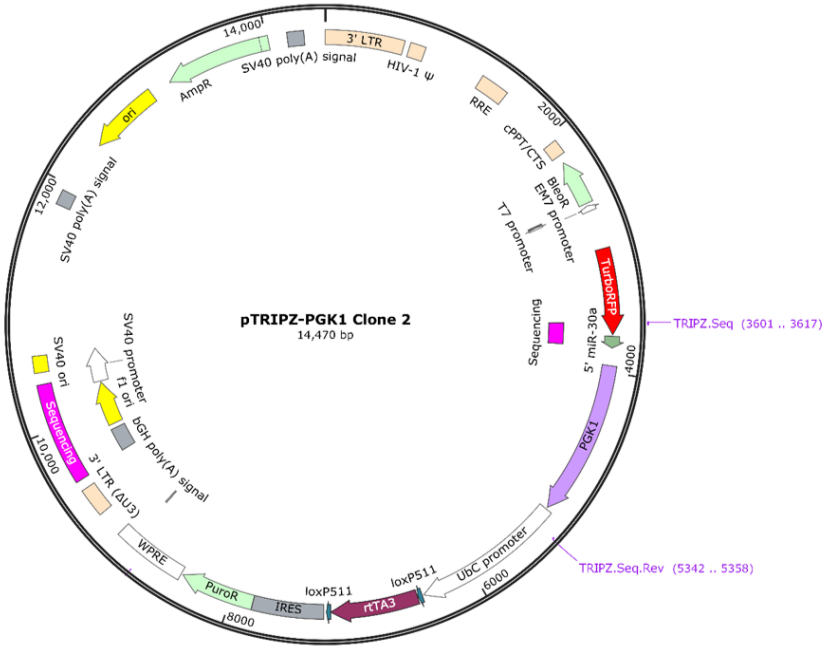

Figure 4.7. Plasmid map showing the primer binding sites and sequencing products of the pTRIPZ-HIS/FLAG/HA-PGK1 plasmid extracted from clone 2.
Binding sites of the TRIPZ-Seq (3601-3617 bp site; forward strand) and TRIPZ.Seq.Rev (5342-5358 bp site; reverse strand) primers (17 bp annealing) are represented by light purple text. Sequencing from the TRIPZ-Seq primer was successful, generating an 1138 bp amplicon sequence (pink plasmid feature). The sequence read from site 3601-3805, and then jumped to site 9548 reading for another 825 bp to site 10372; skipping 5742 bp of the plasmid sequence. Sequencing from the TRIPZ.Seq.Rev primer was unsuccessful. The pTRIPZ vector map was downloaded from Addgene and modified with SnapGene to include to *PGK1* insert sequence (purple plasmid feature).

4.2.2 Transfection efficiency of MCF-7 and MDA-MB-231 cells transfected with GFP

Sequencing could not validate the insertion of the full length *PGK1* gene into the lentiviral vector. Therefore, the strategy was shifted to transiently overexpress PGK1 protein in MCF-7 and MDA-MB-231 breast cancer cells to levels observed by co-culture with CAA (Chapter 3; Figure 3.9) and for long enough to perform endpoint analyses (54 hours; Chapter 2; Figure 2.3).

To test transfection efficiency, MCF-7 and MDA-MB-231 cells were transfected with green fluorescent protein (*GFP*) coding plasmids at a 1:2 ratio of µg DNA to µL of jetPRIME® transfection reagent. Transfection efficiency was determined as the percentage of GFP positive cells using fluorescent microscopy and FACS analysis (Figure 4.8).

Microscopy counted, on average, 35.17% and 35.92% GFP positive cells for MCF-7 (n= 3) and MDA-MB-231 (n= 3) transfections (complete data not shown). Visual inspection detected a slight shift towards rounder cell morphology, and more dead floating cells caused by transfection in both MCF-7 and MDA-MB-231 transfections (Figure 4.8A and C). FACS analysis calculated 40.6% and 46.9% GFP positive cells for MCF-7 and MDA-MB-231 transfections, respectively, and detected a reduction in cell viability due to transfection; as evident in the lower cell counts compared to controls (Figure 4.8B and D). Of the GFP positive cells, FACS analysis demonstrated that some cells had higher GFP expression than others. Transfection efficiencies and conditions were deemed acceptable for subsequent transfection experiments.

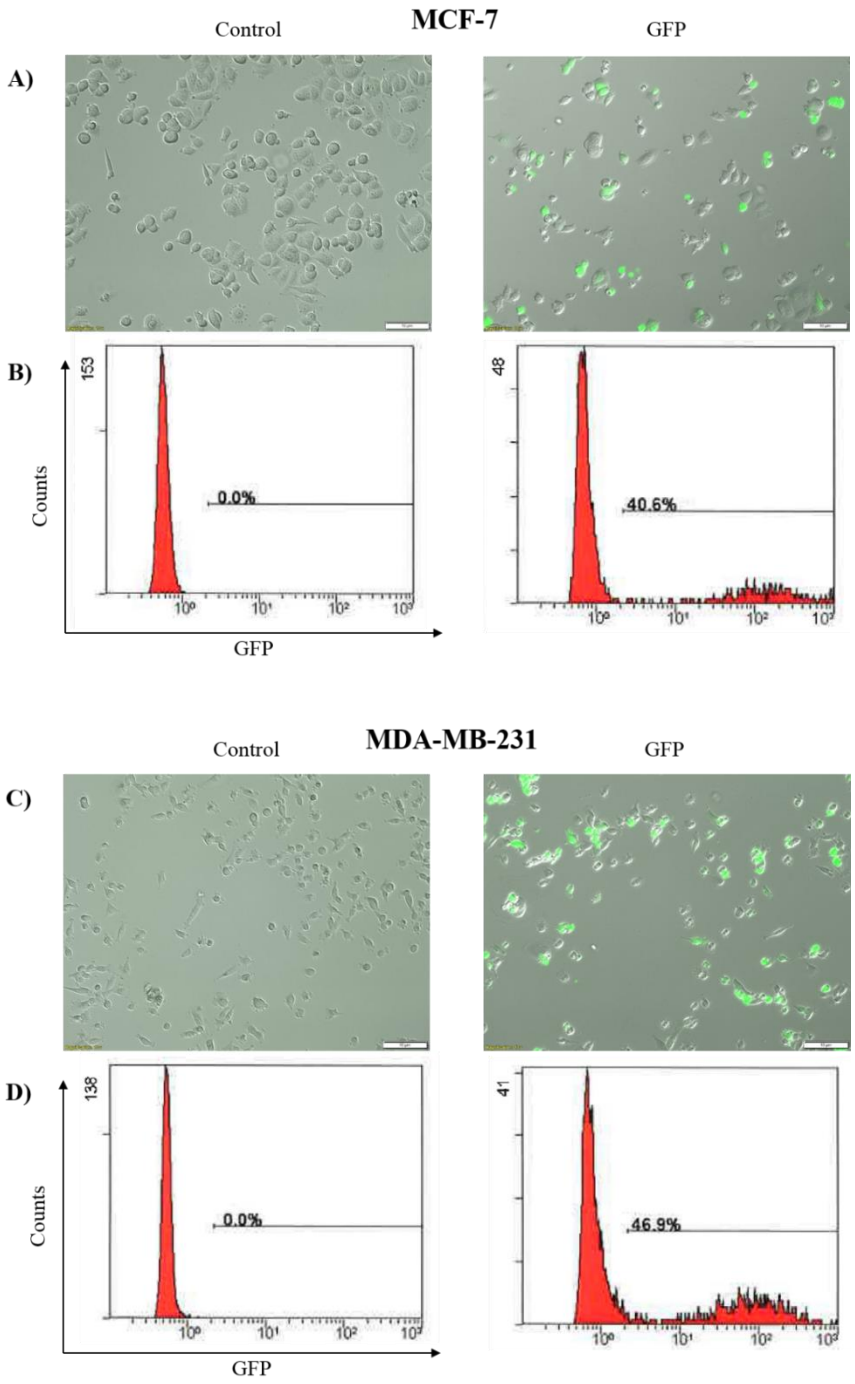

Figure 4.8. Transfection efficiency in MCF-7 and MDA-MB-231 cells using jetPRIME® reagent.

MCF-7 (A and B) and MDA-MB-231 (C and D) cells were transfected with the pEGFP-n1 plasmid, and the GFP signal was quantified by live cell fluorescent microscopy and FACS. A and C) Representative microscopy images show GFP positive cells as green fluorescent signal measured using FITC at 10X magnification. B and D) Single parameter histograms show FACS data as GFP negative cells (left peak) and GFP positive cells (right peak); distinguished by the gate set at a maximum of 0.5% GFP signal in the control conditions. Figures on the left are control cells without transfection reagent or DNA. Figures on the right are transfected cells.

4.2.3 Transfection of MCF-7 and MDA-MB-231 cells to transiently overexpress PGK1

MCF-7 and MDA-MB-231 cells were transfected with a plasmid encoding the *PGK1* gene (pFRT/TO/HIS/FLAG/HA-PGK1; Figure 2.2) using the jetPRIME® reagent at a ratio of 1:2 (2 µg DNA: 4µL transfection reagent). Cells were lysed after 54 hours and lysates were measured for PGK1 protein expression by Western blot analysis with an antibody specific to PGK1. A full blot showing the specificity of the PGK1 antibody is depicted in Supplementary Figure A.3.

Western blotting for PGK1 showed a double band in the cells transfected with the *PGK1* encoding plasmid (Figure 4.9). In the pFRT/TO/HIS/FLAG/HA-PGK1 plasmid the *PGK1* gene is located downstream of the poly-HIS-FLAG-HA tag sequence that is located between the *PGK1* sequence and the CMV promoter (Chapter 2; Figure 2.2). Providing the poly-HIS (24 bp), FLAG (24 bp) and HA (27 bp) tags are being transcribed and translated onto the N-terminus of PGK1 enzyme, the additional amino acids would increase the molecular weight of the PGK1 protein by approximately 3.2 kDa. Western blotting for the FLAG epitope tag confirmed the expression of the tag within the increased molecular weight PGK1 band; measuring at approximately 48 kDa (determined by comparison to the protein ladder) (Figure 4.9).

Western blot analysis confirmed that 54 hours post transfection, PGK1 protein expression was increased by 135.4% (2.35-fold) in MCF-7, and 49.4% (1.49-fold) in MDA-MB-231 transfected cells. PGK1 expression included both the untagged and FLAG tagged protein (Figure 4.10). This data indicates that transient overexpression of PGK1 protein in MCF-7 and MDA-MB-231 cells was successful.

PGK1 protein expression was increased in MDA-MB-231 cells to similar levels seen in response to transwell co-culture with CAA (1.48-fold; Chapter 3; Figure 3.9). After transfection MCF-7 cells increased PGK1 expression to levels greater than what was observed in response to co-culture with CAA (1.45-fold; Chapter 3; Figure 3.9). Western blot analysis shows greater expression of untagged PGK1 protein in MDA-MB-231 compared MCF-7 cells (Figure 4.10).

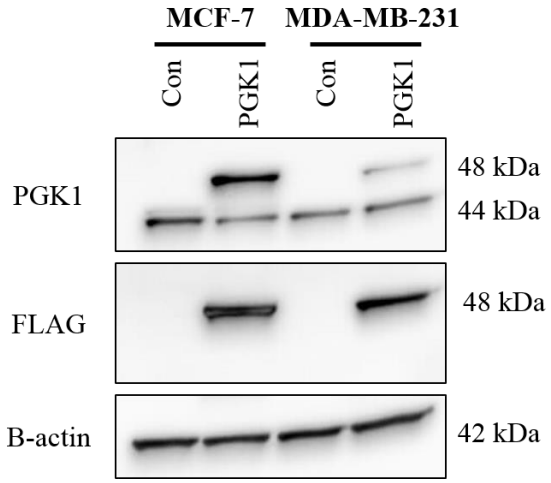

Figure 4.9. FLAG expression of transiently transfected MCF-7 and MDA-MB-231 cells 54 hours post transfection.

Western blot of MCF-7 and MDA-MB-231 cells transfected with the pFRT/TO/HIS/FLAG/HA-PGK1 plasmid encoding PGK1. Transfection showed double immunoreactive bands for PGK1 at the correct (44 kDa) and larger molecular size (48 kDa), and an immunoreactive band for FLAG at the larger molecular weight PGK1 band location (48 kDa). No FLAG expression was detected in control cells without transfection reagent or DNA (Con). β-actin was used as a loading control.

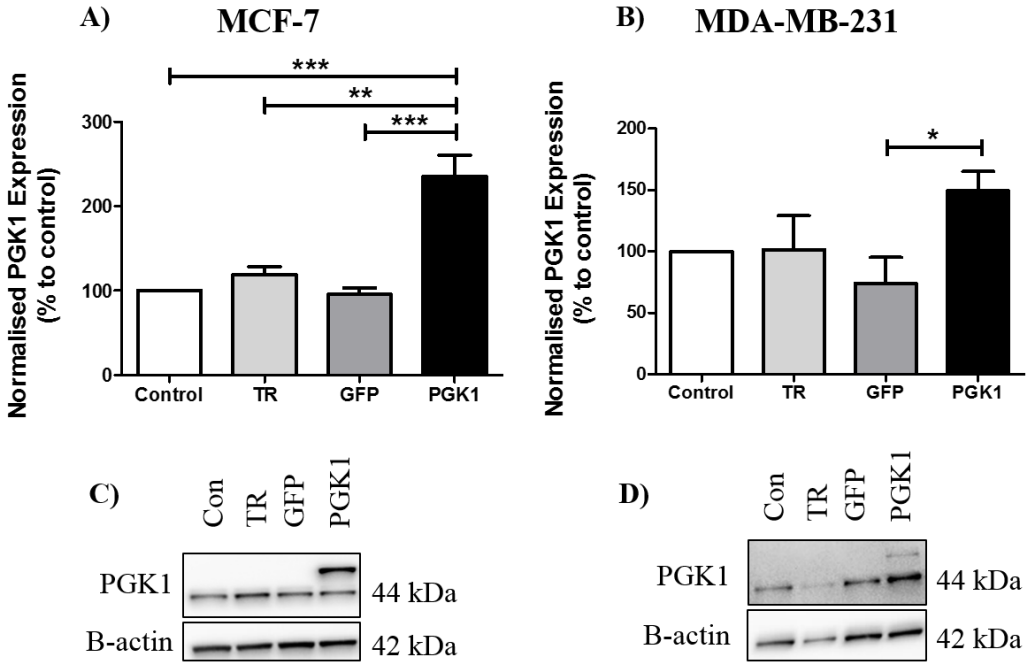

Figure 4.10. PGK1 expression of transiently transfected MCF-7 and MDA-MB-231 cells 54 hours post transfection.

A and B) PGK1 protein expression of transiently transfected MCF-7 (n= 6) and MDA-MB-231 cells (n= 6). Transfection reagent and DNA were excluded from control (con) cells. DNA was excluded from transfection reaction only (TR) cells, and transfection with pEGFP-n1 was used as a vehicle control (GFP). PGK1 expression was normalised to control, and data are presented as mean ± SEM. Statistical significance was evaluated by One-way ANOVA with *post-hoc* Tukey's Multiple Comparison Test; *$p<0.05$; **$p<0.01$; ***$p<0.001$. Representative Western blot of C) MCF-7 (n= 3) and D) MDA-MB-231 (n= 3) cells transfected with the pFRT/TO/HIS/FLAG/HA-PGK1 plasmid encoding *PGK1* shows a double immunoreactive band for PGK1 at the correct (44 kDa) and larger molecular size (48 kDa). β-actin expression was used as a loading control.

4.2.4 Effect of PGK1 overexpression on lactate production in MCF-7 and MDA-MB-231 cells

MCF-7 and MDA-MB-231 cells transfected with *GFP* and *PGK1* encoding plasmids were seeded at higher densities than controls (cells grown alone or with jetPRIME® transfection reagent), to account for the observed reduced cell viability post-transfection with the *GFP* encoding plasmid (Figure 4.8; Section 4.2.2). Therefore, to account for cell seeding differences and to reassess viability, MCF-7 and MDA-MB-231 cell numbers (live and dead) were determined using an automated cell counter. Live cell number measurements were used to normalise lactate concentration data.

To determine whether PGK1 protein overexpression alters the amount of lactate produced by MCF-7 and MDA-MB-231 cells, lactate concentration was measured using the L-Lactate Assay Kit in MCF-7 and MDA-MB-231 cells 54 hours after transfection, and in the media conditioned for 48 hours by PGK1 overexpressing MCF-7 and MDA-MB-231 cells. Lactate concentrations were normalised to live cell numbers measured 54 hours after transfection.

4.2.4.1 Measurement of live cell number in transiently transfected MCF-7 and MDA-MB-231 cells

The number of live MCF-7 cells did not significantly differ between transfection conditions 54 hours after transfection (Figure 4.11A). The number of live MDA-MB-231 cells transfected with *PGK1* encoding plasmids was significantly lower than untreated and transfection reagent control live cell numbers ($p<0.05$; Figure 4.11B). There was no significant difference in live cell number between the *GFP* and *PGK1* plasmid transfected MDA-MB-231 cells ($p>0.05$; Figure 4.11B). The live cell number and viability of MCF-7 and MDA-MB-231 cells treated with jetPrime® transfection reagent only (TR) was not significantly different from live cell number and viability of control cells (Figure 4.11A-D). MCF-7 and MDA-MB-231 cell viability was lower in cells transfected with *PGK1* or *GFP* encoding plasmids, compared to untreated and transfection reagent controls (Figure 4.11C and D, respectively). This suggests that reductions in MDA-MB-231 live cell number following plasmid transfection is not a consequence of transfection reagent toxicity, but rather the introduction of *GFP* and *PGK1* expressing plasmids. Moreover, by using higher seeding densities this study was able to counteract the reduced viability caused by transfection in MCF-7, but not MDA-MB-231 cells.

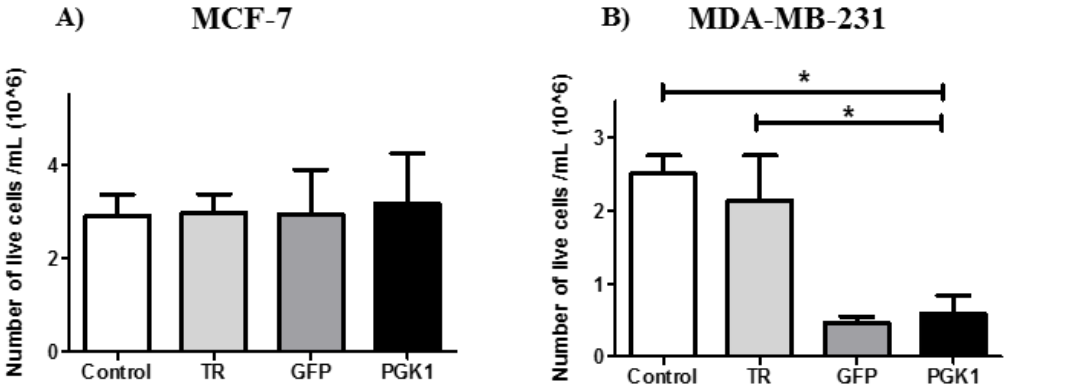

C)

MCF-7	Average Cell Viability (%)
Con	97.3
TR	96.7
GFP	90.3
PGK1	89.7

D)

MDA-MB-231	Average Cell Viability (%)
Con	98.0
TR	97.3
GFP	93.7
PGK1	94.0

Figure 4.11. Number of live cells after transfection with PGK1 in MCF-7 and MDA-MB-231 cells.

The number (10^6 live cells per mL) and viability (%) of MCF-7 (A and C; n= 3) and MDA-MB-231 (B and D; n= 3) cells 54 hours after transfection with a *PGK1* encoding plasmid was determined by automated cell counting. Transfection reagent and DNA were excluded from control (Con) cells. DNA was excluded from transfection reaction only (TR) cells, and transfection with pEGFP-n1 was used as a vehicle control (GFP). Statistical significance was evaluated by One-way ANOVA and *post-hoc* Bonferroni's Multiple Comparison Test. Data are presented as mean ± SEM; *$p<0.05$.

4.2.4.2 Detecting lactate production in, and extracellular lactate secreted by, MCF-7 and MDA-MB-231 cells overexpressing PGK1 protein

Intracellular lactate levels (cell lysate) in MCF-7 and MDA-MB-231 cells were not significantly different in PGK1 overexpressing cells compared to untreated, transfection reagent, and GFP transfected controls (Figure 4.12A and B, respectively). Lactate concentrations in the conditioned media of *PGK1* plasmid transfected MCF-7 cells was not significantly different to untreated, transfection reagent and GFP transfected controls ($p>0.05$; Figure 4.12A). Compared to *PGK1* plasmid transfection, GFP expression in MDA-MB-231 cells resulted in significantly higher concentration of lactate in the conditioned media ($p<0.001$; Figure 4.12B). Whereas, lactate concentrations were higher in the conditioned media of *PGK1* plasmid transfected cells when compared to untreated controls ($p<0.05$; Figure 4.12B). Therefore, PGK1 overexpression did not alter lactate concentration in MCF-7 cells, but may elicit an upregulation of lactate efflux by MDA-MB-2131 cells. However, this increase in lactate efflux is likely the consequence of introducing a foreign expressing plasmid, as evidenced by the significant increase in lactate accumulating in the conditioned media of *GFP* transfected MDA-MB-231 cells.

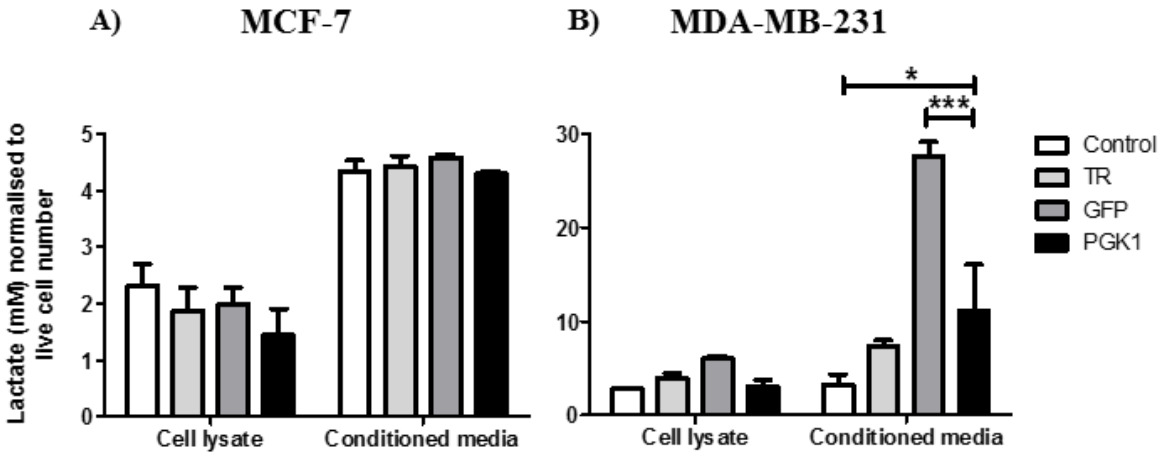

Figure 4.12. Production and secretion of lactate from MCF-7 and MDA-MB-231 cells overexpressing PGK1.

Lactate concentrations were measured in A) MCF-7 (n= 3) and B) MDA-MB-231 (n= 3) cell lysates 54 hours after transfection, and in conditioned media from A) MCF-7 (n= 3) and B) MDA-MB-231 (n= 3) cells incubated for 48 hours. Transfection reagent and DNA were excluded from control (Control) cells. DNA was excluded from transfection reaction only (TR) cells, and transfection with pEGFP-n1 was used as a vehicle control (GFP). Lactate concentrations were normalised to live cell number, and data are presented as mean ± SEM. Statistical significance was evaluated by Two-way ANOVA with *post-hoc* Bonferroni correction.*$p<0.05$; ***$p< 0.001$.

4.2.5 Effect of PGK1 overexpression on MCF-7 and MDA-MB-231 cell proliferation

To assess cell proliferation, MCF-7 and MDA-MB-231 cells overexpressing PGK1 were subjected to a sulforhodamine B (SRB) assay 54 hours after transfection. In this study, cell proliferation was extrapolated from protein content, as SRB binds to protein and SRB concentration can be measured in solution by reading absorbance at 565 nm.

MCF-7 cells showed a trend toward reduced proliferation when transfected with *PGK1* and *GFP* expressing plasmids (Figure 4.13A). MDA-MB-231 cells transfected with *PGK1* encoding plasmids showed a significant reduction in proliferation compared to untreated controls ($p<0.001$; Figure 4.13B). Both MCF-7 and MDA-MB-231 cells showed no significant difference in proliferation between *PGK1* and *GFP* plasmid transfection ($p>0.05$; Figure 4.13A and B, respectively). Treatment with the transfection reagent showed a small but insignificant increase in MCF-7 cell proliferation, and a small but insignificant decrease in MDA-MB-231 cell proliferation, when compared to control. This suggests that decreased proliferation in plasmid transfected cells is not a consequence of transfection reagent toxicity, but rather is likely the consequence of introducing *GFP* and *PGK1* expressing plasmids.

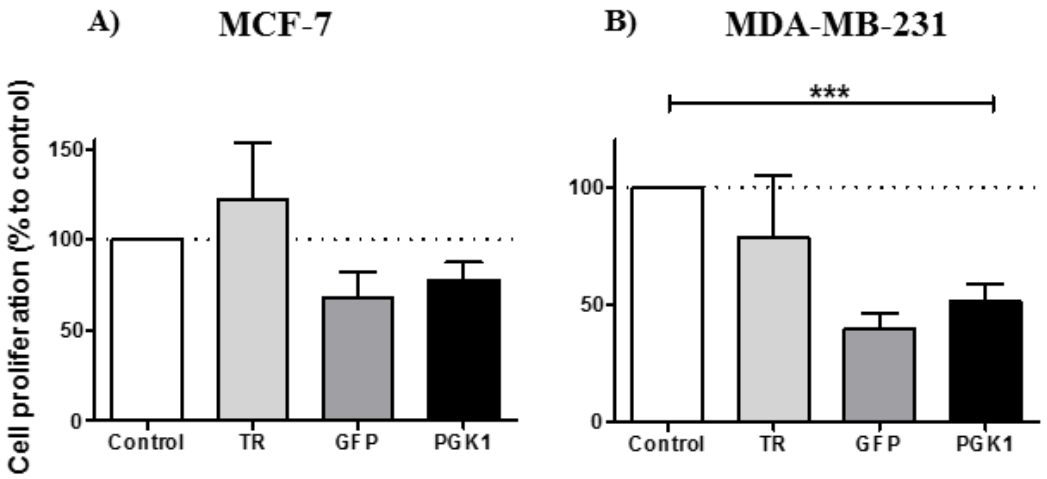

Figure 4.13. Proliferation of MCF-7 and MDA-MB-231 cells overexpressing PGK1. Cell proliferation was measured using an SRB assay in A) MCF-7 (n= 6) and B) MDA-MB-231 cells (n= 6) 54 hours post transfection. Transfection reagent and DNA was excluded from control (Con) cells. DNA was excluded from transfection reaction only (TR) cells, and transfection with pEGFP-n1 was used as a vehicle control (GFP). Cell proliferation was normalised to control, and data are presented as mean ± SEM. Statistical significance was evaluated by One-way ANOVA and *post-hoc* Bonferroni's Multiple Comparison Test. ***p< 0.001.

4.2.6 Effect of PGK1 overexpression on chemotherapy response in MCF-7 and MDA-MB-231 cells

4.2.6.1 Calculating IC50 doses of breast cancer chemotherapies for MCF-7 and MDA-MB-231 cells

To assess the dose-dependent effect of paclitaxel and 4-hydroperoxycyclophosphamide (active metabolite of cyclophosphamide) on metabolic cell activity, MCF-7 and MDA-MB-231 cells were treated for 24 hours with paclitaxel concentrations ranging from 0.5-100 µM for MCF-7 and 0.5-200 µM for MDA-MB-231, and 4-hydroperoxycyclophosphamide concentrations ranging from 1-100 µM for both MCF-7 and MDA-MB-231 (Table 4.1). At the highest concentration of paclitaxel and 4-hydroperoxycyclophosphamide, MCF-7 cells were exposed to 1.5% ethanol (paclitaxel) and 0.29% DMSO (4-hydroperoxycyclophosphamide), respectively, and MDA-MB-231 cells were exposed to 0.75% ethanol (paclitaxel) and 0.29% DMSO (4-hydroperoxycyclophosphamide), respectively (Table 4.1).

Table 4.1. Paclitaxel and 4-hydroperoxycyclophosphamide concentrations used to determine dose-response of MCF-7 and MDA-MB-231 cells.

MCF-7	MDA-MB-231	MCF-7 and MDA-MB-231
Paclitaxel (µM)	**Paclitaxel (µM)**	**4-H-Cyclo (µM)**
0.5	0.5	1
2	2	2
10	10	5
20	20	10
50	40	20
100	50	50
200 (EtOH 1.50%)	100 (EtOH 0.75%)	100 (DMSO 0.29%)

EtOH: ethanol; Ethanol is used to solubilise paclitaxel. **DMSO:** dimethyl sulfoxide. DMSO is used to solubilise. **4-H-Cyclo**: 4-hydroperoxycyclophosphamide.

MTT analysis demonstrated that, at increasing doses of paclitaxel and 4-hydroperoxycyclophosphamide, the number of metabolically viable MCF-7 and MDA-MB-231 cells decreased in a dose-dependent manner (R^2>0.90; Figure 4.14). IC50s for paclitaxel and 4-hydroperoxycyclophosphamide were, 61.94 µM and 24.60 µM in MCF-7, and 20.23 µM and 23.33 µM in MDA-MB-231, respectively (Figure 4.14). After 24 hours, 200 µM of paclitaxel reduced the number of viable MCF-7 cells to 1.5%, and 100 µM of paclitaxel completely eliminated viability in MDA-MB-231 cells. Additionally, there were no viable MCF-7 and MDA-MB-231 cells after 24 hour exposure to 100 µM of 4-hydroperoxycyclophosphamide. The viability of MCF-7 and MDA-MB-231 cells was not affected by 1.5% or 0.75% ethanol, or 0.29% of dimethyl sulfoxide (DMSO) after 24 hours(Figure 4.14); validating that the decrease in cell viability measured during paclitaxel and 4-hydroperoxycyclophosphamide treatment was not due to ethanol or DMSO present in the solution.

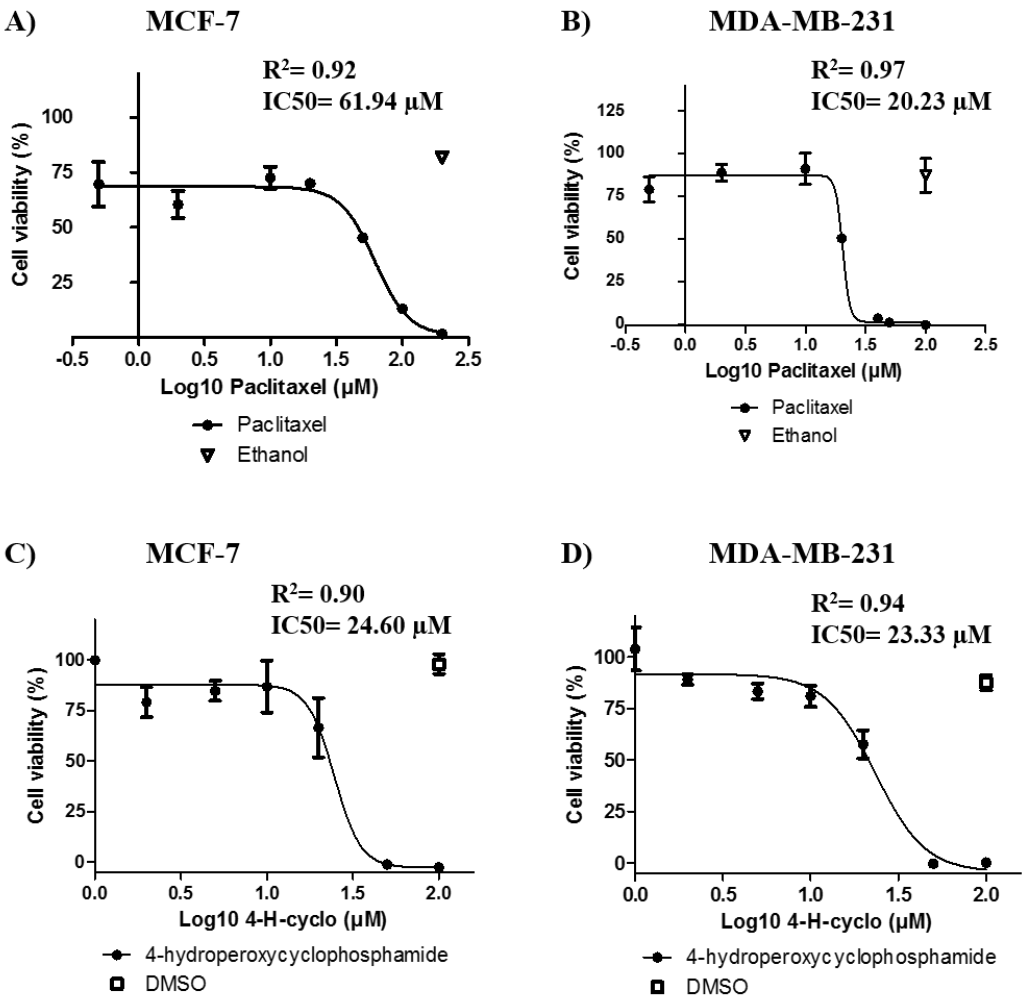

Figure 4.14. Dose-response curves of MCF-7 and MDA-MB-231 cells treated with paclitaxel and 4-hydroperoxycyclophosphamide.
MTT assay analysis was used to measure cell viability in relation to untreated cells (100% viability) in MCF-7 and MDA-MB-231 cells (each with n= 3 biological replicates). Paclitaxel and 4-hydroperoxycyclophosphamide (4-H-Cyclo) concentrations were log transformed, and IC50 values were evaluated using non-linear fit dose-response curves constructed with variable slope modelling (four parameter).

4.2.6.2 Measuring cell viability in chemotherapy treated MCF-7 and MDA-MB-231 cells overexpressing PGK1

To assess the effect of PGK1 overexpression on chemotherapy response, MCF-7 and MDA-MB-231 cells overexpressing PGK1 were treated with IC50 doses of paclitaxel and 4-hydroperoxycyclophosphamide for 24 hours. Cell viability measured by MTT assay was normalised to untreated controls for MCF-7 and MDA-MB-231 (Figure 4.15A and B, respectively).

MCF-7

In untreated (no chemotherapy) MCF-7 cells, increased expression of PGK1 did not significantly alter cell viability when compared to untreated, transfection reagent, and GFP transfected controls, although on average a 24.50% reduction was observed compared to untreated control ($p>0.05$; Figure 4.15A). Paclitaxel treatment significantly reduced MCF-7 cell viability in control cells (white bars) by 36.22% ($p<0.001$) and PGK1 overexpressing cells (black bars) by 36.03% ($p<0.001$), when compared to their equivalent untreated control cells (Figure 4.15B). Similarly, 4-hydroperoxycyclophosphamide treatment significantly reduced viability by 24.78% in PGK1 overexpressing cells compared to untreated PGK1 overexpressing MCF-7 cells ($p<0.05$; Figure 4.15B).

MDA-MB-231

PGK1 overexpression significantly reduced MDA-MB-231 cell viability by 46.58% in untreated (no chemotherapy) cells compared to untreated control ($p<0.01$; Figure 4.15B). In untreated (no chemotherapy) MDA-MB-231 cells, cell viability of PGK1 overexpressing cells was not significantly different to GFP expressing and transfection reagent controls ($p>0.05$; Figure 4.15B). When compared to equivalent untreated cells, paclitaxel treatment significantly reduced cell viability by 41.40% in control cells (white bars; $p<0.05$), and produced a small but not statistically significant reduction in cell viability of 18.68% for PGK1 overexpressing cells (black bars; $p>0.05$; Figure 4.15B). Treatment with 4-hydroperoxycyclophosphamide caused non-significant reductions in cell viability in control, transfection reagent, GFP expressing or PGK1 overexpressing cells when compared to equivalent untreated cells ($p>0.05$; Figure 4.15B).

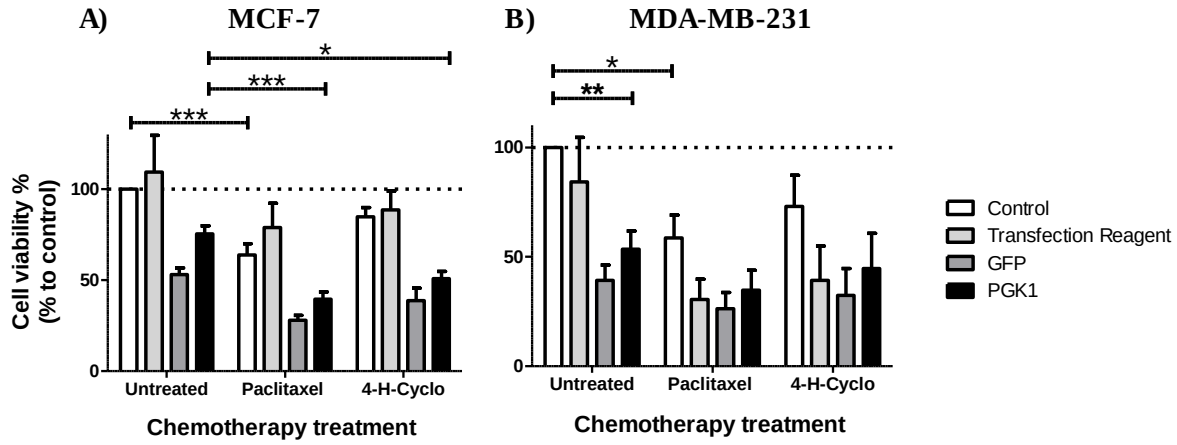

Figure 4.15. Chemotherapy response of MCF-7 and MDA-MB-231 cells overexpressing PGK1.

Response to a 24 hour treatment with IC50 concentration paclitaxel and 4-hydroperoxycyclophosphamide (4-H-Cyclo) was determined by comparing differences in A MCF-7 (n= 6) and B) MDA-MB-231 (n= 6) cell viability (measured by MTT assay) to untreated cells (medium without chemotherapy). Data was normalised to untreated control cells (horizontal black dotted line). Transfection reagent and DNA was excluded from control (Control) cells (white bars). DNA was excluded from transfection reaction only cells (light grey bars), and transfection with pEGFP-n1 was used as a transfection vehicle control (GFP; dark grey bars). Data are presented as mean ± SEM. Statistical significance was evaluated by Two-way ANOVA with *post-hoc* Bonferroni correction comparing PGK1 overexpression (black bars) to controls. *$p<0.05$; **$p<0.01$; ***$p< 0.001$.

4.2.7 Relative levels of PGK1 in a panel of breast cancer cell lines

To assess whether differences in clinically important phenotypes are associated with differences in PGK1 expression *in vitro*, Western blot analysis was used to measure relative PGK1 protein levels in ER+ (n= 2), HER2 enriched (n= 2) and triple negative (n= 5) breast cancer cell lines cultured under standard growth conditions. The transcriptional characteristics, and the molecular and histological tumour subtypes, of the human breast cancer cell lines used in this study are described in Table 4.2.

Expression of PGK1 protein did not significantly differ across the majority of the breast cancer cell lines studied, though PGK1 expression was significantly higher in the HCC38 cell line compared to all other cell lines except HCC70 ($p<0.05$, $P<0.01$, and $p<0.001$). BT20 cells also exhibited significantly lower PGK1 expression than HCC70 cells ($p<0.05$; Figure 4.16A). The largest difference in PGK1 expression was between two triple negative cell lines, HCC38 and BT20 ($p<0.001$; Figure 4.16A). In comparison to MDA-MB-231 cells, MCF-7 cells exhibited higher PGK1 levels, although the difference was not significant ($p>0.05$; Figure 4.16A). On average, the relative levels of PGK1 did not significantly differ between breast cancer cell line subtypes, or between breast cancer subtypes and the MCF-10A normal breast cell line (Figure 4.16C).

Table 4.2. Clinical and pathological features of breast tumours used to derive breast cancer cell lines used in this study.

Cell Line	ER	PR	HER2	*TP53*	Molecular subtype	Histological tumour type
BT20	-	-	-	Mutant	Basal-like	IDC
HCC1954	-	-	+	Mutant	HER2 enriched	DC
HCC38	-	-	-	Mutant	Basal-like	DC
HCC70	-	-	-	Mutant	Basal-like	DCIS
MCF-7	+	+	-	Wild Type	Luminal A	IDC
MDA-MB-231	-	-	-	Mutant	Basal-like	AC
MDA-MB-468	-	-	-	Mutant	Basal-like	AC
SKBR3	-	-	+	Mutant	HER2 enriched	AC
T47D	+	+	-	Mutant	Luminal A	IDC

ER: Oestrogen receptor; **PR**: Progesterone receptor; **HER2:** human epidermal growth factor receptor 2; **IDC:** Invasive ductal carcinoma; **DC**: Ductal carcinoma; **AC**: Adenocarcinoma; **+/-**: positive/negative.
ER/PR/HER2 and *TP53* status: as indicated by Neve *et al.* [335].

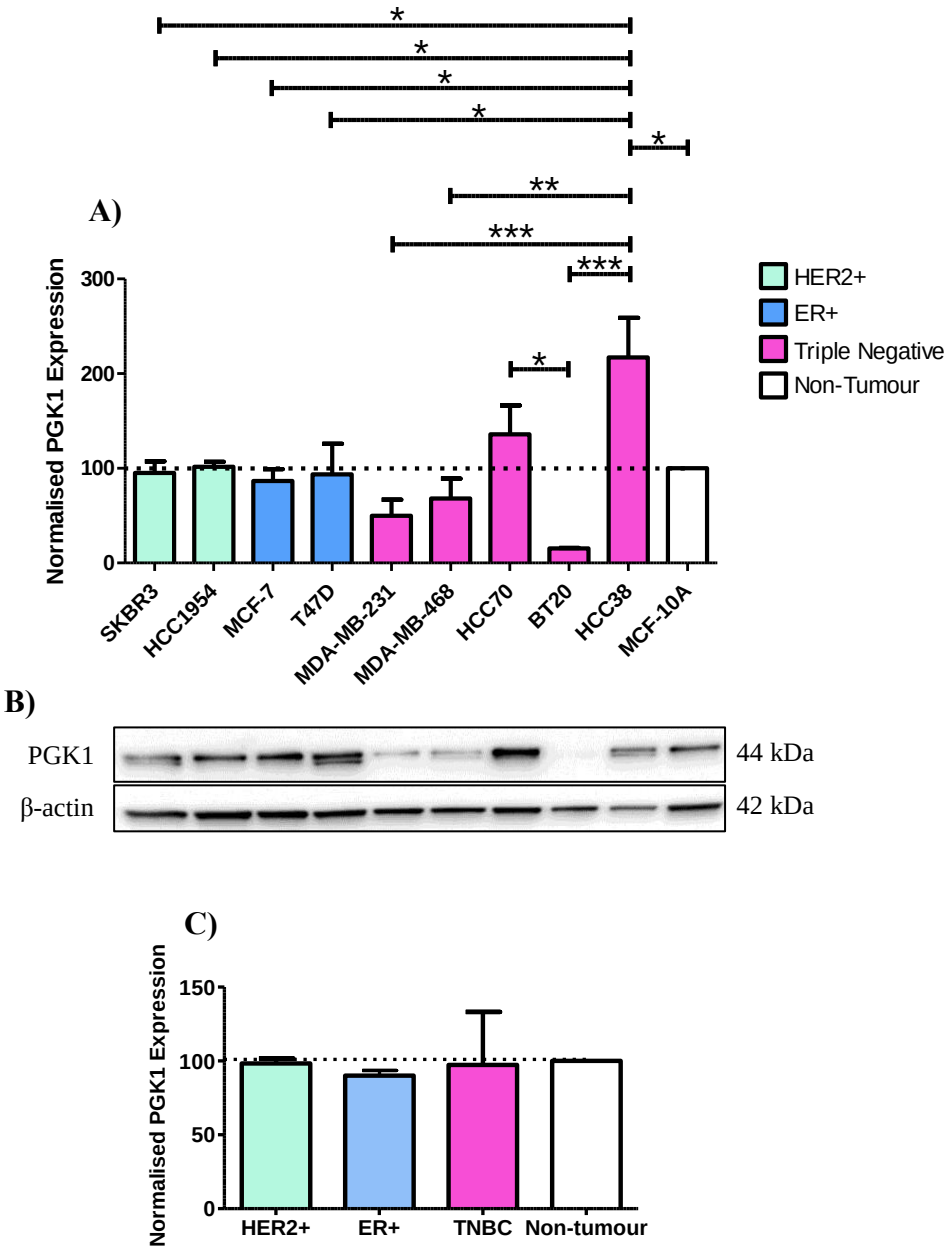

Figure 4.16. PGK1 protein expression levels in breast cancer cell lines.
A) Basal expression of PGK1 was measured using Western blot analysis in human epidermal growth factor receptor 2 overexpressing (HER2+; n= 2), oestrogen receptor positive (ER+; n= 2), and triple negative (TNBC; n= 5) breast cancer cell lines (n= 3, each cell line). B) Representative Western blot of PGK1 expression in a panel of breast cancer cell lines. C) PGK1 expression in breast cancer cell lines averaged across the HER2+, ER+, and TNBC subtypes. For normalisation, β-actin expression was used as a loading control, and relative protein levels of PGK1 were normalised to MCF-10A loaded on each gel (+, non-tumour control). Data are presented as mean ± SEM. Statistical significance was evaluated by One-way ANOVA and *post-hoc* Tukey's Multiple Comparison Test; *p<0.05; **p<0.01; ***p<0.001.

4.2.8 *PGK1* expression in Cancer Cell Line Encyclopedia (CCLE) breast cancer cell lines

The hormone receptor (oestrogen and progesterone) and HER2 enrichment status of the breast cancer cell lines from the Cancer Cell Line Encyclopedia (CCLE) dataset, was used for categorisation into clinically important molecular subtypes including, luminal (ER+ and/or PR+, HER2+/-; n= 15), HER2 enriched/HER+ (ER-, PR-, HER2+; n= 8), and triple negative/basal-like (ER-, PR-, HER2-; n= 22) (Table 4.3).

Gene expression analysis of this dataset showed that *PGK1* mRNA exhibits significant difference between triple negative (ER-, PR- and HER2-) and HER2 enriched cell lines (ER-, PR- and HER+), with higher expression in cell lines that show increased HER2 expression ($p<0.05$; Figure 4.17). No significant differences in *PGK1* mRNA expression were observed between luminal and HER2 enriched, or between luminal and triple negative breast cancer cell lines. MCF-7 cells exhibited lower *PGK1* mRNA expression compared to MDA-MB-231 cells (Figure 4.17). According to the Cancer Dependency Map (DepMap), the sensitivity of breast cancer cell lines to paclitaxel and cyclophosphamide is not significantly associated with differences in *PGK1* mRNA expression (Figure 4.18).

Table 4.3. Molecular characteristics, subtypes and *PGK1* mRNA expression of breast cancer cell lines from Cancer Cell Line Encyclopedia (CCLE) assessed in this study.

Cell Line	ER status	PR status	HER2 enrichment	Subtype	PGK1 expression (RNAseq)
AU565_BREAST	-	-	+	HER2	7.622
BT20_BREAST	-	-	-	TN	6.051
BT474_BREAST	+	+	+	Lum	6.800
BT483_BREAST	+	+/-	-	Lum	7.015
BT549_BREAST	-	-	-	TN	6.735
CAL120_BREAST	-	-	-	TN	6.840
CAL148_BREAST	-	-	-	TN	6.738
CAL51_BREAST	-	-	-	TN	6.083
CAL851_BREAST	-	-	-	TN	7.375
CAMA1_BREAST	+	+/-	-	Lum	6.512
DU4475_BREAST	-	-	-	TN	6.141
EFM19_BREAST	+	+	-	Lum	6.643
EFM192A_BREAST	+	+	+	Lum	6.775
HCC1143_BREAST	-	-	-	TN	6.879
HCC1187_BREAST	-	-	-	TN	6.757
HCC1395_BREAST	-	-	-	TN	6.324
HCC1419_BREAST	-	-	+	HER2	6.795
HCC1428_BREAST	+	+	-	Lum	7.073
HCC1500_BREAST	+	+	-	Lum	7.175
HCC1569_BREAST	-	-	+	HER2	7.455
HCC1599_BREAST	-	-	-	TN	5.992
HCC1806_BREAST	-	-	-	TN	5.245
HCC1937_BREAST	-	-	-	TN	5.988
HCC1954_BREAST	-	-	+	HER2	7.992
HCC202_BREAST	-	-	+	HER2	6.524
HCC2157_BREAST	-	-	-	TN	6.297
HCC2218_BREAST	-	-	+	HER2	6.725
HCC38_BREAST	-	-	-	TN	5.321
HCC70_BREAST	-	-	-	TN	7.075
HDQP1_BREAST	-	-	-	TN	5.769
HS578T_BREAST	-	-	-	TN	7.677
KPL1_BREAST	+	-	-	Lum	6.697
MCF7_BREAST	+	+	-	Lum	7.103
MDAMB134VI_BREAST	+	-	-	Lum	5.889
MDAMB157_BREAST	-	-	-	TN	6.314
MDAMB175VII_BREAST	+	-	-	Lum	6.268
MDAMB231_BREAST	-	-	-	TN	7.876
MDAMB361_BREAST	+	+/-	+	Lum	7.076
MDAMB415_BREAST	+	+/-	-	Lum	6.433
MDAMB436_BREAST	-	-	-	TN	7.545
MDAMB453_BREAST	-	-	+	HER2	7.190
MDAMB468_BREAST	-	-	-	TN	6.642
SKBR3_BREAST	-	-	+	HER2	6.791

Table continues on the next page

T47D_BREAST	+	+	-	Lum	6.236
UACC812_BREAST	+	+/-	+	Lum	6.940
UACC893_BREAST	-	-	+	HER2	7.616
ZR751_BREAST	+	+/-	-	Lum	6.980
ZR7530_BREAST	+	-	+	Lum	6.440

ER: oestrogen receptor, **HER2**: Human epidermal growth factor receptor 2 (HER2 enriched subtype), **Lum**: Luminal subtype; **PR**: progesterone receptor; **TN:** triple negative/basal subtype; **+/-**: positive/negative.

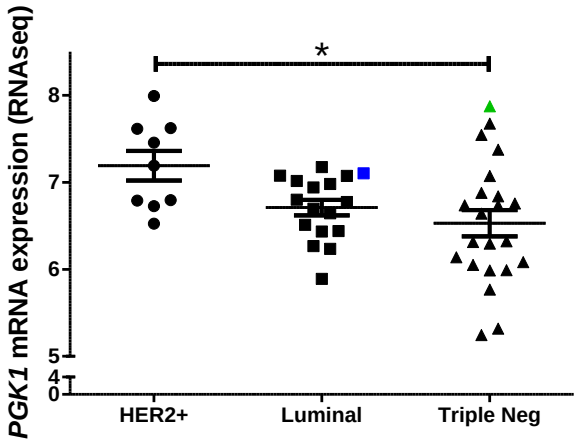

Figure 4.17. *PGK1* mRNA expression in breast cancer cell lines grouped by subtype.
Gene expression analysis of *PGK1* was reported by Cancer Cell Line Encyclopedia (CCLE). *PGK1* expression is shown for n= 48 breast cancer cell lines categorised by molecular subtype including, HER2+/HER2 overexpressing (ER-, PR-, HER2+; n= 9), Luminal (ER+ and/or PR+, HER2+/-; n= 17), and triple negative/basal-like (ER-, PR-, HER2-; n= 22) breast cancer. Blue square represents the MCF-7 cell line, and green triangle represents the MDA-MB-231 cell line. Error bars represent mean ± SEM. Statistical significance was evaluated by One-way ANOVA and *post-hoc* Tukey's Multiple Comparison Test; *p<0.05. ER: oestrogen receptor; PR: progesterone receptor, HER2: human epidermal growth factor receptor 2; RNAseq: ribonucleic acid sequencing.

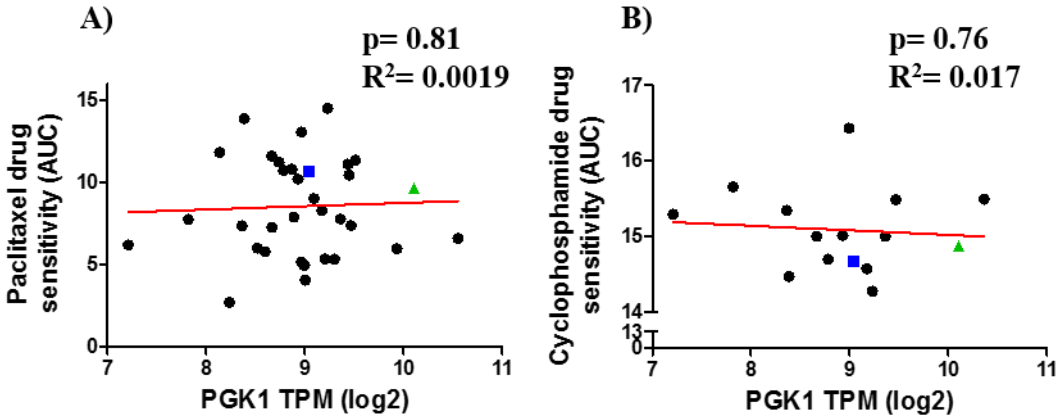

Figure 4.18. Correlation between *PGK1* transcript expression and breast cancer cell sensitivity to chemotherapy.
Breast cancer cell line sensitivity to A) paclitaxel (n= 33) and B) cyclophosphamide (n= 15) was determined by area under the curve (AUC), and is correlated with the expression of *PGK1* presented as transcripts per million (TPM); as reported by the Cancer Dependency Map (DepMap) project. Blue squares represent the MCF-7 cell line, and green triangles represent the MDA-MB-231 cell line. Statistical significance was evaluated by Pearson's correlation.

4.2.9 Expression of *PGK1* in breast tumours

To assess whether *PGK1* mRNA expression is associated with clinicopathological features and expression of other *PGK1* related genes in breast tumours, this study utilised publically available breast tumour datasets; The Cancer Genome Atlas (TCGA) and Molecular Taxonomy of Breast Cancer International Consortium (METABRIC). *PGK1* mRNA expression was compared with the presence or absence of the clinical biomarkers oestrogen receptor (ER), progesterone receptor (PR) and *ERBB2* expression (human epidermal growth factor receptor 2; HER2) status, and with the expression of hypoxia inducible factor 1α *(HIF-1α)* and solute carrier family 16 member 3 (*SLC16A3;* encoding for monocarboxylate transporter 4 [MCT4] protein) genes.

Gene expression analysis suggests that *PGK1* mRNA displays significant differences between ER positive and negative (+/-), PR+/- and HER2+/- breast tumours, with higher expression in ER- ($p<0.001$; Figure 4.19A and B), PR- ($p<0.001$; Figure 4.19C and D) and HER2+ ($p<0.01$ and $p<0.001$; Figure 4.19E and F, respectively) breast tumours. *PGK1* mRNA expression was significantly differentially regulated in luminal A breast tumours, with lower expression in luminal A breast tumours compared to all other subtypes, including luminal B, HER2 enriched, basal, and claudin-low breast tumours ($p<0.001$;Figure 4.20). *PGK1* mRNA expression is significantly positively correlated with both *HIF-1* and *SLC16A3* expression ($p<0.0001$), although the correlations were weak (correlation coefficient < 0.40; Figure 4.21).

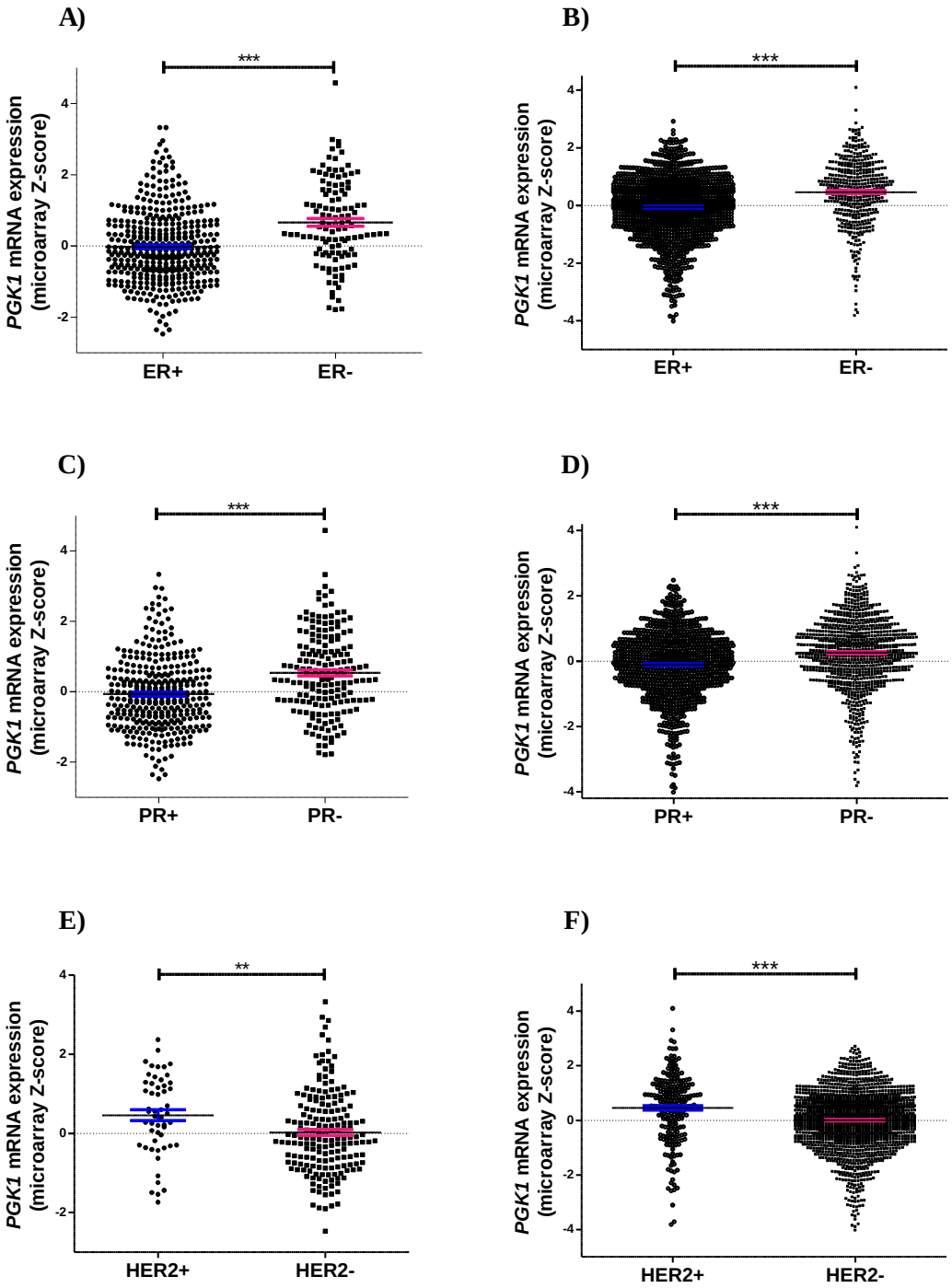

Figure 4.19. *PGK1* mRNA expression in breast tumours from the TCGA and METABRIC datasets.

There were a total of n= 521 TCGA (A, C and E) and n= 1904 METABRIC (B, D and F) breast tumours. Difference in *PGK1* expression (microarray z-score) in breast tumours that are A and B) ER positive (n= 405 TCGA; n= 1459 METABRIC) and ER negative (n= 117 TCGA; n= 445 METABRIC), C and D) PR positive (n= 344 TCGA; n= 1009 METABRIC) and PR negative (n= 177 TCGA; n= 895 METABRIC), and E and F) HER2 enriched (n= 53 TCGA; n= 236 METABRIC) and HER2 negative (n= 181 TCGA; n= 1668 METABRIC). Error bars represent mean ± SEM (blue and pink). Statistical significance was evaluated by unpaired two-tailed t-test. ** $p<0.01$; ***$p< 0.001$.

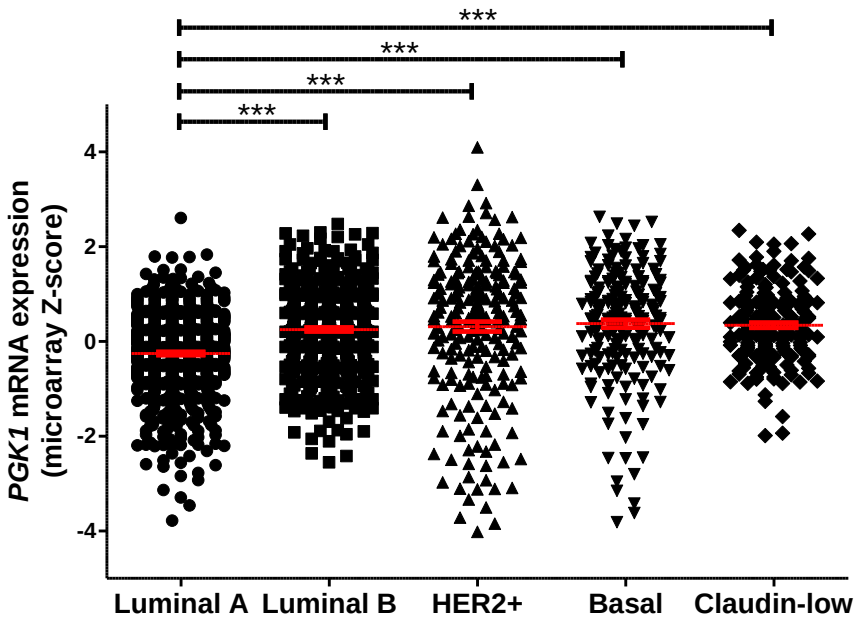

Figure 4.20. *PGK1* mRNA expression in METABRIC breast tumours grouped by subtype.
Difference in *PGK1* mRNA expression between breast tumour subtypes (total, n=1904) including luminal A (n= 679), luminal B (n= 461), HER2+ (n= 220), basal (n= 199), and claudin-low (n= 199). Statistical significance was evaluated by One-way ANOVA and *post-hoc* Tukey's Multiple Comparison Test. Error bars represent mean ± SEM (red bars). ***p<0.001.

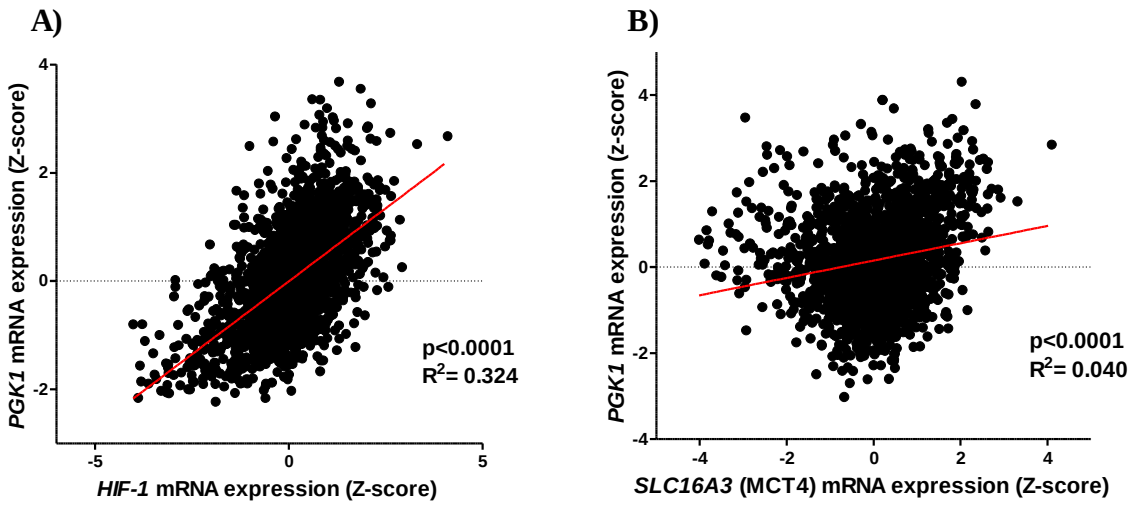

Figure 4.21. Correlation of *PGK1* with *HIF-1* and *SLC16A3* mRNA expression in METABRIC breast tumours.
PGK1 mRNA expression correlated with A) *HIF-1* mRNA expression and B) *SLC16A3* mRNA expression in METABRIC breast tumours (n= 1904). Statistical significance was evaluated with Pearson's correlation.

4.3 Discussion

Phosphoglycerate kinase 1 (PGK1) was upregulated in breast cancer cells co-cultured with mature breast adipocytes in the previous study chapter (Chapter 3). PGK1 catalyses the reversible conversion of 1,3-diphosphoglycerate to 3-phosphoglycerate, the first ATP generating step of glycolysis [370], and has been observed to be more highly expressed in breast tumours compared to normal breast tissue [399]. Moreover, increased PGK1 protein expression has been associated with breast cancer progression and poorer prognosis [349,371]. However, the influence of elevated PGK1 expression on breast cancer cell metabolism, growth and response to chemotherapy has yet to be investigated *in vitro.*

In this study, the PGK1 enzyme was transiently overexpressed in the molecularly distinct hormone receptor positive MCF-7 and triple negative MDA-MB-231 breast cancer cell lines. In MCF-7 cells, this overexpression led to increased sensitivity to chemotherapy, but made little to no difference in cell proliferation, viability or lactate production. Conversely, in MDA-MB-231 cells, transfection with *PGK1* expressing plasmids resulted in reduced cell proliferation and viability, and significantly increased lactate in the conditioned media. However, transfection with *GFP* expressing plasmids induced similar effects in MDA-MB-231 cells, suggesting phenotypic changes in MDA-MB-231 cells are likely to be in response to expression of plasmid DNA, rather than PGK1 overexpression specifically. From these data, we propose that overexpression of PGK1 *in vitro* could be promoting chemotherapy sensitivity in hormone receptor positive breast cancer cells in a glycolysis independent manner, and may be abrogating proliferation and viability in hormone receptor negative breast cancer cells, although this requires further investigation.

In addition, analysis using publicly available data showed *PGK1* mRNA expression to be significantly higher in HER2 enriched (HER2+) compared to HER2 negative (HER2-) breast cancers (Figure 4.17 and Figure 4.19), suggesting that gene expression of *PGK1 in vivo* may be associated with this clinically important breast tumour biomarker.

4.3.1 Effect of PGK1 overexpression on MCF-7 and MDA-MB-231 cell phenotypes *in vitro*

Previous studies overexpressing PGK1 protein in hepatocellular and gastric cancer cell lines suggest that elevated PGK1 abundance is tolerated by non-breast tumour cells grown

in vitro [364,365]. To the best of our knowledge, this study is the first to report overexpression of PGK1 in human breast cancer cells.

4.3.1.1 Lactate production

Cancer cells have been shown to reprogram their metabolism to preferentially perform aerobic glycolysis in order to fulfil their energetic requirements, a phenomenon referred to as the 'Warburg effect'[380]. Aerobic glycolysis consists of an increase in the conversion of glucose into pyruvate, even under high oxygen conditions, in which cancer cells correspondingly exhibit increases in glucose uptake and production of lactate [380,396]. In this study, intracellular lactate concentrations measured in MCF-7 and MDA-MB-231 cells, and extracellular lactate secreted by MCF-7 cells, was not altered by PGK1 overexpression. There was a notable increase in the concentration of lactate in the conditioned media of MDA-MB-231 cells overexpressing PGK1 compared to untreated cells, although this increase was significantly lower than the lactate concentrations evident in the conditioned media of MDA-MB-231 cells transfected with a *GFP* expressing plasmid, suggestive of a plasmid expression effect. Thus, exclusively upregulating PGK1 does not seem to notably encourage aerobic glycolysis in MCF-7 cells, but may be increasing the production and subsequent secretion of lactate in MDA-MB-231 cells, although further analysis of the transfection model would need to be performed to validate these findings.

Altered expression of PGK1 in human breast cancer cells has been previously associated with changes in energy production, where knockdown of *PGK1* decreased the concentration of ATP produced in both the cytoplasm and mitochondria of MCF-7 and MDA-MB-231 cells [372]. The decrease in cytosolic ATP reported following knockdown of *PGK1* in MDA-MB-231 cells could suggest a reduction in the rate of aerobic glycolysis [372], which would support the elevated levels of lactate in the conditioned media of PGK1 overexpressing MDA-MB-231 cells measured in the current study (Figure 4.12). Moreover, the reduction in cytosolic and mitochondrial ATP measured after *PGK1* expression was decreased [372], provides evidence to suggest that changes in lactate concentrations of PGK1 overexpressing MCF-7 cells were undetected because pyruvate produced via glycolysis was likely preferentially fuelling the TCA cycle in these cells, rather than being converted into lactate. Overall, these findings suggest that alterations in PGK1 mRNA and protein expression may be influencing breast cancer cell metabolism. Further research would benefit from more direct measures of the glycolytic and mitochondrial respiratory flux in human breast cancers with variable PGK1 expression.

Lactate levels in the conditioned media of MDA-MB-231 cells were higher than for MCF-7 cells, across all experimental conditions. Secretion of lactate from tumour cells occurs through the hypoxia-induced lactate transporter monocarboxylate transporter 4 (MCT4) [396], which has low affinity to pyruvate, and so in highly glycolytic tumour cells, upregulation of MCT4 expression promotes lactate dehydrogenase enzymes to convert pyruvate to lactate [400]. MCT4 is commonly increased in tumour cells [401–403], including breast cancer cells [379]. Under both normal oxygen and hypoxic conditions, MCT4 gene expression (known as solute carrier family 16 member 3, *SLC16A3*) is observed to be much higher in hormone receptor negative MDA-MB-231 cells than hormone receptor positive MCF-7 cells [379]. In addition, triple negative breast tumours have been shown to basally express higher levels of MCT4 protein [404], suggesting that triple negative tumours may be innately better equipped to secrete excess lactate produced during increased glycolytic flux. The current study did not assess MCT4 expression in MCF-7 and MDA-MB-231 cells overexpressing PGK1 protein, but did observe a positive correlation between *PGK1* and *SLC16A3* gene expression in a large cohort (METABRIC) of breast tumours, in which 398 tumours had basal-like or claudin-low molecular phenotypes (Figure 4.21). Thus, it could be speculated that MCT4 expression may be elevated in PGK1 overexpressing MDA-MB-231 cells, facilitating enhanced lactate secretion, and thus quantification of MCT4 expression in future investigations of the effects of PGK1 overexpression would be worthwhile.

Until recently, it was assumed that PGK1 primarily promoted tumourigenesis by catalysing a key step in the glycolytic pathway. However, evidence is accumulating to show that PGK1 has a number of other mechanistically distinct functions, which are determined by subcellular localisation [373–375]. In the cytosol, PGK1 can phosphorylate Beclin 1 (BECN1) at S30 under hypoxia stimulation or glutamine deprivation, encouraging the initiation of autophagy [375]. Under hypoxia PGK1 has been observed to translocate to the mitochondria, where it acts as a protein kinase phosphorylating pyruvate dehydrogenase kinase 1 (PDHK1) at T338. Phosphorylation of PDHK1 leads to the inhibition of the pyruvate dehydrogenase complex causing reduced mitochondrial pyruvate utilisation, and thus increased lactate production through promotion of aerobic glycolysis [374]. Moreover, PGK1 has been shown to bind to DNA polymerases α and ε in the nucleus, upregulating the synthesis of DNA [405,406], and has recently been determined to translocate from the cytosol to the nucleus, where it co-localises with HIV-Tat Specific Factor 1 (HTATSF1) [407]. Another study suggests that PGK1 expressed in the nucleus of brain cancer cells binds to CDC7 and promotes DNA helicase

recruitment, DNA replication and cell proliferation [408]. Furthermore, PGK1 secreted by fibrosarcoma cells may be acting as a disulphide reductase by binding and reducing disulphide bonds of plasmin, thus permitting the cleavage of plasminogen and promoting formation of angiostatin in the extracellular compartment, inhibiting tumour angiogenesis [373,409]. Taken together, these studies suggest that overexpression of PGK1 in the breast cancer cells used in this study may not be exclusively affecting metabolic activity, but rather influencing an array of cellular functions.

In addition to playing a role in determining sub-cellular localisation, a number of reports show that post-translation modification of PGK1, including phosphorylation, acetylation and ubiquitination, may regulate the glycolytic and non-glycolytic activity of PGK1 in tumour cells [374,375,408,410–412]. In liver cancer cells, acetylation of PGK1 at K323 enhanced its metabolic activity, and was associated with poorer prognosis in clinical tumours [412]. Another study showed that it was acetylation of PGK1 at K388 that lead to its binding with, and phosphorylation of BECN1 [375]. The translocation of PGK1 into the mitochondria where it phosphorylates PDHK1 is reliant on it being phosphorylated at S203 [374], and binding of PGK1 to CDC7 in the nucleus is dependent on it being phosphorylated at S256 [408]. Furthermore, non-small cell lung cancer (NSCLC) cell growth was suppressed following post-translation ubiquitin-mediated degradation of PGK1, regulated by Rab11-binding protein Rab11-FIP2 [411]. Therefore, to better understand the functional role of PGK1 shown to be upregulated in advanced breast cancers, future research would benefit from analysing both the post-translational modifications and the sub-cellular localisation of PGK1 in breast cancer cells *in vivo*.

4.3.1.2 Cell proliferation

PGK1 overexpression significantly reduced cell proliferation and live cell number in MDA-MB-231 cells, although this was concurrent with GFP induced reductions in MDA-MB-231 cell proliferation and live cell number (Figure 4.11 and Figure 4.13). MCF-7 cells showed an insignificant decrease in cell proliferation following PGK1 overexpression (Figure 4.13). If induced by PGK1 overexpression, reductions in live cell number and proliferation would be unexpected based on previous *in vivo* findings that suggest increased PGK1 expression is associated with larger more advanced stage tumours and poorer survival outcomes in patients treated with paclitaxel [349,371]. Moreover, *in vitro* observations have previously determined that the knockdown of 17beta-hydroxysteroid dehydrogenase type 5

(17β-HSD5) upregulated PGK1 expression and increased rates of proliferation in MCF-7 cells [413], and that the activation of peroxisome proliferator-activated receptor γ (PPARγ) decreased PGK1 expression and initiated apoptosis in MCF-7 and MDA-MB-231 breast cancer cells [372]. Thus, other than the likely influence of plasmid DNA transfection, it is possible that other factors associated with the cell lines may have influenced the lowered survival and replication of the breast cancer cells in this study.

In comparison to MDA-MB-231 cells, MCF-7 cells seemed to better tolerate the expression of plasmid DNA. Importantly though, any reductions in breast cancer cell proliferation and live cell number were not associated with transfection reagent toxicity. It has recently been suggested that GFP expression in cells can induce oxidative stress that affects expression of genes involved in important biological pathways [414]. Therefore, it is possible enforced GFP expression in this study may be inhibiting the proliferation and live cell number of the transfected breast cancer cells. However, this does not explain the reduction in proliferation evident in cells overexpressing PGK1. Thus, future investigations would benefit from the transfection of a similar sized 'empty' vector, to determine whether the expression of plasmid DNA is influencing the survival and replication of MCF-7 and MDA-MB-231 cells.

It is possible that differences in response to *GFP* and *PGK1* transfection in MCF-7 and MDA-MB-231 cells may be driven in part by differences in oncogenic mutations intrinsic to the breast cancer cell lines [384]. P53 is a tumour suppressor that has well-established roles in protecting malignant cell development but also tumour progression [415]. MCF-7 cells carry a wildtype *TP53* gene, whereas the more invasive MDA-MB-231 cells have a mutant *TP53* gene [384]. P53 is recognized for its use as a prognostic marker in breast cancer [385], and interestingly, can influence how cells respond to altered expression of certain genes and proteins [415,416]. Thus, it may be interesting for further studies to consider the influence of PGK1 protein upregulation on p53 activity in cell lines with differing *TP53* status.

4.3.1.3 Chemotherapy response

In this study, transient overexpression of PGK1 protein led to an insignificant decrease in the viability of MCF-7 cells. However, in combination with paclitaxel or cyclophosphamide, PGK1 overexpression in MCF-7 cells significantly reduced the viability of the cells. In comparison to MCF-7 cells, MDA-MB-231 cells showed a significant decrease in viability with PGK1 overexpression, but this decrease in viability was not exacerbated by

paclitaxel or cyclophosphamide treatment. To the best of our knowledge this is the first study to report on the association between PGK1 protein expression and sensitivity to both paclitaxel and cyclophosphamide in MDA-MB-231 cells. The current observations of reduced viability in chemotherapy treated PGK1 overexpressing MCF-7 cells are supported by a previous investigation that found PGK1 expression to be downregulated in adriamycin- and paclitaxel-resistant MCF-7 cells [417]. Taken together, these findings suggest that increased expression of the PGK1 enzyme may make MCF-7 cells more susceptible to the cytotoxic effects of chemotherapy.

Increased PGK1 expression has been observed in adriamycin-resistant leukaemia cells [418], cisplatin-resistant ovarian carcinoma cells [419,420], and PGK1 overexpression has been associated with the induction of a multi-drug resistance phenotype in human osteogenic sarcoma cells [367]. Furthermore, previous investigations have shown that by knocking down PGK1 protein expression in endometrial and gastric carcinoma cells, the inhibitory/cytotoxic effects of chemotherapy are enhanced [368,398]. Thus, expression of PGK1 appears to play a key role in chemotherapy resistance in many cancer types. Based on *in vitro* findings in MCF-7 cells[417] and current study results (Figure 4.18), the role of PGK1 in breast cancer may not concord with other cancers. However, previous *in vivo* investigations in breast tumours suggest that the role PGK1 is similar to findings in other cancers. PGK1 expression was decreased in breast tumours that exhibited a response to chemotherapy treatment [421], and higher PGK1 expression in breast tumours from patients treated with paclitaxel resulted in worse overall survival [349]; suggesting that PGK1 overexpression is prognostic of chemotherapy resistance in the clinical setting, particularly to paclitaxel. Thus, further research assessing the effects of PGK1 protein expression on breast tumour response to chemotherapies are warranted.

Paclitaxel and cyclophosphamide were chosen for use in this study as they are currently utilised chemotherapeutics in the clinical treatment of patients with breast cancer. Paclitaxel and cyclophosphamide achieve cytotoxicity by targeting cell replication processes. Paclitaxel inhibits mitosis, causing cell cycle arrest, by stabilising microtubules and preventing the reorganisation of the microtubule network that is essential during mitosis [422,423]. After rapid hepatic metabolism, metabolites of cyclophosphamide form crosslinks between and within DNA strands that are irreversible and interfere with DNA replication and transcription, resulting in cell apoptosis [271]. In this study, the aim was to reduce control cell viability by approximately 50% during paclitaxel and cyclophosphamide treatment, yet

neither chemotherapy achieved this reduction. It is possible that variation in experimental design between the dose-response and PGK1 overexpression experiments altered the chemotherapeutic effects. Nevertheless, PGK1 overexpression was not able to protect the viability of the breast cancer cells from chemotherapy treatment, despite the cytotoxicity being lower than expected.

Cyclophosphamide is a prodrug that *in vivo* undergoes hepatic metabolism into its main active metabolite, 4-hydroperoxycyclophosphamide. 4-hydroperoxycyclophosphamide exists in equilibrium with its tautomer, aldophosphamide, which can diffuse into cells. When cells are low in aldehyde dehydrogenase (ALDH) levels, aldophosphamide is converted into phosphoramide mustard which forms crosslinks between and within DNA strands at N7 position of guanine, causing cellular apoptosis [271]. ALDH is a well-established marker of breast cancer stem cells, and higher ALDH expression has been associated with poor clinical outcome, resistance to chemotherapeutic agents, and positive HER2 expression in breast cancer [424–426]. The current study did not address the levels of ALDH expression in the breast cancer cells treated with 4-hydroperoxycyclophosphamide, and whether transfection with GFP or PGK1 encoding plasmids altered the ALDH levels. Interestingly, both breast cancer cell lines used in this study chapter are known to be negative for HER2 overexpression [335], which suggests inherently lower levels of ALDH are present in these cells. However, it is still possible that ALDH levels influenced the cytotoxic effects of 4-hydroperoxycyclophosphamide, but this requires further investigation.

4.3.1.4 Considerations of the PGK1 overexpression experimental model

The current study initially selected the TRIPZ inducible lentiviral system for transducing *PGK1* into the MCF-7 and MDA-MB-231 cell genomes based on its high transduction efficiency in non-dividing cell populations and its ability to stably integrate introduced material into the host genome. This study attempted the insertion of the HIS/FLAG/HA tagged *PGK1* gene sequence into the TRIPZ vector backbone between the *Xho*I and *Mlu*I restriction sites, and was able to confirm successful ligation of the insert at *Xho*I. However, sequencing could not validate ligation of the insert at *Mlu*I despite successful insertion with this site in previous studies overexpressing catalase in human colon carcinoma cells and E-cadherin in human epidermoid carcinoma cells using the TRIPZ lentiviral system; achieved by replacing the shRNA cassette, between the *Age*I and *Mlu*I restriction sites, with the coding sequences for these genes [427,428].

Instead of stable transduction, PGK1 expression in this study was upregulated in MCF-7 and MDA-MB-231 breast cancer cells by transfection with an established *PGK1* expressing vector using the JetPRIME® polymer-based transfection reagent. A major advantage of cationic polymer molecules, such as the JetPRIME® reagent, is they form polymer-DNA complexes that are taken up by the host cell via endocytosis [429,430], and therefore in comparison to viral transduction, polymer-based transfection has much lower cytotoxicity and promotes transfection efficiency by condensing the transfected DNA [429–431]. Furthermore, by performing polymer transfection for transient upregulation of PGK1 protein, this study avoided the potential for host cell mutagenesis, which can occur with lentiviral vectors randomly integrating into the host genome, disrupting essential genes and potentially causing oncogene activation [432].

The current analysis indicated that transfected breast cancer cells expressed two different forms of PGK1 protein, the endogenous PGK1 enzyme and a slightly larger variant determined as the PGK1 enzyme fused with an N-terminal poly-HIS-FLAG-HA tag. Transfected MDA-MB-231 cells mostly expressed the endogenous untagged PGK1 protein, whereas MCF-7 cells expressed more of the larger tagged PGK1 protein following transfection, and thus the analysis of PGK1 protein overexpression in MCF-7 cells may have been impacted by this. Although, the exact structure and function of the tagged PGK1 protein was not investigated in the current analysis, it was assumed that the small size of the tag was unlikely to obscure the conformational domains of the protein, and therefore both forms were considered to constitute active PGK1 enzymes in the analysis of results.

According to microscopic images taken to assess EGFP transfection efficiency, the number of expressing vectors transfected into each MCF-7 and MDA-MB-231 cell varied across the cell populations. Thus, it was considered that non-transfected cells with basal levels of PGK1 protein expression may have influenced the measured effects of the PGK1 overexpressing populations. However, the average expression of PGK1 protein across the cell populations was established to be increased in both cell lines, and for this reason, overexpression of PGK1 was analysed and interpreted for its effect over the cell population, rather than any potential impact at the single cell level. Selection for vector DNA expression to isolate only transfected cells could be considered for future research using this study's transfection protocol [433].

The MCF-7 cells showed higher PGK1 expression following transfection than the MDA-MB-231 cells in this study, however, the MDA-MB-231 cells exhibited higher transfection efficiencies. It is well recognised that transfection efficiency differs between mammalian cell lines [434], and in agreement with this study the transfection efficiency of foreign DNA has been shown to be higher in MDA-MB-231 compared to MCF-7 cells using variety of different transfection reagents [435]. Higher PGK1 protein expression in MCF-7 cells may be explained by the fact that transfection with encoding DNA (*GFP* and *PGK1*) resulted in a statistically significant reduction in MDA-MB-231 live cell number, proliferation, and viability, whereas, MCF-7 cells only exhibited a statistically significant reduction in viability following transfection with a GFP encoding plasmid. Taken together, these results suggest that plasmid DNA transfection into MDA-MB-231 cells may be easier than MCF-7 cells, yet MCF-7 cells seem to tolerate the introduction of the foreign DNA, and/or the subsequent expression of the plasmid encoded proteins better than MDA-MB-231 cells.

Lastly, in this study, transfection with a *GFP* encoding plasmid was used as a vehicle control for *PGK1* plasmid transfection, and interestingly, GFP expression exhibited a greater reduction in MCF-7 and MDA-MB-231 cell viability than PGK1 protein overexpression. Recently, GFP expression in cells was found to induce oxidative stress that affected the expression of genes involved in important biological pathways, including decreased stabilisation and activity of HIF-1α [414]. HIF-1α is known to regulate the expression of genes associated with cell metabolism [393,394]. Therefore, it could be hypothesised that GFP expression is causing an increase in oxidative stress that is leading to reduced HIF-1α activity, and subsequently decreased metabolic viability. MDA-MB-231 cells expressing GFP in this study showed elevated secretion of lactate. GFP expressing MDA-MB-231 cells increased lactate secretion more than PGK1 overexpressing MDA-MB-231 cells, suggesting that elevated lactate secretion may not be occurring in direct response to PGK1 overexpression. It is possible that the source of elevated lactate in MDA-MB-231 conditioned media is intracellular lactate released during cell death, which would correlate with the increased number of dead MDA-MB-231 cells observed after plasmid mediated expression of GFP and PGK1.

4.3.2 Association with clinical biomarkers and expression of PGK1 in breast cancer

Molecular phenotypes of breast tumours are relevant to the clinical prognosis and treatment of the disease [104,105,107,111,112]. PGK1 protein expression was previously determined to have no association with any particular breast tumour molecular subtype [349], and prior to the current analysis the association between *PGK1* gene expression and breast cancer molecular subtypes had not been assessed. In this study, breast cancer cell lines showed significantly higher *PGK1* expression in HER2 enriched compared to triple negative breast cancer cells, whereas, breast tumours showed no difference in *PGK1* expression between HER2 enriched, luminal B, basal-like or claudin-low tumours (Figure 4.17), although did exhibit lower *PGK1* expression in breast tumours characterised as being luminal A compared to all other breast tumour subtypes (Figure 4.20). Based on these findings, it could be speculated that mRNA and protein expression of PGK1 is not likely molecular subtype dependent, but rather responds predominantly to HER2 signalling in breast cancer.

Analysis of *PGK1* gene expression in large publicly available datasets (TCGA, METBRIC), determined that *PGK1* was significantly upregulated in HER2 overexpressing (HER2+) compared to HER2- breast tumours (Figure 4.19). These results are supported by previous investigations, observing elevated expression of PGK1 in HER2 enriched tumours as measured by mass spectrometry [369,436] and immunohistochemistry [349], suggesting that mRNA and protein expression of PGK1 in breast tumours overexpressing HER2 are likely positively correlated; although this has yet to be addressed directly. Moreover, it has been shown that the monoclonal antibody Herceptin, through its partial blocking of the HER2 signalling pathway, considerably decreased the expression of PGK1 in the HER2+ SKBR3 breast cancer cell line [369], providing strong evidence for a direct association between HER2 signalling and PGK1 regulation in breast cancer. PGK1 protein expression measured in a panel of breast cancer cell lines in this study was not differentially expressed between HER2+ and HER2- subtypes, however the sample numbers were small making results vulnerable to outliers, and thus these differences would likely change with larger sample sizes. Overall, results from this chapter along with investigations by others, suggests that PGK1 may represent a co-expressing HER2 related enzyme. As the majority of the work carried out in this study chapter was performed in HER2 negative breast cancer cell lines, further

investigation is required to better determine the biological and clinical implications of PGK1 overexpression in HER2 enriched breast cancers.

In the cohort of breast tumours assessed in this study (METABRIC), *PGK1* expression was paralleled with an increase in *SLC16A3* (encoding for MCT4 protein) and *HIF-1α* expression (Figure 4.21). PGK1 and MCT4 expression are well known to be regulated by hypoxia in a HIF-1α dependent manner [392,393,437], and this is true in breast cancer [371,404]. Larger more aggressive tumours that show greater resistance to cancer therapeutics have been shown to be more hypoxic [438], and in breast cancer, larger more advanced stage tumours, poorer disease-free survival, and worse overall survival in patients treated with paclitaxel, have all been correlated with elevated expression of PGK1 [349,371]. An elevated hypoxic signature is a negative prognostic factor in breast cancer [439], where simultaneous presentation of HER2 overexpression and HIF-1α reactivity has been linked with breast cancer aggression [440]. Therefore, it is possible that the HIF-1α-PGK1 signalling axis is aiding in the promotion of HER2 overexpressing breast cancers, and thus, may be a potential target for future study and therapeutic development.

4.4 Summary

The data presented in this chapter showed that transfection of MCF-7 and MDA-MB-231 breast cancer cells transiently upregulated expression of PGK1, however, overexpression of PGK1 did not promote cell growth or survival. Elevated PGK1 expression did not alter live cell number, proliferation, or lactate production in MCF-7 cells, yet increased sensitivity to chemotherapy. Moreover, despite overexpression of PGK1 increasing the level of lactate released by MDA-MB-231 cells into the media, elevated expression of PGK1 reduced cell proliferation and viability in these cells, and similar effects were evident in GFP transfected MDA-MB-231 cells, therefore implicating the expression of plasmid DNA, rather than PGK1 overexpression, in the manifestation of these phenotypic alterations. Overall, the transient transfection model utilised for PGK1 overexpression in this study requires further optimisation. Thus, further research is still required to fully understand the biological role of PGK1 in breast cancer.

Chapter 5

Influence of obesity-related systemic inflammation on hepatic cytochrome P450 activity in women with breast cancer: A patient feasibility study

5.1 Introduction

Obese women with breast cancer have increased levels of circulating obesity-related inflammatory cytokines, and poorer pathological response rates to chemotherapy [63,116,122]. In contrast, combined aerobic and resistance exercise implemented during adjuvant chemotherapy has displayed a trend toward improved breast cancer disease free survival outcomes, particularly for women who were overweight or obese [188]. Two systematic reviews have concluded there is biological relevance in the association between exercise and breast cancer outcome, as physical activity can positively alter levels of circulating inflammatory cytokines and other cancer-related biomarkers [441,442]. A number of biological mechanisms have been proposed to explain the complex relationships between systemic inflammation and breast cancer outcome, with many of these focused around the direct interaction between inflammatory markers and breast tumour cells [148–150]. To date, less attention has been directed toward the impact of systemic inflammation on the hepatic metabolism of clinically important breast cancer chemotherapy agents that operate under very narrow therapeutic windows. Thus, this study hypothesises that elevated circulating inflammatory cytokines decrease activity of drug metabolizing enzymes in obese women receiving chemotherapy for breast cancer, and secondly that concentrations of circulating inflammatory markers in these women are influenced by obesity and levels of physical activity.

A number of hepatic cytochrome P450 (CYP) drug metabolising enzymes, including CYP1A2, CYP2C9, CYP2C19, CYP2D6, and CYP3A4, are involved in metabolism of currently utilised breast cancer chemotherapy, such as tamoxifen, cyclophosphamide, dexamethasone, doxorubicin and paclitaxel [264,266]. Alteration in the activity of these CYP enzymes may lead to altered efficacy or toxicity in breast cancer patients being treated with chemotherapies [264,265,267]. Evidence for inflammation-induced repression of hepatic CYP expression has been presented *in vitro* [300–303]. Altered CYP activity has been observed in inflammatory-associated disease states, including HIV and hepatitis C infection, liver disease and cancer [283,306–310,316]. However, only one study has observed alterations in CYP activity associated with levels of circulating inflammatory markers, in which decreased activity of the CYP3A4 was correlated with an increase in circulating C-reactive protein (CRP; a marker of inflammation associated with the acute phase response) expression in advanced cancer patients [317].

Whether in whole animal models or human subjects, *in vivo* CYP activity has been studied using CYP-specific probe drugs. Using concurrent oral administration of five probe drugs in twelve healthy Korean males, Ryu *et al*. demonstrated that the activity of CYP1A2, CYP2C9, CYP2C19, CYP2D6, and CYP3A4 could be evaluated using only a 4 hour blood sample and a 0-8 hour urine collection [290]. *In vivo* metabolic activity of CYP1A2, CYP2C9, CYP2C19, CYP2D6, and CYP3A4 after single administration of losartan and midazolam, or dosing with a well-known three drug cocktail of caffeine, omeprazole and dextromethorphan, was not significantly different from the metabolic activity exhibited after the administration of all five probe drugs concurrently, named the 'Inje cocktail'; indicating no probe-drug component interactions [290]. Subsequently, the use of the 'Inje cocktail' to assess metabolising activity of CYP1A2, CYP2C9, CYP2C19, CYP2D6, and CYP3A4 has been investigated in drug-drug interaction studies, by co-administering the probe drugs alongside other drugs of interest [443,444]. However, to the best of our knowledge, the use of the 'Inje cocktail' to assess drug-drug or disease-drug interactions resulting in altered CYP activity has not yet been carried out in cancer patients.

This study chapter carried out an exploratory patient study recruiting non-obese (BMI < 30) and obese (BMI ≥ 30) women being treated with chemotherapy for stage II or III breast cancer. *In vivo* activity of CYP1A2, CYP2C9, CYP2C19, CYP2D6, and CYP3A4 was assessed using the 'Inje' probe drug cocktail and mass spectrometry analysis, and was subsequently related to serum concentrations of inflammatory cytokines quantified by

immunoassays. Differences in body morphometry and daily step counts were measured in order to assess whether alterations in CYP activity may be attributable to obesity or physical activity influencing the levels of circulating inflammatory cytokines.

5.1.1 Aims

The aim of this study chapter was to explore the association between body morphometry, physical activity, circulating inflammatory cytokines and metabolising activity of CYP enzymes in women being treated with chemotherapy for early stage II or III breast cancer. This was assessed by:

1) Assessing body mass index (BMI), waist to hip ratio (WHR) and body fat percentage before chemotherapy (following diagnosis, and prior to starting neoadjuvant or adjuvant chemotherapy) and again after chemotherapy (following dose six of paclitaxel).
2) Measuring daily step counts for the 21 days following adriamycin-cyclophosphamide (AC) cycle one, 7 days after both paclitaxel dose one and dose six, and relating step counts to body morphometry measures.
3) Quantifying the concentration of selected circulating inflammatory cytokines in serum samples collected before chemotherapy, after AC cycle one, following paclitaxel dose one and dose six and relating these to body morphometry and step count measures.
4) Investigating metabolising activity of CYP enzymes before and after chemotherapy and relating any changes in metabolising activity during chemotherapy with changes in circulating inflammatory cytokine concentrations.

5.1.2 Experimental approach

A schematic diagram outlining the study protocol is shown in Figure 2.4. The experimental approaches taken for this clinical study chapter are described in detail at the beginning of each relevant results section (see Sections 5.2.1.1, 5.2.2.1, 5.2.3.1, and 5.2.4.1).

5.1.3 Acknowledgments

Mass spectrometry assessment of the probe drug cocktail compounds was optimised and performed by Mei Zhang and Assoc. Prof. Matthew Doogue (University of Otago Christchurch, Department of Medicine, Clinical Pharmacology). Advice for the statistical analysis of data generated during this study was provided by Prof Chris Frampton

(Biostatistician, University of Otago Christchurch, Department of Medicine). I would like to thank Helen Morrin (CSTB curator, University of Otago Christchurch, Department of Pathology and Biomedical Sciences) for her expertise in clinical trial ethics and study design. I also thank Anne Smith and the rest of the Christchurch Oncology Research Unit (CORU) research team (Oncology, CDHB) for their dedication to aiding in participant recruitment and sampling. I would also like to acknowledge the team of breast oncologists at CDHB for their engagement in this study. Lastly and very importantly, I would like to say a huge thank you to all the women who participated in this study.

5.2 Results

5.2.1 Participant recruitment

5.2.1.1 Experimental approach

Recruitment took place between 1/3/2017 and 25/12/18. Patients were screened by study nurses based on a range of inclusion and exclusion criteria (Section 2.10.2 and Appendix B). Potential participants were then approached by medical oncologists at their first oncology appointment. Recruited participants gave informed written consent for their participation in the study, the use of their specimens (blood and urine) for research purposes, and access to their medical records.

5.2.1.2 Recruitment rates

Ethical approval for this study originally included recruitment of women with stage II and III breast cancer being treated with adjuvant adriamycin-cyclophosphamide (AC)-paclitaxel chemotherapy. Based on slower than anticipated rates of recruitment, this study amended the protocol, approximately three months after recruitment started (on 7/6/2017), to include women with stage II and III breast cancer receiving neoadjuvant chemotherapy. Recruitment onto this study did not alter clinical treatment for the participant (see Figure 2.4 for a schematic of the study schedule).

Mosaiq electronic records (Elekta, Stockholm, Sweden) were used to determine the recruitment rates onto this study. There were 107 stage II or III breast cancer patients receiving AC and paclitaxel chemotherapy (neoadjuvant or adjuvant) registered on Mosaiq under the Canterbury Regional Cancer & Haematology Service at Christchurch Hospital (CDHB) between 1/3/2017 and 6/8/2018 (Figure 5.1). Over the same period (1/3/2017 and 6/8/2018) eleven participants were recruited onto this study, a recruitment rate of 10.28% (11/107; Figure 5.1). 31.8% of the registered patients (34/107) were considered ‘not eligible’ for this study based on other exclusion criteria, and 57.9% of the registered patients (62/107) were considered ‘not recruited’ despite being eligible for this study (Figure 5.1). ‘Not eligible’ patients were excluded mostly because they lived out of Christchurch, and thus, were receiving a portion of their treatment at other oncology centres including Ashburton, Greymouth, and Timaru hospitals; making the additional clinical visits required to participate in this study unfeasible for those patients. Further factors rendering patients ineligible were, starting neoadjuvant chemotherapy prior to 7/6/2017, hepatitis C, and receiving paclitaxel dosing prior to AC cycles. Anecdotally, the most notable deterrent to consent for those

patients that were approached but were considered ‘not recruited’ was the additional time commitment; especially for full time workers and women with families (data not shown).

Following assessment of recruitment rates, another study participant was recruited between 6/8/2018 and 25/12/2018, and thus, the final number of participants recruited onto this study was twelve (n=12).

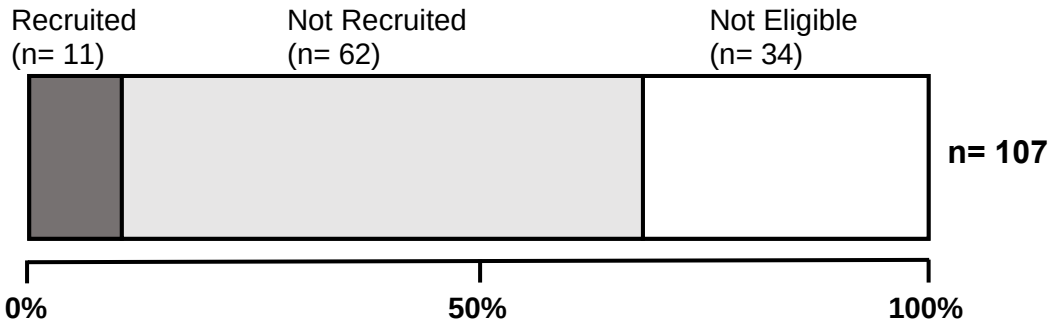

Figure 5.1. Recruitment rates.
Recruitment of women with stage II and II breast cancer receiving adriamycin-cyclophosphamide (AC) and paclitaxel (neoadjuvant or adjuvant) who were registered on HCS under the Canterbury Regional Cancer & Haematology Service at Christchurch Hospital (CDHB) between 1/3/2017 and 6/8/2018 (total n= 107).

5.2.2 Demographics and body morphometry

5.2.2.1 Experimental approach

Body morphometry was measured using body mass index (BMI), waist to hip ratio (WHR) and body fat and muscle mass percentages calculated for each participant at baseline (before chemotherapy) and following dose six of paclitaxel (after chemotherapy) (Chapter 2; Section 2.10.3). BMI was calculated from height and weight, by dividing a participant's weight in kilograms by their height in meters squared (BMI= kg/m^2). WHR was calculated as the waist circumference divided by the hip circumference. Body fat and muscle mass percentages were determined using the Tanita Body Composition Analyser (Chapter 2; Section 2.10.4). Associations between BMI, WHR and body fat percentage before chemotherapy, and the change in body morphometry during chemotherapy, was assessed.

Waist and hip circumference measures were missed from participant 1 following paclitaxel dose six, and therefore, changes in WHR during chemotherapy could not be calculated. Due to clinical complications participant 7 was only able to complete two out of the twelve (2/12) scheduled paclitaxel doses, and was withdrawn from the study. Therefore, participant 7 did not have body morphometry measures taken after chemotherapy, and thus, any change during chemotherapy could not be assessed.

5.2.2.2 Participant demographics and body morphometry

Overall, this study recruited twelve women with stage II or III breast cancer being treated with neoadjuvant or adjuvant chemotherapy at Christchurch Hospital (Table 5.1). Reported ethnicity of participants were NZ European (n= 9), NZ Māori (n= 1), English (n= 1), and other (n= 1) (Table 5.1). At the time of recruitment (baseline), participants were aged from 40 to 68 years (Table 5.1). Six participants were aged 49 years or below (and were considered pre-menopausal), and six were aged 50 years or above (and were considered post-menopausal). Half of the participants received neoadjuvant chemotherapy (n= 6), and half (n= 6) received adjuvant chemotherapy following surgery (Table 5.1). At baseline, BMI ranged from 20.7 to 39.4, WHR ranged from 0.770 to 0.938, body fat percentage ranged from 20.5% to 51.7%, and muscle mass percentage ranged from 45.9% to 75.48% (Table 5.1). According to BMI at baseline, seven participants were non-obese (BMI < 30), and five participants were obese (obese; BMI ≥ 30), whereas, WHR measures suggest that five participants were non-obese (WHR < 0.85) and seven participants were obese (WHR ≥ 0.85) at baseline (Table 5.1).

None of the study participants had their adriamycin-cyclophosphamide or paclitaxel chemotherapy treatments dose-capped based on body surface area (BSA) (Table 5.2).

Table 5.1. Patient information and baseline body morphometry measurements for the study participants.

Participant	Age	Ethnicity	Chemo Regime	Weight (kg)	Height (cm)	BMI	WHR	Body Fat %	Muscle Mass %
1	68	NZ European	Adjuvant	86.1	159	34.1	0.938	43.3	53.77
2	43	NZ European	Adjuvant	84.8	161	33.1	0.915	42.2	54.83
3	60	NZ European	Adjuvant	73	163	27.5	0.914	43.4	53.7
4	48	NZ Māori	Neoadjuvant	56.4	165	20.7	0.840	27.6	68.62
5	49	NZ European	Adjuvant	68.4	160	26.6	0.871	37.9	58.91
6	44	Other	Neoadjuvant	94.7	167	34.0	0.840	43.1	54.05
7	40	NZ European	Neoadjuvant	112.4	169	39.4	0.860	51.7	45.90
8	67	NZ European	Adjuvant	64.7	154	27.3	0.880	34.1	62.40
9	50	English	Adjuvant	61.2	166	22.2	0.770	28.7	67.60
10	50	NZ European	Neoadjuvant	72.2	163	27.2	0.800	20.5	75.48
11	42	NZ European	Neoadjuvant	61.3	155	25.5	0.847	33.5	63.13
12	65	NZ European	Neoadjuvant	73	154	30.8	0.856	41.9	55.07

BMI: Body mass index; **WHR:** Waist to hip ratio.

Table 5.2. Predicted doses based on BSA, and actual doses of adriamycin-cyclophosphamide and paclitaxel received by study participants.

Participant	BSA* (AC)	Predicted A (mg)	Actual A** (mg)	Predicted C (mg)	Actual C*** (mg)	BSA* (Pac)	Predicted Pac (mg)	Actual**** Pac (mg)
1	1.91	114	115	1140	1150	1.91	150	150
2	1.9	114	115	1140	1150	1.9	150	150
3	1.82	108	110	1080	1100	1.82	150	150
4	1.64	98.4	100	984	1000	1.66	132	130
5	1.74	104.4	105	1044	1050	1.84	145.6	140
6	2.07	124.2	120	1242	1200	2.1	168	170
7	2.2	132	135	1320	1350	2.2	176	180
8	1.64	98.4	95	984	950	1.63	130	130
9	1.72	103.2	100	1032	1000	1.71	136	140
10	1.79	107.4	105	1074	1050	1.79	143	140
11	1.6	96	95	960	950	1.62	130	130
12	1.73	103.8	105	1038	1050	1.7	136	140

BSA: body surface area; **AC:** adriamycin-cyclophosphamide; **Pac:** paclitaxel; **mg**: milligrams.
*BSA is calculated by multiplying height (cm) by weight (kg), dividing by 3600, and then calculating the square root.
**Adriamycin dosed based on BSA and rounded to the nearest 5mg
***Cyclophosphamide dosed based on BSA and rounded to the nearest 50mg
****Paclitaxel dosed based on BSA and rounded to the nearest 10mg

5.2.2.3 Correlation between different body morphometry measures before chemotherapy

To determine whether the different body morphometry measures taken at baseline were correlated, this study compared BMI, WHR and body fat percentage measurements taken at baseline (n= 12 participants), and the associations are presented in Figure 5.2.

In this group of women diagnosed with stage II or III breast cancer (n= 12 participants), body fat percentage was significantly positively correlated with both BMI (R^2= 0.846) and WHR (R^2= 0.639), in which both associations were significant ($p<0.05$; Figure 5.2A and C). BMI and WHR measures were positively correlated, but not significantly (R^2= 0.530, p=0.076; Figure 5.2B).

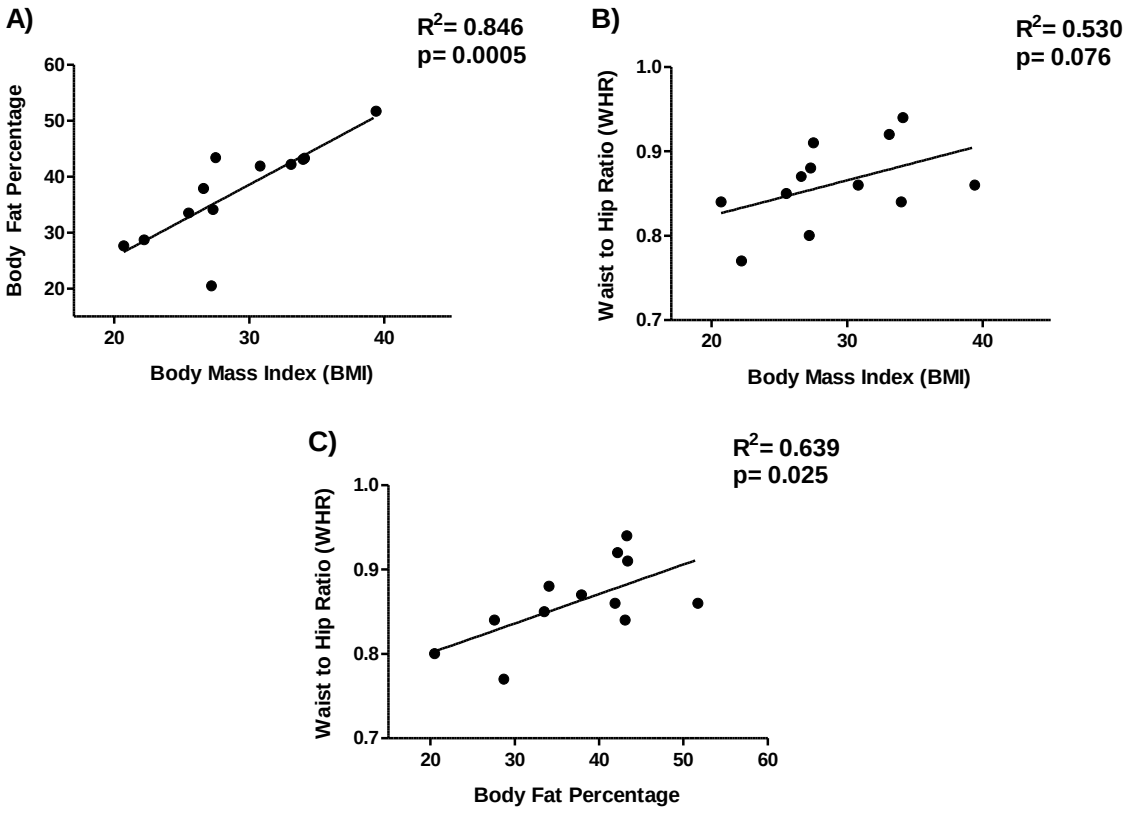

Figure 5.2. Correlation between body morphometry measures at baseline.
Participants had body mass index (BMI; n= 12), waist to hip ratio (WHR; n= 12) and body fat percentage (n= 12) measured before chemotherapy. A and C) Analysis showed a significant positive association of body fat percentage with BMI and WHR, and B) a positive association between BMI and WHR. Statistical analysis was performed using Spearman correlation analysis. Significance was determined as $p<0.05$.

5.2.2.4 Change in body composition during chemotherapy

In order to examine changes in body morphometry during chemotherapy, this study compared BMI, WHR and body fat percentage measurements taken before and after chemotherapy. Individual changes in body morphometry are presented in Figure 5.3, and the average change in body morphometry across all participants is displayed in Figure 5.4. Muscle mass measurements are presented in Figure 5.5 and Figure 5.6.

The largest change in BMI was a 28% increase (participant 5; 26.6 before chemotherapy to 34.0 after chemotherapy); indicating a transition from the overweight to obese category (Figure 5.3A). Only one participant had a decrease in BMI during chemotherapy (participant 12); BMI decreased from 30.80 before chemotherapy to 29.60 after chemotherapy (4% decrease; Figure 5.3A). All other participants displayed 0-7% increases in BMI during chemotherapy (Figure 5.3A).

During chemotherapy, three participants displayed notable changes in body fat percentage, two participants showed increases of 53% (from 20.5% before chemotherapy to 31.40% after chemotherapy; participant 10) and 15% (from 37.9% before chemotherapy to 43.40% after chemotherapy; participant 5), and one participant exhibited a 16.4% decrease (from 34.10% before chemotherapy to 29.30% after chemotherapy; participant 8) (Figure 5.3B). All other participants displayed 0-6% differences in body fat percentage during chemotherapy (Figure 5.3B). The largest difference in muscle mass percentage was participant 10, decreasing from 75.48% to 62.20% (Figure 5.5).

The largest change in WHR was by participant 5, with a decrease from 0.87 before chemotherapy to 0.79 after chemotherapy (a 10.2% decrease); thus changing this participant from the obese to non-obese category (Figure 5.3C). All other participants displayed 0-7% differences in WHR during chemotherapy (Figure 5.3C).

On average across all participants, BMI showed a significant increase from before to after chemotherapy ($n= 11$; $p< 0.05$), whereas, WHR ($n= 10$) and body fat percentage ($n= 11$) were not significantly different (Figure 5.4). Similarly, muscle mass did not change significantly during chemotherapy ($n= 11$; $p>0.05$; Figure 5.6).

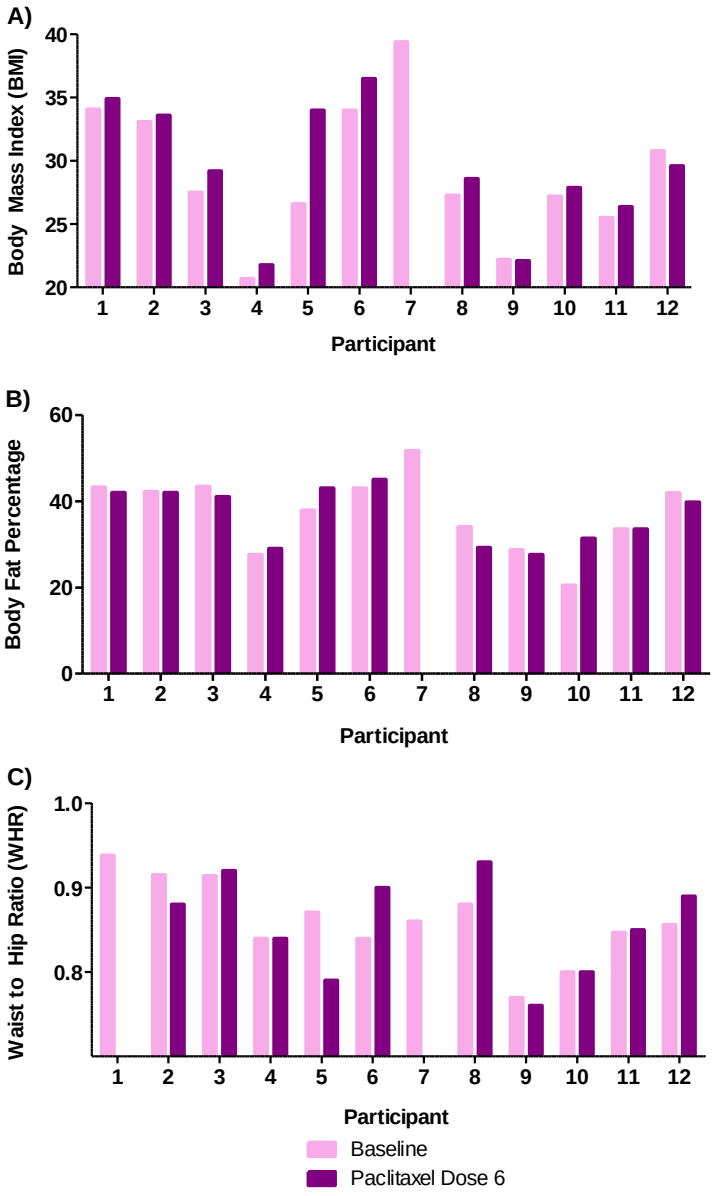

Figure 5.3. Body morphometry measures recorded before and after chemotherapy.
A) Body mass index (BMI) of the participants was measured at baseline (n= 12) and following dose six of paclitaxel (n= 11). B) Body fat percentage was assessed for each participant at baseline (n= 12) and following dose six of paclitaxel (n= 11). C) Waist to hip ratio (WHR) was determined for each participant at baseline (n= 12) and following dose six of paclitaxel (n= 10).

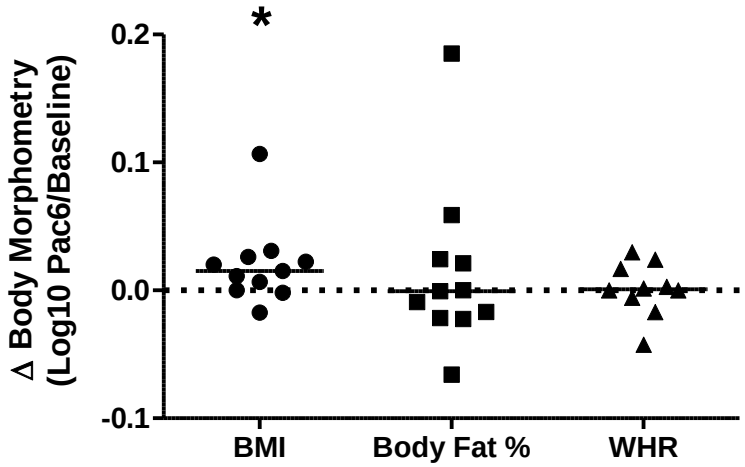

Figure 5.4. Change in body morphometry during chemotherapy.
Body mass index (BMI; n= 11; circles), body fat percentage (n= 11; squares), waist to hip ratio (WHR; n= 10; triangles) measures taken before and after chemotherapy were used to assess the change in body morphometry during chemotherapy (ΔBody Morphometry Log10 Paclitaxel dose6/Baseline). Horizontal dotted line represents no change in body morphometry during chemotherapy. Solid black horizontal lines represent the median values. Statistical analysis was performed by Wilcoxon matched-pairs signed rank tests. *$p<0.05$

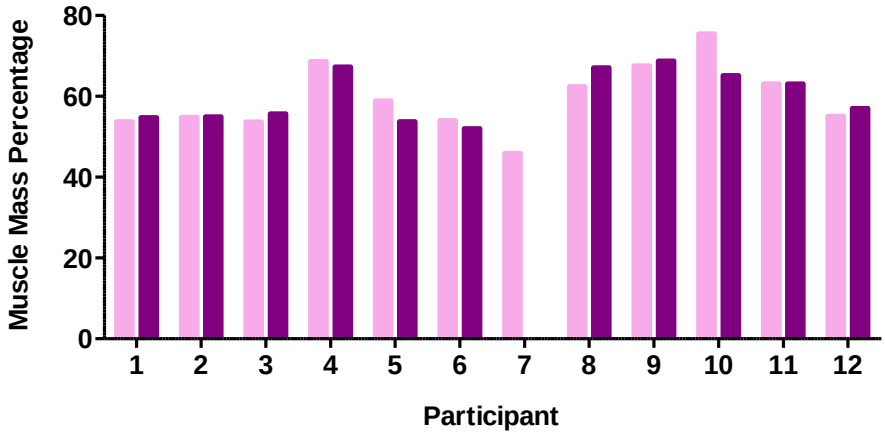

Figure 5.5. Muscle mass percentage before and after chemotherapy.
Muscle mass percentage for each participant was recorded before chemotherapy (pink; n= 12) and following dose six of paclitaxel (purple; n= 11).

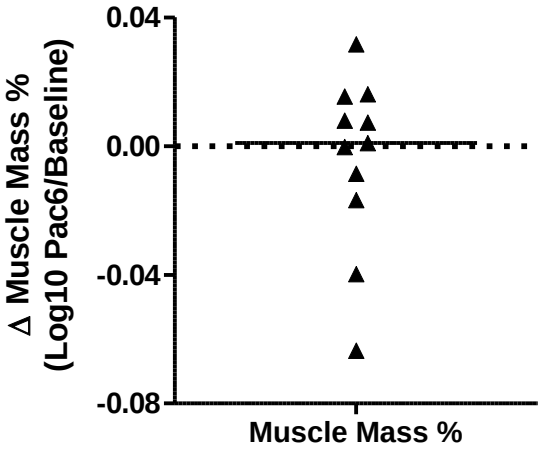

Figure 5.6. Change in muscle mass during chemotherapy.
Muscle mass percentage (n= 11; triangles) measures taken before and after chemotherapy were used to assess the change during chemotherapy (Δ muscle mass log10). Horizontal dotted line represents no change during chemotherapy. Solid black horizontal lines represent the median values. Statistical analysis was performed by Wilcoxon matched-pairs signed rank tests, and $p<0.05$ was considered statistically significant.

5.2.3 Physical activity levels during chemotherapy

5.2.3.1 Experimental approach

To investigate physical activity levels, the number of steps walked each day by study participants was measured using FitBit One® devices for 21 days after AC cycle one, and 7 days after both paclitaxel dose one and dose six (Chapter 2; Section 2.10.5). Average daily step counts were calculated for AC cycle one, paclitaxel dose one, paclitaxel dose six, and all three treatment periods combined (35 days). To assess whether variation in physical activity levels between participants was due to differences in treatment plans, body morphometry, or age, the average daily step count over all three measurement periods was compared between participants that had high and low body fat percentage (split by median), participants that did or did not have surgery prior to starting chemotherapy (adjuvant or neoadjuvant, respectively), and participants that were considered pre- or post-menopausal (split by age of 50 years). Adherence to wearing FitBIt One® devices was evaluated by considering the number of days that steps were recorded compared to the total number of possible days that steps could have been recorded.

Due to technical complications, step count data for two participants (participants 9 and 10) was lost during the 21 days of AC cycle one. One participant (participant 12) misplaced the FitBit One® and, therefore, another 21 days of data over AC cycle one was missed. As a result of clinical complications, participant 7 was only able to complete two out of the twelve (2/12) scheduled paclitaxel doses and was withdrawn from the study before paclitaxel dose six, and therefore did not have step counts measured over this time period of the study.

5.2.3.2 Adherence to wearing the FitBit One® devices during chemotherapy

To determine adherence to wearing the FitBit One® devices, the number of days that participants were scheduled to wear the device was compared to the number of days that the device had step count recorded.

Of the 350 days that participants were scheduled to wear the FitBit One® devices, step counts were recorded for 328 of these days, and thus, the overall adherence rate for wearing the devices was 93.7% (328/350 days; Table 5.3). Adherence rates were highest for the 7 days over paclitaxel dose one (95.2%; 80/84 days; n= 12), when compared to the 21 days of AC cycle one (93.7%; 177/189 days; n= 9), and 7 days of paclitaxel dose six (92.2%; 71/77 days;

n= 11; Table 5.3). 10 out of the 22 missed days were by participant 4, and 9 out of the 22 days were by participant 2.

Table 5.3. Adherence to wearing FitBit One® devices.

	Days Counted	Days Missed	Total Days	Adherence (%)
AC Cycle 1	177	12	189	93.7
Paclitaxel Dose 1	80	4	84	95.2
Paclitaxel Dose 6	71	6	77	92.2
Total	328	22	350	93.7

AC: Adriamycin-cyclophosphamide

5.2.3.3 Cumulative number of steps walked during FitBit One® wearing periods of chemotherapy

To assess the variation in the number of steps walked by the study participants, the number of steps walked each day was measured over AC cycle one (21 days; n= 9 participants), paclitaxel dose one (7 days; n= 12 participants), and paclitaxel dose six (7 days; n= 11 participants), and the cumulative step count for each participant is presented in Figure 5.7.

Over 21 days of AC cycle one, the median cumulative step count was 113,632 steps, and the cumulative step counts ranged from 77,411 (participant 4) to 324,158 steps (participant 8; Figure 5.7A). Participant 5 had the second highest cumulative step count over AC cycle one, with 242,694 steps in total (Figure 5.7A). Over 7 days of paclitaxel dose one, the median cumulative step count was 35,340 steps, and the cumulative step counts ranged from 10,970 (participant 4) to 54,494 steps (participant 9; Figure 5.7B). Participants 1 and 8 had the second and third highest cumulative step counts over paclitaxel dose one, with 48,954 and 48,373 steps, respectively (Figure 5.7B). Over 7 days of paclitaxel dose six, the median cumulative step count was 34,508 steps, and the cumulative step counts ranged from 6,145 (participant 4) to 73,907 steps (participant 9; Figure 5.7C), and participant 6 had the second highest cumulative step count with 61,499 steps in total (Figure 5.7C). Participant 4 only wore the FitBit One® device for two days during paclitaxel dose six, walking 3,194 and 2,951 steps on each of these days (Figure 5.7C).

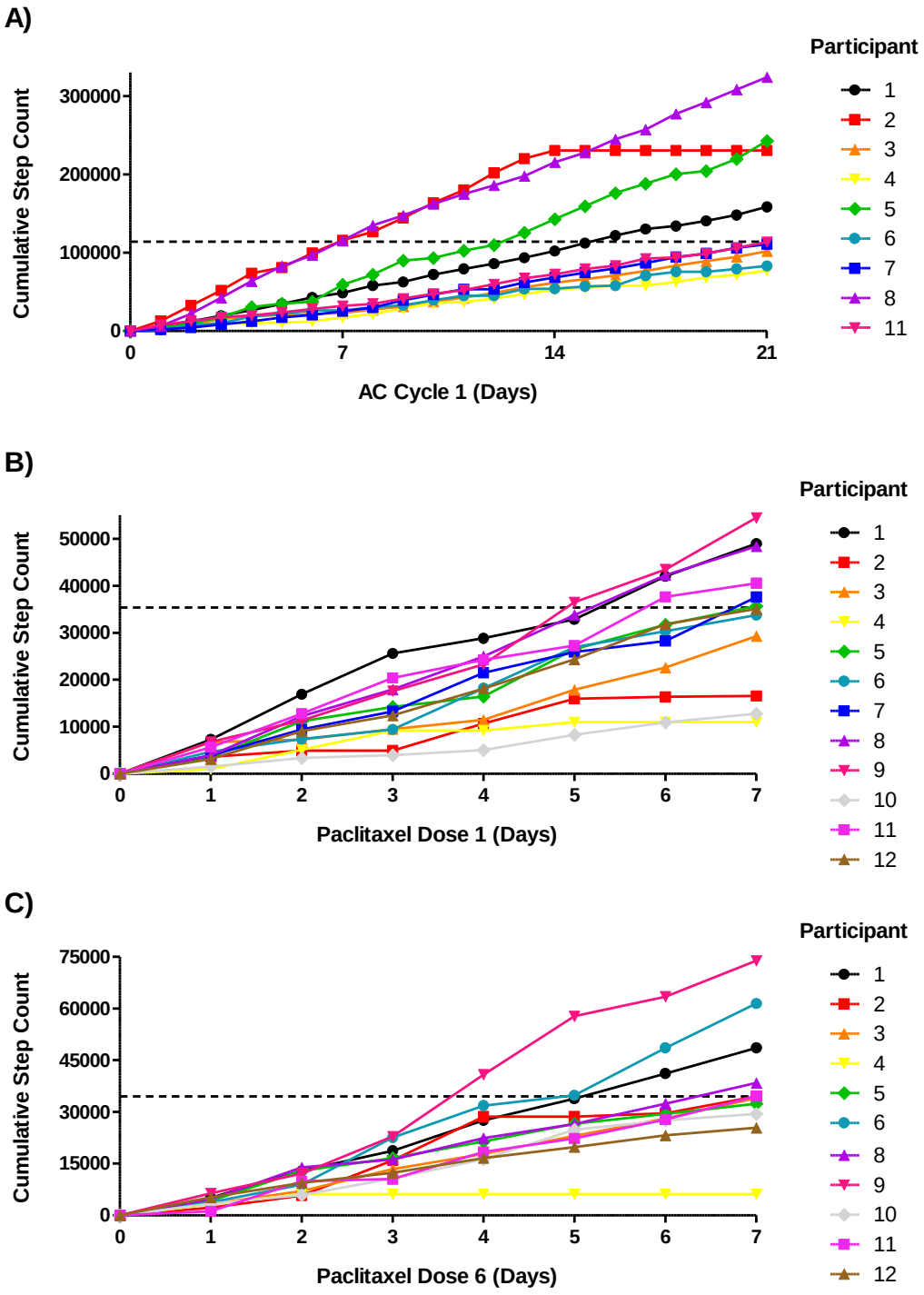

Figure 5.7. Cumulative step counts were assessed using daily step counts during chemotherapy.
The number of steps walked by participants each day during A) AC cycle one (21 days; n= 9 participants), B) paclitaxel dose one (7 days; n= 12 participants) and C) paclitaxel dose six (7 days; n= 11 participants). Horizontal black dotted line represents the median cumulative step count at the end of AC cycle one, and paclitaxel dose one and six.

5.2.3.4 Number of steps walked on average each day during chemotherapy

To determine whether the number of steps walked by participants changes during chemotherapy the number of steps walked each day was measured over AC cycle one (21 days; n= 9 participants), paclitaxel dose one (7 days; n= 12 participants), and paclitaxel dose six (7 days; n= 11 participants), and the average daily step counts are presented in Figure 5.8.

For all participants, the average daily step counts were 8,390 steps for AC cycle one, 4,901 steps for paclitaxel dose one, and 5,716 steps for paclitaxel dose six (Figure 5.8). The average daily step count significantly decreased from AC cycle one to dose one of paclitaxel ($p<0.05$; Figure 5.8). Median values of the average daily step counts were 5546 steps for AC cycle one, 4913 steps for paclitaxel dose one, and 4940 steps for paclitaxel dose six.

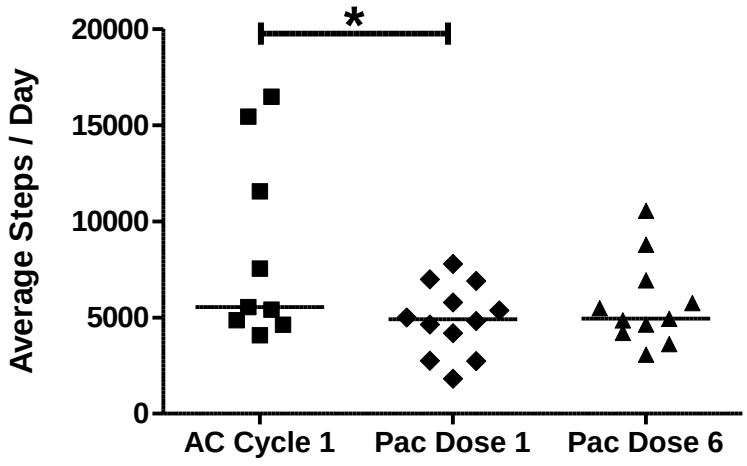

Figure 5.8. Average number of steps walked each day during chemotherapy.
Step counts were measured over AC cycle one (21 days; n= 9 participants; squares), paclitaxel dose one (7 days; n= 12 participants; diamonds) and paclitaxel dose six (7 days; n= 11 participants; triangles). Horizontal solid line represents the median values. Statistical analysis was performed using Wilcoxon matched-pairs signed rank test. *$p<0.05$.

5.2.3.5 Effects of demographics and body morphometry on the number of steps walked during chemotherapy

To determine whether the average daily step counts are effected by differences in participant demographics or body morphometry, the average daily step counts for AC cycle one (21 days; n= 9 participants), paclitaxel dose one (7 days; n= 12 participants), and paclitaxel dose six (7 days; n= 11 participants) were compared between participants with high and low body fat percentage at baseline (split by median= 39.90%), participants that were treated with either adjuvant or neo-adjuavnt chemotherapy, and participants that were pre-menopausal (age < 50 years) or post-menopausal (age ≥ 50 years) at baseline (Figure 5.9).

Variation in the participants average daily step counts over AC cycle one, paclitaxel dose one and paclitaxel dose six was not dependent on the body fat percentage of the participants (Figure 5.9A). To determine the effects of body morphometry on levels of physical activity this study compared body fat percentage, and not BMI, with average daily step counts due to the participants body fat percentage being significantly positively correlated with BMI and WHR (Section 5.2.2.3, Figure 5.2A and C), and the participants BMI significantly changing during chemotherapy, when body fat percentage did not (Section 5.2.2.4, Figure 5.4).

The difference in average daily steps counts during AC cycle one, paclitaxel dose one, and paclitaxel dose six was not significantly affected by whether the participant had surgery prior to chemotherapy ($p > 0.05$), although there was a trend towards lower step counts in neoadjuvant compared to adjuvant participants during AC cycle one ($p=0.06$; Figure 5.9B). Lastly, the menopausal status of the participants did not significantly influence the number of steps walked by the participants during chemotherapy (Figure 5.9C).

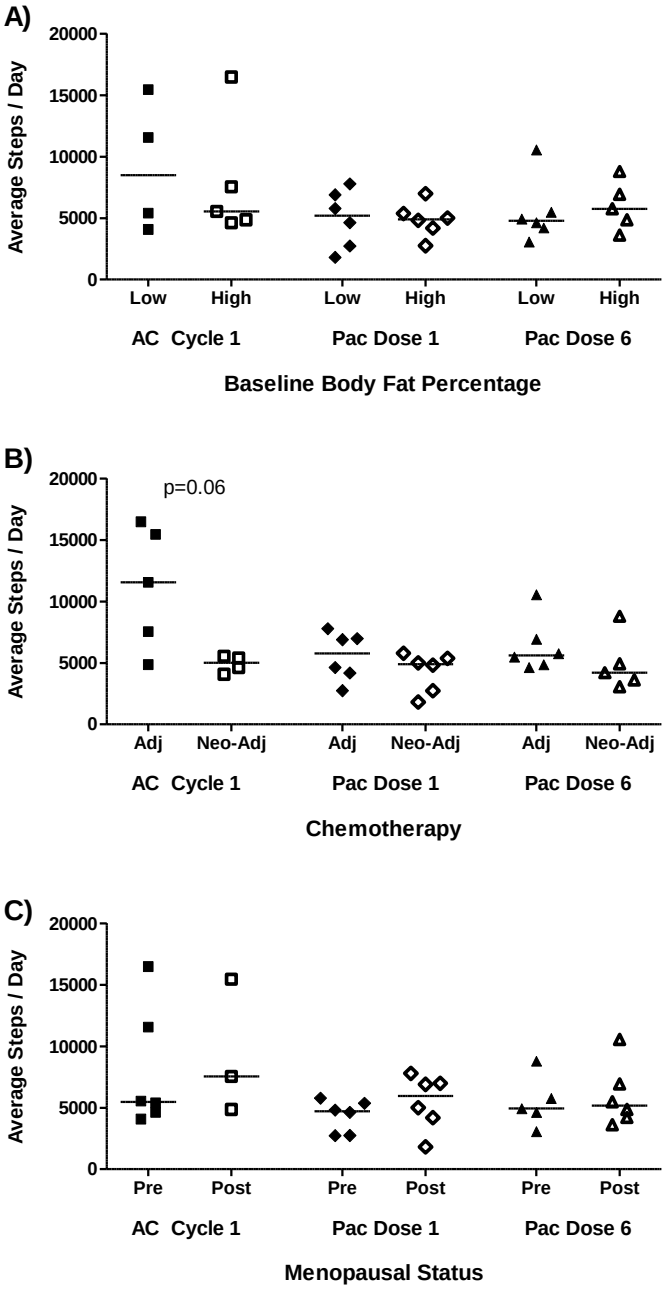

Figure 5.9. Effect of participant demographics and body morphometry on the average number of steps walked each day during chemotherapy.
Daily step counts were recorded using FitBit One® devices and the average daily step counts were calculated for AC cycle one (n= 9; squares), paclitaxel dose one (n= 12; diamonds), and paclitaxel dose six (n= 11; triangles). Average daily step counts were compared between A) participants with low (solid points) and high (transparent points) body fat percentage (split by median= 39.90%) recorded before chemotherapy, B) participants that had either adjuvant (Adj; solid icons) or neoadjuvant (Neo-Adju; transparent icons) chemotherapy, and C) participants that were pre-menopausal (Pre; age<50; solid icons) or post-menopausal (Post; age ≥ 50; transparent icons) at baseline. Horizontal solid black lines represent median values. Statistical analysis was performed using Mann Whitney U tests, and significance was determined as $p<0.05$.

5.2.4 Circulating inflammation markers

5.2.4.1 Experimental approach

To investigate the effect of body morphometry and physical activity on circulating concentrations of inflammatory cytokines during chemotherapy, serum was collected from participants at baseline (before chemotherapy), following AC cycle one, and after paclitaxel dose one and dose six (Chapter 2; Section 2.10.3). Using a human cytokine array, relative expression of 105 inflammatory cytokines were compared between non-obese (BMI < 30; n= 4) and obese (BMI ≥ 30; n= 4) participants by pooling together serum samples (4 x 25 µL = 100 µL) taken before chemotherapy and again after paclitaxel dose six (after chemotherapy) (Chapter 2; Section 2.10.7).

Enzyme linked immunoassays (ELISAs) were used to measure the concentration of circulating inflammatory cytokines (ANG2, BAFF, CRP, GDF-15, IL-1β, IL-4, IL-10, MCP-1, and TNF-α) in each individual serum sample taken from study participants throughout chemotherapy (baseline, AC cycle one, paclitaxel dose one and paclitaxel dose six), using internal linear standards. The inflammatory cytokines of interest were selected for assessment for one of three reasons. First, for being previously associated with decreased CYP expression and/or activity *in vitro* and/or *in vivo* (CRP, IL-1β, IL-4, IL-10, and TNF-α) [159,304,317]. Second, for showing an increase compared to baseline in obese participant serum throughout chemotherapy in this studies inflammatory cytokine array (ANG2, BAFF, and GDF-15) (Section 5.2.4.2). Last, for having a well-established relationship with elevated adiposity and/or obesity in the literature (CRP, MCP-1, and TNF-α) [29,63]. Assessment of IL-6 was not performed in this part of the study due to restricted serum sample volumes. The change in cytokine expression during chemotherapy was compared between participants with high or low body fat percentage (measured before chemotherapy; split by median), and participants with high or low physical activity levels (split by the median average daily step count over all 35 days).

Participant 1 did not have circulating concentrations of ANG2, BAFF, CRP, and GDF-15 measured before chemotherapy due to the small volume of serum collected from participant 1 at baseline. As a result of clinical complications, participant 7 was only able to complete two out of the twelve (2/12) scheduled paclitaxel doses and was withdrawn from the study before paclitaxel dose six, and therefore did not have circulating inflammatory cytokines measured over this time period of the study.

5.2.4.2 Effect of body morphometry on the relative levels of circulating inflammatory cytokines during chemotherapy

To indicate whether differences in body morphometry influence the relative levels of circulating inflammatory cytokines during chemotherapy, the expression of 105 inflammatory cytokines were compared between the pooled serum samples collected from non-obese (BMI < 30) and obese (BMI ≥ 30) participants before and after chemotherapy, using a human cytokine array. The most differently expressed cytokines are presented in Figure 5.11 and Figure 5.12. Human XL Cytokine Array reference Full array images are depicted below in Figure 5.10, and the corresponding cytokines based on array co-ordinates are listed in

Table 5.4.

Of the top 30 most differentially expressed cytokines between non-obese and obese participants, leptin was the only cytokine that was increased in obese compared to non-obese participants both before chemotherapy (obese/non-obese= 3.56) and after chemotherapy (obese/non-obese= 1.95; Figure 5.11). Interleukin 3 (IL-3) showed the greatest difference in expression between obese and non-obese participants before chemotherapy; 12.62-fold in obese participants. Macrophage Inflammatory Protein-3 (MIP3a) exhibited the greatest difference in expression between obese and non-obese participants after chemotherapy; 7.13-fold higher in non-obese participants. Before chemotherapy, all 30 of the most differentially expressed cytokines were more highly expressed in obese compared to non-obese participants (Figure 5.11A). After chemotherapy, 29 out of the 30 most differentially expressed cytokines showed lower expression in obese compared to non-obese participants (Figure 5.11B).

The change in the relative levels of inflammatory cytokines from before to after chemotherapy was also evaluated, and the most differentially expressed cytokines are presented in Figure 5.12. In non-obese participants, all 30 of the most differentially expressed cytokines were higher after chemotherapy than before chemotherapy (Figure 5.12A), whereas, in obese participants 29 out of the 30 most differentially expressed cytokines were lower after chemotherapy than before chemotherapy (Figure 5.12B). B-cell activating factor (BAFF) was the only cytokine that showed higher levels after chemotherapy (compared to before chemotherapy) in obese participants (2.49-fold increase; Figure 5.12).

In obese participants, 8 of the 105 cytokines showed a 1.1-fold or higher (log>0.1761) increase in expression after chemotherapy (compared to before chemotherapy), of which

BAFF, growth/differentiation factor 15 (GDF-15), growth hormone, and angiopoietin-2 (ANG2) were the top four (Figure 5.13).

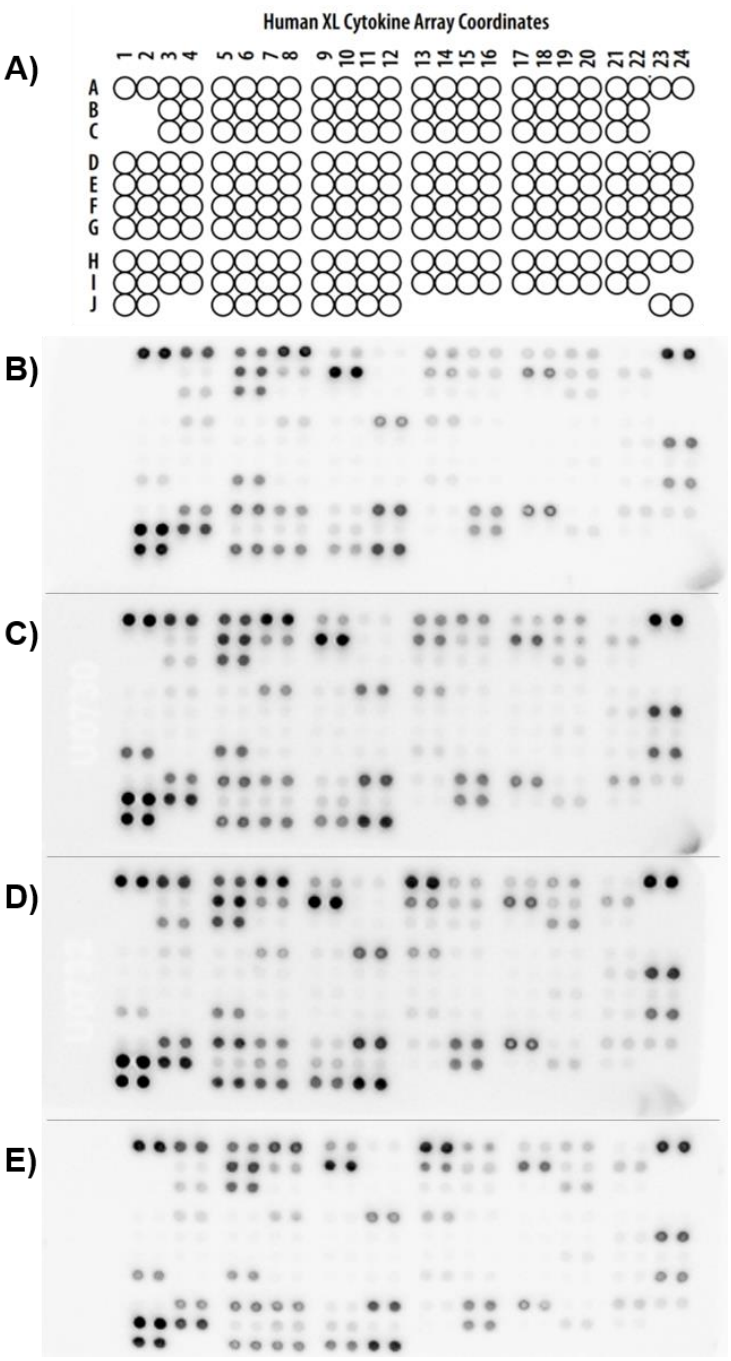

Figure 5.10. Human XL Cytokine Array membrane images.
A) Schematic of the membrane array analyte co-ordinates (not to scale), which included duplicate spots of 105 human cytokines, chemokines and acute phase response proteins. These duplicate spots were measured in the serum of study participants taken B and C) before chemotherapy, and D and E) after chemotherapy. B and D) Serum from four non-obese (BMI<30) participants, and C and E) four obese (BMI>30) participants were pooled together.

Table 5.4. List of Human XL Cytokine Array analytes and the co-ordinates that they map to on the array membrane.

Co-ordinates	Analyte/Control	Co-ordinates	Analyte/Control	Co-ordinates	Analyte/Control	Co-ordinates	Analyte/Control
A1, A2	Reference spots	C13, C14	FGF-19	E23, E24	IL-18 BPa	H5, H6	PDGF-AA
A3, A4	Adiponectin/Acrp30	C15, C16	Flt-3 Ligand	F1, F2	IL-19	H7, H8	PDGF-AB/BB
A5, A6	Angiogenin	C17, C18	G-CSF	F3, F4	IL-22	H9, H10	Pentraxin 3/TSF-14
A7, A8	Angiopoietin-1	C19, C20	GDF-15	F5, F6	IL-23	H11, H12	CXCL4/PF4
A9, A10	Angiopoietin-2	C21, C22	GM-CSF	F7, F8	IL-24	H13, H14	RAGE
A11, A12	Apolipoprotein A1	D1, D2	CXCL1/GRO alpha	F9, F10	IL-27	H15, H16	CCL5/RANTES
A13, A14	BAFF/BLyS/TNFSF13B	D3, D4	Growth Hormone	F11, F12	IL-31	H17, H18	RBP4
A15, A16	BDNF	D5, D6	HGF	F13, F14	IL-32 alpha/beta/gamma	H19, H20	Relaxin-2
A17, A18	CD14	D7, D8	ICAM-1/CD54	F15, F16	IL-33	H21, H22	Resistin
A19, A20	CD30	D9, D10	IFN-gamma	F17, F18	IL-34	H23, H24	SDF-1 alpha
A21, A22	CD31/PECAM-1	D11, D12	IGFBP-2	F19, F20	CXCL10/IP-10	I1, I2	Serpin E1/PAI-1
A23, A24	Reference spots	D13, D14	IGFBP-3	F21, F22	CXCL11/I-TAC	I3, I4	SHBG
B3, B4	CD40 Ligand/TNFSF5	D15, D16	IL-1 alpha/IL-1F1	F23, F24	Kallikrein 3/PSA	I5, I6	ST2/IL1 R4
B5, B6	Chitinase 3-like 1	D17, D18	IL-1 beta/IL-1F2	G1, G2	Leptin	I7, I8	CCL17/TARC
B7, B8	Complement Factor D	D19. D20	IL-1ra/IL-1F3	G3, G4	LIF	I9, I10	TFF3
B9, B10	C-Reactive Protein/CRP	D21, D22	IL-2	G5, G6	Lipocalin-2/NGAL	I11, I12	TfR
B11, B12	Cripto-1	D23, D24	IL-3	G7, G8	CCL2/MCP-1	I13, I14	TGF-alpha
B13, B14	Cystatin C	E1, E2	IL-4	G9, G10	CCL7/MCP-3	I15, I16	Thrombospondin-1
B15, B16	Dkk-1	E3, E4	IL-5	G11, G12	M-CSF	I17, I18	TNF-alpha
B17, B18	DPPIV/CD26	E5, E6	IL-6	G13, G14	MIF	I19, I20	uPAR
B19, B20	EGF	E7, E8	IL-8	G15, G16	CXCL9/MIG	I21, I22	VEGF
B21, B22	Emmprin	E9, E10	IL-10	G17, G18	CCL3/CCL4 MIP-1 alpha/beta	J1, J2	Reference spot
C3, C4	CXCL5/ENA-78	E11, E12	IL-11	G19, G20	CCL20/MIP-3 alpha	J5, J6	Vitamin D BP
C5, C6	Endoglin/CD105	E13, E14	IL-12 p70	G21, G22	CCL19/MIP-3 beta	J7, J8	CD31
C7, C8	Fas Ligand	E15, E16	IL-13	G23, G24	MMP-9	J9, J10	TIM-3
C9, C10	FGF basic	E17, E18	IL-15	H1, H2	Myeloperoxidase	J11, J12	VCAM-1
C11, C12	KGF/FGF-7	E19, E20	IL-16	H3, H4	Osteopontin (OPN)	J23, J24	Negative control
		E21, E22	IL-17A				

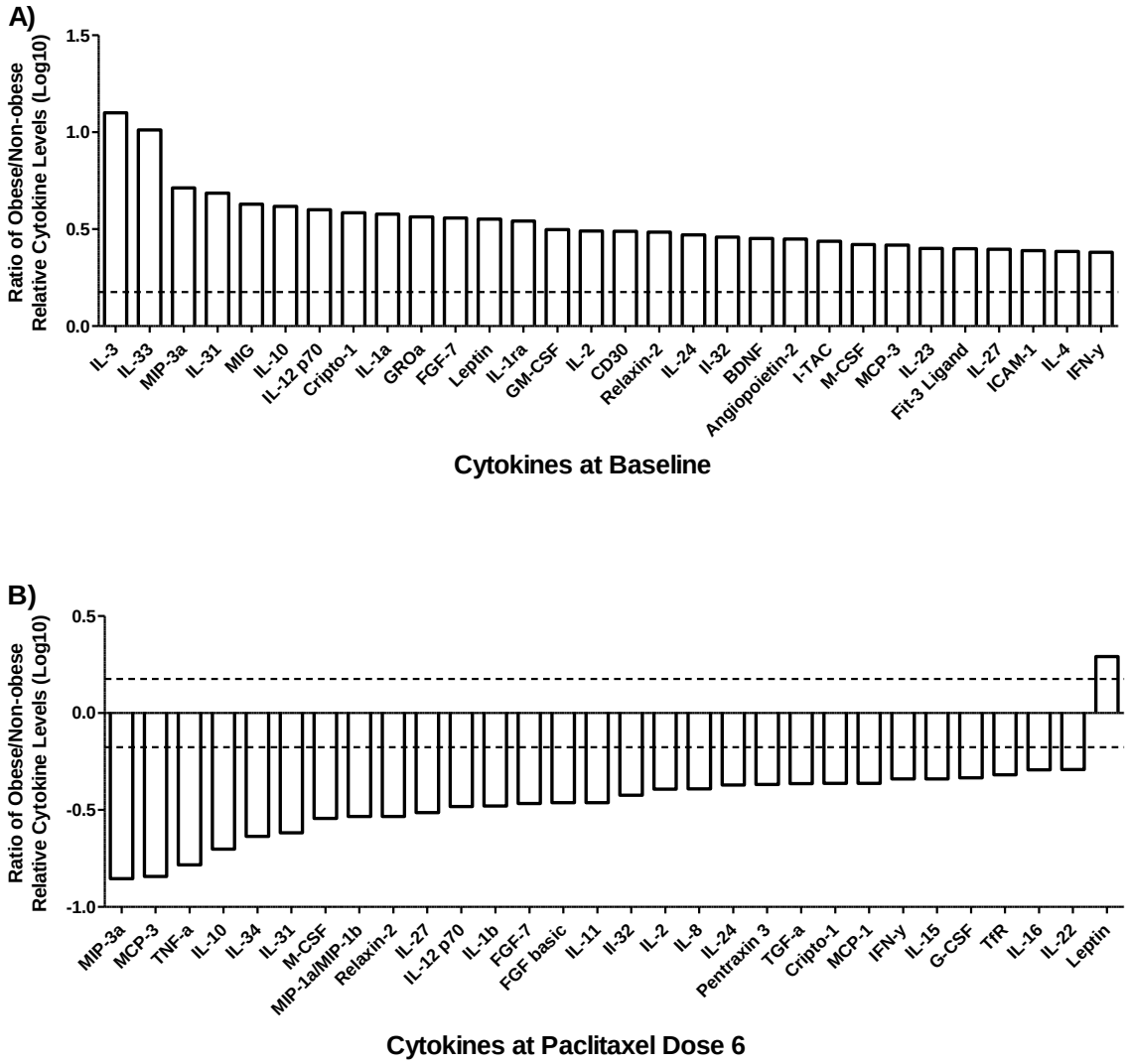

Figure 5.11. Effect of body morphometry on the relative levels of circulating inflammatory cytokines during chemotherapy.

Serum samples were assessed by a human cytokine array (105 human cytokines) to measure the cytokines most differentially expressed between non-obese (BMI < 30; pooled sample from n= 4 participants) and obese (BMI ≥ 30; pooled sample from n= 4 participants) participants (top n= 30 cytokines) A) before chemotherapy and B) after chemotherapy (following paclitaxel dose six). Horizontal dotted lines represent a 1.5 fold change (log10 of 1.5 = ± 0.1761).

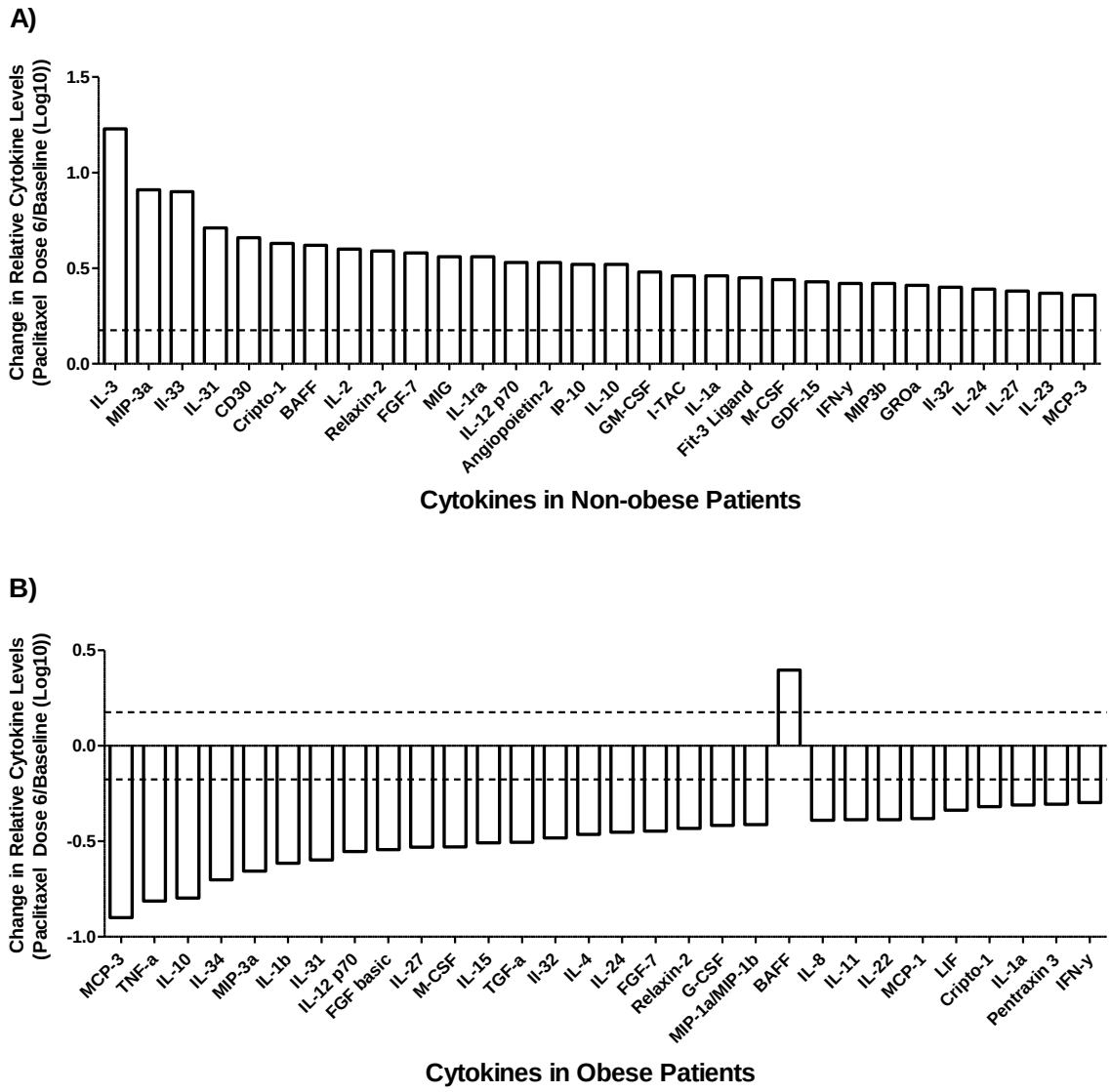

Figure 5.12. The change in relative levels of circulating inflammatory cytokines from before to after chemotherapy.

Serum samples were assessed by a human cytokine array (105 human cytokines) to measure the cytokines most differentially expressed between baseline and paclitaxel dose six (top n= 30 cytokines) in A) non-obese (BMI < 30; pooled sample from n= 4 participants) and B) obese (BMI $\geq$ 30; pooled sample from n= 4 participants) participants. Horizontal dotted lines represent a 1.5 fold change (log10 of 1.5 = $\pm$ 0.1761).

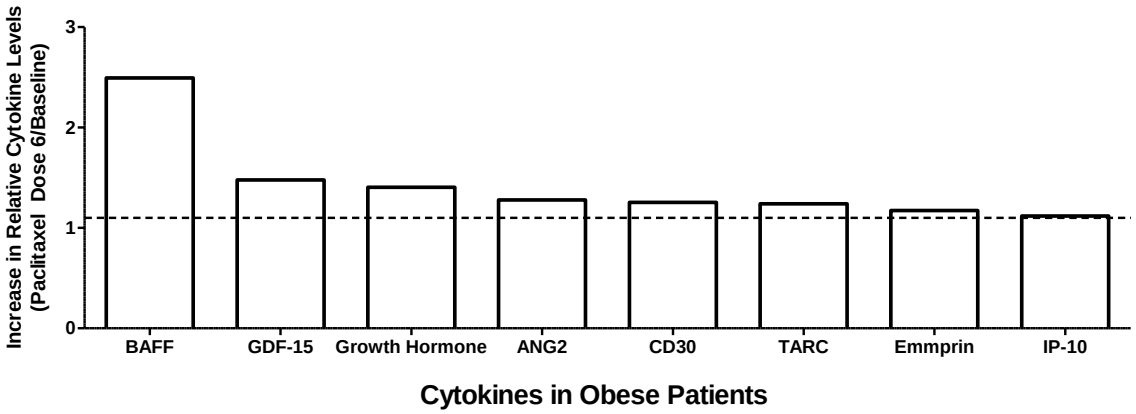

Figure 5.13. The circulating inflammatory cytokines showing a relative increase from before to after chemotherapy in obese participants.
Serum samples were assessed by a human cytokine array (105 human cytokines) to measure the cytokines most differentially expressed between baseline (pooled sample from n= 4 participants) and paclitaxel dose six (pooled sample from n= 4 participants) in obese (BMI ≥ 30) participants. Horizontal dotted lines represent a 1.1-fold change.

5.2.4.3 Change in circulating concentrations of selected inflammatory cytokines during chemotherapy

To determine whether circulating inflammatory cytokines are changing during chemotherapy, concentrations of the inflammatory cytokines ANG2, BAFF, CRP, GDF-15, IL-1β, IL-4, IL-10, MCP-1, and TNF-α were measured in serum samples collected from each participant before chemotherapy (baseline), and again following AC cycle one, paclitaxel dose one and paclitaxel dose six, with the measured concentrations presented in Figure 5.14.

Across all participants, the circulating concentrations of BAFF were significantly higher at paclitaxel dose one (median= 4064 pg/mL) and paclitaxel dose six (median= 3776 pg/mL) compared to baseline (median= 1472 pg/mL; $p<0.05$; Figure 5.14B). Circulating concentrations of IL-10 were significantly lower at paclitaxel dose one (median= 12.53 pg/mL) and paclitaxel dose six (median= 3.61 pg/mL) compared to AC cycle one (Median= 14.0 pg/mL; $p<0.05$; Figure 5.14E). Paclitaxel dose six concentrations of IL-10 (median= 3.61 pg/mL) were lower than baseline IL-10 concentrations (median= 9.75 pg/mL), but not significantly ($p>0.05$; Figure 5.14E). Across all participants, the circulating concentrations of ANG2, CRP, GDF-15, and MCP-1 did not significantly differ throughout chemotherapy ($p>0.05$; Figure 5.14A, C, D, and F). Median circulating concentrations of CRP and GDF-15 increase from baseline to AC cycle one, and increase again from AC cycle one to paclitaxel dose one, and remain higher than baseline at paclitaxel dose six, but not significantly ($p>0.05$; Figure 5.14D). Circulating concentration of MCP-1 decreased from baseline (median= 397.7 pg/mL) to AC cycle one (median= 365.8 pg/mL), but increased by paclitaxel dose six (median= 504.8 pg/mL) to levels higher than baseline, but not significantly ($p>0.05$). Expression of the IL-1β, IL-4, and TNF-α inflammatory cytokines were below the detectable range in serum from study participants.

A separate investigation of the change in circulating inflammatory cytokine concentrations from before to after chemotherapy, by relating cytokine levels after paclitaxel dose six back to levels recorded before chemotherapy, showed a significant increase in the levels of BAFF, GDF-15, and MCP-1 ($p<0.05$), and significant decrease in IL-10 ($p<0.05$; Figure 5.15).

Lastly, the concentrations of inflammatory cytokines before chemotherapy were not significantly different between participants treated with either neoadjuvant or adjuvant

chemotherapy (p>0.05; Figure 5.16), suggesting surgery prior to starting chemotherapy was not influencing the levels of circulating inflammatory cytokines in the adjuvant participants.

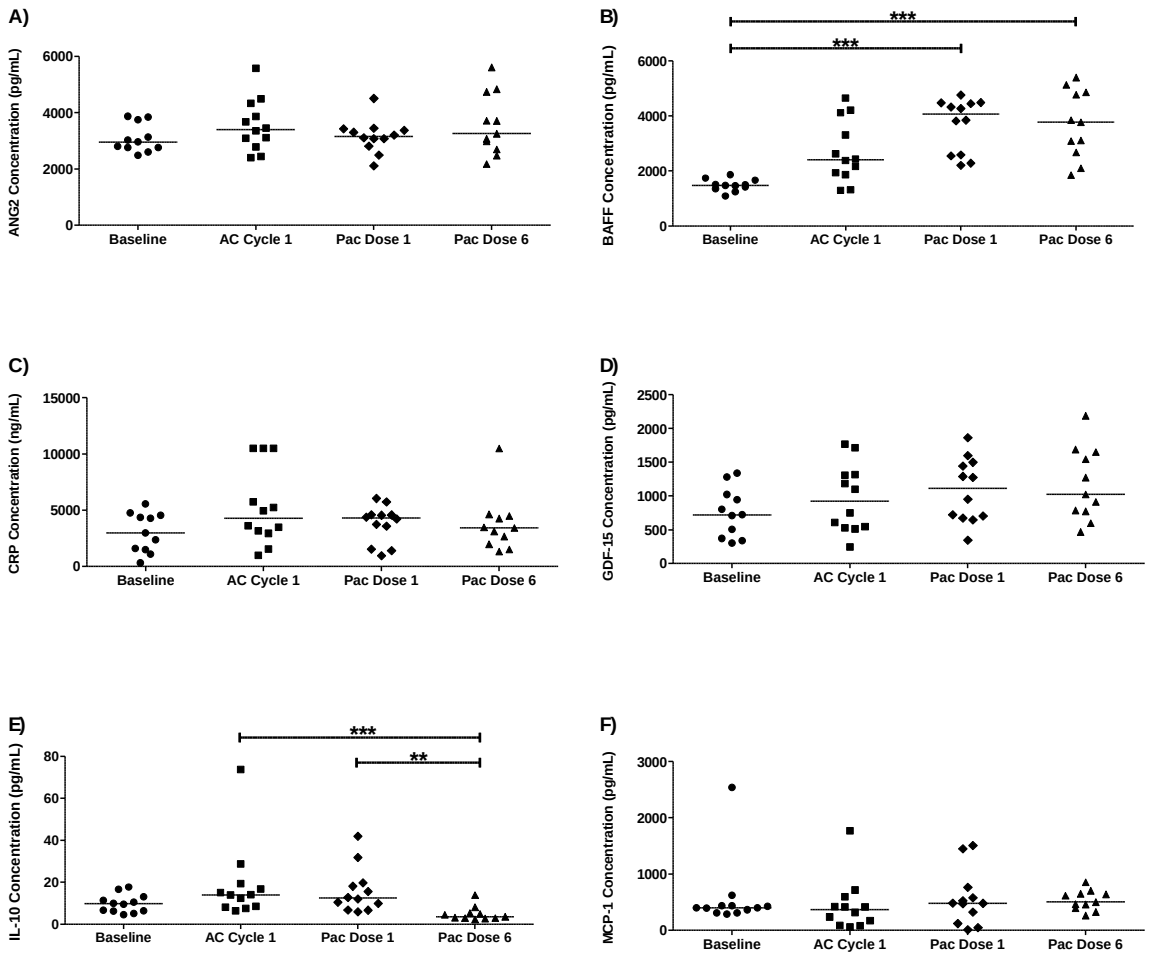

Figure 5.14. Circulating inflammatory cytokine concentrations measured during chemotherapy.

Inflammatory cytokines. A) ANG2, B) BAFF, C) CRP, D) GDF-15, E) IL-10, and F) MCP-1 were measured in participant serum using enzyme-linked immunosorbent assays at baseline (n= 11 for ANG2, BAFF, CRP and GDF-15, and n= 12 for IL-10 and MCP-1; circles), AC cycle one (n= 12; squares), paclitaxel dose one (n= 12; diamonds), and paclitaxel dose six (n= 11; triangles). Black horizontal solid lines represent the median values. Statistical analysis was perform with the Kruskal-Wallis test using Dunn's Multiple Comparison Testing *p<0.01; **p<0.01; ***p<0.001.

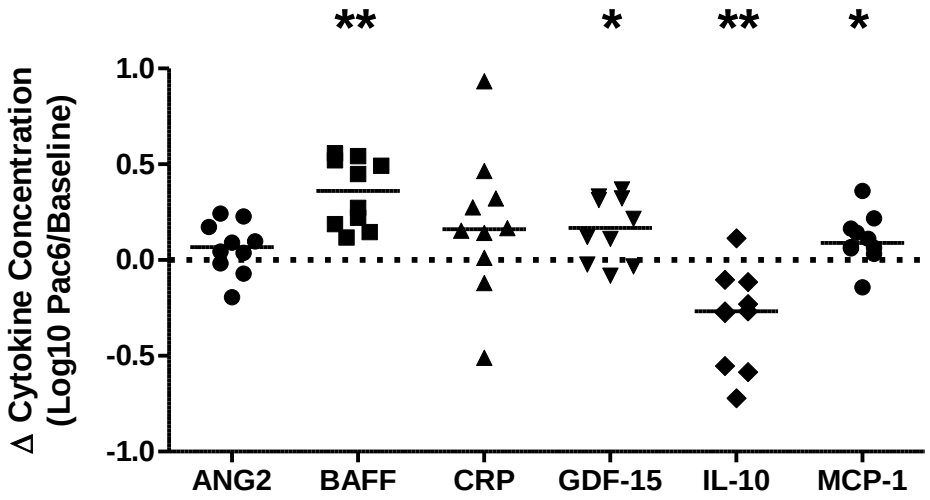

Figure 5.15. Change in circulating inflammatory cytokines measured during chemotherapy.

Inflammatory cytokines ANG2, BAFF, CRP, GDF-15, IL-10, and MCP-1 were measured in participant serum using enzyme-linked immunosorbent assays before chemotherapy (n= 10), and after chemotherapy (after paclitaxel dose six; n= 10). Black horizontal solid lines represent median values. The black horizontal dotted line represents no difference in cytokine concentration from baseline to paclitaxel dose six, and points above or below the dotted line represent an increase or decrease in cytokine concentration during chemotherapy, respectively. Statistical analysis was performed using the Wilcoxon matched-pairs signed rank test. *$p<0.05$; **$p<0.01$.

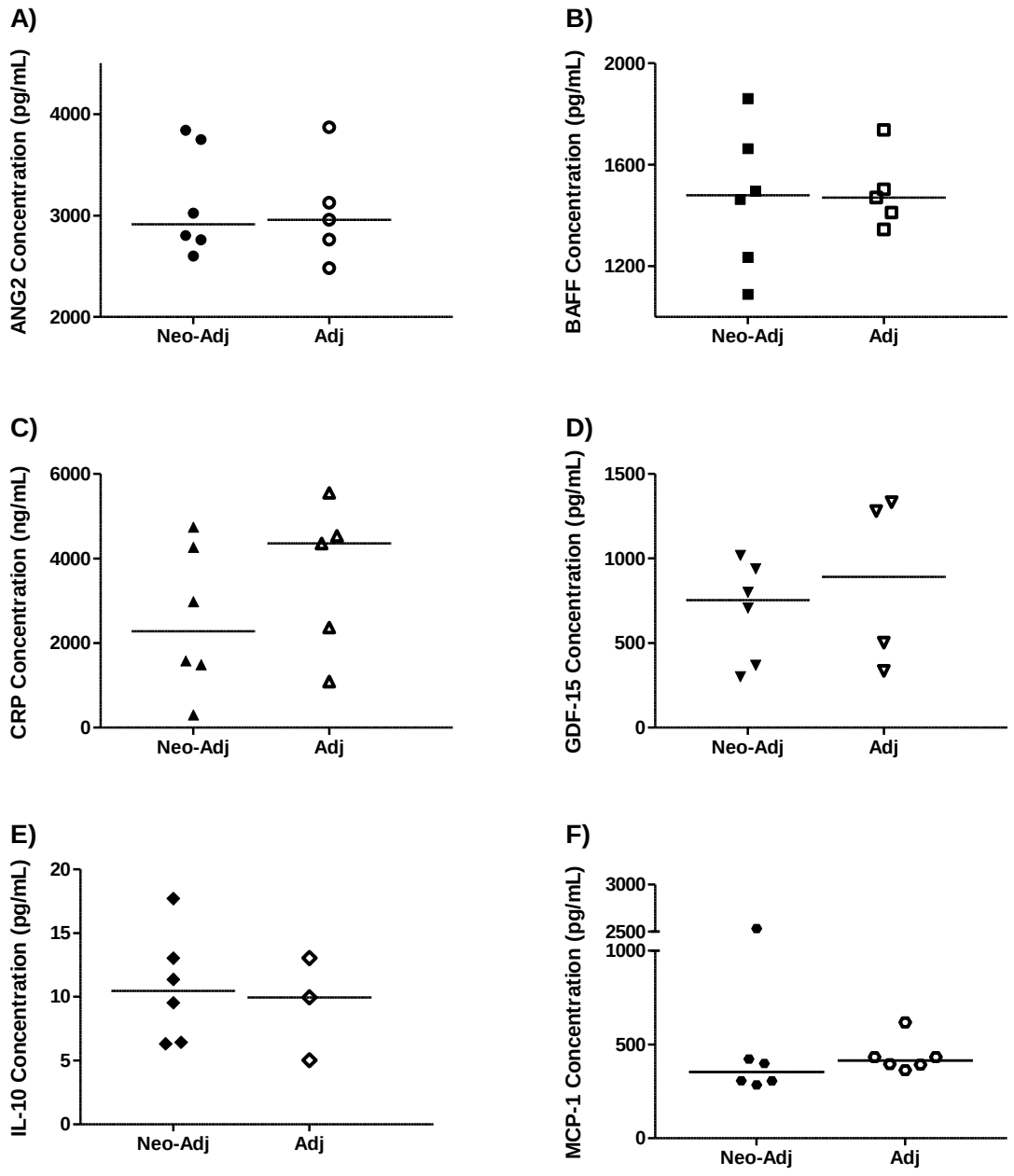

Figure 5.16. Effects of surgery on concentrations of circulating inflammatory cytokines before chemotherapy.

The concentration of A) ANG2, B) BAFF, C) CRP, D) GDF-15, E) IL-10, and F) MCP-1 were measured in serum samples collected from each participant before starting chemotherapy, and were compared between participants treated with neoadjuvant (n= 6; solid points) and adjuvant (n= 6; transparent points) chemotherapy. Black horizontal solid lines represent the median values. Statistical analysis was performed using Mann-Whitney U testing, and significance was determined as $p<0.05$.

5.2.4.4 Effect of body morphometry on changes in circulating concentrations of selected inflammatory cytokines during chemotherapy

To determine whether the change in circulating inflammatory cytokines was affected by differences in body morphometry at baseline (prior to starting chemotherapy), and the change in BMI and body fat percentage during chemotherapy, the change in levels of inflammatory cytokines ANG2, BAFF, CRP, GDF-15, IL-10 and MCP-1 between baseline and paclitaxel dose six were compared between participants that had either low (n= 6) or high (n= 5) body fat percentage (split by median= 39.90%) at baseline (Figure 5.17), and correlated with the change in body fat percentage and BMI between baseline and paclitaxel dose six (Figure 5.18 and Figure 5.19).

Change in concentrations of all six cytokines from baseline to paclitaxel dose six was not dependent on differences in body fat percentage at baseline ($p>0.05$; Figure 5.17). To determine the effects of body morphometry on the changes in circulating inflammatory cytokines during chemotherapy, this study compared baseline body fat percentage with the change in cytokine concentrations, as body fat percentage was significantly positively correlated with both BMI and WHR at baseline (Section 5.2.2.3, Figure 5.2A and C).

Changes in IL-10 concentrations were significantly positively correlated with changes in body fat percentage ($R^2=0.685$, $p=0.025$; Figure 5.18E). Whereas, changes in the remaining cytokines were not correlated with changes in body fat percentage or BMI ($p>0.05$; Figure 5.18 and Figure 5.19).

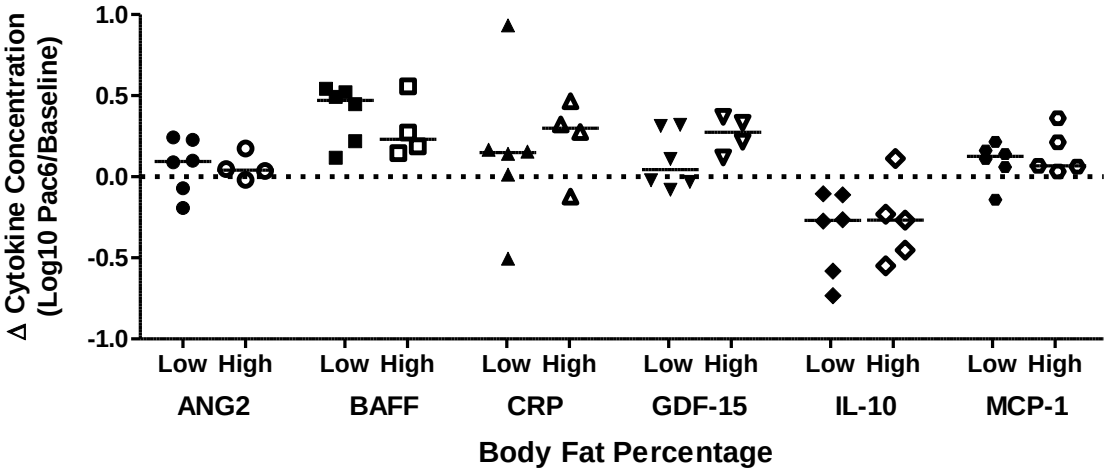

Figure 5.17. Effect of body morphometry on the change in circulating inflammatory cytokines measured during chemotherapy.

The change in concentration of ANG2, BAFF, CRP, GDF-15, IL-10, and MCP-1 inflammatory cytokines from baseline to paclitaxel dose six, measured in serum using enzyme-linked immunosorbent assays, was compared between participants with low (n= 6) or high (n= 4 for ANG2, BAFF, CRP and GDF-15, and n= 5 for IL-10 and MCP-1) body fat percentage (split by median= 39.90%) recorded before chemotherapy. Black horizontal solid lines represent median values. The black horizontal dotted line represents no difference in cytokine concentration from baseline to paclitaxel dose six, and points above or below the dotted line represent an increase or decrease in cytokine concentration during chemotherapy, respectively. Statistical analysis was performed using Mann Whitney U testing, and significance was determined as $p<0.05$.

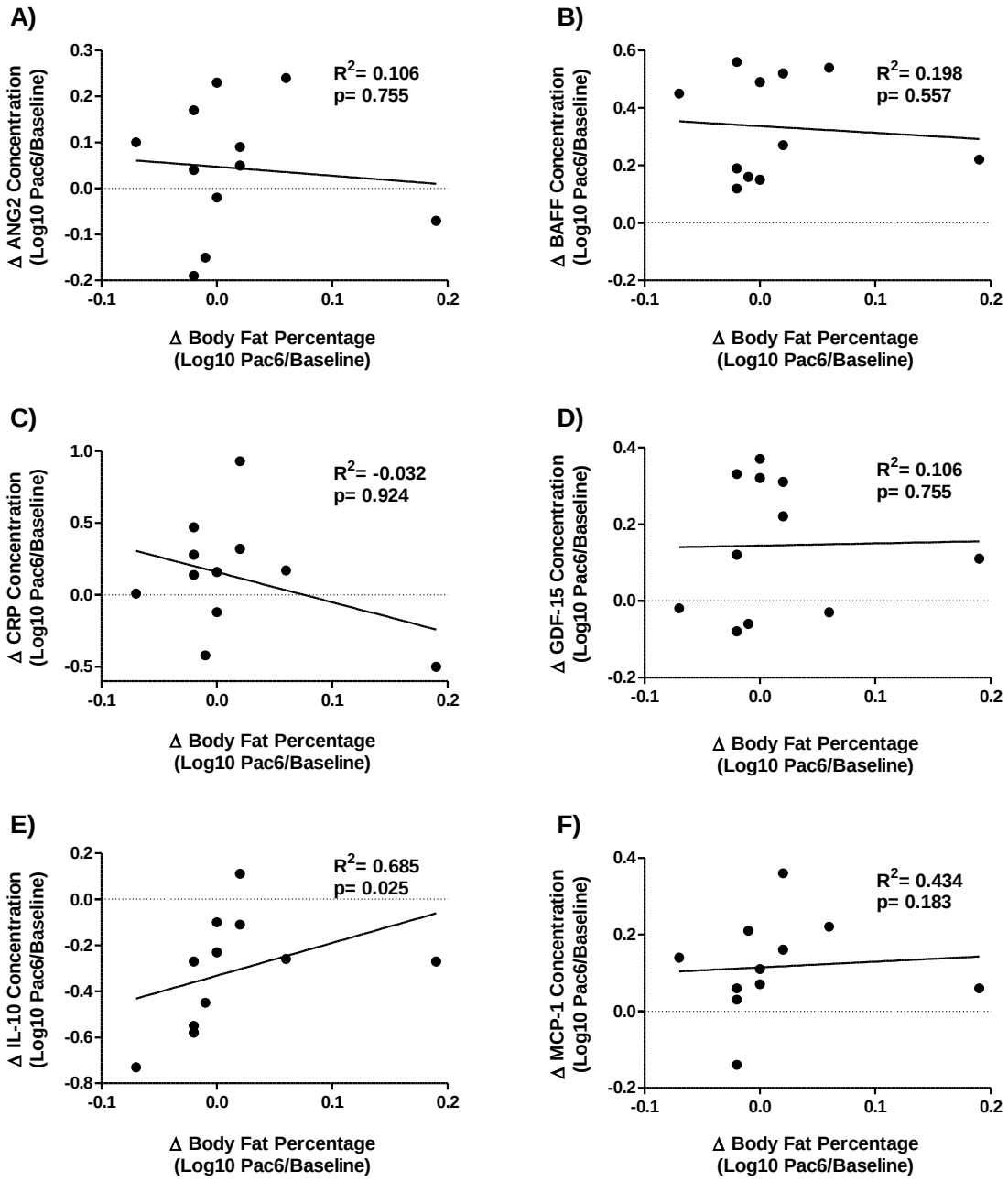

Figure 5.18. Correlation between the change in inflammatory cytokines and the change in body fat percentage during chemotherapy.

The change in A) ANG, B) BAFF, C) CRP, D) GDF-15, E) IL-10 and F) MCP-1 cytokine concentrations from before to after chemotherapy (log10), was correlated with the change in body fat percentage from before to after chemotherapy (log10; n= 11). Black solid lines represent linear regression line of best fit. Horizontal black dotted lines represent no change in inflammatory cytokine concentration from baseline to paclitaxel dose six, and points above or below this represent an increase or decrease in inflammatory cytokine concentration, respectively. Statistical analysis was performed using Spearman correlation analysis, and significance was determined as $p<0.05$.

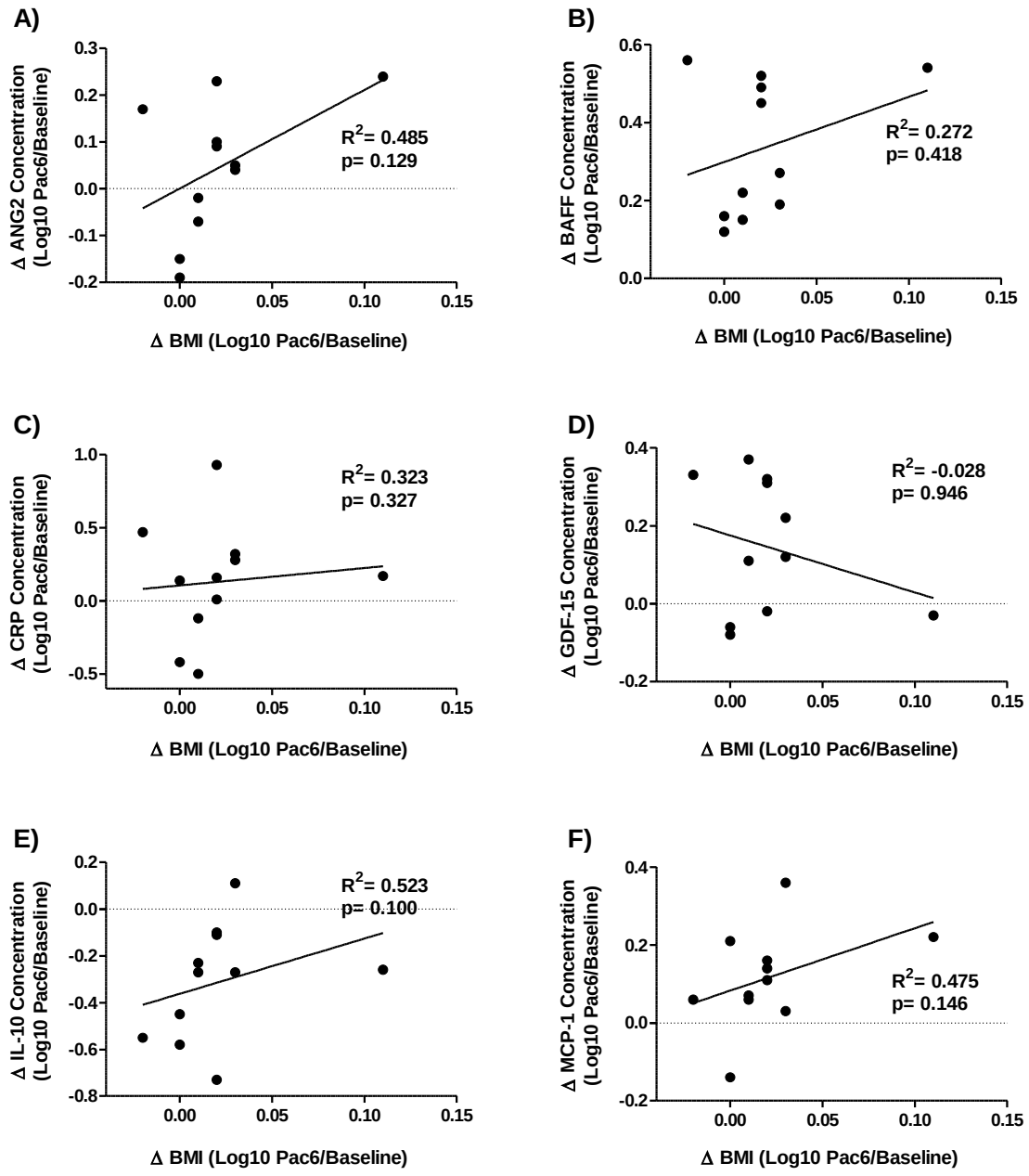

Figure 5.19. Correlation between the change in inflammatory cytokines and the change in body mass index (BMI) during chemotherapy.

The change in A) ANG, B) BAFF, C) CRP, D) GDF-15, E) IL-10 and F) MCP-1 cytokine concentrations from before to after chemotherapy (log10), was correlated with the change in BMI from before to after chemotherapy (log10; n= 11). Black solid lines represent linear regression line of best fit. Horizontal black dotted lines represent no change in inflammatory cytokine concentration from baseline to paclitaxel dose six, and points above or below this represent an increase or decrease in inflammatory cytokine concentration, respectively. Statistical analysis was performed using Spearman correlation analysis, and significance was determined as $p<0.05$.

5.2.4.5 Effect of physical activity levels on the change in circulating concentrations of selected inflammatory cytokines during chemotherapy

To determine whether the change in circulating inflammatory cytokines was affected by differences in physical activity levels during chemotherapy, the change in concentration of ANG2, BAFF, CRP, GDF-15, IL-10 and MCP-1 inflammatory cytokines from before to after (following paclitaxel dose six) chemotherapy was compared between participants that had either low (n= 5) or high (n= 5 for ANG2, BAFF, CRP and GDF-15, and n= 6 for IL-10 and MCP-1) average daily step counts (split by median= 5537 steps) recorded for AC cycle one, paclitaxel dose one, and paclitaxel dose six combined (Figure 5.20).

The change in cytokine concentration from before to after chemotherapy was not significantly dependent on differences in physical activity levels measured during chemotherapy ($p>0.05$; Figure 5.20).

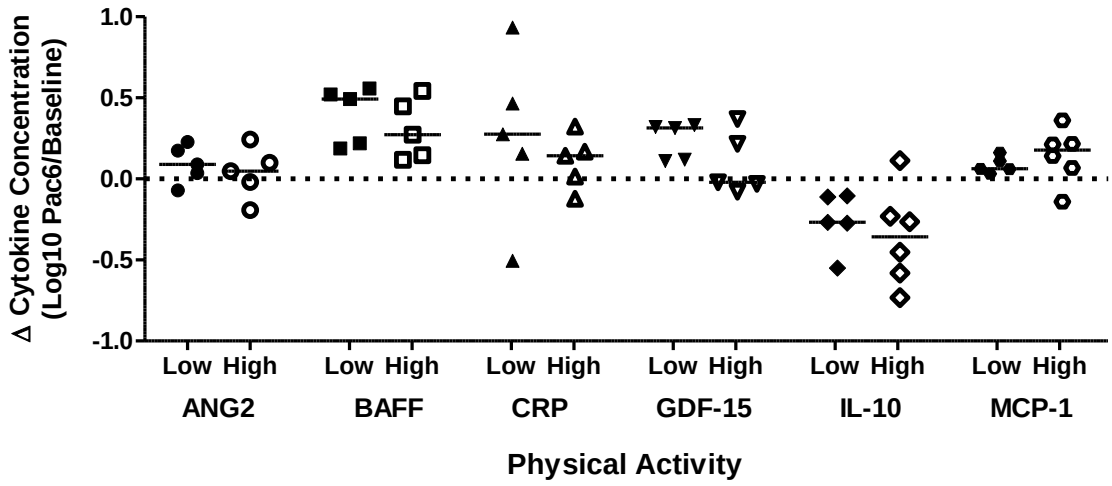

Figure 5.20. Effect of physical activity levels on the change in circulating inflammatory cytokines measured during chemotherapy.
The change in concentration of ANG2, BAFF, CRP, GDF-15, IL-10, and MCP-1 inflammatory cytokines from baseline to paclitaxel dose six, measured in serum using enzyme-linked immunosorbent assays, was compared between participants that had low (n= 5) or high (n= 5 for ANG2, BAFF, CRP and GDF-15, and n= 6 for IL-10 and MCP-1) average daily step counts (split by median= 5537 steps) recorded during AC cycle one, paclitaxel dose one and paclitaxel dose six using FitBit One® devices. Black horizontal solid lines represent median values. The black horizontal dotted line represents no difference in cytokine concentration from baseline to paclitaxel dose six, and points above or below the dotted line represent an increase or decrease in cytokine concentration during chemotherapy, respectively. Statistical analysis was performed using Mann Whitney U testing, and significance was determined as $p<0.05$.

5.2.5 Metabolising activity of liver CYP enzymes during chemotherapy

5.2.5.1 Experimental approach

To determine the metabolising activity of CYP1A2, CYP2C9, CYP2C19, CYP2D6 and CYP3A4 *in vivo*, this study measured the concentration of probe drugs, including caffeine, losartan, omeprazole, dextromethorphan, and midazolam, and their phase I metabolites, paraxanthine, E-3174, 5-hydroxyomeprazole, dextrophan, and α-hydroxymidazolam, respectively, using mass spectrometry. Probe drugs were administered to participants as a single oral dose at baseline (before chemotherapy) and again following paclitaxel dose six (after chemotherapy), and probe drug concentrations were compared to metabolite concentrations at each time point. Caffeine, omeprazole, midazolam, and their associated metabolites, were measured in serum samples after 4 hours, and losartan, dextromethorphan, and their metabolites, were measured in urine collected for 8 hours following probe drug administration.

To validate the use of serum samples for assessing probe drug and metabolite concentrations, rather than plasma (previously used by Ryu *et al.*[290]), participant 1 had caffeine, omeprazole, midazolam, and the metabolites paraxanthine, 5-hydroxyomeprazole, and α-hydroxymidazolam, quantified in both serum and plasma samples using mass spectrometry.

To check whether participants had abstained from consuming caffeine prior to probe drug administration as requested, this study investigated the concentrations of caffeine, and its metabolite paraxanthine, in serum samples taken before probe drugs were administered (0h), both before and after chemotherapy.

To investigate the change in metabolising activity of CYP enzymes during chemotherapy, the metabolic ratio of losartan, omeprazole, dextromethorphan, and midazolam, to their metabolites, were determined for each participant before and after chemotherapy, and the change in metabolic ratios from before to after chemotherapy was calculated. Moreover, to evaluate the effect of circulating inflammatory cytokines on changes in CYP metabolising activity during chemotherapy, the changes in inflammatory cytokine concentration from before to after chemotherapy were associated with the changes in metabolic ratios from before to after chemotherapy.

Due to extra time commitments and additional clinical visits required for the ‘Inje’ probe drug component of this study, participant 10 only consented to having body

morphometry, physical activity and inflammatory cytokines measured, and therefore did not have CYP metabolising activity measured before or after chemotherapy. Owing to difficulties taking blood samples, participant 11 opted out of the probe drug component following dose six of paclitaxel, and therefore did not have CYP metabolising activity measured after chemotherapy. As a result of clinical complications, participant 7 was only able to complete two out of the twelve (2/12) scheduled paclitaxel doses and was withdrawn from the study before paclitaxel dose six, and therefore did not have CYP metabolising activity measured after chemotherapy. The urine specimen for participant 3 was not collected following the administration of the probe drug cocktail after paclitaxel dose six and therefore, metabolising activity of CYP2C9 and CYP2D6 were not measured after chemotherapy.

5.2.5.2 Measuring the probe drugs and metabolites in serum and plasma

To determine whether the probe drugs and metabolites can be measured in serum as well as plasma samples, the concentration (ng/mL) of caffeine, omeprazole, midazolam, and their metabolites, paraxanthine, 5-hydroxyomeprazole, α-hydroxymidazolam were quantified 4 hours after cocktail administration in serum and plasma samples collected from participant 1.

The largest difference between serum and plasma concentrations was the α-hydroxymidazolam metabolite, with a 10% higher concentration of α-hydroxymidazolam measured in serum than plasma (Table 5.5). Based on the successful detection of parent drugs and metabolites in these serum samples it was deemed acceptable to use serum for the subsequent quantification of caffeine, omeprazole, midazolam, and their metabolites, paraxanthine, 5-hydroxyomeprazole, α-hydroxymidazolam for the remaining study participants.

Table 5.5. Concentration of parent and metabolite components from the 'Inje' probe drug cocktail in plasma and serum samples. Plasma and serum samples were collected 4 hours after cocktail administration from participant 1 following dose six of paclitaxel, and are used to measure metabolising activity of CYP1A2, CYP2C19 and CYP3A4 *in vivo*.

CYP enzyme	Parent and Metabolite	Plasma (ng/mL)	Serum (ng/mL)	Serum/Plasma
CYP1A2	Caffeine	8306.70	8420.00	1.10
	Paraxanthine	1260.00	1350.00	1.07
CYP2C19	Omeprazole	204.00	198.20	0.97
	5-Hydroxyomeprazole	95.30	97.65	1.02
CYP3A4	Midazolam	0.36	0.39	1.08
	α-Hydroxymidazolam	0.20	0.22	1.10

5.2.5.3 Determining levels of caffeine and paraxanthine prior to cocktail administration

To investigate whether participants were able to abstain from consuming caffeine prior to cocktail administration, this study investigated the serum concentrations of caffeine and its metabolite paraxanthine in study participants prior to probe drug cocktail administration (0 h), before chemotherapy and after chemotherapy (Table 5.6).

Before chemotherapy, and prior to 'Inje' cocktail administration, only two participants (participant 4 and 6) had undetectable levels of caffeine, and participant 6 also had undetectable paraxanthine (<5.0 ng/mL; Table 5.6). After chemotherapy, but prior to 'Inje' cocktail administration, participants 4, 5 and 6 had undetectable levels of caffeine, and participant 4 had undetectable levels of paraxanthine (<5.0 ng/mL; Table 5.6). Before cocktail administration, caffeine concentrations ranged from <5.0 to 1876.7 ng/mL and <5.0 to 2066.7 ng/mL in serum samples taken before and after chemotherapy, respectively (Table 5.6). Before cocktail administration, paraxanthine concentrations ranged from <5.0 to 2366.7 ng/mL and <5.0 to 1546.7 ng/mL in serum samples taken before and after chemotherapy, respectively (Table 5.6).

In comparison to caffeine and paraxanthine, all other parent drugs (losartan, omeprazole, dextromethorphan, and midazolam) and their metabolites (E-3174, 5-hydroxyomeprazole, dextrophan, and α-hydroxymidazolam) were below detectable concentrations prior to cocktail administration for the participants where changes in CYP phenotype during chemotherapy was assessed (Supplementary Table A.1).

Based on the variable concentrations of caffeine and paraxanthine in serum samples prior to probe drug administration, it was deemed unacceptable for CYP1A2 metabolising activity to be assessed based on caffeine and paraxanthine measures in serum taken 4 hours after probe drug administration.

Table 5.6. Concentrations of caffeine and paraxanthine in serum samples taken from each participant before probe drug administration.

	Before Chemotherapy (ng/mL)		After Chemotherapy (ng/mL)	
Participant	0h Caffeine	0h Paraxanthine	0h Caffeine	0h Paraxanthine
1	1876.7	1066.7	791.85	610.5
2	32.8	122.7	2066.7	1546.7
3	92.6	261.0	1846.7	926.7
4	< 5.0	91.5	< 5.0	< 5.0
5	70.8	131	< 5.0	15.2
6	< 5.0	< 5.0	< 5.0	55.3
7	41.2	538	n/a	n/a
8	259.7	553.7	115.5	289
9	1706.7	2366.7	63.3	289.3
11	217.3	389	n/a	n/a
12	224.7	471.3	445.3	744

<5.0: concentration of caffeine or paraxanthine was below the detectable limits of the assay.
0h: blood samples were drawn from participants prior to receiving the probe drug cocktail, and serum was prepared for analysis.

5.2.5.4 Phenotype assessment of CYP enzymes before chemotherapy

To determine metabolising activity of CYP enzymes at baseline, the participants were administered the 'Inje' probe drugs cocktail before starting chemotherapy, the concentrations of probe drugs and metabolites were measured in participant serum (n= 11) and urine (n= 11) samples, and parent drug concentrations were compared to the concentrations of their metabolites (Figure 5.21).

The levels of midazolam (median= 0.68 ng/mL) was significantly higher than the α-hydroxymidazolam (median= 0.31 ng/mL) metabolite measured in serum 4 hours after cocktail administration ($p<0.001$; Figure 5.21D). In urine samples, the E-3174 (median= 374.7 ng/mL) metabolite levels displayed lower levels than losartan (median= 524.7 ng/mL; Figure 5.21A), whereas, the dextrophan (median= 170.0 ng/mL) metabolite levels looked to be higher than dextromethorphan (median= 66.30 ng/mL; Figure 5.21C), however, neither difference was significant ($p>0.05$). Serum concentration of omeprazole (median= 118.30 ng/mL) and the 5-hydroxyomeprazole metabolite (median= 126.0 ng/mL) were not significantly different 4 hours after cocktail administration ($p>0.05$), although participant 6 had much higher levels of omeprazole (781 ng/mL) than all other participants (Figure 5.21B).

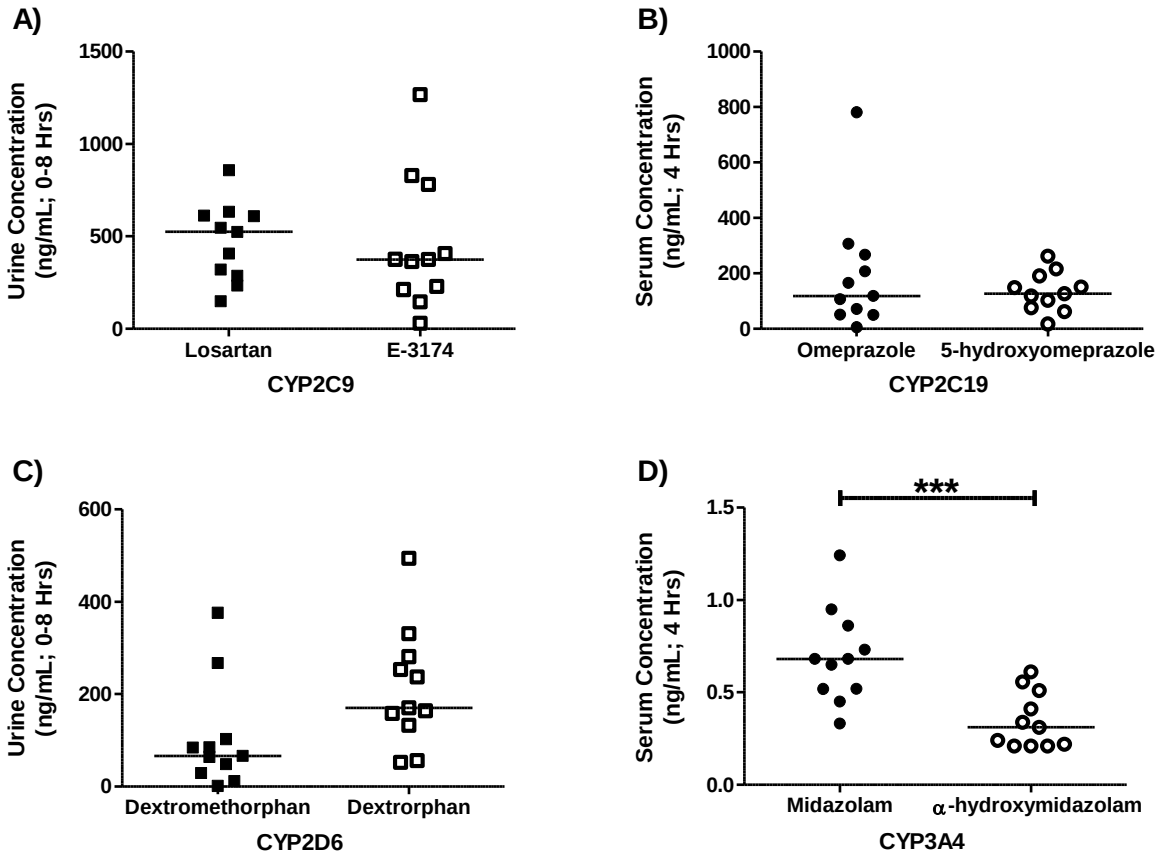

Figure 5.21. Probe drug and metabolite concentration measured before chemotherapy. Prior to starting chemotherapy the concentration (ng/mL) of the probe drugs A) losartan (CYP2C9), B) omeprazole (CYP2C19), C) dextromethorphan (CYP2D6), and D) midazolam (CYP3A4), and their metabolites (paraxanthine, E-3174, 5-hydroxyomeprazole, dextrophan, and α-hydroxymidazolam) were determined using mass spectrometry in serum and urine samples (n= 11). Serum samples were taken 4 hours after probe drug administration, and urine samples were collected for 8 hours following probe drug administration. Horizontal solid black lines represent median values. Statistical analysis was performed using Wilcoxon matched-pairs signed rank testing. ***$p<0.001$.

5.2.5.5 Phenotype assessment of CYP enzymes after chemotherapy

To determine metabolising activity of CYP enzymes after chemotherapy, the participants were administered the probe drugs following paclitaxel dose six and the concentrations of probe drugs and metabolites were measured in participant serum (n= 9) and urine (n= 8), and probe drug concentrations were compared to the concentration of metabolites (Figure 5.22).

The concentration of midazolam (median= 0.64 ng/mL) was significantly higher than the α-hydroxymidazolam (median= 0.30 ng/mL) metabolite measured in serum 4 hours after cocktail administration ($p<0.01$; Figure 5.22D). Lower levels of the E-3174 (median= 250.2 ng/mL) metabolite than losartan (median= 377.2 ng/mL) were displayed in urine samples, although not significantly ($p>0.05$;Figure 5.22A). Serum concentration of omeprazole (median= 82.60 ng/mL) and the 5-hydroxyomeprazole metabolite (median= 82.50 ng/mL) were not significantly different 4 hours after cocktail administration ($p>0.05$; Figure 5.22B). Dextrophan (median= 177.0 ng/mL) metabolite levels were not significantly different from the dextromethorphan (median= 71.85 ng/mL; $p>0.05$), however participant 4 showed much higher levels of dextrophan (3090 ng/mL) than the other participants (Figure 5.22C).

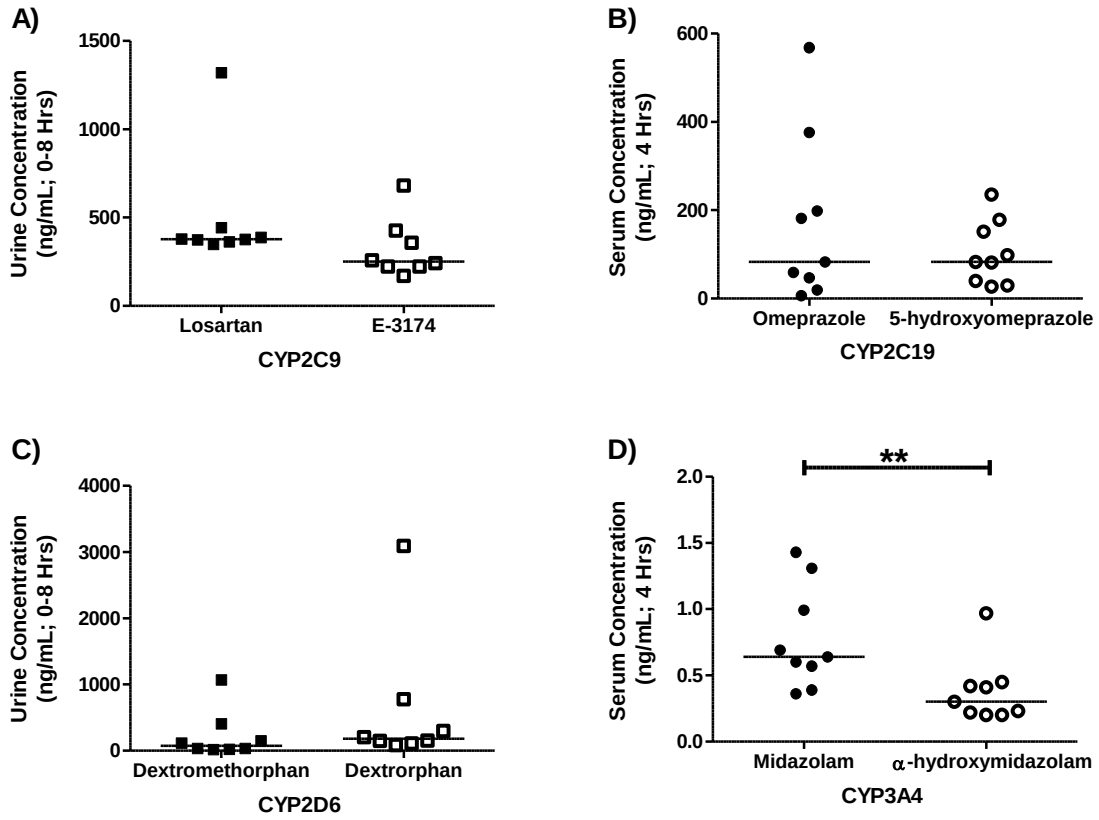

Figure 5.22. Probe drug and metabolite concentration measured after chemotherapy. Following paclitaxel dose six, the concentration (ng/mL) of the probe drugs A) losartan (CYP2C9), B) omeprazole (CYP2C19), C) dextromethorphan (CYP2D6), and D) midazolam (CYP3A4), and their metabolites (paraxanthine, E-3174, 5-hydroxyomeprazole, dextrophan, and α-hydroxymidazolam) were determined using mass spectrometry in serum (n= 9) and urine (n= 8) samples. Serum samples were taken 4 hours after probe drug administration, and urine samples were collected for 8 hours following probe drug administration. Horizontal solid black lines represent median values. Statistical analysis was performed using Wilcoxon matched-pairs signed rank testing. ***$p<0.001$.

5.2.5.6 Change in the metabolising activity of CYP enzymes during chemotherapy

To assess whether metabolising activity of CYP2C9, CYP2C19, CYP2D6 and CYP3A4 changed during chemotherapy, this study calculated the baseline probe drug to metabolite ratio and the probe drug to metabolite ratio following dose six of paclitaxel, and compared the change in ratios from before chemotherapy to after chemotherapy.

On average, there were no significant changes in CYP2C9, CYP2C19, CYP2D6 or CYP3A4 metabolising activity from baseline to paclitaxel dose six in this cohort of breast cancer patients ($p>0.05$; Table 5.7). For CYP2C9, n= 7 participants showed a greater than 1.25-fold change in metabolising activity during chemotherapy, in which two showed an increase in metabolising activity (< -0.097) and five exhibited decreased metabolising activity (> 0.0969; Figure 5.23). Furthermore, for CYP2C19 and CYP2D6, n= 6 participants showed a greater than 1.25-fold change in metabolising activity during chemotherapy, with three displaying an increase in metabolising activity (< -0.097) and three exhibiting a decrease in metabolising activity (> 0.097; Figure 5.23). Lastly for CYP3A4, n= 5 participants showed a greater than 1.25-fold change in metabolising activity during chemotherapy, with two displaying an increase in metabolising activity (< -0.097) and three exhibiting a decrease in metabolising activity (> 0.097; Figure 5.23).

Table 5.7. Changes in CYP metabolic ratios during chemotherapy for breast cancer.

Enzyme	Phenotyping	n	Before Chemo Phenotype Ratio*	After Chemo Phenotype Ratio*	After Chemo / Before Chemo Ratio (90% CI)	p**
CYP2C9	losartan/ E-3174	8	1.54	1.74	1.79 (0.79 - 2.78)	0.55
CYP2C19	omeprazole/ 5-hydroxyomeprazole	9	2.27	3.00	1.02 (0.78 - 1.26)	0.82
CYP2D6	dextromethorphan/ dextrorphan	8	0.65	0.68	1.26 (0.64 - 1.87)	1.00
CYP3A4	midazolam/ α-hydroxymidazolam	9	2.18	2.29	1.08 (0.81 - 1.35)	0.91

CI: confidence interval
*mean ratios; **statistical analysis was performed using Wilcoxon matched-pairs signed rank testing, and significance was determined as $p<0.05$.

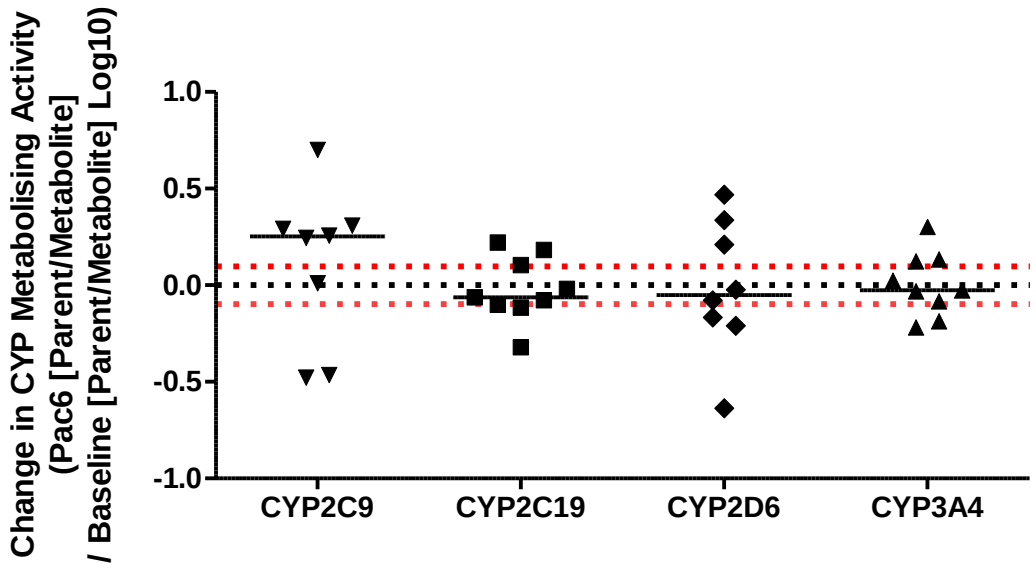

Figure 5.23. Changes in CYP metabolising ratios during chemotherapy for breast cancer.

The change in CYP2C9, CYP2C19, CYP2D6 and CYP3A4 metabolising activity was determined by comparing the probe drug to metabolite ratios from after chemotherapy and before chemotherapy (log10). Horizontal black solid lines represent median values. Horizontal black dotted line represents no change in CYP metabolising activity from baseline to paclitaxel dose six, and points above or below the red dotted horizontal lines represent a decrease or increase, respectively, in CYP metabolising activity of 1.25-fold or greater (log10 of 0.80 - 1.25= ± 0.097) from before chemotherapy to after chemotherapy. Statistical analysis was performed using Wilcoxon matched-pairs signed rank testing, and significance was determined as $p < 0.05$.

5.2.5.7 Effects of circulating inflammatory cytokines on the change in metabolising activity of CYP enzymes during chemotherapy

To assess whether changes in metabolising activity of CYP2C9, CYP2C19, CYP2D6 and CYP3A4 are affected by changes in circulating inflammatory cytokines during chemotherapy, this study correlated the changes in probe drug to metabolite ratio with changes in ANG2, BAFF, CRP, GDF-15, IL-10 and MCP-1 inflammatory cytokine concentrations from baseline to paclitaxel dose six. The correlations are presented in Figure 5.24, Figure 5.25, Figure 5.26, and Figure 5.27.

The change in concentration of the MCP-1 cytokine during chemotherapy was significantly correlated with the change in CYP3A4 metabolising activity during chemotherapy ($p= 0.05$), in which the increase in MCP-1 was associated with a decrease in CYP3A4 metabolising activity during chemotherapy ($R^2= 0.683$; Figure 5.27F).

The change in CYP2C19 metabolising activity during chemotherapy showed a trend ($p > 0.05$) towards a significant correlation with a change in ANG2 ($p= 0.121$; $R^2= 0.567$), BAFF ($p= 0.067$; $R^2= 0.650$) and MCP-1 ($p= 0.121$; $R^2= 0.567$) cytokine concentration during chemotherapy, suggesting that as these cytokines increased during chemotherapy, CYP2C19 showed a trend towards decreased metabolising activity (Figure 5.25A, B and F).

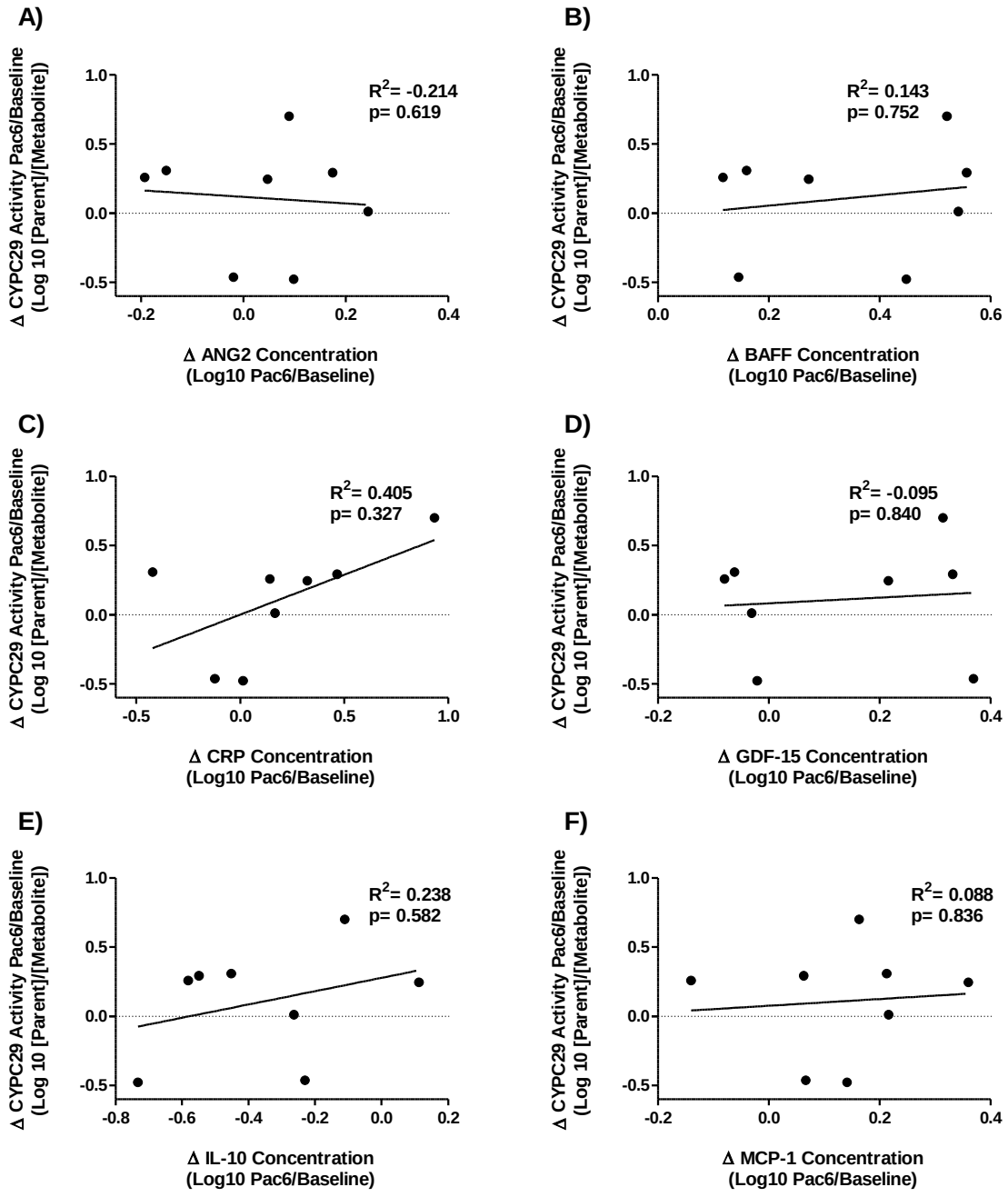

Figure 5.24. Correlation between the change in inflammatory cytokines and the change in CYP2C9 metabolising activity during chemotherapy.

The change in A) ANG, B) BAFF, C) CRP, D) GDF-15, E) IL-10 and F) MCP-1 cytokine concentrations from before to after chemotherapy (log10), was correlated with the change in CYP2C9 metabolising activity from before to after chemotherapy (log10; n= 8). Black solid lines represent linear regression line of best fit. Horizontal black dotted lines represent no change in CYP2C9 metabolising activity from baseline to paclitaxel dose six, and points above or below this represent a decrease or increase in CYP2C9 metabolising activity, respectively. Statistical analysis was performed using Spearman correlation analysis, and significance was determined as $p \leq 0.05$.

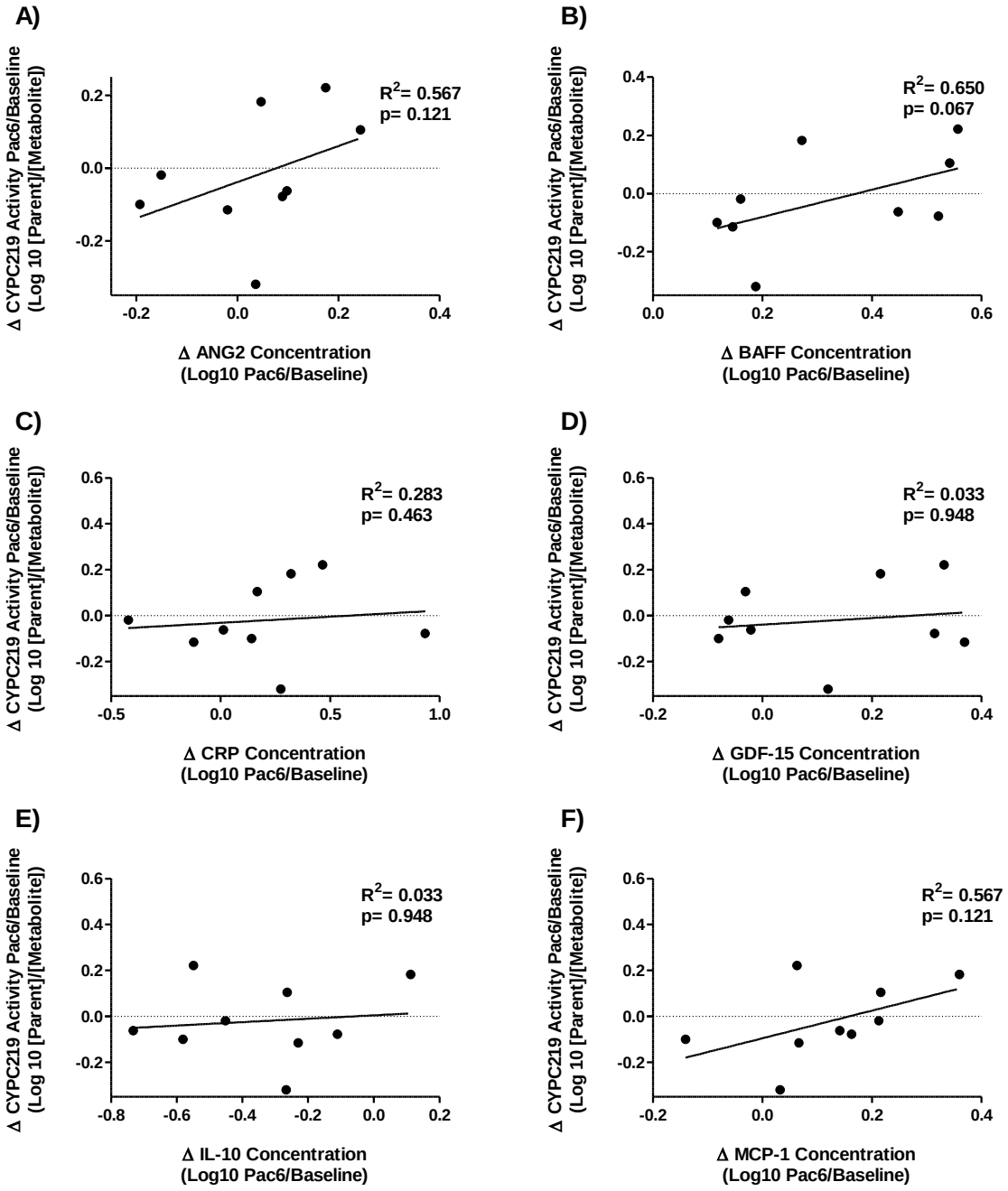

Figure 5.25. Correlation between the change in inflammatory cytokines and the change in CYP2C19 metabolising activity during chemotherapy.

The change in A) ANG, B) BAFF, C) CRP, D) GDF-15, E) IL-10 and F) MCP-1 cytokine concentrations from before to after chemotherapy (log10), was correlated with the change in CYP2C19 metabolising activity from before to after chemotherapy (log10; n= 9). Black solid lines represent linear regression line of best fit. Horizontal black dotted lines represent no change in CYP2C19 metabolising activity from baseline to paclitaxel dose six, and points above or below this represent a decrease or increase in CYP2C19 metabolising activity, respectively. Statistical analysis was performed using Spearman correlation analysis, and significance was determined as $p \leq 0.05$.

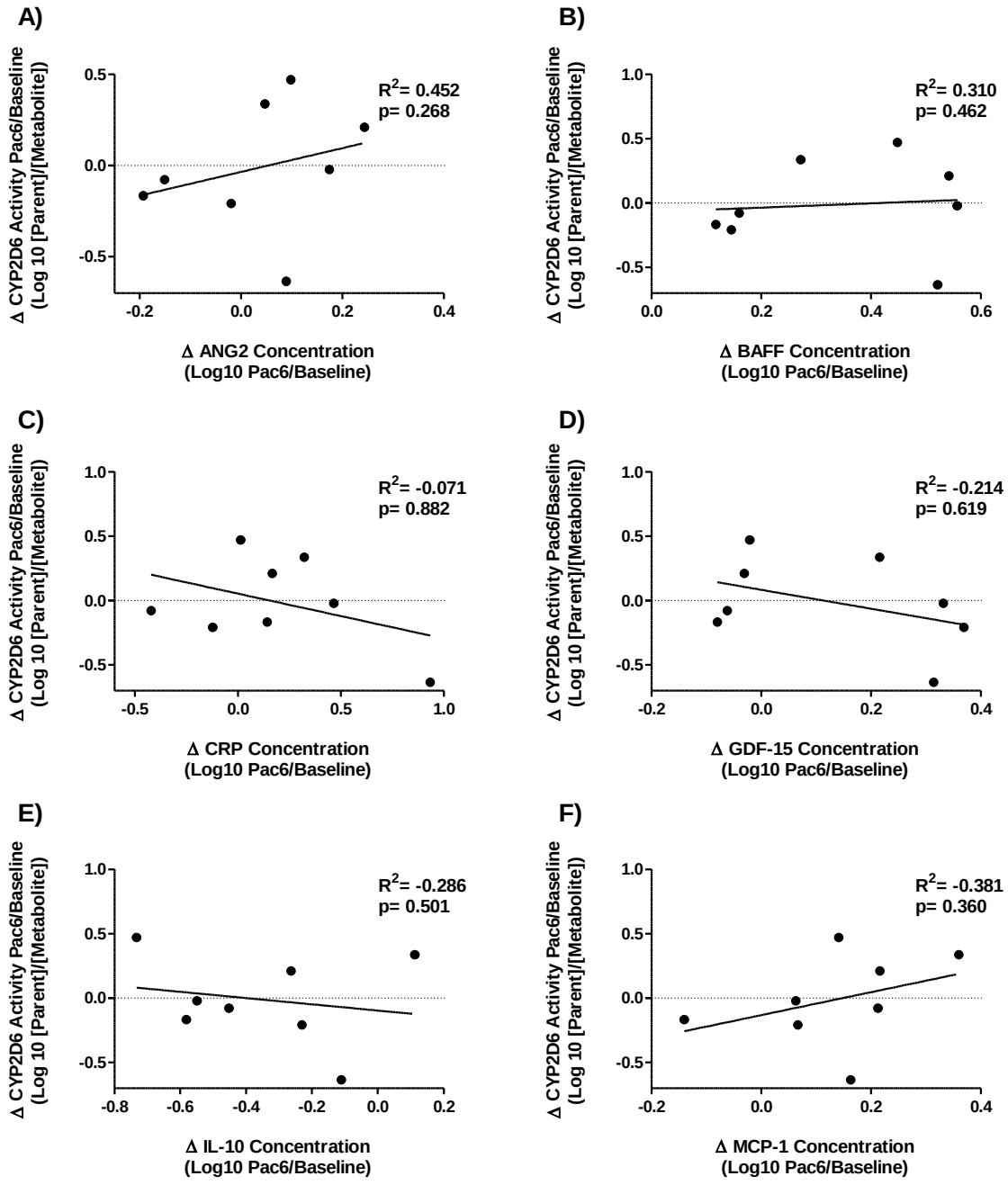

Figure 5.26. Correlation between the change in inflammatory cytokines and the change in CYP2D6 metabolising activity during chemotherapy.

The change in A) ANG, B) BAFF, C) CRP, D) GDF-15, E) IL-10 and F) MCP-1 cytokine concentrations from before to after chemotherapy (log10), was correlated with the change in CYP2D6 metabolising activity from before to after chemotherapy (log10; n= 8). Black solid lines represent linear regression line of best fit. Horizontal black dotted lines represent no change in CYP2D6 metabolising activity from baseline to paclitaxel dose six, and points above or below this represent a decrease or increase in CYP2D6 metabolising activity, respectively. Statistical analysis was performed using Spearman correlation analysis, and significance was determined as $p \leq 0.05$.

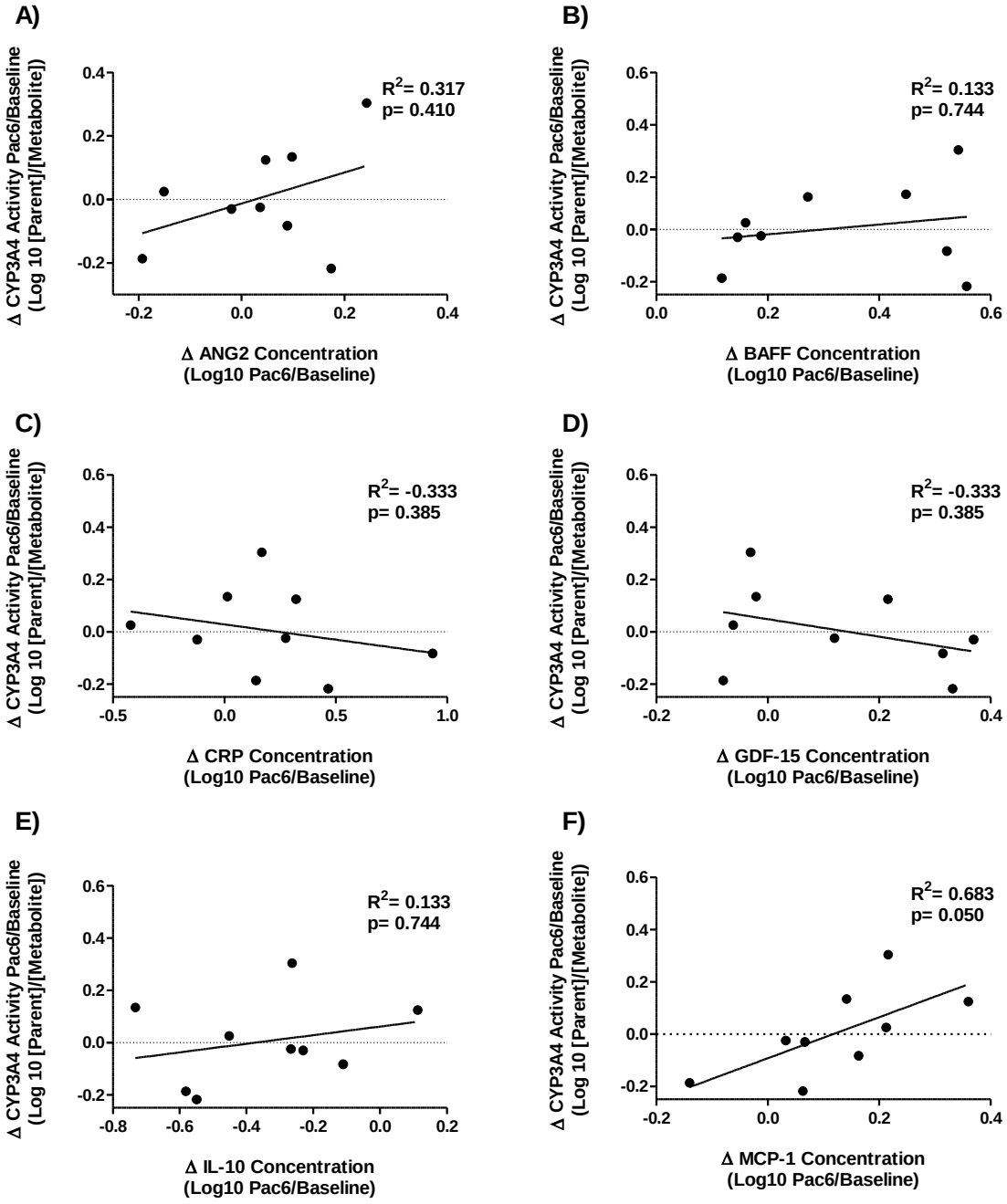

Figure 5.27. Correlation between the change in inflammatory cytokines and the change in CYP3A4 metabolising activity during chemotherapy.
The change in A) ANG, B) BAFF, C) CRP, D) GDF-15, E) IL-10 and F) MCP-1 cytokine concentrations from before to after chemotherapy (log10), was correlated with the change in CYP3A4 metabolising activity from before to after chemotherapy (log10; n= 9). Black solid lines represent linear regression line of best fit. Horizontal black dotted lines represent no change in CYP3A4 metabolising activity from baseline to paclitaxel dose six, and points above or below this represent a decrease or increase in CYP3A4 metabolising activity, respectively. Statistical analysis was performed using Spearman correlation analysis, and significance was determined as $p \leq 0.05$.

5.3 Discussion

Obese women with breast cancer are suggested to have poorer pathological response rates to chemotherapy [122]. Alternatively, physical activity implemented during adjuvant chemotherapy has displayed a trend toward improved breast cancer disease free survival outcomes, particularly for women who were overweight or obese [188]. Obesity and post-diagnosis physical activity are associated with increases in, and lowered levels of circulating inflammatory cytokines, respectively [63,441,442]. The biological mechanisms by which alterations in the levels of circulating inflammatory cytokines are influencing treatment outcomes for women with breast cancer are yet to be elucidated. Metabolism of breast cancer chemotherapy agents occurs primarily by hepatic cytochrome (CYP) P450 drug metabolising enzymes, including CYP1A2, CYP2C9, CYP2C19, CYP2D6, and CYP3A4 [264,266]. Inflammatory cytokines are known to downregulate hepatic CYP expression *in vitro*, and circulating inflammatory cytokines *in vivo* may be causing discordance between CYP genotypes and phenotypes [283,300–305,309,310,316,317]. Unexpected alterations in the metabolism of chemotherapies may be influencing the therapeutic efficacy of these drugs during treatment for breast cancer. Thus, this study determined whether alterations in CYP activity throughout chemotherapy are influenced by levels of circulating inflammatory cytokines in women with breast cancer.

This exploratory patient study is the first to concurrently assess *in vivo* changes in both circulating inflammatory cytokine concentrations and activity of multiple CYP drug metabolising enzymes, during chemotherapy for breast cancer. This chapter presents data from seven non-obese (BMI < 30) and five obese (BMI ≥ 30) women receiving adriamycin-cyclophosphamide (AC) and paclitaxel treatment for stage II or III breast cancer. Due to the small sample size, results from this exploratory study are reported as, and should be considered, preliminary findings.

Results showed that the reduction in the activity of CYP3A4 during chemotherapy was correlated with increased serum concentrations of monocyte chemoattractant protein 1 (MCP-1), although the *in vivo* activity of CYP enzymes across this cohort of women remained unchanged during chemotherapy. In addition, significant increases in serum levels of the pro-inflammatory cytokines B-cell activating factor (BAFF), growth and differentiation factor 15 (GDF-15) and MCP-1, and a decrease in the cytokine interleukin 10 (IL-10), were observed during chemotherapy. Finally, this study observed a significant increase in BMI throughout

chemotherapy, as well as a reduction in daily step counts in the early stages of treatment, however alterations in cytokine concentrations were not dependent on these differences in body morphometry and physical activity.

5.3.1 Exploratory patient study feasibility

5.3.1.1 Participant recruitment

Success of clinical trials depends not only on robust trial designs and protocols, but also on sufficient participant recruitment. In this exploratory patient study, the evaluation of recruitment rates showed that approximately 10% of the stage II and III breast cancer patients receiving AC and paclitaxel chemotherapy at Christchurch Hospital were successfully recruited onto this study. The approximate 10% recruitment rate aligns well with participation rates reported internationally for cancer clinical trials, which sits around 7.7% [445]. Moreover, the recruitment rate achieved here was well above the overall 2-5% enrolment rate reported for adult patients with colorectal and lung cancers [446]. In agreement with survey findings regarding clinical trial participation of cancer patients [447,448], the majority of the patients approached in this exploratory study expressed a willingness to participate. Furthermore, similar to the recent survey reports [448], reasons for rejecting participation in the current study were largely related to the extra time commitment.

Despite having comparatively high recruitment rates, this pilot study recruited lower numbers of participants than initially anticipated, an experience commonly reported for a large proportion of clinical trials in the UK [449]. Moreover, like one third to half of previously assessed clinical trials, this study required an extension on the recruitment time in an attempt to meet the enrolment goal [449,450]. With close to 20% of clinical trials failing due to insufficient participant enrolment [451], it is becoming increasingly important for researchers to assess and publish data on participant recruitment so that interventions that increase recruitment, and thus, the success of clinical trials can be implemented. Overall, the data on recruitment rates from this feasibility study provide valuable information for the clinical trial landscape in New Zealand.

5.3.1.2 'Inje' probe drug cocktail administration

Concurrent assessment of *in vivo* CYP enzyme activity in this study was achieved by administering sub-therapeutic oral doses of five probe drugs, referred to as the 'Inje' cocktail,

and simultaneously assessing the concentration of the probe drugs and their metabolites in serum and urine samples taken 4 and 0-8 hours after cocktail administration, respectively.

The 'Inje' probe drug cocktail was developed by Ryu *et al.,* in which the simultaneous oral administration of caffeine, losartan, omeprazole, dextromethorphan, and midazolam probe drugs, and the single time point for blood and urine sample collection to measure probe drugs and metabolites, were validated for the concurrent assessment of *in vivo* activity of CYP1A2, CYP2C9, CYP2C19, CYP2D6, and CYP3A4, in which no evidence of any probe-drug interactions or drug-associated adverse events were observed [290]. The current study was the first to use a modification of the 'Inje' cocktail to assess the *in vivo* activity of these five CYP enzymes in women receiving chemotherapy for breast cancer. Prior to this study, numerous research investigations have used slight variations of the 'Inje' cocktail to assess CYP activity in healthy human subjects [452–456]. Some were focused on developing analytic techniques for simultaneously assessing the cocktail's probe drugs and metabolites in a single assay [452,454], whereas, others used the 'Inje' cocktail to investigate interactions between CYP activity and co-administered drugs, including rifampicin and belatacept [453,455]. Heo *et al*., developed an assay that simultaneously determined the concentration of another substrate and its metabolite, as well as the 'Inje' probe drug cocktail substrates [456]. In difference to these past studies, the 'Inje' cocktail was used as a tool in the current study to assess for the first time whether *in vivo* activity of the CYP1A2, CYP2C9, CYP2C19, CYP2D6, and CYP3A4 enzymes are affected by treatment with chemotherapy in women with breast cancer.

The current study administered the same or lower doses of the probe drugs when compared to the doses from the original 'Inje' study [290]; with the exception of caffeine which was higher. Other investigations using the 'Inje' cocktail were carried out in healthy volunteers, and used oral doses of the probe drugs that were either similar or higher than the original study [453–456]. The only exception was a study that developed a high-sensitivity LC-MS/MS methodology for simultaneously detecting 10-100 times lower administered doses of the probe drugs in human plasma [452]. Despite inter-study differences in dosage, the 'Inje' probe drugs and metabolites were successfully measured in this, and prior, studies. Moreover, the oral administration of the probe drugs was pharmacologically and clinically well tolerated by the participants, as no probe-drug associated adverse events were documented.

Serum samples collected prior to probe drug administration showed background contamination with both caffeine and its metabolite paraxanthine in the majority of the

participants, despite being asked to abstain from caffeine containing beverages for 24 hours prior to the cocktail visit (Section 5.2.5.3; Table 5.6). Based on this finding, the current investigation did not generate phenotype data for the CYP1A2 enzyme. In contrast, metabolic phenotype data was generated for CYP1A2 by previous studies utilising the 'Inje' probe drug cocktail, suggesting that similar findings of caffeine contamination were not observed [290,452–456]. Future research should consider dosing with mass-labelled caffeine molecules in order to prevent dietary interference. Yet, in comparison to the other CYP enzymes assessed in this study, the contribution of CYP1A2 to *in vivo* breast cancer chemotherapy metabolism is negligible [266], thus, the decision to omit caffeine and paraxanthine assessment, rather than attempting to control for the background levels, is supported.

Intra-patient variability of CYP activity throughout chemotherapy for breast cancer was assessed in this study using the 'Inje' cocktail and pharmacokinetic sampling, performed prior to starting chemotherapy (neoadjuvant and adjuvant participants) and again following dose six of paclitaxel. Changes in CYP2C19 and CYP3A4 during breast cancer chemotherapy were assessed in nine women, with eight women also having changes in CYP2C9 and CYP2D6 activity measured. Despite being an exploratory study, the current study numbers align well with the number of participants investigated in previous 'Inje' cocktail studies, which ranged from four to twenty-two participants [290,452–456]. The cocktail approach to simultaneously phenotyping multiple CYP enzymes, eliminates the need for multiple studies, and thus, reduces the pharmacokinetic variation that would usually be experienced between study populations [288]. It could be argued that by removing the between study variation, it is justifiable to use smaller study numbers for cocktail probe drug phenotyping, particularly in exploratory analyses such as the current investigation.

Overall, this exploratory study exhibited feasibility of the 'Inje' cocktail in cancer patients, as it was used safely and effectively for determining the *in vivo* activity of the CYP2C9, CYP2C19, CYP2D6 and CYP3A4 enzymes in breast cancer chemotherapy patients. Assessment of CYP1A2 activity was hindered by background caffeine contamination in this study's serum samples.

5.3.2 Assessing adiposity during breast cancer chemotherapy

Overall, breast cancer patients in this exploratory study exhibited a small but significant increase in BMI during combination AC and paclitaxel chemotherapy, with no notable changes in WHR, or body fat and muscle mass percentage observed. In agreement

with this, a number of studies in the pre-anthracycline and modern chemotherapy eras, have reported an increase in weight during both adjuvant or neoadjuvant treatment for breast cancer [457,458]. Although, the current observation concluded that body fat and muscle mass percentages are maintained across the cohort as a whole, there was variation in fat and muscle mass changes between participants. Previous body composition analyses have shown that in breast cancer patients, chemotherapy has been associated with an increase in fat mass and a decrease in lean body mass, with or without any significant change in weight [458–460]. In regards to patient outcome, it has been established that both increases and decreases in weight during chemotherapy can negatively impact rates of recurrence and mortality [458,461], suggesting that weight maintenance during chemotherapy may be important for patient outcomes. Therefore, the change in BMI and variation in body composition observed in this study may be of clinical significance. As the recruitment for this pilot study has recently ended, and follow-up is currently on-going, assessment of the association between chemotherapy induced changes in BMI and cancer outcomes of the participants will be of interest in the future.

This exploratory study provided evidence of chemotherapy associated adipose tissue remodelling, particularly in participant 5. In this participant, BMI and body fat percentage were notably increased, yet this participant had the greatest decrease in WHR during chemotherapy. Based on these changes it is speculated that adipose tissue depots were remodelled throughout chemotherapy so that excess energy was stored around the hips rather than the abdominal/waist area. Alongside participant 5, participant 10 more than doubled their adiposity throughout chemotherapy, although based on a stable WHR, it was assumed that their weight gain was evenly distributed. It has been suggested that during weight gain, adipose tissue remodelling upregulates adipocyte lipolysis, which is the breakdown for stored triacylglycerides and increased secretion of free fatty acids [462]. Fatty acids can bind to toll-like receptor 4 transmembrane proteins on macrophages resident within adipose tissues, activating intracellular signalling pathways that increase production of inflammatory cytokines, such as TNF-α and MCP-1 [39]. Moreover, most likely as a result of elevated lipolysis, transportation of fatty acids to the liver, and hepatic *de novo* fatty acid production, are increased during conditions of adipose tissue remodelling [463]. Similar to adipose tissue, fatty acids can stimulate inflammatory cytokine production by hepatic macrophages, fuelling inflammatory signalling that may negatively impact liver function [464]. Thus, by utilising different measures to determine body composition, this exploratory study was able to identify adipose tissue remodelling as a potential source of inflammatory cytokine production during chemotherapy.

A key strength of this exploratory study was the combination of anthropometric measurements and bioelectrical impedance analysis (BIA) for gathering information on multiple components of body morphometry. Classifications for grouping individuals as healthy, overweight and obese are historically based on anthropometric measures, such as BMI, however, other methods and tools have now been developed that can more accurately determine total body adiposity [10,11,465]. One such modality is BIA, which measures resistance of the flow of electrical currents through the body in order to rapidly, painlessly, and non-invasively generate muscle, adipose, bone and water composition data [466,467]. Major benefits of BIA is that it is inexpensive, simple, and transportable; in that the instrument can be moved between sites and delivered to its users [466,467]. The validity, accuracy, and reliability of BIA instruments has been extensively studied and reviewed, and despite sometimes conflicting results, consensus suggests BIA is useful when assessing and comparing adiposity within subgroups [468,469].

Prior to starting chemotherapy, results from the current study showed body fat percentage measured by BIA was significantly positively correlated with BMI and WHR measurements. In agreement with this study, BMI has been previously reported as a good predictor of body fat percentage in a large population of otherwise healthy post-menopausal women [470]. However, in the majority of studies investigating the association between body fat percentage and BMI, the prevalence of obesity in adult populations tends to be underestimated by BMI, although the degree of difference is usually dependent on sex, age and ethnic group [14,16,17]. Discordance between measures is likely due to the fact that anthropometric assessments lack the distinction between fat mass and fat free mass [10]. Nevertheless, results from this study suggest that in this population of women with early stage breast cancer, BMI was a good indicator of patient adiposity.

5.3.3 Assessing physical activity during breast cancer chemotherapy

Based on average daily step count data, this study observed a significant decrease in physical activity levels over the first 12 weeks of chemotherapy, a reduction that remained throughout the following stages of treatment. Similar declines in physical activity levels during chemotherapy have been reported by previous studies in breast cancer patients. Total physical activity was shown to reduce by 8 hours each week over the first half of chemotherapy; with levels remaining low throughout the second half of treatment [202]. Another study assessing activity during a 20 week home-based and supervised resistance training

programme, observed a decrease in physical activity from the early to late stages of chemotherapy [471]. Interestingly, breast cancer patients reporting higher levels of physical activity prior to diagnosis were more inclined to remain physically active throughout chemotherapy [472]. Furthermore, behaviours of reduced physical activity in the later stages of chemotherapy have been shown to continue into life post-treatment [473]. Taken together, these findings suggest that chemotherapy patients would likely benefit from physical activity education and support implemented prior to commencing treatment, to help prevent activity declines in the early stages of therapy.

Similar to previous investigations [196,201,202,474], this study used FitBit™ devices to objectively measure physical activity levels in women receiving chemotherapy for breast cancer; and the objectivity of accelerometer data is a major strength of the current investigation. Compared to FitBit™ measured physical activity levels during chemotherapy, self-reported activity has been shown to be biased, with 59% of participants over-reporting activity levels [196], validating the importance of objective assessment.

In comparison to previous studies using FitBit™ devices, the current analysis achieved a higher rate of FitBit™ wearing adherence during chemotherapy. In this study step count data was recorded for 93.7% of the total FitBit One® wearing days, whereas, other studies reported FitBit™ recordings on an average of 44.5%, 79% and 84% of days where participants provided analysable FitBit™ data [201,202,474]. In contrast to these previous studies [201,202,474], the current investigation had a smaller study population, recorded physical activity over fewer weeks, synced and charged the FitBit™ devices regularly in-house (omitting this as a requirement for study participants), and passively assessed physical activity without implementing an exercise intervention. Thus, it could be speculated that all, or some, of these differences may have contributed to the improved adherence rates to wearing the FitBit™ devices throughout the chemotherapy period in the current investigation.

5.3.4 Change in serum levels of circulating inflammatory cytokines during chemotherapy for breast cancer

Circulating levels of four inflammatory cytokines were significantly changed in the serum of breast cancer patients, over the course of AC and paclitaxel chemotherapy, including an increase in BAFF, GDF-15 and MCP-1, and a decrease in IL-10.

BAFF is a member of the tumour necrosis factor (TNF) ligand superfamily, and soluble forms of BAFF bind receptors mainly expressed on mature B lymphocytes and stimulate B-cell production of immunoglobulins [475]. Moreover, interaction between BAFF and the BAFF receptor (BAFF-R) has been shown to initiate nuclear translocation of NF-κB in mature B cells [476]. BAFF is generally produced and released by myeloid lineage cells [477], although production and secretion of BAFF from adipocytes has also been observed and is enhanced through adipocyte interactions with macrophages and pro-inflammatory cytokines [478–480]. Adipocytes also express BAFF receptors, and thus, in an autocrine manner BAFF has been exhibited to trigger adipocyte production of itself as well as other inflammatory cytokines [479,480]. Overexpression of BAFF in circulation has been associated with malignant B-cell proliferation and survival, initiation and enhancement of autoimmune diseases, and obesity-related systemic inflammation and insulin resistance [476,479,481,482]. Very little evidence has been presented for pathophysiological links between BAFF and breast cancer. What has been shown is that human breast tumours express BAFF [483], and expression of BAFF was increased in human breast cancer cells under hypoxic conditions [484]. Moreover, treatment with BAFF upregulated migration of human breast cancer cell lines in a manner that was dependent on breast cancer cell NF-κB signalling [484]. The current study was the first to investigate serum levels of BAFF in breast cancer patients, therefore, further research is required to unravel the biological significance of chemotherapy induced BAFF upregulation during treatment for breast cancer.

GDF-15, also known as macrophage inhibitory cytokine-1 (MIC-1), is a transforming growth factor beta (TGF-β) superfamily member that was discovered due to its increased expression in activated macrophages [485,486]. Under normal physiological conditions, the expression of GDF-15 is low in most human tissues, but has been shown to dramatically increase during inflammatory conditions, such as injury to organs and cancer [487]. GDF-15 is overexpressed in a variety of tumours, including prostate, breast, and colon [487,488], and is suggested to have anti-tumoural effects in early stages of cancer but, pro-tumourigenic effects in the later stages of disease [487,488]. GDF-15 has been exhibited to be both produced and secreted as an adipokine from subcutaneous and visceral adipose tissue [489], and was markedly increased in human breast tumours following treatment with neoadjuvant chemotherapy [490], suggesting these tissues as possible sources of elevated GDF-15 during chemotherapy in the current study. Elevated serum levels of GDF-15 in advanced prostate cancer patients has been strongly associated with the anorexia-cachexia phenotype [491], moreover adipose tissue GDF-

15 levels are known to be negatively correlated with BMI and body fat percentage in healthy donors [489]. Thus, it is plausible that the increases in GDF-15 seen during chemotherapy in this study were early signs of cancer associated cachexia developing in these women. Taken together, these studies suggest that systemic levels of GDF-15 may be a central regulator in the association between breast cancer, adiposity and inflammation. Further research is required to fully understand the biological role of enhanced GDF-15 expression in breast cancer patients during chemotherapy.

MCP-1, also known as CCL2, is a C-C chemokine family member and a potent chemoattractant, regulating the recruitment and infiltration of monocytes to sites of inflammation [492]. MCP-1 has been implicated for its roles in a number of inflammatory related human diseases, predominantly HIV, cardiovascular disease, cancer, and obesity [492,493]. During obesity, MCP-1 concentrations are increased in inflamed adipose tissue and it has been observed that MCP-1 interacts with hypertrophic adipocytes and adipose tissue resident macrophages to upregulate production of itself and other inflammatory cytokines, such as TNF-α and IL-6; contributing to the low-grade systemic inflammatory condition characteristic of excessive adiposity [29,43,48]. MCP-1 was increased throughout chemotherapy in this study, and although changes in body fat percentage were variable, body fat percentage was not significantly increased throughout chemotherapy in this cohort of women; as discussed earlier (Section 5.3.2). However, in agreement with the current study findings, paclitaxel has been shown to induce an increase in systemic MCP-1 concentrations in ovarian cancer patients [494]. Moreover, treatment with a combination of neoadjuvant chemotherapeutic agents has been shown to induce monocytosis in breast cancer patients that consequently led to a monocyte secreted elevation of serum MCP-1 levels [495]. Although further research is required to fully understand the biological significance of elevated circulating MCP-1 in women receiving chemotherapy for breast cancer, the above supports that it is likely occurring in response to chemotherapy rather than increases in patient adiposity; although it is plausible that interactions with already existing adipose tissues may aid in sustaining increased systemic levels.

IL-10 is produced by almost all leukocytes, and is predominantly known for its role in immunosuppression and pro-inflammatory cytokine inhibition [496]. However, IL-10 has pleiotropic functions in cancer where it has been observed exerting both proliferative and inhibitory effects [496]. Numerous studies have assessed serum levels of IL-10 in breast cancer patients to find no significant difference between different stages of disease [497], or between

women with or without breast cancer [498,499]. In agreement with this study, serum IL-10 levels were shown to reduce in advanced cancer patients who received paclitaxel chemotherapy [500], whereas, in contrast to this study, transient increases in serum IL-10 have been observed in response to weekly paclitaxel treatments in breast cancer patients [501]. Therefore, based on the results of this study it could be speculated that paclitaxel is supressing IL-10 production. However, circulating levels of IL-10 during chemotherapy are likely dynamic and multifaceted.

Previous observations suggest that chemotherapy induced increases in circulating inflammatory cytokines may contribute to the flu-like symptoms, fatigue, depression, cognitive impairment, pain, cachexia, and importantly, poorer responses to chemotherapy and worse cancer related outcomes for the patients [502]. Therefore, in order to better understand possible biological mechanisms causing chemoresistance and tumour progression, many studies have investigated the mechanisms by which tumours and their microenvironments are altering inflammatory signalling and cytokine expression in response to chemotherapy [503,504]. Far fewer studies have directly assessed alterations in the circulating levels of inflammatory cytokines occurring during breast cancer chemotherapy. Therefore, to the best of our knowledge the current study has for the first time shown that concentrations of the inflammatory cytokines ANG2, BAFF, CRP, GDF-15, IL-10, and MCP-1 fluctuate throughout combination AC and paclitaxel chemotherapy for breast cancer.

Consistent with findings from this study, previous observations have shown that treatment with paclitaxel alone can induce alterations in the levels of circulating inflammatory cytokines in breast and ovarian cancer patients, including IFN-γ, IL-2, IL-6, IL-8, GM-CSF, and MCP-1 [494,501,505]. Paclitaxel has been observed to enhance macrophage secretion of TNF-α [506], lung cancer cell production of IL-8 [507], and IL-1β expression in monocytes and breast cancer cells [508], suggesting that immune cells and cancer cells within the tumour microenvironment are a potential source for the circulating inflammatory cytokines that are being regulated during paclitaxel chemotherapy. Research investigating the impact of other chemotherapeutic agents, such as doxorubicin and cyclophosphamide, on alterations in systemic inflammation, is lacking. One study has shown that serum levels of Fas ligand, macrophage migration inhibitory factor (MIF), and epidermal growth factor receptor (EGFR) were increased in breast cancer patients that had pathological complete response to neoadjuvant doxorubicin and paclitaxel chemotherapy [509]. Taken together, it is likely that serum concentrations of inflammatory cytokines can be altered by chemotherapy treatment,

however, knowledge regarding the specific milieu of circulating cytokines that are being regulated, and the exact origin of their production during chemotherapy, is still incomplete and requires further exploration.

5.3.4.1 Effect of body morphometry and physical activity on circulating inflammatory cytokines in women receiving chemotherapy for breast cancer

Changes in circulating inflammatory cytokine concentrations during chemotherapy were not dependent on differences in participant's physical activity levels or body fat percentage; except for changes in serum IL-10 which were positively associated with body fat percentage.

This study is the first to report on associations between physical activity and systemic alterations in the inflammatory cytokines ANG2, BAFF, CRP, GDF-15, IL-10, and MCP-1 in breast cancer patients during chemotherapy. Prior to this study, only a single investigation has assessed the effects of physical activity on markers of systemic inflammation during breast cancer chemotherapy, finding no effect of exercise on serum levels of IL-6 or IL-1 [192]. The majority of the studies that have assessed physical activity in breast cancer survivors, have investigated the effects of exercise interventions following the cessation of treatment. Meta-analyses of these exercise intervention studies have consistently concluded that interventions induce reductions in circulating CRP and TNF-α, particularly when combined aerobic and resistance training was implemented [182–184]. The current investigation passively assessed levels of physical activity, as opposed to implementing an exercise intervention. Thus, it is plausible that the decrease in physical activity levels during chemotherapy observed in this study would have been limited if an intervention had been implemented, and may also explain why there were no physical activity associated changes in the levels of circulating inflammatory cytokines. Based on this, future research investigating the influence of physical activity on systemic inflammation during cancer chemotherapy should consider investigating the effects of a defined physical activity program.

Evidence suggests that physical activity with concurrent weight loss in women with or without breast cancer, decreases levels of circulating inflammatory cytokines and other biomarkers associated with obesity , such as IL-6, TNF-α, and leptin [185,193,510,511]. Results from the current study are in agreement with these previous findings, as patients exhibited an increase in BMI, a reduction in physical activity, and an increase in the circulating pro-inflammatory cytokines BAFF, GDF-15 and MCP-1 during chemotherapy for breast cancer.

The voluntary levels of physical activity performed by the women in this study may not have been great enough to prevent increases in BMI, and consequently were not able to prevent increases in systemic inflammation during chemotherapy. However, changes in inflammatory cytokine levels were not observed to be associated with differences in physical activity levels nor with the changes in body composition. Therefore, it is likely that during chemotherapy, systemic inflammation may be affected by factors other than exercise or obesity.

IL-10 was found to be significantly reduced throughout chemotherapy and is discussed above in Section 5.3.4. In addition, smaller reductions in IL-10 were associated with greater increases in body fat percentage, suggesting that there may be more bioavailable IL-10 in the circulation to inhibit pro-inflammatory cytokines being produced by excess adipose tissue; endorsing the anti-inflammatory properties of IL-10 in cancer [496]. Further research would benefit from investigating the association between IL-10 and body fat percentage in women receiving chemotherapy for breast cancer.

5.3.5 Inflammatory associated changes in CYP activity during chemotherapy

Changes in the *in vivo* activity of CYP2C9, CYP2C19, CYP2D6, and CYP3A4 drug metabolising enzymes during chemotherapy for breast cancer were variable between patients, but did not significantly differ from before to after chemotherapy in the current investigation. Inter-patient variation in the alterations of CYP3A4 activity during chemotherapy were significantly correlated with changes in MCP-1 serum concentrations. More specifically, increased circulating MCP-1 levels were associated with greater reductions in CYP3A4 activity. Furthermore, alterations in activity greater than 1.25-fold were observed in 87.5% of patients where changes in CYP2C9 activity were assessed during chemotherapy.

5.3.5.1 Correlation between circulating MCP-1 and *in vivo* CYP3A4 activity

This is the first study to observe a correlation between increasing serum MCP-1 concentrations and reduced CYP3A4 activity. Prior to the current investigation, one other study has documented an association between *in vivo* function of CYP3A4 and systemic inflammation, in which patients with advanced cancer that had elevated systemic CRP also exhibited decreased CYP3A4 activity; as measured by the erythromycin breath test [317]. Previous *in vitro* investigations of inflammation-induced downregulated CYP activity have focused on the effects of interleukins, interferons, and TNF-α [159], and prior *in vivo* studies

assessing circulating inflammatory cytokines and CYP activity in cancer patients have concentrated on the levels of pro-inflammatory mediators IL-1β, IL-6, IL-8, TNF-α, TGF, and the acute phase response protein, CRP [283,310,317]. In cancer patients, studies measuring *in vivo* activity of CYP enzymes have focused on CYP2C19 and CYP2D6 function [283,309,310,316], and the level of systemic inflammation was either not associated with CYP activity [283,310] or was not assessed [309,316]. Thus, the current investigation has revealed a novel correlation between serum MCP-1 levels and CYP3A4 activity in breast cancer patients receiving chemotherapy.

An association between elevated systemic MCP-1 and decreased CYP3A4 activity could have notable implications in the clinic, as optimal CYP3A4 activity is critical for patients receiving breast cancer chemotherapy. CYP3A4 is the most abundantly expressed member of the CYP3A subfamily, and accounts for approximately one third of total hepatic CYP activity [274]. CYP3A4 is responsible for the metabolism of over 50% of the most widely administered breast cancer therapeutic agents including tamoxifen, cyclophosphamide, docetaxel, doxorubicin and paclitaxel; most of which are heavily utilised in New Zealand clinics [314]. Due to the narrow therapeutic window associated with chemotherapeutic agents [264], altered metabolism of these drugs may have considerable impact on the pathological response to chemotherapy, and thus may influence clinical outcomes.

Different polymorphisms in the CYP genes are known to contribute to inter-individual variation in drug-metabolism [274,276]. However, in contrast to most other CYP drug metabolising enzymes, CYP3A4 exhibits an activity distribution in humans that is not associated with genetic polymorphisms [512–514]. Four *CYP3A4* allelic variants (*CYP3A4*1B, CYP3A4*6, CYP3A4*17* and *CYP3A4*18*) with suspected functional importance were investigated in 134 cancer patients with solid tumours before beginning chemotherapy, and similar to the current study, these patients exhibited extensive inter-patient variability in CYP3A4 activity, but these differences were not associated with any of the single nucleotide polymorphisms measured [512]. In another study that used the phenotypic probe drug midazolam, no functional effects of the genotypic variants *CYP3A4*1B, CYP3A4*17, and CYP3A4*18A* were observed in 58 cancer patients with solid tumours [513]. Lastly, inter-patient variability in paclitaxel pharmacokinetics measured in 97 cancer patients was not explained by the presence of the *CYP3A4*3* genetic variant [514]. Taken together, these studies suggest that the CYP3A4 genotype is not likely to influence CYP3A4 mediated drug metabolism in cancer patients receiving chemotherapy treatment, and that alternative factors aside from

genotype may be mediating any changes in CYP3A4 activity that were observed in the current investigation; for example circulating bio-available inflammatory molecules such as MCP-1.

Inter-patient variation in CYP3A4 observed in the current exploratory study suggests that further research is required to better understand the biological significance of the change in CYP3A4 activity, and that future investigations would benefit from regular assessment of systemic MCP-1 and *in vivo* activity of CYP3A4 in a larger cohort of women throughout chemotherapy.

5.3.5.2 Alterations in *in vivo* CYP2C9 activity during chemotherapy

In vivo CYP2C9 activity, determined using the phenotypic probe drug losartan, was altered by 25% or more throughout chemotherapy in seven out of the eight breast cancer patients investigated in the current investigation. CYP2C9 activity was decreased in five and increased in two of the breast cancer patients during chemotherapy, suggesting that CYP2C9 activity may have worsened in some patients, but improved in others, during chemotherapy for breast cancer.

Changes in CYP2C9 activity during chemotherapy were not associated with the alterations in circulating concentrations of the inflammatory cytokines assessed in this study. It is possible that other inflammatory cytokines that were not measured in the current investigation, may cause a decrease in CYP2C9 activity. CYP2C9 mRNA expression by hepatocytes *in vitro* has been shown to be downregulated by IL-6, however, expression was not affected by treatment with IL-1 or TNF-α in the same investigation [300]. Interestingly, to date, there is no direct clinical evidence for CYP2C9 phenoconversion by cytokines in inflammatory related diseases. CYP2C9 mediated clearance of the metabolic probe tolbutamide has been observed to be similar between patients with, or without, cancer, and was not associated with serum levels of IL-6 and TNF-α which were notably elevated in the cancer patients [515]. Therefore, based on results from the current investigation and previous findings, is it likely that changes in CYP2C9 activity occurring during cancer chemotherapy are not influenced by systemic inflammation but rather are affected by other *in vivo* factors. For example, tamoxifen has been observed to inhibit CYP2C9 activity in a study of thirteen breast cancer patients [516]; although women in the current study were not receiving tamoxifen during the study period. Thus, in conjunction with *in vivo* CYP activity, further research would benefit from in depth assessment of prototypical inducers and inhibitors of CYP enzymes taken by patients during chemotherapy for breast cancer.

5.4 Summary

In this exploratory patient study of twelve women receiving chemotherapy for breast cancer, circulating levels of the inflammatory cytokines BAFF, GDF-15 and MCP-1 were increased, and IL-10 was decreased over chemotherapy. Alterations in circulating inflammatory cytokines were not dependent on differences in physical activity levels or body fat percentage, suggesting that other factors, such as chemotherapy effects, are likely influencing the levels of systemic inflammation in breast cancer patients during chemotherapy. Analysis showed that increases in circulating MCP-1 levels were correlated with reductions in CYP3A4 activity during chemotherapy, supporting the concept that systemic inflammation may result in clinically meaningful alterations in liver CYP activity, and thus, chemotherapy drug metabolism.

Results from this exploratory study show it is feasible to analyse CYP enzyme function and monitor physical activity in patients during treatment, and suggest that *in vivo* research investigating the biological mechanisms by which alterations in the levels of circulating inflammatory cytokines may be influencing treatment outcomes for women with breast cancer are clinically important. Data from this pilot study will form a useful basis for future studies investigating the biological mechanisms by which circulating MCP-1 and other inflammatory cytokines, may be inducing a decrease in *in vivo* CYP3A4 activity, and to address whether such affects are impacting chemotherapy metabolism and patient outcomes following treatment for breast cancer.

Chapter 6

Discussion

The aim of this study was to assess adipose-related biological mechanisms that may be contributing to breast tumour progression. A host of adipocyte-secreted factors including pro-inflammatory cytokines produced by cancer associated adipocytes (CAA) have been observed to promote a more aggressive phenotype in nearby breast cancer cells[150,161,236,256]. These same pro-inflammatory cytokines can be found in circulation in obese individuals [28,29,62,63]. Therefore, these inflammatory cytokines may have systemic effects on other organs and tissues that aid in promotion of breast tumour progression in obese women[148,149].

This study had two components: first, this study addressed the microenvironmental effects of CAA on global protein abundance changes in hormone receptor positive MCF-7 and hormone receptor negative MDA-MB-231 breast cancer cells; and second, this study investigated the systemic effects of obesity-related circulating inflammatory cytokines on *in vivo* cytochrome (CYP) P450 enzyme activity in women receiving chemotherapy for stage II and III breast cancer.

6.1 Local effects of CAA on breast cancer cell progression

It was hypothesised that *in vitro* co-culture with CAA differentially regulates proteome abundance in breast cancer cells, and that the resulting alterations in key molecules and pathways are responsible for promoting a more aggressive breast cancer cell phenotype. Previous studies investigating the mechanisms by which CAA and breast cancer cells interact to promote breast cancer have focused on particular molecules and pathways [245,248,250,258], and prior to this study, global protein abundance changes in breast cancer cells co-cultured with

CAA have not been examined. By assessing global proteome expression differences of hormone receptor positive MCF-7 and hormone receptor negative MDA-MB-231 breast cancer cells co-cultured with CAA (Chapter 3), this study unbiasedly identified, for the first time, greater than 1.5-fold increased expression of the glycolysis enzyme PGK1 in both breast cancer cell lines (Chapter 3; Table 3.2). This finding highlighted PGK1 as a potential key regulator through which breast CAA in the tumour microenvironment may be promoting breast cancer cell progression, and prompted further research investigating the effects of PGK1 overexpression on breast cancer cell phenotypes *in vitro* (Chapter 4).

Transient transfection with a *PGK1* encoding plasmid increased PGK1 protein expression in hormone receptor positive MCF-7 cells by an average of 2.35-fold (Chapter 4; Figure 4.10); a higher increase than co-culture with CAA (Chapter 3; Figure 3.9). In contrast, transfection with the same *PGK1* encoding plasmid increased PGK1 protein expression in hormone receptor negative MDA-MB-231 cells by an average of 1.49-fold (Chapter 4; Figure 4.10), which was similar to the increase in PGK1 protein abundance following co-culture with CAA (Chapter 3; Figure 3.9). Thus, it could be speculated that, in comparison to transfected MCF-7 cells, the transfected MDA-MB-231 cells in this study were being influenced by the effects of PGK1 overexpression in a manner that was more comparable to the effects of co-culture with CAA.

Transient overexpression of PGK1 protein in breast cancer cells *in vitro* increased MCF-7 cells sensitivity to chemotherapy (Chapter 4; Figure 4.15) and decreased live cell number, proliferation, and viability in MDA-MB-231 cells (Chapter 4; Figure 4.11, Figure 4.13, Figure 4.15), which were unexpected observations. Prior to this study, higher protein expression of PGK1 in breast tumours has been associated with resistance to paclitaxel and poorer patient survival [349,371]. In addition, it is established that co-culture with CAA increases proliferation, viability, migration, and invasion, and promotes resistance to tamoxifen, radiotherapy, and doxorubicin chemotherapy in hormone receptor positive and hormone receptor negative breast cancer cells [150,240,245–251,253–255]. Therefore, by investigating the overexpression of PGK1 protein in MCF-7 and MDA-MB-231 cells, it is posited here that, during cross-talk with CAA, upregulation of PGK1 may be contributing to, but not solely responsible for, promoting breast cancer chemotherapy resistance and progression. It is likely that breast tumours expressing higher levels of PGK1 *in vivo* express varying levels of other tumour promoting proteins. In addition, progressive breast cancer phenotypes observed during crosstalk with CAA are not likely to occur following single molecular changes, but

rather in response to a diverse and dynamic fluctuation of breast cancer cell proteome abundances over time. Thus, further research is still needed to fully elucidate the ambiguous role of PGK1 enzyme upregulation in breast cancer cells interacting with CAA. Fortunately, global protein abundance changes determined for MCF-7 and MDA-MB-231 breast cancer cells co-cultured with CAA in this study (Chapter 3), provide a valuable platform for the assessment of other proteins that may be associated with PGK1 upregulation.

The potential impact of PGK1 overexpression on breast cancer migration, invasion, and metastasis, are important avenues of exploration in regard breast cancer progression not addressed in the current study. Increased PGK1 protein expression has been associated with tumour metastasis in a number of cancers [363,366,398], including breast cancer [371], and the overexpression of PGK1 protein in gastric cancer cells dramatically increased the cells' invasive capabilities [365]. Interaction with CAA is known to induce breast cancer cell migration and invasion [150,245,246,258], and PGK1 protein expression was upregulated in MCF-7 and MDA-MB-231 breast cancer cells co-cultured with mature breast adipocytes (Chapter 3; Table 3.2). Based on this, research exploring the effects of PGK1 upregulation on breast cancer cell invasion *in vitro* and breast tumour dissemination *in vivo* would be an important and unexplored area for future investigations.

Co-culture with CAA is suggested to promote human breast cancer cell growth and invasion via the upregulation of mitochondrial fatty acid oxidation [249,261,262]. In addition to fatty acid oxidation, the breast tumour stroma has been recently implicated to play a role in promoting the 'reverse Warburg' effect, in which tumour cells induce an increase in stromal cell aerobic glycolysis, whereby lactate produced in glycolytic stromal cells is transferred to the tumour cells where it fuels oxidative phosphorylation [517–520]. This is derived from the traditional 'Warburg effect', in which tumour cells themselves are suggested to upregulate aerobic glycolysis, increasing tumour cell secretion of lactate into the tumour microenvironment [380]. In this study, MDA-MB-231 cells co-cultured with CAA showed an elevated abundance of a number of proteins involved in glycolysis (Chapter 3; Figure 3.7), the lactate dehydrogenase subunits LDHA and LDHB, and the lactate efflux transporter MCT4 (Supplementary data provided at https://www.otago.ac.nz/mackenzie-cancer/research/otago715163.html), whereas, MCF-7 cells co-cultured with CAA increased the abundance of a number of TCA cycle proteins (Chapter 3; Figure 3.7). Based on these findings, it could be hypothesised that changes in protein abundance during cross-talk with CAA result in metabolic alterations promoting the 'Warburg' phenotype in triple negative

MDA-MB-231 cells, and the 'reverse Warburg' phenotype in hormone receptor positive MCF-7 cells. Depiction of this hypothesis is presented in Figure 6.1 below.

Further results from the current study showed that lactate concentrations may be increased in the conditioned media of MDA-MB-231 cells transiently overexpressing the glycolytic protein PGK1, whilst the intracellular and extracellular concentrations of lactate remained stable in MCF-7 cells overexpressing PGK1 (Chapter 4; Figure 4.12). This supports the hypothesis that protein abundance changes influence metabolic phenotypes in a cell line dependent manner. Similar findings have been reported by Choi *et al.,* showing that cancer and stromal cell expression of metabolic proteins reflected the Warburg' phenotype in triple negative breast tumours, and the 'reverse Warburg' phenotype in luminal breast tumours [521]. Additionally, mouse adipocyte conditioned media has recently been shown to promote the 'reverse Warburg' phenotype in MCF-7 breast cancer cells [522]. Overall, these findings suggest that in breast tumours, cross-talk with CAA may foster a symbiotic metabolic relationship, whereby, changes in breast cancer cell and stromal cell metabolism are likely driven by the molecular subtype of the tumour.

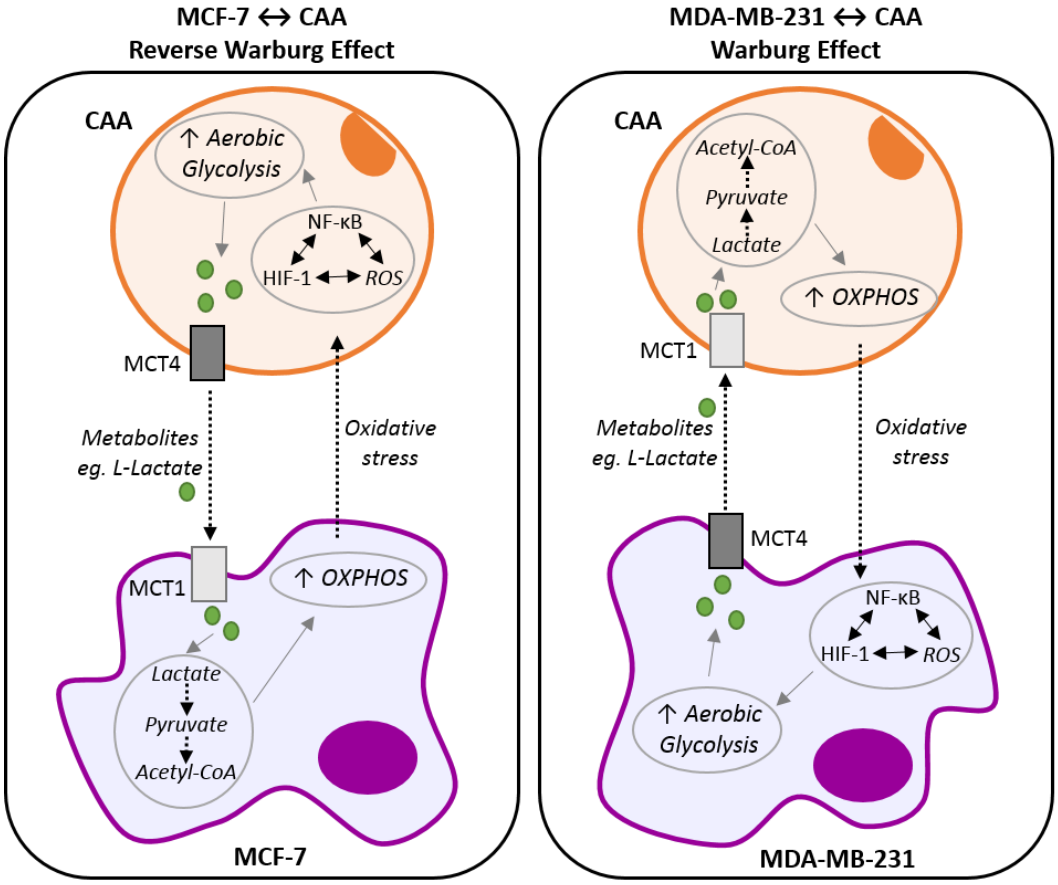

Figure 6.1. Schematic depicting the proposed hypothesis for the metabolic co-operation between cancer associated adipocytes (CAA) and the breast cancer cells studied.
It is hypothesised that cross-talk between breast cancer cells and nearby CAA within the tumour microenvironment alters metabolic symbiosis to promote the 'Warburg' phenotype in triple negative MDA-MB-231 breast cancer cells (ER-, PR-, HER2-), and the 'reverse Warburg' phenotype in hormone receptor positive MCF-7 breast cancer cells (ER+, PR+, HER2-). In mammalian cells, lactate is secreted *via* the efflux transporter monocarboxylate transporter 4 (MCT4), and taken up through the influx transporter monocarboxylate transport 1 (MCT1). Oxidative phosphorylation (OXPHOS) generates reactive oxygen species (ROS) that can stimulate the induction of transcription factors, thus, increasing the expression of proteins involved in a number of processes, including inflammatory signalling and altered metabolism; such as an upregulation of aerobic glycolysis and downregulation of oxidative phosphorylation.

In the current study, intracellular and conditioned media concentrations of lactate were unchanged by PGK1 overexpression in MCF-7 cells (Chapter 4; Figure 4.12). As discussed earlier in Chapter 4, it is possible that additional PGK1 molecules in the transfected cells are moonlighting to perform non-glycolytic functions (Chapter 4; Section 4.3.1.1). However, it is also possible that the overexpression of PGK1 enzymes conferred an increase in glycolytic

flux, but instead of being converted to lactate, pyruvate from glycolysis was being converted to acetyl coenzyme A (acetyl-CoA) and was used to fuel the TCA cycle in the MCF-7 cells. Previous studies have shown that in well oxygenated tumours, aerobic breast tumour cells and stromal cells can exchange and use lactate to generate pyruvate to fuel mitochondrial oxidative phosphorylation [517–520]. Thus, the hypothesised upregulation of the pyruvate to acetyl-CoA conversion could potentially explain the lack of change in lactate concentrations in PGK1 overexpressing MCF-7 cells (Chapter 4; Figure 4.12), and additionally, may provide a link between the upregulation of both PGK1 and TCA cycle proteins identified in MCF-7 cells co-cultured with CAA under normoxic conditions (Chapter 3; Table 3.2 and Figure 3.7).

Transient overexpression of PGK1 protein in MDA-MB-231 breast cancer cells may have induced metabolic alterations that, without the additional support of the CAA in the microenvironment, was not compatible with tumour cell growth and progression *in vitro*. Stromal fibroblasts have been shown to take up lactate derived from lung cancer cells, driving the production of factors that supported tumour cell viability and resistance to tyrosine kinase inhibitors [523]. Thus, it could be speculated that the unexpected reductions in MDA-MB-231 live cell number, proliferation and viability following transient PGK1 protein upregulation (Chapter 4; Figure 4.11, Figure 4.13, and Figure 4.15), may be due to the accumulation of lactate in the conditioned media (Chapter 4; Figure 4.12) poisoning these cells via lactate acidosis, as additional lactate was not being taken up by nearby stromal cells in this experimental model.

This study compared proteome abundance changes in two well-characterised, HER2 negative, breast cancer lines co-cultured with CAA (Chapter 3). Until now, there have been only three studies which investigated the effects of CAA on HER2 positive breast cancer cells, demonstrating that CAA induced an increase in SKBR3 (ER-, PR-, HER2+) cell migration [245], and BT-474 (ER+, PR+, HER2+) and MDA-MB-453 (ER-, PR-, HER2+) cell resistance to doxorubicin and Herceptin [253,254]. Increases in migration and therapy resistance were similarly observed in HER2 negative breast cancer cell lines co-cultured with CAA *in vitro* [245,246,249,251–255]. Interestingly, gene expression analysis performed using two large publicly available datasets (TCGA and METABRIC), demonstrated higher *PGK1* mRNA expression in HER2 positive compared to HER2 negative breast tumours (Chapter 4; Figure 4.19). In addition, a previous investigation showed a downregulation of PGK1 protein levels when HER2 signalling was partially blocked with trastuzumab (Herceptin) treatment [369], suggesting that HER2 signalling in breast cancer may be regulating PGK1 expression.

Therefore, when compared to the HER2 negative breast cancer cell lines used in the current analysis, HER2 positive breast cancer cells co-cultured with CAA may display unique proteome abundances profiles that could highlight important subtype dependent differences and novel therapeutic targets.

In breast cancer cells, ALDH concentrations are thought to be an important contributor in the cytotoxicity of cyclophosphamide chemotherapy, as the formation of cytotoxic metabolites within the cell requires low, rather than high, levels of ALDH [271]. According to the results from this study, co-culture with CAA increased expression of ALDH family members, including AL9A1, AL1B1, and P5CS in MCF-7 cells, and AL1B1 and ALDH2 in MDA-MB-231 cells (Chapter 3; supplementary data provided at https://www.otago.ac.nz/mackenzie-cancer/research/otago715163.html). Thus, it is possible that PGK1 overexpressing MCF-7 and MDA-MB-231 cells may have had elevated expression of ALDH proteins that could have influenced the conversion of aldophosphamide into phosphoramide, affecting DNA crosslinking and the rates of cellular death in cells treated with 4-hydroperoxycyclophosphamide (metabolite of cyclophosphamide). Concentrations of ALDH in experimentally manipulated breast cancer cells should be considered in future research assessing cytotoxicity of cyclophosphamide.

6.1.1 Future directions

The results from Chapters 3 and 4 have identified CAA-induced alterations in MCF-7 and MDA-MB-231 breast cancer cell proteome abundance, whereby, the metabolic enzyme, PGK1, was notably upregulated in both cell lines. Before meaningful clinical implications can be inferred about the impact of increased PGK1 expression on breast cancer metabolism and progression, further *in vitro* and *in vivo* analyses are needed to validate and expand on this study's findings.

As an important first step for future research, it is recommended that proteome abundance alterations are assessed in additional breast cancer cell lines co-cultured with CAA. In order to validate whether the unique protein expression profiles identified in this study's MCF-7 (ER+, PR+, HER2-; luminal subtype) and MDA-MB-231 (ER-, PR-, HER2-; triple negative subtype) cell lines are subtype dependent, other breast cancer cell lines with matching molecular phenotypes, such as T47D (ER+, PR+, HER2-; luminal subtype) and MDA-MB-436 (ER-, PR-, HER2-; triple negative subtype), and different molecular

phenotypes, such as SKBR3 (ER-, PR-, HER2+; HER2 overexpressing subtype) and BT-474 (ER+, PR+, HER2+; HER2 overexpressing subtype), should be investigated. The T47D, MDA-MB-436, SKBR3 and BT-474 cell lines have been previously co-cultured with CAA using the transwell co-culture model [245,248,253,263], and thus, represent examples of cell lines that would be suitable for future proteome abundance investigations. Both breast cancer cell lines used in the current analysis are known to be negative for HER2 overexpression, and consequently, global protein abundance alterations of a HER2 positive breast cancer cell line co-cultured with CAA is yet to be reported. As 15-20% of breast tumours are enriched for HER2 overexpression [524], it is of clinical importance to include the HER2 enriched subtype of breast cancer in future co-culture analyses.

The current *in vitro* investigation quantified breast cancer cell proteome abundance after a 3-day transwell co-culture of breast cancer cells with CAA. Yet, within the tumour microenvironment, cross-talk with CAA is likely to regulate breast cancer cell protein abundance differentially over time. In previous studies, *in vitro* transwell co-cultures of breast cancer cells with CAA performed endpoint analyses at single time points, with co-culture duration most commonly ranging from 24-hours to 3-days [150,245–247,249–251,253–255]. Consequently, knowledge regarding the dynamic effects of CAA on breast cancers over time is lacking. A time-course experiment, collecting lysates and measuring proteome abundances in breast cancer cells co-cultured with CAA over incrementally greater time periods, may provide evidence to better understand the biological mechanisms associated with CAA-mediated breast cancer cell progression. Furthermore, the use of 3D models, whereby, breast cancer cells and CAA are in direct contact, may provide a platform in which co-culture between these two cell types can be extended for longer time periods [241,255,390,525], and thus, should also be considered as an experimental model for extended time course experiments; although extraction and isolation of the breast cancer cell component for proteome analysis would be challenging.

To investigate the impact of PGK1 protein overexpression on breast cancer cell phenotypes, this study only considered proliferation, lactate production and cytotoxicity of chemotherapies as endpoints. Previously, however, increased PGK1 protein expression in primary breast tumours has been associated with the presence of metastatic lesions in human patients [371]. Thus, future analyses could test whether increased PGK1 expression impacts on breast cancer cell migration and invasion *in vitro*, and/or breast tumour dissemination *in vivo;* perhaps using xenograft models. Interestingly, xenografts of human breast cancer cells co-

cultured either with or without CAA and implanted into the mammary fat pad of mice, have shown that CAA increase breast cancer tumorigenesis and metastasis [248,250,257,526]; however, the exact mechanisms responsible for this are still unclear. Therefore, comparison of the proteome abundance profiles between primary and metastatic tumours derived from human xenografts, cultured with or without CAA, may also help to elucidate mechanisms by which CAA are promoting breast cancer cell invasion and metastasis formation *in vivo*.

MCT4 is the main lactate efflux transporter in mammalian cells. In the current analysis, PGK1 and MCT4 were proteins identified by mass spectrometry to be upregulated in MDA-MB-231 breast cancer cells co-cultured with CAA (Chapter 3; supplementary data provided at https://www.otago.ac.nz/mackenzie-cancer/research/otago715163.html) and lactate concentrations were increased in the conditioned media of PGK1 overexpressing MDA-MB-231 cells (Chapter 4; Figure 4.12). Validation of PGK1 protein upregulation, but not MCT4 protein expression, in the CAA co-cultured and *PGK1* encoding plasmid transfected MDA-MB-231 cells, was performed using Western blotting, and therefore, similar validation for increases in MCT4 protein expression are also warranted. Furthermore, during co-culture with CAA, previous studies have documented the transfer of fatty acids from adipocytes to breast cancer cells, and then observed the use of these fatty acids to fuel breast cancer cell mitochondrial fatty acid oxidation, and possibly, cell replication and migration [249,262]. Therefore, in order to assess whether cross-talk with CAA results in metabolic alterations promoting glycolysis and lactate efflux in triple negative breast cancer cells (as discussed above in 6.1), it might also be possible to monitor the transfer of lactate from MDA-MB-231 breast cancer cells to adipocytes during co-culture.

Investigation of PGK1 overexpression in breast cancer cell lines *in vitro* showed that plasmid derived PGK1 proteins were fused with an N-terminal poly-HIS-FLAG-HA tag, but the implications of this tag on PGK1 enzyme function remain unexplained. The use of immunohistochemistry (IHC) to investigate PGK1 protein expression at the invasive margin of human breast tumours *in vivo*, would avoid the potential interference of plasmid derived tags on PGK1 protein function. Additionally, analysis using IHC would identify whether CAA interactions influence breast cancer cell PGK1 expression levels, and would enable the determination of PGK1 subcellular localisation within the tumour cell, providing insight into whether additional PGK1 molecules are involved in glycolysis or other mechanistically distinct, subcellular localisation dependent, functions [373,374,406,408]. Furthermore, molecularly distinct subtypes of breast tumours could be selected for IHC analysis, and thus, the

relationship between HER2 enrichment and PGK1 protein expression in tumour cells interacting with CAA could also be assessed. Interactions between CAA and breast cancer cells at the invasive margin of human breast tumours have been examined using IHC, assessing the expression and localisation of a number of target proteins including IL-6, MMP-2, MMP-9, S100A7, IGF-1, and IGFBP-2 [150,245–248], and thus, similar analysis of PGK1 protein expression could complement these previous investigations.

PGK1 protein overexpression in breast cancer cell lines *in vitro* was determined by Western blotting, however, post-translational modifications were not addressed. Previous investigations have used either mass spectrometry or targeted antibodies to measure post-translational modifications of PGK1 enzymes, including acetylation at K323 and K388, and phosphorylation at S203 and S256; modifications that were found to be associated with alterations in the activity and function of the enzyme [374,375,408,412]. Therefore, testing the extent of post-translational modifications in breast cancer cells overexpressing PGK1 would help confirm the mechanistic functions associated with its upregulation.

6.2 Systemic effects of obesity-associated inflammation on breast cancer chemotherapy metabolism

It was hypothesised that high circulating concentrations of obesity-associated inflammatory cytokines downregulate *in vivo* activity of cytochrome P450 (CYP) enzymes in women receiving chemotherapy for breast cancer. Inflammatory cytokines have been shown to inhibit expression and activity of CYP enzymes *in vitro* [300–303], and a CYP genotype-phenotype discordance has been recorded in a number of inflammatory pathologies *in vivo* [283,306–310,316]. In advanced cancer patients, elevated CRP (a marker of systemic inflammation) has been associated with CYP3A4 downregulation [317], however, prior to this study, the relationship between CYP activity and circulating inflammatory cytokines during breast cancer chemotherapy has never been examined. By concurrently assessing *in vivo* changes in both the circulating inflammatory cytokine concentrations and activity of multiple CYP metabolising enzymes in twelve women receiving chemotherapy for stage II and III breast cancer (Chapter 5), the current study identified for the first time a correlation between increases in serum MCP-1 levels and decreases in CYP3A4 activity during chemotherapy (Chapter 5; Figure 5.27). This finding highlighted MCP-1 as a potential regulator of CYP3A4-

mediated breast cancer chemotherapy metabolism, and thus, when increased systemically, MCP-1 may be playing a role in the manifestation of chemotherapy resistance.

Potential biological mechanisms by which MCP-1 may influence the activity of CYP3A4 in hepatocytes have never been investigated. MCP-1 mediates its chemoattractant properties through binding to its cell surface receptor, C-C chemokine receptor type 2 (CCR2) [492]. Expression of CCR2 is restricted to particular cell types, which includes resident and recruited Kupffer cells (hepatic macrophages), but excludes hepatocytes [492,527]. Thus, MCP-1 is unlikely to be directly influencing hepatocyte CYP3A4 expression and activity. Instead, it is hypothesised here that MCP-1 is indirectly downregulating hepatocyte CYP3A4 activity by binding CCR2 on Kupffer cell surfaces, increasing their production of inflammatory cytokines, such as IL-6 and TNF-α [528]. IL-6 can bind membrane receptors on nearby hepatocytes and promote signalling cascades previously documented to downregulate CYP3A4 transcription [298,299]. Depiction of this hypothesis is presented below in Figure 6.2. In order to test this hypothesis, the binding of MCP-1 to CCR2, and the subsequent release of inflammatory cytokines from liver Kupffer cells in breast cancer patients receiving chemotherapy, needs to be tested.

In the current study, the increase in circulating levels of MCP-1 during chemotherapy was not associated with differences in adiposity or physical activity, suggesting an influence of additional factors on systemic MCP-1 concentrations (Chapter 5; Figure 5.17, Figure 5.18, Figure 5.19, and Figure 5.20). In the earlier discussion (Chapter 5; Section 5.3.4), it was postulated that increases in circulating MCP-1 are being induced by chemotherapy. Chemotherapy has been shown to activate the immune system in breast cancer patients by enhancing natural killer and lymphocyte-activated cytotoxic cell activity [505]. In addition, increases in circulating monocyte levels (monocytosis) and elevated serum MCP-1 concentrations have been associated with neoadjuvant chemotherapy treatment in breast cancer patients [495]. It is possible that during repeated doses of chemotherapy, increases in serum MCP-1 levels are stimulated by the effects on immune cells, and over the course of chemotherapy, interaction between MCP-1 and its receptor, CCR2, may be intensified. Therefore, based on the hypothesis presented above (Figure 6.2), it is suggested that through an influence on the immune system, chemotherapy may be contributing to the development of a perpetuating cycle of monocyte/macrophage infiltration and inflammatory cytokine production in the liver; fostering an inflammatory microenvironment that may influence hepatocyte CYP3A4 expression and activity (Figure 6.2).

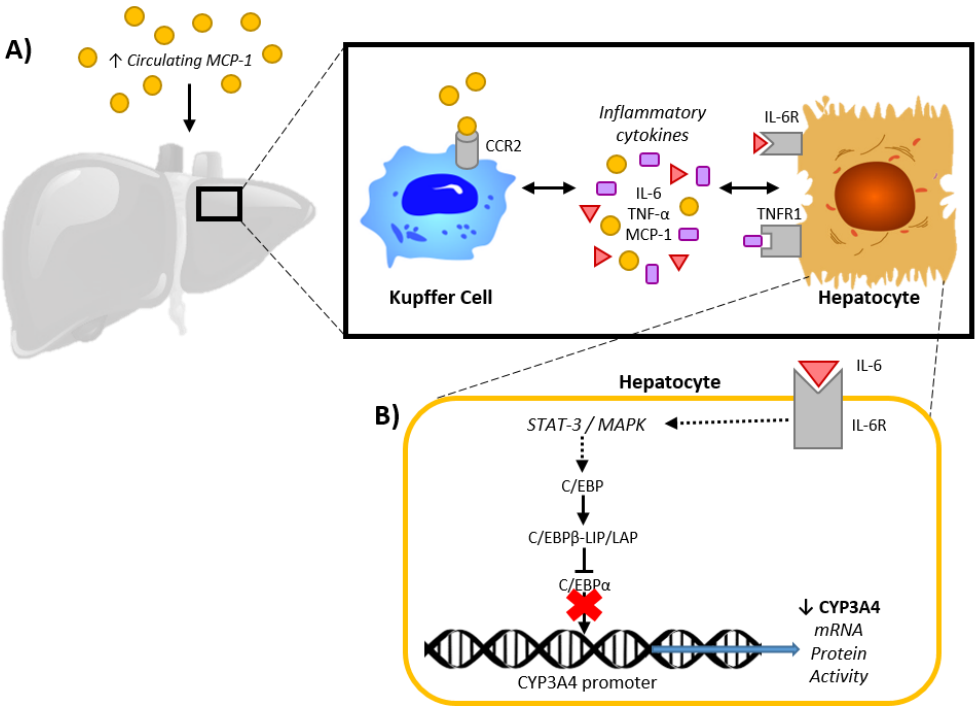

Figure 6.2. Schematic of the proposed hypothesis for monocyte chemoattractant protein 1 (MCP-1) mediated decrease in CYP3A4 activity in the liver of human breast cancer patients.
A) The liver of breast cancer patients is exposed to increased circulating levels of MCP-1 during chemotherapy. Liver Kupffer cells (hepatic macrophages) express the MCP-1 cell surface receptor C-C chemokine receptor type 2 (CCR2), and thus, MCP-1 can bind and induce an increase in the production of other inflammatory cytokines, such as interleukin 6 (IL-6) and tumour necrosis factor alpha (TNF-α), and further increase levels of MCP-1 molecules. IL-6 and TNF-α bind their membrane receptors, interleukin 6 receptor (IL-6R) and tumour necrosis factor receptor 1 (TNFR1), on the surface of nearby hepatocytes, inducing inflammatory signalling cascades that regulate CYP3A4 transcription. B) Schematic of one of the mechanisms by which inflammatory cytokines inhibit CYP3A4 transcription; as reported by Jover *et al*, [298]. Intracellular signalling, following IL-6 binding, induces translation of CCAAT-enhancer-binding protein beta isoform LIP (C/EBPβ-LIP), an antagonist of CCAAT-enhancer-binding protein alpha (C/EBPα); C/EBPα is a known transcription factor that constitutively promotes CYP3A4 expression in hepatocytes [298].

6.2.1 Future directions and clinical implications

The results from this exploratory patient study have identified a potential mechanistic relationship between circulating MCP-1 and activity of CYP3A4 *in vivo*, which may play a role in altering the rates of breast cancer chemotherapy metabolism. Additional studies are required to validate these findings, and assess the potential clinical impacts.

Gathering follow-up data for the study participants is an important first step in assessing whether clinical outcomes, such as disease free survival (DFS) and overall survival (OS), are associated with levels of circulating inflammatory cytokines and/or changes in CYP activity reported during chemotherapy. Poorer recurrence and survival rates have been previously associated with reduced cyclophosphamide and tamoxifen metabolism in breast cancer patients [279,529], however, participants in these studies were followed for 10-25 years in order to assess such endpoints. It is likely that the longitudinal nature required for clinical outcome assessments is what prevented reports on DFS and OS by the other studies that have observed reduced CYP activity in cancer patients [283,309,310,316,317]. Therefore, it will be important to know whether recurrence and survival rates are affected by alterations in circulating inflammatory cytokines and CYP activity in breast cancer patients receiving chemotherapy, as this has yet to be assessed directly. Importantly, data from the current analysis showed that none of the participants had chemotherapy dose-capped based on BSA (Chapter 5; Table 5.2), and thus, dose-capping can be ruled out as a contributing factor towards the findings from the current analysis, and, clinical outcomes that may be assessed in the future.

The correlation between circulating MCP-1 and *in vivo* CYP3A4 activity, and the change in circulating levels of BAFF, GDF-15, IL-10 and MCP-1, need to be validated in a larger population of participants, as this would generate more statistical power. As discussed earlier (Chapter 5; Section 5.3.1), the number of participants in the current study was suitable for determining the tolerability and feasibility of using the 'Inje' probe drug cocktail to measure *in vivo* CYP activity in breast cancer patients during chemotherapy. Yet, with the current study numbers, assessing the influence of other cancer-related co-morbidities and drug-drug interactions on systemic inflammation and CYP activity *in vivo* was not feasible. There are a number of cancer-related pathologies that are associated with an increase in the levels of circulating inflammatory cytokines [502], and, there are many prescribed, but also 'over the counter', drugs that have the potential to induce and inhibit CYP enzymes *in vivo* [293]. Therefore, in order to validate the findings from this feasibility study and assess the impact of other confounding factors on circulating inflammation and *in vivo* CYP activity, a larger patient study is warranted.

Previous studies have established a pro-tumourigenic role of MCP-1 in a number of solid tumours [530], and as such, early stage clinical trials have been carried out to assess the efficacy and safety of MCP-1 blockade using the human monoclonal antibody, CNT0888,

that inhibits MCP-1 binding to CCR2, for use in cancer patients with solid tumours [531,532]. Despite binding to MCP-1 with high affinity *in vitro*, CNT0888 given in combination with standard of care chemotherapies was not able to achieve a pro-longed inhibition of serum MCP-1, and accordingly, was not associated with an anti-tumour response [531,532]. CNT0888 caused a number of adverse effects that included, neutropenia, anemia, nausea, and fatigue, but interestingly, did not alter the pharmacokinetics of the chemotherapeutic agents [531,532]. Based on these trial findings and the fact that mechanisms by which MCP-1 may be downregulating CYP3A4 activity in hepatocytes has never been investigated, it is suggested here, that before assessing the effects of an MCP-1 blockade on CYP activity in breast cancer patients *in vivo*, the mechanistic relationship between circulating MCP-1 and CYP3A4 activity should first be investigated *in vitro*.

An *in vitro* transwell co-culture between human Kupffer cells and hepatocytes, a model previously established to assess the influence of pro-inflammatory cytokines on CYP enzymes [303], could be used to test for the mechanism of action proposed earlier (Section 6.2; Figure 6.2). Before co-culture with hepatocytes, Kupffer cells could be pre-treated with or without recombinant MCP-1 or serum collected from breast cancer patients during chemotherapy. The inflammatory cytokine profiles secreted into the co-culture conditioned medium could be compared between Kupffer cell pre-treatment with or without MCP-1, or with or without serum samples. Furthermore, hepatocytes could be collected following co-culture to measure intracellular gene and protein expression of CYP3A4, in order to test whether interaction with Kupffer cells pre-treated with MCP-1 or serum differentially regulates hepatocyte expression of CYP3A4. It may also be possible to test rates of CYP3A4 activity by measuring midazolam metabolism in this co-culture model.

Exploring genotypes of the CYP2C9, CYP2C19 and CYP2D6 enzymes, and associating common variants with *in vivo* activity of the CYP enzymes measured in the current study, would identify whether functional variation observed between participants was dependent on genotypic differences. Genotyping CYP enzymes would allow us to assess the variation at a single time point, however, this study observed changes in CYP activity during chemotherapy that varied between participants, particularly in CYP2C9 and CYP2D6 (Chapter 5; Figure 5.23), and it is unlikely that genotypic alterations are responsible for changing the activity of these enzymes over such a short time period. It is more likely that endogenous factors, such as circulating inflammatory cytokines and drug-drug interactions, are influencing CYP activity during chemotherapy. Yet, epigenetic changes, such as

hypermethylation of CYP promoters, cannot be ruled out and should also be considered in future investigations.

Changes in circulating inflammatory cytokines during chemotherapy were not associated with differences in physical activity levels in this study. However, there was an observed reduction in the average daily step counts in the early stages of chemotherapy (Chapter 5; Figure 5.8). In addition to reducing adiposity and serum concentrations of circulating inflammatory cytokines, increased levels of physical activity have been shown to improve the quality of life, cardiorespiratory fitness, physical well-being, symptoms of fatigue and depression in breast cancer survivors [533]. Thus, in order to try and counteract the early reductions in physical activity during treatment, it will be clinically important for future investigations in breast cancer patients to implement exercise education and physical training programmes prior to starting chemotherapy.

6.3 Conclusion

In summary, the current thesis describes experimental investigations of the local effects of CAA on breast cancer cell processes *in vitro*, and systemic effects of obesity-associated inflammatory cytokines on cytochrome P450 (CYP) drug metabolising activity in breast cancer patients during chemotherapy.

Firstly, global differences in relative protein abundance were identified and quantified in MCF-7 (ER+, PR+, HER2-) and MDA-MB-231 (ER-, PR-, HER2-) breast cancer cell lines co-cultured with cancer associated adipocytes (CAA) in an *in vitro* transwell system. Proteome abundance profiles indicated that CAA effects are likely to differ according to molecular subtypes. Co-culture with CAA induced an enriched upregulation of TCA cycle proteins in MCF-7 cells, and glycolysis proteins in MDA-MB-231 cells, highlighting the importance of metabolic pathways in breast cancer cells exposed to CAA in the tumour microenvironment. Moreover, the glycolytic protein phosphoglycerate kinase 1 (PGK1), was the only identified protein to be upregulated by more than 1.5-fold in both breast cancer cell lines co-cultured with CAA. In general, this hypothesis generating aspect of the thesis has provided, for the first time, a rich resource of proteome abundance alterations that can be used for future research assessing the role of CAA in breast cancer cell progression.

Secondly, transient overexpression of PGK1 in MCF-7 and MDA-MB-231 breast cancer cell lines *in vitro* exhibited cell-line specific effects, with reduced proliferation and increased lactate in the conditioned media of MDA-MB-231 cells, and increased sensitivity to paclitaxel and cyclophosphamide in MCF-7 cells. These results did not support our hypothesis that increased PGK1 expression is promoting breast cancer cell growth and survival through its influence on metabolism. However, findings did reveal that breast cancer cell viability was negatively affected by the experimental conditions imposed during PGK1 plasmid transfection. Furthermore, *in silico* analysis of *PGK1* expression provided evidence for an association between HER2 signalling and *PGK1* regulation in breast cancer. Taken together, these findings may indicate a non-glycolytic role for PGK1 in high PGK1-expressing breast cancers, and highlight the need for further research to develop a stably overexpressing model for PGK1 and to assess PGK1 overexpression in HER2+ breast cancer.

Thirdly, results from an exploratory clinical trial showed that breast cancer patients receiving chemotherapy exhibited changes in serum levels of a number of circulating inflammatory cytokines that were not associated with adiposity or physical activity. However, increases in serum monocyte chemoattractant protein 1 (MCP-1) correlated with decreases in CYP3A4 activity during chemotherapy. Based on the participants that were assessed, findings from this exploratory study did not support our hypothesis that chronic low levels of obesity-related inflammatory cytokines could inhibit *in vivo* CYP activity, altering chemotherapy metabolism, and that physical activity could mitigate this effect during treatment. However, findings from this study confirmed, for the first time, the feasibility of the 'Inje' cocktail to measure CYP activity in women having treatment for breast cancer, and showed that increased concentrations of circulating inflammatory cytokines are capable of altering CYP activity during chemotherapy. Further studies are required to understand the biological mechanisms by which circulating MCP-1 and other inflammatory cytokines, may be inducing a decrease in *in vivo* CYP3A4 activity, and to address whether such affects are impacting chemotherapy metabolism and patient outcomes following treatment.

Overall, this thesis has, for the first time, generated an extensive list of breast cancer cell protein abundance alterations, induced by *in vitro* co-culture with CAA that may help guide future research targeted towards understanding and mitigating detrimental local interactions between CAA and breast cancer cells *in vivo*. In addition, this thesis has provided novel evidence confirming that it is feasible to analyse CYP function in women receiving chemotherapy for breast cancer using the 'Inje' probe drug cocktail. In this study the 'Inje'

cocktail generated individualised drug metabolising activity, suggesting that in the future similar methodologies could be used for precision chemotherapy drug dosing in order to improve patient outcomes.

References

1. World Health Organisation. Obesity and overweight. *Fact sheet no 311 January 2015* (2015). Available at: https://www.who.int/en/news-room/fact-sheets/detail/obesity-and-overweight. (Accessed: 30th June 2019)
2. Health Effects of Overweight and Obesity in 195 Countries over 25 Years. *N. Engl. J. Med.* **377**, 13–27 (2017).
3. Levesque, R. J. R. Obesity and Overweight. in *Encyclopedia of Adolescence* (2018). doi:10.1007/978-3-319-33228-4_447
4. Chooi, Y. C., Ding, C. & Magkos, F. The epidemiology of obesity. *Metabolism* **92**, 6–10 (2019).
5. Kelly, T., Yang, W., Chen, C. S., Reynolds, K. & He, J. Global burden of obesity in 2005 and projections to 2030. *Int J Obes* **32**, 1431–1437 (2008).
6. Marie, N. G. *et al.* Global, regional, and national prevalence of overweight and obesity in children and adults during 1980–2013: a systematic analysis for the Global Burden of Disease Study 2013. *Lancet* **384**, 766–781 (2014).
7. New Zealand Ministry of Health. Annual Update of Key Results 2014/15: New Zealand Health Survey. Available at: http://www.health.govt.nz/system/files/documents/publications/annual-update-key-results-2014-15-nzhs-dec15-1.pdf.
8. Hill, J. O. Understanding and addressing the epidemic of obesity: an energy balance perspective. *Endocr Rev* **27**, 750–761 (2006).
9. Jivraj, S. Obesity. in *Antenatal Disorders for the MRCOG and Beyond* (2016). doi:10.1017/CBO9781107585799.013
10. Burkhauser, R. V. & Cawley, J. Beyond BMI: The value of more accurate measures of fatness and obesity in social science research. *J. Health Econ.* (2008). doi:10.1016/j.jhealeco.2007.05.005
11. Prentice, A. M. & Jebb, S. A. Beyond body mass index. *Obesity Reviews* (2001). doi:10.1046/j.1467-789x.2001.00031.x
12. Rothman, K. J. BMI-related errors in the measurement of obesity. *Int. J. Obes.* (2008). doi:10.1038/ijo.2008.87
13. National Obesity Observatory. Body Mass Index as a measure of obesity. *Natl. Heal. Serv.* (2009).
14. Romero-Corral, A. *et al.* Accuracy of body mass index in diagnosing obesity in the adult general population. *Int. J. Obes.* (2008). doi:10.1038/ijo.2008.11
15. Flegal, K. M. *et al.* Comparisons of percentage body fat, body mass index, waist circumference, and waist-stature ratio in adults. *Am. J. Clin. Nutr.* (2009). doi:10.3945/ajcn.2008.26847
16. Frankenfield, D. C., Rowe, W. A., Cooney, R. N., Smith, J. S. & Becker, D. Limits of body mass index to detect obesity and predict body composition. *Nutrition* (2001). doi:10.1016/S0899-9007(00)00471-8
17. Padwal, R., Leslie, W. D., Lix, L. M. & Majumdar, S. R. Relationship among body fat percentage, body mass index, and all-cause mortality: A Cohort Study. *Ann. Intern. Med.* (2016). doi:10.7326/M15-1181
18. Deurenberg, P., Deurenberg-Yap, M. & Guricci, S. Asians are different from Caucasians and from each other in their body mass index/body fat per cent relationship. *Obes. Rev.* **3**, 141–146 (2002).
19. Duncan, J. S., Duncan, E. K. & Schofield, G. *Ethnic-specific body mass index cut-off points for overweight and obesity in girls*. *Journal of the New Zealand Medical Association NZMJ* **123**, (2010).
20. Cancello, R. & Clement, K. Review article: Is obesity an inflammatory illness? Role of low-grade inflammation and macrophage infiltration in human white adipose tissue. *BJOG An Int. J. Obstet. Gynaecol.* **113**, 1141–1147 (2006).
21. Gesta, S., Tseng, Y. H. & Kahn, C. R. Developmental origin of fat: Tracking obesity to its source. *Cell* **131**, 242–256 (2007).
22. Esteve Ràfols, M. Adipose tissue: Cell heterogeneity and functional diversity. *Endocrinol. y Nutr. (English Ed.* **61**, 100–112 (2014).
23. Lee, M.-J., Wu, Y. & Fried, S. K. Adipose tissue heterogeneity: Implication of depot differences in adipose tissue for obesity complications. *Mol. Aspects Med.* **34**, 1–11 (2013).
24. Vohl, M. M. *et al.* Brief Genetic Analysis A Survey of Genes Differentially Expressed in Subcutaneous and Visceral Adipose Tissue in Men. *Obes. Res.* **12**, 1217–1222 (2004).
25. Trayhurn, P. & Wood, I. S. Adipokines: inflammation and the pleiotropic role of white adipose tissue. *Br. J. Nutr.* **92**, 347–355 (2004).
26. Juge-Aubry, C. E., Henrichot, E. & Meier, C. A. Adipose tissue: a regulator of inflammation. *Best Pract. Res. Clin. Endocrinol. Metab.* **19**, 547–566 (2005).

27. Wozniak, S. E., Gee, L. L., Wachtel, M. S. & Frezza, E. E. Adipose tissue: the new endocrine organ? A review article. *Dig. Dis. Sci.* **54**, 1847–1856 (2009).
28. Ellulu, M. S. *et al.* Obesity and Inflammation : The Linking Mechanism and the Complications. *Archives of Medical Science* 851–863 (2016).
29. Caruso, C., Balistreri, C. R. & Candore, G. The role of adipose tissue and adipokines in obesity-related inflammatory diseases. *Mediators Inflamm.* **2010**, (2010).
30. Lago, F., Gómez, R., Gómez-Reino, J. J., Dieguez, C. & Gualillo, O. Adipokines as novel modulators of lipid metabolism. *Trends Biochem. Sci.* **34**, 500–510 (2009).
31. Fontana, L., Eagon, J. C., Trujillo, M. E., Scherer, P. E. & Klein, S. Visceral fat adipokine secretion is associated with systemic inflammation in obese humans. *Diabetes* **56**, 1010–1013 (2007).
32. Vázquez-Vela, M. E. F., Torres, N. & Tovar, A. R. White Adipose Tissue as Endocrine Organ and Its Role in Obesity. *Archives of Medical Research* (2008). doi:10.1016/j.arcmed.2008.09.005
33. Gregor, M. F. & Hotamisligil, G. S. Inflammatory mechanisms in obesity. *Annu. Rev. Immunol.* **29**, 415–445 (2011).
34. Gregor, M. F. & Hotamisligil, G. S. Adipocyte stress: the endoplasmic reticulum and metabolic disease. *J. Lipid Res.* **48**, 1905–1914 (2007).
35. Trayhurn, P. Hypoxia and Adipose Tissue Function and Dysfunction in Obesity. *Physiol. Rev.* (2013). doi:10.1152/physrev.00017.2012
36. Shi, H. *et al.* TLR4 links innate immunity and fatty acid – induced insulin resistance. *J. Clin. Invest.* **116**, 3015–3025 (2006).
37. Vitseva, O. I. *et al.* Inducible Toll-like Receptor and NF-κB Regulatory Pathway Expression in Human Adipose Tissue. *Obesity* **16**, 932–937 (2008).
38. Wang, B., Wood, I. S. & Trayhurn, P. Hypoxia induces leptin gene expression and secretion in human preadipocytes: Differential effects of hypoxia on adipokine expression by preadipocytes. *J. Endocrinol.* (2008). doi:10.1677/JOE-08-0156
39. Suganami, T. & Ogawa, Y. Adipose tissue macrophages: their role in adipose tissue remodeling. *J. Leukoc. Biol.* **88**, 33–39 (2010).
40. Morris, D. L., Singer, K. & Lumeng, C. N. Adipose tissue macrophages: phenotypic plasticity and diversity in lean and obese states. *Curr. Opin. Clin. Nutr. Metab. Care* **14**, 341 (2011).
41. Hotamisligil, G. S., Arner, P., Caro, J. F., Atkinson, R. L. & Spiegelman, B. M. Increased adipose tissue expression of tumor necrosis factor-alpha in human obesity and insulin resistance. *J. Clin. Invest.* **95**, 2409 (1995).
42. Wang, B. & Trayhurn, P. Acute and prolonged effects of TNF-α on the expression and secretion of inflammation-related adipokines by human adipocytes differentiated in culture. *Pflügers Arch.* **452**, 418–427 (2006).
43. Bruun, J. M., Lihn, A. S., Pedersen, S. B. & Richelsen, B. Monocyte chemoattractant protein-1 release is higher in visceral than subcutaneous human adipose tissue (AT): implication of macrophages resident in the AT. *J. Clin. Endocrinol. Metab.* **90**, 2282–2289 (2005).
44. Skurk, T., Alberti-Huber, C., Herder, C. & Hauner, H. Relationship between adipocyte size and adipokine expression and secretion. *J. Clin. Endocrinol. Metab.* **92**, 1023–1033 (2007).
45. Jernås, M. *et al.* Separation of human adipocytes by size: hypertrophic fat cells display distinct gene expression. *FASEB J.* **20**, 1540–1542 (2006).
46. Fain, J. N., Madan, A. K., Hiler, M. L., Cheema, P. & Bahouth, S. W. Comparison of the release of adipokines by adipose tissue, adipose tissue matrix, and adipocytes from visceral and subcutaneous abdominal adipose tissues of obese humans. *Endocrinology* **145**, 2273–2282 (2004).
47. Suganami, T., Nishida, J. & Ogawa, Y. A paracrine loop between adipocytes and macrophages aggravates inflammatory changes role of free fatty acids and tumor necrosis factor α. *Arterioscler. Thromb. Vasc. Biol.* **25**, 2062–2068 (2005).
48. Weisberg, S. P. *et al.* Obesity is associated with macrophage accumulation in adipose tissue. *J. Clin. Invest.* **112**, 1796–1808 (2003).
49. Cancello, R. *et al.* Reduction of macrophage infiltration and chemoattractant gene expression changes in white adipose tissue of morbidly obese subjects after surgery-induced weight loss. *Diabetes* **54**, 2277–2286 (2005).
50. Lumeng, C. N., DelProposto, J. B., Westcott, D. J. & Saltiel, A. R. Phenotypic switching of adipose tissue macrophages with obesity is generated by spatiotemporal differences in macrophage subtypes. *Diabetes* **57**, 3239–3246 (2008).
51. Gordon, S. & Martinez, F. O. Alternative activation of macrophages: mechanism and functions. *Immunity* **32**, 593–604 (2010).
52. Fujisaka, S. *et al.* Regulatory mechanisms for adipose tissue M1 and M2 macrophages in diet-induced obese mice. *Diabetes* **58**, 2574–2582 (2009).

53. Kratz, M. *et al.* Metabolic dysfunction drives a mechanistically distinct proinflammatory phenotype in adipose tissue macrophages. *Cell Metab.* **20**, 614–625 (2014).
54. Russo, L. & Lumeng, C. N. Properties and functions of adipose tissue macrophages in obesity. *Immunology* **155**, 407–417 (2018).
55. Springer, N. L. *et al.* Obesity-Associated Extracellular Matrix Remodeling Promotes a Macrophage Phenotype Similar to Tumor-Associated Macrophages. *Am. J. Pathol.* **189**, 2019–2035 (2019).
56. Corrêa, L., Heyn, G. & Magalhaes, K. The Impact of the Adipose Organ Plasticity on Inflammation and Cancer Progression. *Cells* **8**, 662 (2019).
57. Cinti, S. *et al.* Adipocyte death defines macrophage localization and function in adipose tissue of obese mice and humans. *J. Lipid Res.* **46**, 2347–2355 (2005).
58. Gornicka, A. *et al.* Adipocyte hypertrophy is associated with lysosomal permeability both in vivo and in vitro: role in adipose tissue inflammation. *Am. J. Physiol. Metab.* **303**, E597–E606 (2012).
59. Hotamisligil, G. S. Endoplasmic reticulum stress and the inflammatory basis of metabolic disease. *Cell* **140**, 900–917 (2010).
60. Strissel, K. J. *et al.* Adipocyte death, adipose tissue remodeling, and obesity complications. *Diabetes* **56**, 2910–2918 (2007).
61. Vaysse, C. *et al.* Inflammation of mammary adipose tissue occurs in overweight and obese patients exhibiting early-stage breast cancer. *npj Breast Cancer* **3**, 19 (2017).
62. Maachi, M. *et al.* Systemic low-grade inflammation is related to both circulating and adipose tissue TNFα, leptin and IL-6 levels in obese women. *Int. J. Obes.* **28**, 993–997 (2004).
63. Park, H. S., Park, J. Y. & Yu, R. Relationship of obesity and visceral adiposity with serum concentrations of CRP, TNF-α and IL-6. *Diabetes Res. Clin. Pract.* **69**, 29–35 (2005).
64. Castell, J. V. *et al.* Interleukin-6 is the major regulator of acute phase protein synthesis in adult human hepatocytes. *FEBS Lett.* **242**, 237–239 (1989).
65. Choi, J., Joseph, L. & Pilote, L. Obesity and C-reactive protein in various populations: a systematic review and meta-analysis. *Obes. Rev.* **14**, 232–244 (2013).
66. Guh, D. P. *et al.* The incidence of co-morbidities related to obesity and overweight: A systematic review and meta-analysis. *BMC Public Health* (2009). doi:10.1186/1471-2458-9-88
67. Hruby, A. *et al.* Determinants and Consequences of Obesity. *Am. J. Public Health* **106**, 1656–62 (2016).
68. Calle, E. E., Rodriguez, C., Walker-Thurmond, K. & Thun, M. J. Overweight, obesity, and mortality from cancer in a prospectively studied cohort of U.S. Adults. *N. Engl. J. Med.* (2003). doi:10.1056/NEJMoa021423
69. Parekh, N., Chandran, U. & Bandera, E. V. Obesity in Cancer Survival. *Annu. Rev. Nutr.* (2012). doi:10.1146/annurev-nutr-071811-150713
70. Reeves, G. K. *et al.* Cancer incidence and mortality in relation to body mass index in the Million Women Study: cohort study. *BMJ* **335**, 1134 (2007).
71. Renehan, A. G., Tyson, M., Egger, M., Heller, R. F. & Zwahlen, M. Body-mass index and incidence of cancer: a systematic review and meta-analysis of prospective observational studies. *Lancet* **371**, 569–578 (2008).
72. Renehan, A. G. *et al.* Incident cancer burden attributable to excess body mass index in 30 European countries. *Int. J. Cancer* **126**, 692–702 (2010).
73. Bhaskaran, K. *et al.* Body-mass index and risk of 22 specific cancers: a population-based cohort study of 5·24 million UK adults. *Lancet* **384**, 755–765 (2014).
74. Arnold, M. *et al.* Global burden of cancer attributable to high body-mass index in 2012: a population-based study. *Lancet Oncol.* **16**, 36–46 (2015).
75. Hines, R. B. *et al.* Effect of comorbidity and body mass index on the survival of African-American and Caucasian patients with colon cancer. *Cancer* (2009). doi:10.1002/cncr.24598
76. Navarro, W. H. *et al.* Effect of Body Mass Index on Mortality of Patients with Lymphoma Undergoing Autologous Hematopoietic Cell Transplantation. *Biol. Blood Marrow Transplant.* (2006). doi:10.1016/j.bbmt.2005.12.033
77. Parker, A. S. *et al.* Greater body mass index is associated with better pathologic features and improved outcome among patients treated surgically for clear cell renal cell carcinoma. *Urology* (2006). doi:10.1016/j.urology.2006.05.024
78. Schlesinger, S. *et al.* Postdiagnosis body mass index and risk of mortality in colorectal cancer survivors: a prospective study and meta-analysis. *Cancer Causes Control* (2014). doi:10.1007/s10552-014-0435-x
79. Hakimi, A. A. *et al.* An epidemiologic and genomic investigation into the obesity paradox in renal cell carcinoma. *J. Natl. Cancer Inst.* (2013). doi:10.1093/jnci/djt310
80. Amptoulach, S., Gross, G. & Kalaitzakis, E. Differential impact of obesity and diabetes mellitus on

survival after liver resection for colorectal cancer metastases. *J. Surg. Res.* (2015). doi:10.1016/j.jss.2015.05.059
81. Brunner, A. M. *et al.* Association between baseline body mass index and overall survival among patients over age 60 with acute myeloid leukemia. *Am. J. Hematol.* (2013). doi:10.1002/ajh.23462
82. Tsang, N. M. *et al.* Overweight and obesity predict better overall survival rates in cancer patients with distant metastases. *Cancer Med.* (2016). doi:10.1002/cam4.634
83. Lennon, H., Sperrin, M., Badrick, E. & Renehan, A. G. The Obesity Paradox in Cancer: a Review. *Current Oncology Reports* (2016). doi:10.1007/s11912-016-0539-4
84. Strulov Shachar, S. & Williams, G. R. The Obesity Paradox in Cancer—Moving Beyond BMI. *Cancer Epidemiol. Prev. Biomarkers* **26**, 13–16 (2017).
85. Trestini, I., Carbognin, L., Bonaiuto, C., Tortora, G. & Bria, E. The obesity paradox in cancer: clinical insights and perspectives. *Eat. Weight Disord. - Stud. Anorexia, Bulim. Obes.* **23**, 185–193 (2018).
86. Calle, E. E. & Kaaks, R. Overweight, obesity and cancer: Epidemiological evidence and proposed mechanisms. *Nat. Rev. Cancer* **4**, 579–591 (2004).
87. Renehan, A. G., Roberts, D. L. & Dive, C. Obesity and cancer: pathophysiological and biological mechanisms. *Arch Physiol Biochem* **114**, 71–83 (2008).
88. Park, J., Morley, T. S., Kim, M., Clegg, D. J. & Scherer, P. E. Obesity and cancer—mechanisms underlying tumour progression and recurrence. *Nat. Rev. Endocrinol* **10**, 455–465 (2014).
89. Pérez-Hernández, A. I., Catalán, V., Gómez-Ambrosi, J., Rodríguez, A. & Frühbeck, G. Mechanisms linking excess adiposity and carcinogenesis promotion. *Frontiers in Endocrinology* (2014). doi:10.3389/fendo.2014.00065
90. Teoh, S. L. & Das, S. Tumour biology of obesity-related cancers: understanding the molecular concept for better diagnosis and treatment. *Tumor Biol.* 1–18 (2016). doi:10.1007/s13277-016-5357-7
91. Quail, D. F. & Dannenberg, A. J. The obese adipose tissue microenvironment in cancer development and progression. *Nat. Rev. Endocrinol.* 1 (2018). doi:10.1038/s41574-018-0126-x
92. Divella, R., De Luca, R., Abbate, I., Naglieri, E. & Daniele, A. Obesity and cancer: the role of adipose tissue and adipo-cytokines-induced chronic inflammation. *J. Cancer* **7**, 2346–2359 (2016).
93. Spyrou, N., Avgerinos, K. I., Mantzoros, C. S. & Dalamaga, M. Classic and Novel Adipocytokines at the Intersection of Obesity and Cancer: Diagnostic and Therapeutic Strategies. *Curr. Obes. Rep.* 1–16 (2018). doi:10.1007/s13679-018-0318-7
94. Iyengar, N. & Hudis, C. Obesity and cancer: local and systemic mechanisms. *Annu. Rev.* (2015).
95. Geisler, J., Haynes, B., Ekse, D., Dowsett, M. & Lonning, P. E. Total body aromatization in postmenopausal breast cancer patients is strongly correlated to plasma leptin levels. *J. Steroid Biochem. Mol. Biol.* **104**, 27–34 (2007).
96. Eliassen, A. H. & Hankinson, S. E. Endogenous hormone levels and risk of breast, endometrial and ovarian cancers: Prospective studies. in *Innovative Endocrinology of Cancer* **630**, 148–165 (2008).
97. Renehan, A. G., Frystyk, J. & Flyvbjerg, A. Obesity and cancer risk: the role of the insulin-IGF axis. *Trends Endocrinol. Metab.* **17**, 328–336 (2006).
98. Poloz, Y. & Stambolic, V. Obesity and cancer, a case for insulin signaling. *Cell death & disease* (2015). doi:10.1038/cddis.2015.381
99. Smith, L. A., O'Flanagan, C. H., Bowers, L. W., Allott, E. H. & Hursting, S. D. Translating Mechanism-Based Strategies to Break the Obesity-Cancer Link: A Narrative Review. *Journal of the Academy of Nutrition and Dietetics* (2017). doi:10.1016/j.jand.2017.08.112
100. The Global Cancer Observatory. Cancer fact sheet. *World Heal. Organ.* (2018). doi:https://gco.iarc.fr/today/data/factsheets/cancers/39-All-cancers-fact-sheet.pdf
101. New Zealand Ministry of Health. Selected Cancers Statistics 2015, 2016, 2017. (2017).
102. New Zealand Breast Cancer Foundation. Breast Cancer. *What is breast cancer?* Available at: https://www.breastcancerfoundation.org.nz/breast-awareness/breast-cancer-facts/what-is-breast-cancer. (Accessed: 3rd July 2019)
103. Perou, C. M. *et al.* Molecular portraits of human breast tumours. *Nature* **406**, 747–752 (2000).
104. Koboldt, D. C. *et al.* Comprehensive molecular portraits of human breast tumours. *Nature* **490**, 61–70 (2012).
105. Soliman, N. A. & Yussif, S. M. Ki-67 as a prognostic marker according to breast cancer molecular subtype. *Cancer Biol. Med.* **13**, 496–504 (2016).
106. Perou, C. M. Molecular stratification of triple-negative breast cancers. *Oncologist* **15 Suppl 5**, 39–48 (2010).
107. Maximiano, S., Magalhães, P., Guerreiro, M. P. & Morgado, M. Trastuzumab in the Treatment of Breast Cancer. *BioDrugs* **30**, 75–86 (2016).
108. Marcom, P. K. Breast Cancer. in *Genomic and Precision Medicine: Primary Care: Third Edition* (2017). doi:10.1016/B978-0-12-800685-6.00010-2

109. Pohlmann, P. R., Mayer, I. A. & Mernaugh, R. Resistance to trastuzumab in breast cancer. *Clinical Cancer Research* (2009). doi:10.1158/1078-0432.CCR-09-0636
110. Vu, T. & Claret, F. X. Trastuzumab: Updated Mechanisms of Action and Resistance in Breast Cancer. *Front. Oncol.* (2012). doi:10.3389/fonc.2012.00062
111. Carey, L. A. *et al.* The triple negative paradox: Primary tumor chemosensitivity of breast cancer subtypes. *Clin. Cancer Res.* (2007). doi:10.1158/1078-0432.CCR-06-1109
112. Anders, C. & Carey, L. A. Understanding and treating triple-negative breast cancer. *Oncology (Williston Park).* (2008).
113. Malhotra, G. K., Zhao, X., Band, H. & Band, V. Histological, molecular and functional subtypes of breast cancers. *Cancer Biology and Therapy* (2010). doi:10.4161/cbt.10.10.13879
114. Xia, X. *et al.* Body mass index and risk of breast cancer: a nonlinear dose-response meta-analysis of prospective studies. *Sci Rep* **4**, 7480 (2014).
115. Amadou, A. *et al.* Overweight, obesity and risk of premenopausal breast cancer according to ethnicity: a systematic review and dose-response meta-analysis. *Obes Rev* **14**, 665–678 (2013).
116. Picon-Ruiz, M., Morata-Tarifa, C., Valle-Goffin, J. J., Friedman, E. R. & Slingerland, J. M. Obesity and adverse breast cancer risk and outcome: Mechanistic insights and strategies for intervention. *CA. Cancer J. Clin.* **67**, 378–397 (2017).
117. Nattenmüller, C. J. *et al.* Obesity as risk factor for subtypes of breast cancer: results from a prospective cohort study. *BMC Cancer* **18**, 616 (2018).
118. Donato, G. B., Fuchs, S. C., Oppermann, K., Bastos, C. & Spritzer, P. M. Association between menopause status and central adiposity measured at different cutoffs of waist circumference and waist-to-hip ratio. *Menopause* **13**, 280–5 (2006).
119. Lovejoy, J. C., Champagne, C. M., De Jonge, L., Xie, H. & Smith, S. R. Increased visceral fat and decreased energy expenditure during the menopausal transition. *Int. J. Obes.* (2008). doi:10.1038/ijo.2008.25
120. Harris, H. R., Willett, W. C., Terry, K. L. & Michels, K. B. Body Fat Distribution and Risk of Premenopausal Breast Cancer in the Nurses' Health Study II. *J Natl Cancer Inst* **103**, 273–278 (2011).
121. Abe, R., Kumagai, N., Kimura, M., Hirosaki, A. & Nakamura, T. Biological characteristics of breast cancer in obesity. *Tohoku J. Exp. Med.* **120**, 351–9 (1976).
122. Fontanella, C. *et al.* Impact of body mass index on neoadjuvant treatment outcome: a pooled analysis of eight prospective neoadjuvant breast cancer trials. *Breast Cancer Res. Treat.* **150**, 127–139 (2015).
123. Robinson, P. J., Bell, R. J. & Davis, S. R. Obesity is associated with a poorer prognosis in women with hormone receptor positive breast cancer. *Maturitas* **79**, 279–286 (2014).
124. Ewertz, M., Jensen, M. & Gunnarsdóttir, K. Effect of obesity on prognosis after early-stage breast cancer. *J. Clin.* **29**, 25–31 (2011).
125. Kaviani, A., Neishaboury, M., Mohammadzadeh, N., Ansari-Damavandi, M. & Jamei, K. Effects of Obesity on Presentation of Breast Cancer, Lymph Node Metastasis and Patient Survival: A Retrospective Review. *Asian Pacific J. Cancer Prev.* **14**, 2225–2229 (2013).
126. Protani, M., Coory, M. & Martin, J. H. Effect of obesity on survival of women with breast cancer: Systematic review and meta-Analysis. *Breast Cancer Res. Treat.* **123**, 627–635 (2010).
127. Chan, D. S. M. *et al.* Body mass index and survival in women with breast cancer—systematic literature review and meta-analysis of 82 follow-up studies. *Ann. Oncol.* **25**, 1901–1914 (2014).
128. Dignam, J. J. Obesity and breast cancer prognosis: an expanding body of evidence. *Ann. Oncol.* **15**, 850–851 (2004).
129. Niraula, S., Ocana, A., Ennis, M. & Goodwin, P. J. Body size and breast cancer prognosis in relation to hormone receptor and menopausal status: a meta-analysis. *Breast Cancer Res Treat* **134**, 769–781 (2012).
130. Pajares, B. *et al.* Obesity and survival in operable breast cancer patients treated with adjuvant anthracyclines and taxanes according to pathological subtypes: a pooled analysis. *Breast Cancer Res.* **15**, R105 (2013).
131. Del Fabbro, E. *et al.* The Relationship Between Body Composition and Response to Neoadjuvant Chemotherapy in Women with Operable Breast Cancer. *Oncologist* **17**, 1240–1245 (2012).
132. Chen, S. *et al.* Obesity or Overweight Is Associated with Worse Pathological Response to Neoadjuvant Chemotherapy among Chinese Women with Breast Cancer. *PLoS One* **7**, e41380 (2012).
133. Karpińska, A., Safranow, K., Kładny, J. & Sulżyc-Bielicka, V. The Influence Of Obesity On Results Of AT (Doxorubicin Plus Docetaxel) Neoadjuvant Chemotherapy In Locally Advanced Breast Cancer Patients. *Polish J. Surg.* **87**, 231–237 (2015).
134. Hunter, R. J. *et al.* Dosing chemotherapy in obese patients: Actual versus assigned body surface area (BSA). *Cancer Treat. Rev.* **35**, 69–78 (2009).
135. Griggs, J. J., Sorbero, M. E. S. & Lyman, G. H. Undertreatment of obese women receiving breast

cancer chemotherapy. *Arch. Intern. Med.* **165**, 1267–1273 (2005).
136. Lyman, G. H. Weight-based chemotherapy dosing in obese patients with cancer: back to the future. *J. Oncol. Pract.* **8**, e62-4 (2012).
137. Lyman, G. H. & Sparreboom, A. Chemotherapy dosing in overweight and obese patients with cancer. *Nature Reviews Clinical Oncology* (2013). doi:10.1038/nrclinonc.2013.108
138. Goodwin, P. J. Obesity and breast cancer outcomes: How much evidence is needed to change practice? *Journal of Clinical Oncology* (2016). doi:10.1200/JCO.2015.64.7503
139. Farr, A. *et al.* The effect of obesity on pathological complete response and survival in breast cancer patients receiving uncapped doses of neoadjuvant anthracycline-taxane-based chemotherapy. *Breast* (2017). doi:10.1016/j.breast.2017.04.001
140. Andò, S. *et al.* Obesity, Leptin and Breast Cancer: Epidemiological Evidence and Proposed Mechanisms. *Cancers (Basel).* **11**, (2019).
141. Iyengar, N. M., Gucalp, A., Dannenberg, A. J. & Hudis, C. A. Obesity and Cancer Mechanisms: Tumor Microenvironment and Inflammation. *J Clin Oncol* **34**, 4270–4276 (2016).
142. Iyengar, N. M., Hudis, C. A. & Dannenberg, A. J. Obesity and inflammation: new insights into breast cancer development and progression. *Am. Soc. Clin. Oncol. Educ. Book* **33**, 46–51 (2013).
143. Lapeire, L., Denys, H., Cocquyt, V. & De Wever, O. When fat becomes an ally of the enemy: adipose tissue as collaborator in human breast cancer. *Horm. Mol. Biol. Clin. Investig.* **23**, 21–38 (2015).
144. Goodwin, P. J. *et al.* Fasting insulin and outcome in early-stage breast cancer: Results of a prospective cohort study. *J. Clin. Oncol.* (2002). doi:10.1200/JCO.20.1.42
145. Pierce, B. L. *et al.* Elevated biomarkers of inflammation are associated with reduced survival among breast cancer patients. *J. Clin. Oncol.* **27**, 3437–3444 (2009).
146. Niu, J. *et al.* The Association between Leptin Level and Breast Cancer: A Meta-Analysis. *PLoS One* (2013). doi:10.1371/journal.pone.0067349
147. Brown, S. B. & Hankinson, S. E. Endogenous estrogens and the risk of breast, endometrial, and ovarian cancers. *Steroids* (2015). doi:10.1016/j.steroids.2014.12.013
148. Nicolini, A., Carpi, A. & Rossi, G. Cytokines in breast cancer. *Cytokine and Growth Factor Reviews* (2006). doi:10.1016/j.cytogfr.2006.07.002
149. Dethlefsen, C., Højfeldt, G. & Hojman, P. The role of intratumoral and systemic IL-6 in breast cancer. *Breast Cancer Res. Treat.* **138**, 657–664 (2013).
150. Dirat, B. *et al.* Cancer-associated adipocytes exhibit an activated phenotype and contribute to breast cancer invasion. *Cancer Res.* **71**, 2455–65 (2011).
151. Ishikawa, M., Kitayama, J. & Nagawa, H. Enhanced Expression of Leptin and Leptin Receptor (OB-R) in Human Breast Cancer. *Clin. Cancer Res.* **10**, 4325–4331 (2004).
152. Schmidt, S., Monk, J. M., Robinson, L. E. & Mourtzakis, M. The integrative role of leptin, oestrogen and the insulin family in obesity-associated breast cancer: potential effects of exercise. *Obes. Rev.* **16**, 473–487 (2015).
153. LeRoith, D. & Roberts, C. T. The insulin-like growth factor system and cancer. *Cancer Letters* (2003). doi:10.1016/S0304-3835(03)00159-9
154. Creighton, C. J. *et al.* Insulin-like growth factor-I activates gene transcription programs strongly associated with poor breast cancer prognosis. *J. Clin. Oncol.* (2008). doi:10.1200/JCO.2007.13.4429
155. Creighton, C. J. *et al.* A gene transcription signature of obesity in breast cancer. *Breast Cancer Res. Treat.* **132**, 993–1000 (2012).
156. Liedtke, S. *et al.* Postmenopausal Sex hormones in relation to body fat distribution. *Obesity* (2012). doi:10.1038/oby.2011.383
157. Key, T. Steroid hormone measurements from different types of assays in relation to body mass index and breast cancer risk in postmenopausal women: Reanalysis of eighteen prospective studies. *Steroids* (2015). doi:10.1016/j.steroids.2014.09.001
158. Kakugawa, Y. *et al.* Associations of obesity and physical activity with serum and intratumoral sex steroid hormone levels among postmenopausal women with breast cancer: analysis of paired serum and tumor tissue samples. *Breast Cancer Res. Treat.* (2017). doi:10.1007/s10549-016-4094-3
159. Shah, R. & Smith, R. Inflammation-induced phenoconversion of polymorphic drug metabolizing enzymes: hypothesis with implications for personalized medicine. *Drug Metab. Dispos.* **43**, 400–410 (2015).
160. Iyengar, N. M. *et al.* Systemic Correlates of White Adipose Tissue Inflammation in Early-Stage Breast Cancer. *Clin. Cancer Res.* **22**, 2283–89 (2016).
161. Walter, M., Liang, S., Ghosh, S., Hornsby, P. J. & Li, R. Interleukin 6 secreted from adipose stromal cells promotes migration and invasion of breast cancer cells. *Oncogene* **28**, 2745–2755 (2009).
162. Morris, P. G. *et al.* Inflammation and increased aromatase expression occur in the breast tissue of obese women with breast cancer. *Cancer Prev. Res. (Phila).* **4**, 1021–9 (2011).

163. Iyengar, N. M. *et al.* Menopause is a determinant of breast adipose inflammation. *Cancer Prev. Res.* **8**, 349–358 (2015).
164. Mullooly, M. *et al.* Relationship between crown-like structures and sex-steroid hormones in breast adipose tissue and serum among postmenopausal breast cancer patients. *Breast Cancer Res.* **19**, 8 (2017).
165. Iyengar, N. M. *et al.* Metabolic Obesity, Adipose Inflammation and Elevated Breast Aromatase in Women with Normal Body Mass Index. *Cancer Prev Res* **1**, (2017).
166. Frisch, R. E. *et al.* Lower prevalence of breast cancer and cancers of the reproductive system among former college athletes compared to non-athletes. *Br. J. Cancer* **52**, 885–91 (1985).
167. Friedenreich, C. M. & Cust, A. E. Physical activity and breast cancer risk: impact of timing, type and dose of activity and population subgroup effects. *Br. J. Sports Med.* **42**, 636–47 (2008).
168. Wu, Y., Zhang, D. & Kang, S. Physical activity and risk of breast cancer: a meta-analysis of prospective studies. *Breast Cancer Res. Treat.* **137**, 869–882 (2013).
169. Ibrahim, E. M. & Al-Homaidh, A. Physical activity and survival after breast cancer diagnosis: meta-analysis of published studies. *Med. Oncol.* **28**, 753–765 (2011).
170. Zhong, S. *et al.* Association between physical activity and mortality in breast cancer: a meta-analysis of cohort studies. *Eur. J. Epidemiol.* **29**, 391–404 (2014).
171. Li, T. *et al.* The dose-response effect of physical activity on cancer mortality: findings from 71 prospective cohort studies. *Br. J. Sports Med.* **50**, 339–45 (2016).
172. Schmid, D. & Leitzmann, M. F. Association between physical activity and mortality among breast cancer and colorectal cancer survivors: a systematic review and meta-analysis. *Ann. Oncol.* **25**, 1293–1311 (2014).
173. Lahart, I. M., Metsios, G. S., Nevill, A. M. & Carmichael, A. R. Physical activity, risk of death and recurrence in breast cancer survivors: A systematic review and meta-analysis of epidemiological studies. *Acta Oncol. (Madr).* **54**, 635–654 (2015).
174. World Health Organisation. Physical Activity and Adults. *Global Strategy on Diet, Physical Activity and Health* (2015). Available at: https://www.who.int/dietphysicalactivity/factsheet_adults/en/. (Accessed: 1st July 2019)
175. McTiernan, A. Mechanisms linking physical activity with cancer. *Nature Reviews Cancer* (2008). doi:10.1038/nrc2325
176. Hojman, P., Gehl, J., Christensen, J. F. & Pedersen, B. K. Molecular Mechanisms Linking Exercise to Cancer Prevention and Treatment. *Cell Metabolism* (2018). doi:10.1016/j.cmet.2017.09.015
177. Christensen, J. F., Simonsen, C. & Hojman, P. Exercise Training in Cancer Control and Treatment. in *Comprehensive Physiology* **9**, 165–205 (Wiley, 2019).
178. Mathur, N. & Pedersen, B. K. Exercise as a Mean to Control Low-Grade Systemic Inflammation. *Mediators Inflamm.* **2008**, 1–6 (2008).
179. Irwin, M. L. *et al.* Relationship of obesity and physical activity with C-peptide, leptin, and insulin-like growth factors in breast cancer survivors. *Cancer Epidemiol. Biomarkers Prev.* **14**, 2881–8 (2005).
180. Gómez, A. M. *et al.* Exercise training and cytokines in breast cancer survivors. *Int. J. Sports Med.* **32**, 461–7 (2011).
181. Jones, S. B. *et al.* Effect of Exercise on Markers of Inflammation in Breast Cancer Survivors: The Yale Exercise and Survivorship Study. *Cancer Prev. Res.* **6**, 109–118 (2013).
182. Meneses-Echavez, J. F. *et al.* The effect of exercise training on mediators of inflammation in breast cancer survivors: a systematic review with meta-analysis. *Cancer Epidemiol. Biomarkers Prev.* (2016). doi:10.1158/1055-9965.EPI-15-1061
183. Kang, D.-W. *et al.* Effects of Exercise on Insulin, IGF-axis, Adipocytokines, and Inflammatory Markers in Breast Cancer Survivors: A Systematic Review and Meta-Analysis. *Cancer Epidemiol. Prev. Biomarkers* (2016).
184. Khosravi, N., Stoner, L., Farajivafa, V. & Hanson, E. D. Exercise training, circulating cytokine levels and immune function in cancer survivors: A meta-analysis. *Brain. Behav. Immun.* (2019). doi:10.1016/J.BBI.2019.08.187
185. Dieli-Conwright, C. M. *et al.* Adipose tissue inflammation in breast cancer survivors: effects of a 16-week combined aerobic and resistance exercise training intervention. *Breast Cancer Res. Treat.* **168**, 147–157 (2017).
186. Dethlefsen, C. *et al.* Exercise regulates breast cancer cell viability: systemic training adaptations versus acute exercise responses. *Breast Cancer Res. Treat.* **159**, 469–479 (2016).
187. Dethlefsen, C., Pedersen, K. S. & Hojman, P. Every exercise bout matters: linking systemic exercise responses to breast cancer control. *Breast Cancer Res. Treat.* **162**, 399–408 (2017).
188. Courneya, K., Segal, R., McKenzie, D. & Dong, H. Effects of exercise during adjuvant chemotherapy on breast cancer outcomes. *Med Sci Sport.* **46**, 1744–1751 (2014).

189. Courneya, K. S. *et al.* Effects of exercise dose and type during breast cancer chemotherapy: multicenter randomized trial. *J. Natl. Cancer Inst.* **105**, 1821–32 (2013).
190. Van Waart, H. *et al.* Effect of low-intensity physical activity and moderate- to high-intensity physical exercise during adjuvant chemotherapy on physical fitness, fatigue, and chemotherapy completion rates: Results of the PACES randomized clinical trial. *J. Clin. Oncol.* (2015). doi:10.1200/JCO.2014.59.1081
191. Courneya, K. S. *et al.* Subgroup effects in a randomised trial of different types and doses of exercise during breast cancer chemotherapy. *Br. J. Cancer* **111**, 1718–1725 (2014).
192. van Vulpen, J. K. *et al.* Effects of physical exercise on markers of inflammation in breast cancer patients during adjuvant chemotherapy. *Breast Cancer Res. Treat.* **168**, 421–431 (2018).
193. Scott, E. *et al.* Effects of an exercise and hypocaloric healthy eating program on biomarkers associated with long-term prognosis after early-stage breast cancer: a randomized controlled trial. *Cancer Causes Control* **24**, 181–191 (2013).
194. Swisher, A. K. *et al.* Exercise and dietary advice intervention for survivors of triple-negative breast cancer: effects on body fat, physical function, quality of life, and adipokine profile. *Support. Care Cancer* **23**, 2995–3003 (2015).
195. James, P. *et al.* Comparing GPS, Log, Survey, and Accelerometry to Measure Physical Activity. *Am. J. Health Behav.* **40**, 123–131 (2016).
196. Wagoner, C. W. *et al.* Establishing physical activity in breast cancer: self-report versus activity tracker. *Breast Cancer Res. Treat.* (2019). doi:10.1007/s10549-019-05263-3
197. Klinker, C., Schipperijn, J. & Christian, H. Using accelerometers and global positioning system devices to assess gender and age differences in children's school, transport, leisure and home based. *Int J Behav Nutr* (2014).
198. Webber, S. & Porter, M. Monitoring mobility in older adults using global positioning system (GPS) watches and accelerometers: a feasibility study. *J Aging Phys Act* (2009).
199. Rodriguez, D., Brown, A. & Troped, P. Portable global positioning units to complement accelerometry-based physical activity monitors. *Med. Sci. Sport.* (2005).
200. Takacs, J. *et al.* Validation of the Fitbit One activity monitor device during treadmill walking. *J. Sci. Med. Sport* **17**, 496–500 (2014).
201. Nyrop, K. A. *et al.* Measuring and understanding adherence in a home-based exercise intervention during chemotherapy for early breast cancer. *Breast Cancer Research and Treatment* 1–13 (2017). doi:10.1007/s10549-017-4565-1
202. Nelson, S. H. *et al.* Continuous, objective measurement of physical activity during chemotherapy for breast cancer: the Activity in Treatment pilot study. *Transl. Behav. Med.* (2019). doi:10.1093/tbm/ibz079
203. Gresham, G. *et al.* Wearable activity monitors to assess performance status and predict clinical outcomes in advanced cancer patients. *npj Digit. Med.* **1**, 27 (2018).
204. Weber, C. E. & Kuo, P. C. The tumor microenvironment. *Surg. Oncol.* **21**, 172–177 (2012).
205. Bhome, R. *et al.* A top-down view of the tumor microenvironment: structure, cells and signaling. *Front. Cell Dev. Biol.* (2015). doi:10.3389/fcell.2015.00033
206. Balkwill, F. R., Capasso, M. & Hagemann, T. The tumor microenvironment at a glance. *J. Cell Sci.* (2012). doi:10.1242/jcs.116392
207. Hanahan, D. & Coussens, L. M. Accessories to the Crime: Functions of Cells Recruited to the Tumor Microenvironment. *Cancer Cell* (2012). doi:10.1016/j.ccr.2012.02.022
208. Wang, M. *et al.* Role of tumor microenvironment in tumorigenesis. *J. Cancer* **8**, 761 (2017).
209. Hirata, E. & Sahai, E. Tumor Microenvironment and Differential Responses to Therapy. *Cold Spring Harb. Perspect. Med.* **7**, a026781 (2017).
210. Paget, S. The distribution od secondary growths in cancer of the breast. *Lancet* **133**, 571–573 (1889).
211. Fidler, I. J. & Poste, G. *From the Archives The "seed and soil" hypothesis revisited*. *www.thelancet.com/oncology* **9**, (2008).
212. Bissell, M. J., Hall, H. G. & Parry, G. How does the extracellular matrix direct gene expression? *J. Theor. Biol.* **99**, 31–68 (1982).
213. Rønnov-Jessen, L. & Bissell, M. J. Breast cancer by proxy: can the microenvironment be both the cause and consequence? *Trends Mol. Med.* **15**, 5–13 (2009).
214. Artacho-Cordón, A., Artacho-Cordón, F., Ríos-Arrabal, S., Calvente, I. & Núñez, M. I. Tumor microenvironment and breast cancer progression. *Cancer Biol. Ther.* **13**, 14–24 (2012).
215. Mittal, S., Brown, N. J. & Holen, I. The breast tumor microenvironment: role in cancer development, progression and response to therapy. *Expert Rev. Mol. Diagn.* **18**, 227–243 (2018).
216. Hu, M. & Polyak, K. Microenvironmental regulation of cancer development. *Curr. Opin. Genet. Dev.* **18**, 27–34 (2008).

217. DeCosse, J. J., Gossens, C. L., Kuzma, J. F. & Unsworth, B. R. Breast Cancer: Induction of Differentiation by Embryonic Tissue. *Science (80-.).* **181**, 1057–1058 (1973).
218. Soysal, S. D., Tzankov, A. & Muenst, S. E. Role of the Tumor Microenvironment in Breast Cancer. *Pathobiology* **82**, 142–152 (2015).
219. Fukino, K., Shen, L., Patocs, A., Mutter, G. L. & Eng, C. Genomic Instability Within Tumor Stroma and Clinicopathological Characteristics of Sporadic Primary Invasive Breast Carcinoma. *JAMA* **297**, 2103 (2007).
220. Hu, M. *et al.* Distinct epigenetic changes in the stromal cells of breast cancers. *Nat. Genet.* **37**, 899–905 (2005).
221. Yang, J., Li, X., Liu, X. & Liu, Y. The role of tumor-associated macrophages in breast carcinoma invasion and metastasis. *Int. J. Clin. Exp. Pathol.* **8**, 6656–64 (2015).
222. Yang, M., Ma, B., Shao, H., Clark, A. M. & Wells, A. Macrophage phenotypic subtypes diametrically regulate epithelial-mesenchymal plasticity in breast cancer cells. *BMC Cancer* **16**, 419 (2016).
223. Chen, Y., Zhang, S., Wang, Q. & Zhang, X. Tumor-recruited M2 macrophages promote gastric and breast cancer metastasis via M2 macrophage-secreted CHI3L1 protein. *J. Hematol. Oncol.* **10**, 36 (2017).
224. Polyak, K., Haviv, I. & Campbell, I. G. Co-evolution of tumor cells and their microenvironment. *Trends Genet.* **25**, 30–38 (2009).
225. Ethier, J.-L., Desautels, D., Templeton, A., Shah, P. S. & Amir, E. Prognostic role of neutrophil-to-lymphocyte ratio in breast cancer: a systematic review and meta-analysis. doi:10.1186/s13058-016-0794-1
226. Folgueira, M. A. A. K. *et al.* Markers of breast cancer stromal fibroblasts in the primary tumour site associated with lymph node metastasis: a systematic review including our case series. *Biosci. Rep.* **33**, (2013).
227. Barone, I. *et al.* Leptin mediates tumor-stromal interactions that promote the invasive growth of breast cancer cells. *Cancer Res.* **72**, 1416–27 (2012).
228. Yu, Y. *et al.* Cancer-associated fibroblasts induce epithelial–mesenchymal transition of breast cancer cells through paracrine TGF-β signalling. *Br. J. Cancer* **110**, 724–732 (2014).
229. Amornsupak, K. *et al.* Cancer-associated fibroblasts induce high mobility group box 1 and contribute to resistance to doxorubicin in breast cancer cells. *BMC Cancer* **14**, 955 (2014).
230. Dirat, B., Bochet, L., Escourrou, G., Valet, P. & Muller, C. Unraveling the Obesity and Breast Cancer Links: A Role for Cancer-Associated Adipocytes? in *Adipose Tissue Development* **19**, 45–52 (KARGER, 2010).
231. Tan, J., Buache, E., Chenard, M.-P., Dali-Youcef, N. & Rio, M.-C. Adipocyte is a non-trivial, dynamic partner of breast cancer cells. *Int. J. Dev. Biol.* **55**, 851–859 (2011).
232. Wang, Y.-Y. *et al.* Adipose tissue and breast epithelial cells: A dangerous dynamic duo in breast cancer. *Cancer Lett.* **324**, 142–151 (2012).
233. Hursting, S. D. & Dunlap, S. M. Obesity, metabolic dysregulation, and cancer: a growing concern and an inflammatory (and microenvironmental) issue. *Ann. N. Y. Acad. Sci.* **1271**, 82–87 (2012).
234. Wen, W. Q. *et al.* Meta-analysis of genome-wide association studies in East Asian-ancestry populations identifies four new loci for body mass index. *Hum. Mol. Genet.* **23**, 5492–5504 (2014).
235. Vona-Davis, L. & Rose, D. P. Adipokines as endocrine, paracrine, and autocrine factors in breast cancer risk and progression. *Endocr. Relat. Cancer* **14**, 189–206 (2007).
236. Strong, A. L. *et al.* Leptin produced by obese adipose stromal/stem cells enhances proliferation and metastasis of estrogen receptor positive breast cancers. *Breast Cancer Res.* **17**, 112 (2015).
237. Iyengar, P. *et al.* Adipocyte-secreted factors synergistically promote mammary tumorigenesis through induction of anti-apoptotic transcriptional programs and proto-oncogene stabilization. *Oncogene* **22**, 6408–6423 (2003).
238. Carter, J. C. & Church, F. C. Mature breast adipocytes promote breast cancer cell motility. *Exp. Mol. Pathol.* **92**, 312–317 (2012).
239. Grisouard, J. *et al.* Targeting AMP-activated protein kinase in adipocytes to modulate obesity-related adipokine production associated with insulin resistance and breast cancer cell proliferation. *Diabetol. Metab. Syndr.* **3**, 16 (2011).
240. D 'esposito, V. *et al.* Adipocyte-released insulin-like growth factor-1 is regulated by glucose and fatty acids and controls breast cancer cell growth in vitro. *Diabetologia* **55**, 2811–22 (2012).
241. Bochet, L. *et al.* Adipocyte-derived fibroblasts promote tumor progression and contribute to the desmoplastic reaction in breast cancer. *Cancer Res* **73**, 5657–5668 (2013).
242. Lapeire, L. *et al.* Cancer-associated adipose tissue promotes breast cancer progression by paracrine oncostatin M and Jak/STAT3 signaling. *Cancer Res.* **74**, 6806–19 (2014).
243. Drew, B. G. *et al.* Estrogen receptor (ER)α-regulated lipocalin 2 expression in adipose tissue links

obesity with breast cancer progression. *J. Biol. Chem.* **290**, 5566–81 (2015).
244. Fujisaki, K. *et al.* Cancer-mediated adipose reversion promotes cancer cell migration via IL-6 and MCP-1. *Breast Cancer Res. Treat.* **150**, 255–263 (2015).
245. Sakurai, M. *et al.* Interaction with adipocyte stromal cells induces breast cancer malignancy via S100A7 upregulation in breast cancer microenvironment. *Breast Cancer Res.* **19**, 70 (2017).
246. Wang, C., Gao, C., Meng, K., Qiao, H. & Wang, Y. Human Adipocytes Stimulate Invasion of Breast Cancer MCF-7 Cells by Secreting IGFBP-2. *PLoS One* **10**, e0119348 (2015).
247. D'Esposito, V. *et al.* Adipose microenvironment promotes triple negative breast cancer cell invasiveness and dissemination by producing CCL5. *Oncotarget* **7**, 24495–509 (2016).
248. Picon-Ruiz, M. *et al.* Tumor and Stem Cell Biology Interactions between Adipocytes and Breast Cancer Cells Stimulate Cytokine Production and Drive Src/Sox2/miR-302b–Mediated Malignant Progression. *Cancer Res.* **76**, 491–504 (2016).
249. Balaban, S. *et al.* Adipocyte lipolysis links obesity to breast cancer growth: adipocyte-derived fatty acids drive breast cancer cell proliferation and migration. *Cancer Metab.* **5**, (2017).
250. Huang, C.-K. *et al.* Adipocytes promote malignant growth of breast tumours with monocarboxylate transporter 2 expression via β-hydroxybutyrate. *Nat. Commun.* **8**, 14706 (2017).
251. Bochet, L. *et al.* Cancer-associated adipocytes promotes breast tumor radioresistance. *Biochem. Biophys. Res. Commun.* **411**, 102–106 (2011).
252. De Angel, R. E. *et al.* Stearoyl gemcitabine nanoparticles overcome obesity-induced cancer cell resistance to gemcitabine in a mouse postmenopausal breast cancer model. *Cancer Biol. Ther.* **14**, 357–364 (2013).
253. Lehuédé, C. *et al.* Adipocytes promote breast cancer resistance to chemotherapy, a process amplified by obesity: role of the major vault protein (MVP). *Breast Cancer Res.* **21**, 7 (2019).
254. Duong, M. N. *et al.* Adipose cells promote resistance of breast cancer cells to trastuzumab-mediated antibody-dependent cellular cytotoxicity. *Breast Cancer Res.* **17**, 57 (2015).
255. Bougaret, L. *et al.* Adipocyte/breast cancer cell crosstalk in obesity interferes with the anti-proliferative efficacy of tamoxifen. *PLoS One* **13**, e0191571 (2018).
256. Hsieh, C. C. & Huang, Y. S. Aspirin breaks the crosstalk between 3T3-L1 adipocytes and 4T1 breast cancer cells by regulating cytokine production. *PLoS One* **11**, 1–17 (2015).
257. Rowan, B. G. *et al.* Human Adipose Tissue-Derived Stromal/Stem Cells Promote Migration and Early Metastasis of Triple Negative Breast Cancer Xenografts. *PLoS One* **9**, e89595 (2014).
258. Vazquez Rodriguez, G., Abrahamsson, A., Jensen, L. D. E. & Dabrosin, C. Adipocytes Promote Early Steps of Breast Cancer Cell Dissemination via Interleukin-8. *Front. Immunol.* **9**, 1767 (2018).
259. Hoy, A. J., Balaban, S. & Saunders, D. N. Adipocyte–Tumor Cell Metabolic Crosstalk in Breast Cancer. *Trends Mol. Med.* **23**, 381–392 (2017).
260. Martinez-Outschoorn, U. E. *et al.* Energy transfer in "parasitic" cancer metabolism Mitochondria are the powerhouse and Achilles' heel of tumor cells. *Cell Cycle* **10**, 4208–4216 (2011).
261. Nieman, K. M. *et al.* Adipocytes promote ovarian cancer metastasis and provide energy for rapid tumor growth. *Nat. Med.* **17**, 1498–1503 (2011).
262. Wang, Y. Y. *et al.* Mammary adipocytes stimulate breast cancer invasion through metabolic remodeling of tumor cells. *JCI insight* **2**, e87489 (2017).
263. Nickel, A. *et al.* Adipocytes induce distinct gene expression profiles in mammary tumor cells and enhance inflammatory signaling in invasive breast cancer cells. *Sci. Rep.* **8**, 9482 (2018).
264. Beijnen, J. H. & Schellens, J. H. M. Drug interactions in oncology. *Lancet Oncol.* **5**, 489–496 (2004).
265. Rochat, B. Role of Cytochrome P450 Activity in the Fate of Anticancer Agents and in Drug Resistance. *Clin. Pharmacokinet.* **44**, 349–366 (2005).
266. Harmsen, S., Meijerman, I. & Beijnen, J. The role of nuclear receptors in pharmacokinetic drug–drug interactions in oncology. *Cancer Treat. Rev.* **33**, 369–380 (2007).
267. Kivisto, K., Kroemer, H. & Eichelbaum, M. The role of human cytochrome P450 enzymes in the metabolism of anticancer agents: implications for drug interactions. *Br. J. Clin. Pharmacol.* (1995). doi:10.1111/j.1365-2125.1995.tb05796.x
268. Evans, W. & Relling, M. Pharmacogenomics: translating functional genomics into rational therapeutics. *Science (80-.).* **286**, 487–491 (1999).
269. Krishna, D. R. & Klotz, U. Extrahepatic Metabolism of Drugs in Humans. *Clin. Pharmacokinet.* **26**, 144–160 (1994).
270. Osborne, C. K. Tamoxifen in the Treatment of Breast Cancer. *N. Engl. J. Med.* **339**, 1609–1618 (1998).
271. Moore, M. J. Clinical Pharmacokinetics of Cyclophosphamide. *Clin. Pharmacokinet.* **20**, 194–208 (1991).
272. Speth, P. A. J., van Hoesel, Q. G. C. M. & Haanen, C. Clinical Pharmacokinetics of Doxorubicin. *Clin.*

Pharmacokinet. **15**, 15–31 (1988).
273. Sonnichsen, D. S. & Relling, M. V. Clinical Pharmacokinetics of Paclitaxel. *Clin. Pharmacokinet.* **27**, 256–269 (1994).
274. Zanger, U. M. & Schwab, M. Cytochrome P450 enzymes in drug metabolism: Regulation of gene expression, enzyme activities, and impact of genetic variation. *Pharmacol. Ther.* **138**, 103–141 (2013).
275. MacLeod, S. L. *et al.* Cancer therapy and polymorphisms of cytochromes P450. *Clin. Chem. Lab. Med.* **38**, 883–7 (2000).
276. Kirchheiner, J. *et al.* Pharmacogenetics of antidepressants and antipsychotics: the contribution of allelic variations to the phenotype of drug response. *Mol. Psychiatry* **9**, 442–473 (2004).
277. Dahl, M. L., Johansson, I., Bertilsson, L., Ingelman-Sundberg, M. & Sjöqvist, F. Ultrarapid hydroxylation of debrisoquine in a Swedish population. Analysis of the molecular genetic basis. *J. Pharmacol. Exp. Ther.* **274**, 516–520 (1995).
278. Sim, S. C. *et al.* A common novel CYP2C19 gene variant causes ultrarapid drug metabolism relevant for the drug response to proton pump inhibitors and antidepressants. *Clin. Pharmacol. Ther.* **79**, 103–113 (2006).
279. Petros, W. P. *et al.* Associations Between Drug Metabolism Genotype, Chemotherapy Pharmacokinetics, and Overall Survival in Patients With Breast Cancer. *J. Clin. Oncol.* **23**, 6117–6125 (2005).
280. Shah, R. R. & Shah, D. R. Personalized medicine: is it a pharmacogenetic mirage? *Br. J. Clin. Pharmacol.* **74**, 698–721 (2012).
281. Shah, R. & Smith, R. Addressing phenoconversion: the Achilles' heel of personalized medicine. *Br. J. Clin. Pharmacol.* **79**, 222–240 (2015).
282. Streetman, D., Bleakley, J. & Kim, J. Combined phenotypic assessment of CYP1A2, CYP2C19, CYP2D6, CYP3A, N-acetyltransferase-2, and xanthine oxidase with the "Cooperstown cocktail". *Clinical* (2000).
283. Helsby, N. A. *et al.* CYP2C19 pharmacogenetics in advanced cancer: compromised function independent of genotype. *Br. J. Cancer* **99**, 1251–1255 (2008).
284. de Andrés, F. & LLerena, A. Simultaneous Determination of Cytochrome P450 Oxidation Capacity in Humans: A Review on the Phenotyping Cocktail Approach. *Curr. Pharm. Biotechnol.* **17**, 1159–1180 (2016).
285. Keller, G. A., Gago, M. L. F., Diez, R. A. & Di Girolamo, G. In vivo Phenotyping Methods: Cytochrome P450 Probes with Emphasis on the Cocktail Approach. *Curr. Pharm. Des.* **23**, (2017).
286. Schellens, J. H., van der Wart, J. H., Brugman, M. & Breimer, D. D. Influence of enzyme induction and inhibition on the oxidation of nifedipine, sparteine, mephenytoin and antipyrine in humans as assessed by a "cocktail" study design. *J. Pharmacol. Exp. Ther.* **249**, (1989).
287. Frye, R. F., Matzke, G. R., Adedoyin, A., Porter, J. A. & & Branch, R. A. Validation of the five-drug "Pittsburgh cocktail" approach for assessment of selective regulation of drug-metabolizing enzymes. *Clinical* (1997).
288. Fuhr, U., Jetter, A. & Kirchheiner, J. Appropriate Phenotyping Procedures for Drug Metabolizing Enzymes and Transporters in Humans and Their Simultaneous Use in the "Cocktail" Approach. *Clin. Pharmacol. Ther.* **81**, 270–283 (2007).
289. Derungs, A., Donzelli, M., Berger, B. & Noppen, C. Effects of Cytochrome P450 Inhibition and Induction on the Phenotyping Metrics of the Basel Cocktail: A Randomized Crossover Study. *Clinical* (2016).
290. Ryu, J., Song, I., Sunwoo, Y. & Shon, J. Development of the "Inje Cocktail" for High-throughput Evaluation of Five Human Cytochrome P450 Isoforms in vivo. *Clinical* **82**, 531–540 (2007).
291. Gressier, F., Verstuyft, C., Hardy, P. & Becquemont, L. Response to CYP2D6 substrate antidepressants is predicted by a CYP2D6 composite phenotype based on genotype and comedications with CYP2D6 inhibitors. *J. Neural* (2015).
292. De Andrés, F. *et al.* To Genotype or Phenotype for Personalized Medicine? CYP450 Drug Metabolizing Enzyme Genotype-Phenotype Concordance and Discordance in the Ecuadorian Population. *Omi. A J. Integr. Biol.* **20**, 699–710 (2016).
293. Lynch, T. & Price, A. The effect of cytochrome P450 metabolism on drug response, interactions, and adverse effects. *Am. Fam. Physician* **76**, 391–396 (2007).
294. Kruijtzer, C. M. F. *et al.* Phase II and pharmacologic study of weekly oral paclitaxel plus cyclosporine in patients with advanced non-small-cell lung cancer. *J. Clin. Oncol.* **20**, 4508–16 (2002).
295. Scripture, C. D. & Figg, W. D. Drug interactions in cancer therapy. *Nature Reviews Cancer* (2006). doi:10.1038/nrc1887
296. Riechelmann, R. P. & Del Giglio, A. Drug interactions in oncology: How common are they? *Annals of Oncology* (2009). doi:10.1093/annonc/mdp369

297. Aitken, A. E., Richardson, T. A. & Morgan, E. T. Regulation of drug-metabolizing enzymes and transporters in inflammation. *Annu. Rev. Pharmacol. Toxicol.* **46**, 123–149 (2006).
298. Jover, R., Bort, R., Gómez-Lechón, M. J. & Castell, J. V. Down-regulation of human CYP3A4 by the inflammatory signal interleukin-6: molecular mechanism and transcription factors involved. *FASEB J.* **16**, 1799–1801 (2002).
299. Martínez-Jimé Nez, C. P., Gó Mez-Lechó, M. J., Castell, J. V & Jover, R. Transcriptional Regulation of the Human Hepatic CYP3A4: Identification of a New Distal Enhancer Region Responsive to CCAAT/Enhancer-Binding Protein Isoforms (Liver Activating Protein and Liver Inhibitory Protein). *Mol. Pharmacol.* **67**, 2088–2101 (2005).
300. Aitken, A. E. & Morgan, E. T. Gene-Specific Effects of Inflammatory Cytokines on Cytochrome P450 2C, 2B6 and 3A4 mRNA Levels in Human Hepatocytes. *Drug Metab. Dispos.* **35**, 1687–93 (2007).
301. Dickmann, L. J., Patel, S. K., Rock, D. A., Wienkers, L. C. & Slatter, J. G. Effects of Interleukin-6 (IL-6) and an Anti-IL-6 Monoclonal Antibody on Drug-Metabolizing Enzymes in Human Hepatocyte Culture. *Drug Metab. Dispos.* **39**, 1415–1422 (2011).
302. Dickmann, L., Patel, S., Wienkers, L. & Slatter, J. Effects of Interleukin 1β (IL-1β) and IL-1β/Interleukin 6 (IL-6) Combinations on Drug Metabolizing Enzymes in Human Hepatocyte Culture. *Curr. Drug Metab.* **13**, 930–937 (2012).
303. Nguyen, T. V *et al.* Establishment of a Hepatocyte-Kupffer Cell Coculture Model for Assessment of Proinflammatory Cytokine Effects on Metabolizing Enzymes and Drug Transporters. *DRUG Metab. Dispos. Drug Metab Dispos* **43**, 774–785 (2015).
304. Shedlofsky, S. I., Israel, B. C., McClain, C. J., Hill, D. B. & Blouin, R. A. Endotoxin administration to humans inhibits hepatic cytochrome P450-mediated drug metabolism. *J. Clin. Invest.* **94**, 2209–14 (1994).
305. Shedlofsky, S. I., Israel, B. C., Tosheva, R. & Blouin, R. A. Endotoxin depresses hepatic cytochrome P450-mediated drug metabolism in women. *Br. J. Clin. Pharmacol.* **43**, 627–632 (1997).
306. Rost, K. L., Brockmöller, J., Esdorn, F. & Roots, I. Phenocopies of poor metabolizers of omeprazole caused by liver disease and drug treatment. *J. Hepatol.* **23**, 268–77 (1995).
307. O'Neil, W. M. *et al.* Genotype and phenotype of cytochrome P 450 2D6 in human immunodeficiency virus-positive patients and patients with acquired immunodeficiency syndrome. *Eur. J. Clin. Pharmacol.* **56**, 231–240 (2000).
308. Girardin, F. *et al.* Liver kidney microsomal type 1 antibodies reduce the CYP2D6 activity in patients with chronic hepatitis C virus infection. *J. Viral Hepat.* **19**, 568–573 (2012).
309. Williams, M. L. *et al.* A discordance of the cytochrome P450 2C19 genotype and phenotype in patients with advanced cancer. *Br. J. Clin. Pharmacol.* **49**, 485–488 (2002).
310. Burns, K. E., Goldthorpe, M. A., Porteus, F., Browett, P. & Helsby, N. A. CYP2C19 genotype–phenotype discordance in patients with multiple myeloma leads to an acquired loss of drug-metabolising activity. *Cancer Chemother. Pharmacol.* **73**, 651–655 (2014).
311. Hanahan, D. & Weinberg, R. A. Hallmarks of cancer: the next generation. *Cell* **144**, 646–674 (2011).
312. Roxburgh, C. S. D. & McMillan, D. C. Cancer and systemic inflammation: treat the tumour and treat the host. *Br. J. Cancer* **110**, 1409–12 (2014).
313. Shinko, D., Diakos, C. I., Clarke, S. J. & Charles, K. A. Cancer-Related Systemic Inflammation: The Challenges and Therapeutic Opportunities for Personalized Medicine. *Clin. Pharmacol. Ther.* **102**, 599–610 (2017).
314. Kacevska, M., Robertson, G. R., Clarke, S. J. & Liddle, C. Inflammation and CYP3A4-mediated drug metabolism in advanced cancer: impact and implications for chemotherapeutic drug dosing. *Expert Opin. Drug Metab. Toxicol.* **4**, 137–149 (2008).
315. Jin, Y. *et al.* CYP2D6 genotype, antidepressant use, and tamoxifen metabolism during adjuvant breast cancer treatment. *J. Natl. Cancer Inst.* **97**, 30–9 (2005).
316. de Graan, A.-J. M. *et al.* Dextromethorphan As a Phenotyping Test to Predict Endoxifen Exposure in Patients on Tamoxifen Treatment. *J. Clin. Oncol.* **29**, 3240–3246 (2011).
317. Rivory, L. P., Slaviero, K. A. & Clarke, S. J. Hepatic cytochrome P450 3A drug metabolism is reduced in cancer patients who have an acute-phase response. *Br. J. Cancer* **87**, 277–280 (2002).
318. Harvey, R. D. & Morgan, E. T. Cancer, Inflammation, and Therapy: Effects on Cytochrome P450–Mediated Drug Metabolism and Implications for Novel Immunotherapeutic Agents. *Clin. Pharmacol. Ther.* **96**, 449–457 (2014).
319. Kotlyar, M. & Carson, S. W. Effects of obesity on the cytochrome P450 enzyme system. *Int. J. Clin. Pharmacol. Ther.* **37**, 8–19 (1999).
320. Tomankova, V., Anzenbacher, P. & Anzenbacherova, E. Effects of obesity on liver cytochromes P450 in various animal models. *Biomed. Pap.* **161**, 144–151 (2017).
321. Morrin, H. *et al.* The Christchurch Tissue Bank to support cancer research. *N. Z. Med. J.* **118**, U1735

(2005).
322. Lee, M.-J., Wu, Y. & Fried, S. K. A Modified Protocol to Maximize Differentiation of Human Preadipocytes and Improve Metabolic Phenotypes. *Obesity* **20**, 2334–2340 (2012).
323. Timenetsky, J., Santos, L. M., Buzinhani, M. & Mettifogo, E. Detection of multiple mycoplasma infection in cell cultures by PCR. *Braz J Med Biol Res Brazilian J. Med. Biol. Res.* **39**, 907–914 (2006).
324. Vichai, V. & Kirtikara, K. Sulforhodamine B colorimetric assay for cytotoxicity screening. *Nat. Protoc.* (2006). doi:10.1038/nprot.2006.179
325. Mosmann, T. Rapid colorimetric assay for cellular growth and survival: Application to proliferation and cytotoxicity assays. *J. Immunol. Methods* (1983). doi:10.1016/0022-1759(83)90303-4
326. Consortium, G. O. Gene Ontology Annotations and Resources. *Nucleic Acids Res.* **41**, D530–D535 (2013).
327. Mi, H., Muruganujan, A. & Thomas, P. D. PANTHER in 2013: modeling the evolution of gene function, and other gene attributes, in the context of phylogenetic trees. *Nucleic Acids Res.* **41**, D377-86 (2013).
328. Mi, H., Muruganujan, A., Casagrande, J. T. & Thomas, P. D. Large-scale gene function analysis with the PANTHER classification system. *Nat. Protoc.* **8**, 1551–1566 (2013).
329. Mi, H. & Thomas, P. PANTHER Pathway: An Ontology-Based Pathway Database Coupled with Data Analysis Tools. in 123–140 (Humana Press, 2009). doi:10.1007/978-1-60761-175-2_7
330. Curtis, C. *et al.* The genomic and transcriptomic architecture of 2,000 breast tumours reveals novel subgroups. *Nature* (2012). doi:10.1038/nature10983
331. Zhang, M., Moore, G., Doogue, M. & Strother, M. Simultaneous determination of the phenotyping cocktail drugs and their cytochrome P450-specific probe metabolites in human serum and urine by liquid chromatography/tandem mass spectrometry. in *Australasian Society of Clinical and Experimental Pharmacologists and Toxicologists* Abstract 422 (2018).
332. United States Food and Drug Administration. *Guidance for Industry In Vivo Drug Metabolism/Drug Interaction Studies-Study Design, Data Analysis, and Recommendations for Dosing and Labeling*. (1999).
333. Calderón-González, K. G. *et al.* Determination of the protein expression profiles of breast cancer cell lines by quantitative proteomics using iTRAQ labelling and tandem mass spectrometry. *J. Proteomics* (2015). doi:10.1016/j.jprot.2015.04.018
334. Fuller, H. R. & Morris, G. E. Quantitative Proteomics Using iTRAQ Labeling and Mass Spectrometry. *Integr. Proteomics* (2012). doi:10.5772/31469
335. Neve, R. M. *et al.* A collection of breast cancer cell lines for the study of functionally distinct cancer subtypes. *Cancer Cell* **10**, 515–27 (2006).
336. Holliday, D. L. & Speirs, V. Choosing the right cell line for breast cancer research. *Breast Cancer Research* (2011). doi:10.1186/bcr2889
337. Rezaul, K. *et al.* Differential protein expression profiles in estrogen receptor-positive and -negative breast cancer tissues using label-free quantitative proteomics. *Genes Cancer* **1**, 251–71 (2010).
338. Bresnick, A. R., Weber, D. J. & Zimmer, D. B. S100 proteins in cancer. *Nat. Rev. Cancer* **15**, 96–109 (2015).
339. Lizarbe, M. A., Barrasa, J. I., Olmo, N., Gavilanes, F. & Turnay, J. Annexin-Phospholipid Interactions. Functional Implications. *Int. J. Mol. Sci.* **14**, 2652 (2013).
340. Jaiswal, J. K. & Nylandsted, J. S100 and annexin proteins identify cell membrane damage as the Achilles heel of metastatic cancer cells. *Cell Cycle* **14**, 502–9 (2015).
341. Myrvang, H. K., Guo, X., Li, C. & Dekker, L. V. Protein interactions between surface annexin A2 and S100A10 mediate adhesion of breast cancer cells to microvascular endothelial cells. *FEBS Lett.* **587**, 3210–3215 (2013).
342. Aranda, J. F. *et al.* MYADM regulates Rac1 targeting to ordered membranes required for cell spreading and migration. *Mol. Biol. Cell* **22**, 1252–1262 (2011).
343. Pettersson, M., Dannaeus, K., Nilsson, K. & Jönsson, J.-I. Isolation of MYADM, a novel hematopoietic-associated marker gene expressed in multipotent progenitor cells and up-regulated during myeloid differentiation. *J. Leukoc. Biol.* **67**, 423–431 (2000).
344. Chaerkady, R. *et al.* A quantitative proteomic approach for identification of potential biomarkers in hepatocellular carcinoma. *J. Proteome Res.* **7**, 4289–98 (2008).
345. Feral, C. C. *et al.* CD98hc (SLC3A2) mediates integrin signaling. *Proc. Natl. Acad. Sci. U. S. A.* **102**, 355–60 (2005).
346. Sommer, A. *et al.* A proteomic analysis of chemoresistance development via sequential treatment with doxorubicin reveals novel players in MCF‐7 breast cancer cells. *Int. J. Mol. Med.* **42**, 1987–1997 (2018).

347. Wang, Z., Liu, Q., Chen, Q., Zhu, R. & Zhu, H. [Overexpression of NDRG1: relationship with proliferative activity and invasiveness of breast cancer cell line and breast cancer metastasis]. *Zhonghua bing li xue za zhi = Chinese J. Pathol.* **35**, 333–8 (2006).
348. Pelden, S., Insawang, T., Thuwajit, C. & Thuwajit, P. The trefoil factor 1 (TFF1) protein involved in doxorubicin-induced apoptosis resistance is upregulated by estrogen in breast cancer cells. *Oncol. Rep.* **30**, 1518–1526 (2013).
349. Sun, S. *et al.* Phosphoglycerate kinase-1 is a predictor of poor survival and a novel prognostic biomarker of chemoresistance to paclitaxel treatment in breast cancer. *Br. J. Cancer* **112**, 1332–1339 (2015).
350. Cangul, H. Hypoxia upregulates the expression of the NDRG1 gene leading to its overexpression in various human cancers. *BMC Genet.* **5**, 27 (2004).
351. Fang, B. A. *et al.* Molecular functions of the iron-regulated metastasis suppressor, NDRG1, and its potential as a molecular target for cancer therapy. *Biochim. Biophys. Acta - Rev. Cancer* **1845**, 1–19 (2014).
352. Bandyopadhyay, S. *et al.* Role of the putative tumor metastasis suppressor gene Drg-1 in breast cancer progression. *Oncogene* **23**, 5675–5681 (2004).
353. Mao, X.-Y. *et al.* Increased N-myc downstream-regulated gene 1 expression is associated with breast atypia-to-carcinoma progression. *Tumor Biol.* **32**, 1271–1276 (2011).
354. Ring, B. Z. *et al.* Novel prognostic immunohistochemical biomarker panel for estrogen receptor-positive breast cancer. *J. Clin. Oncol.* **24**, 3039–47 (2006).
355. Gillesby, B. E. & Zacharewski, T. R. pS2 (TFF1) levels in human breast cancer tumor samples: correlation with clinical and histological prognostic markers. *Breast Cancer Res. Treat.* **56**, 251–263 (1999).
356. Amiry, N. *et al.* Trefoil Factor-1 (TFF1) Enhances Oncogenicity of Mammary Carcinoma Cells. *Endocrinology* **150**, 4473–4483 (2009).
357. Buache, E. *et al.* Deficiency in trefoil factor 1 (TFF1) increases tumorigenicity of human breast cancer cells and mammary tumor development in TFF1-knockout mice. *Oncogene* **30**, 3261–3273 (2011).
358. Evans, C. *et al.* An insight into iTRAQ: where do we stand now? *Anal. Bioanal. Chem.* **404**, 1011–1027 (2012).
359. Lane, D. J. R., Saletta, F., Rahmanto, Y. S., Kovacevic, Z. & Richardson, D. R. N-myc Downstream Regulated 1 (NDRG1) Is Regulated by Eukaryotic Initiation Factor 3a (eIF3a) during Cellular Stress Caused by Iron Depletion. *PLoS One* **8**, e57273 (2013).
360. Hwang, T. L., Liang, Y., Chien, K. Y. & Yu, J. S. Overexpression and elevated serum levels of phosphoglycerate kinase 1 in pancreatic ductal adenocarcinoma. *Proteomics* **6**, 2259–2272 (2006).
361. Wang, J. *et al.* Characterization of phosphoglycerate kinase-1 expression of stromal cells derived from tumor microenvironment in prostate cancer progression. *Cancer Res.* **70**, 471–480 (2010).
362. Yan, H. *et al.* Over-expression of cofilin-1 and phosphoglycerate kinase 1 in astrocytomas involved in pathogenesis of radioresistance. *CNS Neurosci. Ther.* **18**, 729–736 (2012).
363. Ahmad, S. S. *et al.* Phosphoglycerate kinase 1 as a promoter of metastasis in colon cancer. *Int. J. Oncol.* **43**, 586–590 (2013).
364. Xie, H. *et al.* PGK1 Drives Hepatocellular Carcinoma Metastasis by Enhancing Metabolic Process. *Int. J. Mol. Sci.* **18**, (2017).
365. Zieker, D. *et al.* Phosphoglycerate kinase 1 a promoting enzyme for peritoneal dissemination in gastric cancer. *Int. J. Cancer* **126**, 1513–1520 (2010).
366. Ameis, H. M. *et al.* PGK1 as predictor of CXCR4 expression, bone marrow metastases and survival in neuroblastoma. *PLoS One* **8**, (2013).
367. Duan, Z. *et al.* Overexpression of human phosphoglycerate kinase 1 (PKG1) induces a multidrug resistance phenotype. *Anticancer Res.* **22**, 1933–1941 (2002).
368. Schneider, C. C. *et al.* Metabolic alteration – Overcoming therapy resistance in gastric cancer via PGK-1 inhibition in a combined therapy with standard chemotherapeutics. *Int. J. Surg.* **22**, 92–98 (2015).
369. Zhang, D. *et al.* Proteomic Study Reveals That Proteins Involved in Metabolic and Detoxification Pathways Are Highly Expressed in HER-2/ neu -positive Breast Cancer*. *Mol. Cell. Proteomics* **4**, 1686–1696 (2005).
370. Bernstein, B. E. & Hol, W. G. J. Crystal structures of substrates and products bound to the phosphoglycerate kinase active site reveal the catalytic mechanism. *Biochemistry* **37**, 4429–4436 (1998).
371. Fu, D. *et al.* PGK1 is a Potential Survival Biomarker and Invasion Promoter by Regulating the HIF-1α–Mediated Epithelial-Mesenchymal Transition Process in Breast Cancer. *Cell. Physiol. Biochem.* **51**, 2434–2444 (2018).

372. Shashni, B., Sakharkar, K. R., Nagasaki, Y. & Sakharkar, M. K. Glycolytic enzymes PGK1 and PKM2 as novel transcriptional targets of PPARγ in breast cancer pathophysiology. *J. Drug Target.* **21**, 161–174 (2013).
373. Lay, A. J. *et al.* Phosphoglycerate kinase acts in tumour angiogenesis as a disulphide reductase. *Nature* **408**, 869–873 (2000).
374. Li, X. *et al.* Mitochondria-Translocated PGK1 Functions as a Protein Kinase to Coordinate Glycolysis and the TCA Cycle in Tumorigenesis. *Mol. Cell* **61**, (2016).
375. Qian, X., Li, X. & Lu, Z. Protein kinase activity of the glycolytic enzyme PGK1 regulates autophagy to promote tumorigenesis. *Autophagy* **13**, 1246–1247 (2017).
376. Lu, Z. & Hunter, T. Metabolic Kinases Moonlighting as Protein Kinases. *Trends Biochem. Sci.* **43**, 301–310 (2018).
377. Fantin, V., St-Pierre, J. & Leder, P. Attenuation of LDH-A expression uncovers a link between glycolysis, mitochondrial physiology, and tumor maintenance. *Cancer Cell* **9**, 425–434 (2006).
378. Mack, N., Mazzio, E. A., Bauer, D., Flores-Rozas, H. & Soliman, K. F. A. Stable shRNA Silencing of Lactate Dehydrogenase A (LDHA) in Human MDA-MB-231 Breast Cancer Cells Fails to Alter Lactic Acid Production, Glycolytic Activity, ATP or Survival. *Anticancer Res.* **37**, 1205–1212 (2017).
379. Baenke, F. *et al.* Functional screening identifies MCT4 as a key regulator of breast cancer cell metabolism and survival. *J. Pathol.* **237**, 152–165 (2015).
380. Koppenol, W. H., Bounds, P. L. & Dang, C. V. Otto Warburg's contributions to current concepts of cancer metabolism. *Nat. Rev. Cancer* **11**, 325–337 (2011).
381. Lanning, N. J. *et al.* Metabolic profiling of triple-negative breast cancer cells reveals metabolic vulnerabilities. *Cancer Metab.* **5**, 6 (2017).
382. Diedrich, J. D. *et al.* Bone marrow adipocytes promote the Warburg phenotype in metastatic prostate tumors via HIF-1a activation. *Oncotarget* **7**, 64854–64877 (2016).
383. Bruce, C. R. *et al.* Overexpression of carnitine palmitoyltransferase-1 in skeletal muscle is sufficient to enhance fatty acid oxidation and improve high-fat diet-induced insulin resistance. *Diabetes* **58**, 550–8 (2009).
384. Kao, J. *et al.* Molecular profiling of breast cancer cell lines defines relevant tumor models and provides a resource for cancer gene discovery. *PLoS One* **4**, e6146 (2009).
385. Gasco, M., Shami, S. & Crook, T. The p53 pathway in breast cancer. *Breast Cancer Res.* **4**, 70–76 (2002).
386. Mukohara, T. PI3K mutations in breast cancer: prognostic and therapeutic implications. *Breast Cancer Targets Ther.* 111 (2015). doi:10.2147/BCTT.S60696
387. Contractor, T. & Harris, C. R. p53 negatively regulates transcription of the pyruvate dehydrogenase kinase Pdk2. *Cancer Res.* **72**, 560–567 (2012).
388. Wang, F. *et al.* Mammary fat of breast cancer: gene expression profiling and functional characterization. *PLoS One* **9**, e109742 (2014).
389. van Marken Lichtenbelt, W. D. *et al.* Cold-Activated Brown Adipose Tissue in Healthy Men. *N. Engl. J. Med.* **360**, 1500–1508 (2009).
390. Manabe, Y., Toda, S., Miyazaki, K. & Sugihara, H. Mature adipocytes, but not preadipocytes, promote the growth of breast carcinoma cells in collagen gel matrix culture through cancer-stromal cell interactions. *J. Pathol.* **201**, 221–228 (2003).
391. Duong, M. N. *et al.* The fat and the bad: Mature adipocytes, key actors in tumor progression and resistance. *Oncotarget* **8**, 57622–57641 (2017).
392. Semenza, G. L., Roth, P. H., Fang, H. M. & Wang, G. L. Transcriptional regulation of genes encoding glycolytic enzymes by hypoxia-inducible factor 1. *J. Biol. Chem.* (1994).
393. Semenza, G. L. HIF-1: upstream and downstream of cancer metabolism. *Current Opinion in Genetics and Development* (2010). doi:10.1016/j.gde.2009.10.009
394. Robin, E. D., Murphy, B. J. & Theodore, J. Coordinate regulation of glycolysis by hypoxia in mammalian cells. *J. Cell. Physiol.* (1984). doi:10.1002/jcp.1041180311
395. Mathupala, S. P., Colen, C. B., Parajuli, P. & Sloan, A. E. Lactate and malignant tumors: a therapeutic target at the end stage of glycolysis. *J. Bioenerg. Biomembr.* **39**, 73–7 (2007).
396. Feron, O. Pyruvate into lactate and back: From the Warburg effect to symbiotic energy fuel exchange in cancer cells. *Radiotherapy and Oncology* **92**, 329–333 (2009).
397. Guo, S. *et al.* PGK1 and GRP78 overexpression correlates with clinical significance and poor prognosis in Chinese endometrial cancer patients. *Oncotarget* (2017). doi:10.18632/oncotarget.23090
398. Zhou, J.-W., Tang, J.-J., Sun, W. & Wang, H. PGK1 facilities cisplatin chemoresistance by triggering HSP90/ERK pathway mediated DNA repair and methylation in endometrial endometrioid adenocarcinoma. *Mol. Med.* **25**, 11 (2019).
399. Chouchane, L. *et al.* Protein alterations in infiltrating ductal carcinomas of the breast as detected by

nonequilibrium pH gradient electrophoresis and mass spectrometry. *J. Biomed. Biotechnol.* (2008). doi:10.1155/2008/564127
400. Dimmer, K.-S., Friedrich, B., Lang, F., Deitmer, J. W. & Broer, S. The low-affinity monocarboxylate transporter MCT4 is adapted to the export of lactate in highly glycolytic cells. *Biochem. J.* (2015). doi:10.1042/bj3500219
401. Ganapathy, V., Thangaraju, M. & Prasad, P. D. Nutrient transporters in cancer: Relevance to Warburg hypothesis and beyond. *Pharmacology and Therapeutics* (2009). doi:10.1016/j.pharmthera.2008.09.005
402. Pinheiro, C. *et al.* Increased expression of monocarboxylate transporters 1, 2, and 4 in colorectal carcinomas. *Virchows Arch.* (2008). doi:10.1007/s00428-007-0558-5
403. Kroemer, G. & Pouyssegur, J. Tumor Cell Metabolism: Cancer's Achilles' Heel. *Cancer Cell* (2008). doi:10.1016/j.ccr.2008.05.005
404. Doyen, J. *et al.* Expression of the hypoxia-inducible monocarboxylate transporter MCT4 is increased in triple negative breast cancer and correlates independently with clinical outcome. *Biochem. Biophys. Res. Commun.* **451**, 54–61 (2014).
405. Popanda, O., Fox, G. & Thielmann, H. W. Modulation of DNA polymerases alpha, delta and epsilon by lactate dehydrogenase and 3-phosphoglycerate kinase. *Biochim. Biophys. Acta* (1998).
406. Boukouris, A. E., Zervopoulos, S. D. & Michelakis, E. D. Metabolic Enzymes Moonlighting in the Nucleus: Metabolic Regulation of Gene Transcription. *Trends in Biochemical Sciences* (2016). doi:10.1016/j.tibs.2016.05.013
407. Yu-Wen Tseng, Yu-Chan Chang, and M. H. Translocation and Targeting of PGK1 to HTATSF1 Regulate Cancer Cell Metastatic Ability. in *Experimental Biology* (2019).
408. Li, X. *et al.* Nuclear PGK1 Alleviates ADP-Dependent Inhibition of CDC7 to Promote DNA Replication. *Mol. Cell* (2018). doi:10.1016/j.molcel.2018.09.007
409. Butera, D. *et al.* Characterization of a reduced form of plasma plasminogen as the precursor for angiostatin formation. *J. Biol. Chem.* (2014). doi:10.1074/jbc.M113.539924
410. Zhang, Y. *et al.* Macrophage-Associated PGK1 Phosphorylation Promotes Aerobic Glycolysis and Tumorigenesis. *Mol. Cell* (2018). doi:10.1016/j.molcel.2018.06.023
411. Dong, W., Li, H. & Wu, X. Rab11-FIP2 suppressed tumor growth via regulation of PGK1 ubiquitination in non-small cell lung cancer. *Biochem. Biophys. Res. Commun.* (2019). doi:10.1016/j.bbrc.2018.11.108
412. Hu, H. *et al.* Acetylation of PGK1 promotes liver cancer cell proliferation and tumorigenesis. *Hepatology* **65**, 515–528 (2017).
413. Xu, Dan, Aka, J., Wang, R. & Lin, S.-X. 17beta-hydroxysteroid dehydrogenase type 5 is negatively correlated to apoptosis inhibitor GRP78 and tumor-secreted protein PGK1, and modulates breast cancer cell viability and proliferation. *J. Steroid Biochem. Mol. Biol.* **171**, 270–280 (2017).
414. Ganini, D. *et al.* Fluorescent proteins such as eGFP lead to catalytic oxidative stress in cells. *Redox Biol.* **12**, 462–468 (2017).
415. Mantovani, F., Collavin, L. & Del Sal, G. Mutant p53 as a guardian of the cancer cell. *Cell Death and Differentiation* (2019). doi:10.1038/s41418-018-0246-9
416. Freed-Pastor, W. A. & Prives, C. Mutant p53: One name, many proteins. *Genes Dev.* (2012). doi:10.1101/gad.190678.112
417. Chuthapisith, S., Layfield, R., Kerr, I., Hughes, C. & Eremin, O. Proteomic profiling of MCF-7 breast cancer cells with chemoresistance to different types of anti-cancer drugs. *Int. J. Oncol.* (2007). doi:10.3892/ijo.30.6.1545
418. Peng, X. *et al.* A proteomic investigation into adriamycin chemo-resistance of human leukemia K562 cells. *Mol. Cell. Biochem.* (2011). doi:10.1007/s11010-011-0730-8
419. Gong, F. *et al.* Proteomic analysis of cisplatin resistance in human ovarian cancer using 2-DE method. *Mol. Cell. Biochem.* (2011). doi:10.1007/s11010-010-0648-6
420. Lincet, H. *et al.* Comparative 2D-DIGE proteomic analysis of ovarian carcinoma cells: Toward a reorientation of biosynthesis pathways associated with acquired platinum resistance. *J. Proteomics* (2012). doi:10.1016/j.jprot.2011.10.030
421. Cortesi, L. *et al.* Identification of protein clusters predictive of response to chemotherapy in breast cancer patients. *J. Proteome Res.* (2009). doi:10.1021/pr900239h
422. Horwitz, S. B. Taxol (paclitaxel): mechanisms of action. *Ann. Oncol. Off. J. Eur. Soc. Med. Oncol.* **5 Suppl 6**, S3-6 (1994).
423. Weaver, B. A. How Taxol/paclitaxel kills cancer cells. *Mol. Biol. Cell* **25**, 2677–81 (2014).
424. Ginestier, C. *et al.* ALDH1 Is a Marker of Normal and Malignant Human Mammary Stem Cells and a Predictor of Poor Clinical Outcome. *Cell Stem Cell* **1**, 555–567 (2007).
425. Morimoto, K. *et al.* Stem cell marker aldehyde dehydrogenase 1-positive breast cancers are

characterized by negative estrogen receptor, positive human epidermal growth factor receptor type 2, and high Ki67 expression. *Cancer Sci.* **100**, 1062–1068 (2009).
426. Tanei, T. *et al.* Association of Breast Cancer Stem Cells Identified by Aldehyde Dehydrogenase 1 Expression with Resistance to Sequential Paclitaxel and Epirubicin-Based Chemotherapy for Breast Cancers. *Clin. Cancer Res.* **15**, 4234–4241 (2009).
427. Brandt, K. E. *et al.* Augmentation of intracellular iron using iron sucrose enhances the toxicity of pharmacological ascorbate in colon cancer cells. *Redox Biol.* (2018). doi:10.1016/j.redox.2017.08.017
428. Padmashali, R., You, H., Karnik, N., Lei, P. & Andreadis, S. T. Adherens junction formation inhibits lentivirus entry and gene transfer. *PLoS One* (2013). doi:10.1371/journal.pone.0079265
429. De Smedt, S. C., Demeester, J. & Hennink, W. E. Cationic polymer based gene delivery systems. *Pharmaceutical Research* (2000). doi:10.1023/A:1007548826495
430. Samal, S. K. *et al.* Cationic polymers and their therapeutic potential. *Chemical Society Reviews* (2012). doi:10.1039/c2cs35094g
431. Park, T. G., Jeong, J. H. & Kim, S. W. Current status of polymeric gene delivery systems. *Advanced Drug Delivery Reviews* (2006). doi:10.1016/j.addr.2006.03.007
432. Pfeifer, A. & Verma, I. M. GENE THERAPY : Promises and Problems. *Annu. Rev. Genomics Hum. Genet.* **2**, 177–211 (2001).
433. Mortensen, R. M. & Kingston, R. E. Selection of transfected mammalian cells. *Current Protocols in Molecular Biology* (2009). doi:10.1002/0471142727.mb0905s62
434. Yamano, S., Dai, J. & Moursi, A. M. Comparison of Transfection Efficiency of Nonviral Gene Transfer Reagents. *Mol. Biotechnol.* **46**, 287–300 (2010).
435. Wang, T., Larcher, L. M., Ma, L. & Veedu, R. N. Systematic Screening of Commonly Used Commercial Transfection Reagents towards Efficient Transfection of Single-Stranded Oligonucleotides. *Molecules* **23**, (2018).
436. Schulz, D. M. *et al.* Identification of differentially expressed proteins in triple-negative breast carcinomas using DIGE and mass spectrometry. *J. Proteome Res.* (2009). doi:10.1021/pr900071h
437. Ullah, M. S., Davies, A. J. & Halestrap, A. P. The plasma membrane lactate transporter MCT4, but not MCT1, is up-regulated by hypoxia through a HIF-1α-dependent mechanism. *J. Biol. Chem.* (2006). doi:10.1074/jbc.M511397200
438. Vaupel, P. & Mayer, A. Hypoxia in cancer: Significance and impact on clinical outcome. *Cancer and Metastasis Reviews* (2007). doi:10.1007/s10555-007-9055-1
439. Milani, M. & Harris, A. L. Targeting tumour hypoxia in breast cancer. *Eur. J. Cancer* **44**, 2766–2773 (2008).
440. Konecny, G. E. *et al.* Association between HER-2/neu and Vascular Endothelial Growth Factor Expression Predicts Clinical Outcome in Primary Breast Cancer Patients. *Clin. Cancer Res.* **10**, 1706–1716 (2004).
441. Ballard-Barbash, R. *et al.* Physical activity, biomarkers, and disease outcomes in cancer survivors: a systematic review. *J. Natl. Cancer Inst.* **104**, 815–40 (2012).
442. Löf, M., Bergström, K. & Weiderpass, E. Physical activity and biomarkers in breast cancer survivors: A systematic review. *Maturitas* **73**, 134–142 (2012).
443. Guo, Y., Chen, Y., Tan, Z., Klaassen, C. D. & Zhou, H. Repeated administration of berberine inhibits cytochromes P450 in humans. *Eur. J. Clin. Pharmacol.* **68**, 213–217 (2012).
444. Kim, D.-S., Kim, Y., Jeon, J.-Y. & Kim, M.-G. Effect of Red Ginseng on cytochrome P450 and P-glycoprotein activities in healthy volunteers. *J. Ginseng Res.* **40**, 375–381 (2016).
445. Byrne, M. M., Tannenbaum, S. L., Glück, S., Hurley, J. & Antoni, M. Participation in Cancer Clinical Trials. *Med. Decis. Mak.* **34**, 116–126 (2014).
446. Fouad, M. N. *et al.* Enrollment of Patients With Lung and Colorectal Cancers Onto Clinical Trials. *J. Oncol. Pract.* **9**, e40–e47 (2013).
447. Moorcraft, S. Y. *et al.* Patients' willingness to participate in clinical trials and their views on aspects of cancer research: results of a prospective patient survey. *Trials* **17**, 17 (2016).
448. Kessel, K. A. *et al.* Cancer clinical trials – Survey evaluating patient participation and acceptance in a university-based Comprehensive Cancer Center (CCC). *Clin. Transl. Radiat. Oncol.* **13**, 44–49 (2018).
449. McDonald, A. M. *et al.* What influences recruitment to randomised controlled trials? A review of trials funded by two UK funding agencies. *Trials* **7**, 9 (2006).
450. Campbell, M. *et al.* Recruitment to randomised trials: strategies for trial enrolment and participation study. The STEPS study. *Health Technol. Assess. (Rockv).* **11**, (2007).
451. Fogel, D. B. Factors associated with clinical trials that fail and opportunities for improving the likelihood of success: A review. *Contemp. Clin. trials Commun.* **11**, 156–164 (2018).
452. Oh, K.-S., Park, S.-J., Shinde, D. D., Shin, J.-G. & Kim, D.-H. High-sensitivity liquid chromatography–tandem mass spectrometry for the simultaneous determination of five drugs and their

cytochrome P450-specific probe metabolites in human plasma. *J. Chromatogr. B* **895**–**896**, 56–64 (2012).
453. Inui, N. *et al.* Chronological Effects of Rifampicin Discontinuation on Cytochrome P450 Activity in Healthy Japanese Volunteers, Using the Cocktail Method. *Clin. Pharmacol. Ther.* **94**, 702–708 (2013).
454. Tanaka, S. *et al.* Simultaneous LC-MS/MS Analysis of the Plasma Concentrations of a Cocktail of 5 Cytochrome P450 Substrate Drugs and Their Metabolites. *Biol. Pharm. Bull* **10**, 79 (2014).
455. Williams, D. *et al.* Use of a cocktail probe to assess potential drug interactions with cytochrome P450 after administration of belatacept, a costimulatory immunomodulator. *Br. J. Clin. Pharmacol.* **83**, 370–380 (2017).
456. Heo, J.-K. *et al.* Simultaneous Determination of Five Cytochrome P450 Probe Substrates and Their Metabolites and Organic Anion Transporting Polypeptide Probe Substrate in Human Plasma Using Liquid Chromatography-Tandem Mass Spectrometry. *Pharmaceutics* **10**, (2018).
457. Demark-Wahnefried, W., Winer, E. P. & Rimer, B. K. Why women gain weight with adjuvant chemotherapy for breast cancer. *J. Clin. Oncol.* **11**, 1418–29 (1993).
458. Makari-Judson, G., Braun, B., Jerry, D. J. & Mertens, W. C. Weight gain following breast cancer diagnosis: Implication and proposed mechanisms. *World J. Clin. Oncol.* **5**, 272 (2014).
459. Freedman, R. J. *et al.* Weight and Body Composition Changes during and after Adjuvant Chemotherapy in Women with Breast Cancer. *J. Clin. Endocrinol. Metab.* **89**, 2248–2253 (2004).
460. Vance, V., Mourtzakis, M., McCargar, L. & Hanning, R. Weight gain in breast cancer survivors: prevalence, pattern and health consequences. *Obes. Rev.* **12**, 282–294 (2011).
461. Thivat, E. *et al.* Weight change during chemotherapy changes the prognosis in non metastatic breast cancer for the worse. *BMC Cancer* **10**, 648 (2010).
462. Mentoor, I., Engelbrecht, A.-M. & Nell, T. Fatty acids: Adiposity and breast cancer chemotherapy, a bad synergy? *Prostaglandins, Leukot. Essent. Fat. Acids* **140**, 18–33 (2019).
463. Verna, E. C. & Berk, P. D. Role of fatty acids in the pathogenesis of obesity and fatty liver: Impact of bariatric surgery. *Seminars in Liver Disease* (2008). doi:10.1055/s-0028-1091985
464. Krenkel, O. & Tacke, F. Liver macrophages in tissue homeostasis and disease. *Nat. Rev. Immunol.* **17**, 306–321 (2017).
465. Wells, J. C. K. & Fewtrell, M. S. Measuring body composition. *Archives of Disease in Childhood* (2006). doi:10.1136/adc.2005.085522
466. Kushner, R. F. Bioelectrical impedance analysis: A review of principles and applications. *Journal of the American College of Nutrition* (1992).
467. Mialich, M. S., Maria, J., Sicchieri, F., Afonso, A. & Junior, J. Analysis of Body Composition : A Critical Review of the Use of Bioelectrical Impedance Analysis. *Int. J. Clin. Nutr. 2014, Vol. 2, No. 1, 1-10* (2014). doi:10.12691/ijcn-2-1-1
468. Dehghan, M. & Merchant, A. T. Is bioelectrical impedance accurate for use in large epidemiological studies? *Nutrition Journal* (2008). doi:10.1186/1475-2891-7-26
469. Kabiri, L. S., Hernandez, D. C. & Mitchell, K. Reliability, validity, and diagnostic value of a pediatric bioelectrical impedance analysis scale. *Child. Obes.* (2015). doi:10.1089/chi.2014.0156
470. Blew, R. M. *et al.* Assessing the Validity of Body Mass Index Standards in Early Postmenopausal Women. *Obes. Res.* **10**, 799–808 (2002).
471. Lund, L. W., Ammitzbøll, G., Hansen, D. G., Andersen, E. A. W. & Dalton, S. O. Adherence to a long-term progressive resistance training program, combining supervised and home-based exercise for breast cancer patients during adjuvant treatment. *Acta Oncol. (Madr).* **58**, 650–657 (2019).
472. Wagoner, C. W. *et al.* Self-Reported Physical Activity at Breast Cancer Diagnosis is Associated with Greater Physical Activity During Chemotherapy. *Med. Sci. Sport. Exerc.* **50**, 707–708 (2018).
473. Kirkham, A. A. *et al.* Exercise Prescription and Adherence for Breast Cancer: One Size Does Not FITT All. *Med. Sci. Sport. Exerc* **50**, 177–186 (2018).
474. Dreher, N. *et al.* Fitbit usage in breast cancer patients undergoing chemotherapy. *Clin. Breast Cancer* (2019). doi:10.1016/J.CLBC.2019.05.005
475. Moore, P. A. *et al.* BLyS: Member of the Tumor Necrosis Factor Family and B Lymphocyte Stimulator. *Science (80-.).* **285**, 260–263 (1999).
476. Mackay, F., Silveira, P. A. & Brink, R. B cells and the BAFF/APRIL axis: fast-forward on autoimmunity and signaling. *Curr. Opin. Immunol.* **19**, 327–336 (2007).
477. Nardelli, B. *et al.* Synthesis and release of B-lymphocyte stimulator from myeloid cells. *Blood* **97**, 198–204 (2001).
478. Do, M.-S. *et al.* Inflammatory Gene Expression Patterns Revealed by DNA Microarray Analysis in TNF-α-treated SGBS Human Adipocytes. *Yonsei Med. J.* **47**, 729 (2006).
479. Kim, Y.-H., Choi, B.-H., Cheon, H.-G. & Do, M.-S. B cell activation factor (BAFF) is a novel adipokine that links obesity and inflammation. *Exp. Mol. Med.* **41**, 208 (2009).

480. Kim, M.-Y., Kim, D.-H. & Do, M.-S. B-cell-activating factor is a regulator of adipokines and a possible mediator between adipocytes and macrophages. *Exp. Mol. Med.* **45**, e4–e4 (2013).
481. Kim, D.-H. & Do, M.-S. BAFF knockout improves systemic inflammation via regulating adipose tissue distribution in high-fat diet-induced obesity. *Exp. Mol. Med.* **47**, e129–e129 (2015).
482. Hamada, M. *et al.* B Cell-Activating Factor Controls the Production of Adipokines and Induces Insulin Resistance. *Obesity* **19**, 1915–1922 (2011).
483. Pelekanou, V. *et al.* Expression of TNF-superfamily members BAFF and APRIL in breast cancer: Immunohistochemical study in 52 invasive ductal breast carcinomas. *BMC Cancer* **8**, 76 (2008).
484. Zhu, J. *et al.* BlyS is up-regulated by hypoxia and promotes migration of human breast cancer cells. *J. Exp. Clin. Cancer Res.* **31**, 31 (2012).
485. Bootcov, M. R. *et al.* MIC-1, a novel macrophage inhibitory cytokine, is a divergent member of the TGF-β superfamily. *Proc. Natl. Acad. Sci. U. S. A.* (1997). doi:10.1073/pnas.94.21.11514
486. Fairlie, W. D. *et al.* MIC-1 is a novel TGF-β superfamily cytokine associated with macrophage activation. *Journal of Leukocyte Biology* (1999). doi:10.1002/jlb.65.1.2
487. Bauskin, A. R. *et al.* Role of Macrophage Inhibitory Cytokine-1 in Tumorigenesis and Diagnosis of Cancer: Figure 1. *Cancer Res.* **66**, 4983–4986 (2006).
488. Mimeault, M. & Batra, S. K. Divergent molecular mechanisms underlying the pleiotropic functions of macrophage inhibitory cytokine-1 in cancer. *J. Cell. Physiol.* **224**, 626–635 (2010).
489. Ding, Q. *et al.* Identification of Macrophage Inhibitory Cytokine-1 in Adipose Tissue and Its Secretion as an Adipokine by Human Adipocytes. *Endocrinology* **150**, 1688–1696 (2009).
490. Modlich, O., Prisack, H.-B., Munnes, M., Audretsch, W. & Bojar, H. Immediate Gene Expression Changes After the First Course of Neoadjuvant Chemotherapy in Patients with Primary Breast Cancer Disease. *Clin. Cancer Res.* **10**, 6418–6431 (2004).
491. Johnen, H. *et al.* Tumor-induced anorexia and weight loss are mediated by the TGF-β superfamily cytokine MIC-1. *Nat. Med.* **13**, 1333–1340 (2007).
492. Deshmane, S. L., Kremlev, S., Amini, S. & Sawaya, B. E. Monocyte chemoattractant protein-1 (MCP-1): an overview. *J. Interferon Cytokine Res.* **29**, 313–26 (2009).
493. Kanda, H. *et al.* MCP-1 contributes to macrophage infiltration into adipose tissue, insulin resistance, and hepatic steatosis in obesity. *J. Clin. Invest.* **116**, 1494–1505 (2006).
494. Penson, R. T. *et al.* Cytokines IL-1beta, IL-2, IL-6, IL-8, MCP-1, GM-CSF and TNFalpha in patients with epithelial ovarian cancer and their relationship to treatment with paclitaxel. *Int. J. Gynecol. Cancer* **10**, 33–41 (2000).
495. Liu, L. *et al.* Chemotherapy Induces Breast Cancer Stemness in Association with Dysregulated Monocytosis. *Clin. Cancer Res.* **24**, 2370–2382 (2018).
496. Hamidullah, Changkija, B. & Konwar, R. Role of interleukin-10 in breast cancer. *Breast Cancer Res. Treat.* **133**, 11–21 (2012).
497. Kozłowski, L., Zakrzewska, I., Tokajuk, P. & Wojtukiewicz, M. Z. Concentration of interleukin-6 (IL-6), interleukin-8 (IL-8) and interleukin-10 (IL-10) in blood serum of breast cancer patients. *Rocz. Akad. Med. Bialymst.* **48**, 82–4 (2003).
498. Lyon, D. E., McCain, N. L., Walter, J. & Schubert, C. Cytokine comparisons between women with breast cancer and women with a negative breast biopsy. *Nurs. Res.* **57**, 51–8 (2008).
499. Rao, V. S., Alabi, A., Dyer, C. E., Greenman, J. & Drew, P. J. IL-10 and IL-12 expression in breast cancer patients and effect of therapy. *J. Clin. Oncol.* **26**, 14016 (2008).
500. Tong, A. W. *et al.* Cellular Immune Profile of Patients With Advanced Cancer Before and After Taxane Treatment. *Am. J. Clin. Oncol. Cancer Clin. Trials* **23**, 463–472 (2000).
501. Pusztai, L. *et al.* Changes in plasma levels of inflammatory cytokines in response to paclitaxel chemotherapy. *Cytokine* **25**, 94–102 (2004).
502. Seruga, B., Zhang, H., Bernstein, L. J. & Tannock, I. F. Cytokines and their relationship to the symptoms and outcome of cancer. *Nat. Rev. Cancer* **8**, 887–899 (2008).
503. Vyas, D., Laput, G. & Vyas, A. Chemotherapy-enhanced inflammation may lead to the failure of therapy and metastasis. *Onco. Targets. Ther.* **7**, 1015 (2014).
504. Jones, V. S. *et al.* Cytokines in cancer drug resistance: Cues to new therapeutic strategies. *Biochim. Biophys. Acta - Rev. Cancer* **1865**, 255–265 (2016).
505. Tsavaris, N., Kosmas, C., Vadiaka, M., Kanelopoulos, P. & Boulamatsis, D. Immune changes in patients with advanced breast cancer undergoing chemotherapy with taxanes. *Br. J. Cancer* **87**, 21–27 (2002).
506. Bogdan, C. & Ding, A. Taxol, a microtubule-stabilizing antineoplastic agent, induces expression of tumor necrosis factor α and interleukin-1 in macrophages. *J. Leukoc. Biol.* **52**, 119–121 (1992).
507. Collins, T. S., Lee, L.-F. & Ting, J. P.-Y. Paclitaxel up-regulates interleukin-8 synthesis in human lung carcinoma through an NF-κB- and AP-1-dependent mechanism. *Cancer Immunol. Immunother.* **49**,

78–84 (2000).
508. White, C. M., Martin, B. K., Lee, L.-F., Haskill, J. S. & Ting, J. P.-Y. Effects of paclitaxel on cytokine synthesis by unprimed human monocytes, T lymphocytes, and breast cancer cells. *Cancer Immunol. Immunother.* **46**, 104–112 (1998).
509. Nolen, B. M. *et al.* Serum biomarker profiles and response to neoadjuvant chemotherapy for locally advanced breast cancer. *Breast Cancer Res.* **10**, R45 (2008).
510. Byers, T. & Sedjo, R. L. Does intentional weight loss reduce cancer risk? *Diabetes, Obes. Metab.* **13**, 1063–1072 (2011).
511. Pakiz, B., Flatt, S. W., Bardwell, W. A., Rock, C. L. & Mills, P. J. Effects of a Weight Loss Intervention on Body Mass, Fitness, and Inflammatory Biomarkers in Overweight or Obese Breast Cancer Survivors. *Int. J. Behav. Med.* **18**, 333–341 (2011).
512. Baker, S. D. *et al.* Factors Affecting Cytochrome P-450 3A Activity in Cancer Patients. *Clin. Cancer Res.* **10**, 8341–8350 (2004).
513. Lepper, E. R. *et al.* Effect of common CYP3A4 and CYP3A5 variants on the pharmacokinetics of the cytochrome P450 3A phenotyping probe midazolam in cancer patients. *Clin. Cancer Res.* **11**, 7398–7404 (2005).
514. Henningsson, A. *et al.* Association of CYP2C8, CYP3A4, CYP3A5, and ABCB1 polymorphisms with the pharmacokinetics of paclitaxel. *Clin. Cancer Res.* **11**, 8097–8104 (2005).
515. Shord, S. S. *et al.* Cytochrome P450 2C9 mediated metabolism in people with and without cancer. *Int. J. Clin. Pharmacol. Ther.* **46**, 365–74 (2008).
516. Boruban, M. C., Yasar, U., Babaoglu, M. O., Sencan, O. & Bozkurt, A. Tamoxifen Inhibits Cytochrome P450 2C9 Activity in Breast Cancer Patients. *J. Chemother.* **18**, 421–424 (2006).
517. Pavlides, S. *et al.* The reverse Warburg effect: Aerobic glycolysis in cancer associated fibroblasts and the tumor stroma. *Cell Cycle* **8**, 3984–4001 (2009).
518. Pavlides, S. *et al.* Loss of stromal caveolin-1 leads to oxidative stress, mimics hypoxia and drives inflammation in the tumor microenvironment, conferring the "reverse Warburg effect": A transcriptional informatics analysis with validation. *Cell Cycle* **9**, 2201–2219 (2010).
519. Bonuccelli, G. *et al.* Ketones and lactate "fuel" tumor growth and metastasis. *Cell Cycle* **9**, 3506–3514 (2010).
520. Martinez-Outschoorn, U. E. *et al.* Oxidative stress in cancer associated fibroblasts drives tumor-stroma co-evolution. *Cell Cycle* **9**, 3276–3296 (2010).
521. Choi, J., Kim, D. H., Jung, W. H. & Koo, J. S. Metabolic interaction between cancer cells and stromal cells according to breast cancer molecular subtype. *Breast Cancer Res.* **15**, R78 (2013).
522. Luis, C. *et al.* Warburg Effect Inversion: Adiposity shifts central primary metabolism in MCF-7 breast cancer cells. *Life Sci.* **223**, 38–46 (2019).
523. Apicella, M. *et al.* Increased Lactate Secretion by Cancer Cells Sustains Non-cell-autonomous Adaptive Resistance to MET and EGFR Targeted Therapies. *Cell Metab.* **28**, 848–865 (2018).
524. Loibl, S. & Gianni, L. HER2-positive breast cancer. *Lancet* **389**, 2415–2429 (2017).
525. Delort, L. *et al.* Reciprocal Interactions between Breast Tumor and Its Adipose Microenvironment Based on a 3D Adipose Equivalent Model. *PLoS One* **8**, e66284 (2013).
526. Gourdon, D. *et al.* Implanted adipose progenitor cells as physicochemical regulators of breast cancer. *Proc. Natl. Acad. Sci.* (2012). doi:10.1073/pnas.1121160109
527. Miura, K., Yang, L., van Rooijen, N., Ohnishi, H. & Seki, E. Hepatic recruitment of macrophages promotes nonalcoholic steatohepatitis through CCR2. *Am. J. Physiol. - Gastrointest. Liver Physiol.* **302**, G1310-1321 (2012).
528. Wyler, S. L., D'Ingillo, S. L., Lamb, C. L. & Mitchell, K. A. Monocyte chemoattractant protein-1 is not required for liver regeneration after partial hepatectomy. *J. Inflamm. (United Kingdom)* **13**, (2016).
529. Newman, W. G. *et al.* Impaired tamoxifen metabolism reduces survival in familial breast cancer patients. *Clin. Cancer Res.* **14**, 5913–5918 (2008).
530. Lim, S. Y., Yuzhalin, A. E., Gordon-Weeks, A. N. & Muschel, R. J. Targeting the CCL2-CCR2 signaling axis in cancer metastasis. *Oncotarget* **7**, 28697 (2016).
531. Sandhu, S. K. *et al.* A first-in-human, first-in-class, phase i study of carlumab (CNTO 888), a human monoclonal antibody against CC-chemokine ligand 2 in patients with solid tumors. *Cancer Chemother. Pharmacol.* **71**, 1041–1050 (2013).
532. Brana, I. *et al.* Carlumab, an anti-C-C chemokine ligand 2 monoclonal antibody, in combination with four chemotherapy regimens for the treatment of patients with solid tumors: an open-label, multicenter phase 1b study. *Target. Oncol.* **10**, 111–123 (2015).
533. McNeely, M. L. *et al.* Effects of exercise on breast cancer patients and survivors: a systematic review and meta-analysis. *Can. Med. Assoc. J.* **175**, 34–41 (2006).

Appendix A

Supplementary Material

A.1 Supplementary material for Chapter 2

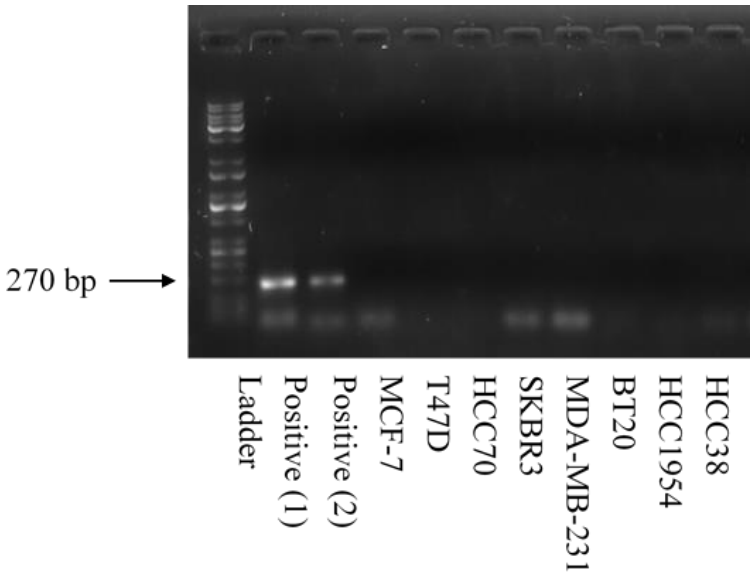

Supplementary Figure A.1.Representative image of human breast cancer cell lines tested for mycoplasma.
PCR using primers designed for the generic detection of Mollicutes (270bp). GPO3 5' GGGAGCAAACACGAT AGATACCCT 3', MGSO 5' TGCACCATC TGTCACTCTGTTAACCTC 3'. Cell lines were free of contamination.

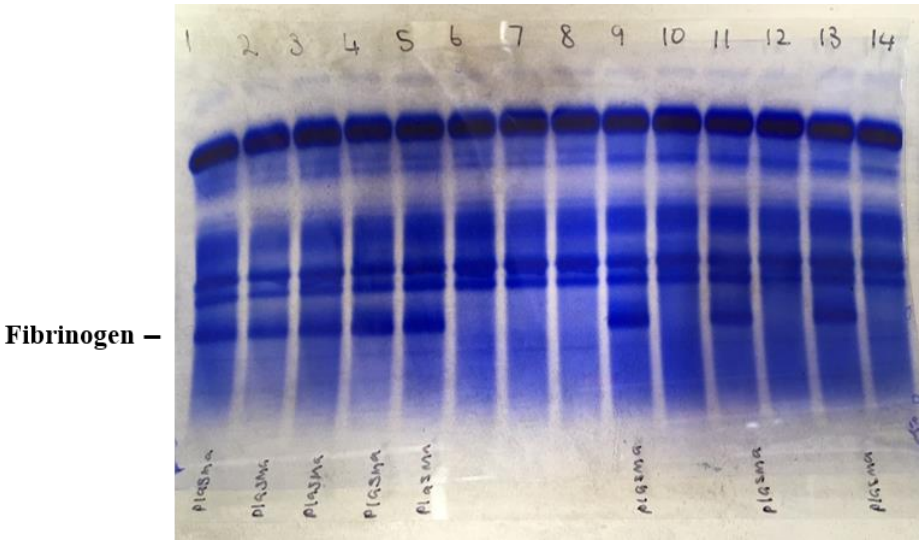

Supplementary Figure A.2. Representative image of serum protein electrophoresis performed on all blood patient plasma and serum samples.
Complete absence of a fibrinogen band indicates a pure serum sample. Samples with fibrinogen bands were considered plasma.

A.2 Supplementary material for Chapter 4

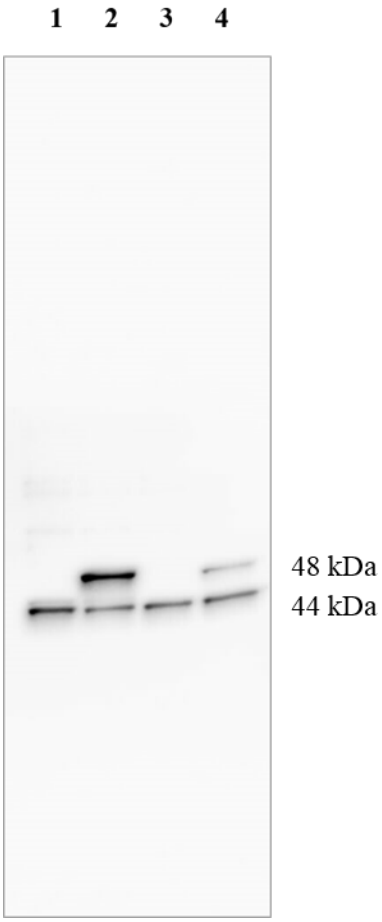

Supplementary Figure A.3. Representative image of a full Western blot for PGK1. Relative PGK1 expression was assessed in control and transfected MCF-7 and MDA-MB-231 cells. Cells were transfected with the pFRT/TO/HIS/FLAG/HA-PGK1 plasmid encoding PGK1. Lane 1) control MCF-7, Lane 2) transfected (PGK1) MCF-7, Lane 3) control MDA-MB-231, and Lane 4) transfected MDA-MB-231. Transfection showed double immunoreactive bands for PGK1 at the correct (44 kDa) and larger molecular size (48 kDa). β-actin was used as a loading control.

A.3 Supplementary material for Chapter 5

Supplementary Table A.1.Concentrations (ng/mL) of probe drugs and metabolites in serum and urine samples collected from each participant before probe drug administration.

Before Chemotherapy (0Hr samples)								
Participant	**Losartan**	**E-3174**	**Omeprazole**	**5-Hydroxyomeprazole**	**Dextromethorphan**	**Dextrorphan**	**Midazolam**	**α-Hydroxymidazolam**
1	< 5.0	< 5.0	< 5.0	< 5.0	< 1.25	< 5.0	< 0.2	< 0.2
2	< 5.0	< 5.0	< 5.0	< 5.0	< 1.25	< 5.0	< 0.2	< 0.2
3	< 5.0	< 5.0	< 5.0	< 5.0	< 1.25	< 5.0	< 0.2	< 0.2
4	< 5.0	< 5.0	< 5.0	< 5.0	< 1.25	< 5.0	< 0.2	< 0.2
5	< 5.0	< 5.0	< 5.0	< 5.0	< 1.25	< 5.0	< 0.2	< 0.2
6	< 5.0	< 5.0	< 5.0	< 5.0	< 1.25	< 5.0	< 0.2	< 0.2
8	< 5.0	< 5.0	< 5.0	< 5.0	< 1.25	< 5.0	< 0.2	< 0.2
9	< 5.0	< 5.0	< 5.0	< 5.0	< 1.25	< 5.0	< 0.2	< 0.2
12	< 5.0	< 5.0	< 5.0	< 5.0	< 1.25	< 5.0	< 0.2	< 0.2
After Chemotherapy (0Hr samples)								
Participant	**Losartan**	**E-3174**	**Omeprazole**	**5-Hydroxyomeprazole**	**Dextromethorphan**	**Dextrorphan**	**Midazolam**	**α-Hydroxymidazolam**
1	< 5.0	< 5.0	< 5.0	< 5.0	< 1.25	< 5.0	< 0.2	< 0.2
2	< 5.0	< 5.0	< 5.0	< 5.0	< 1.25	< 5.0	< 0.2	< 0.2
3	< 5.0	< 5.0	< 5.0	< 5.0	< 1.25	< 5.0	< 0.2	< 0.2
4	< 5.0	< 5.0	< 5.0	< 5.0	< 1.25	< 5.0	< 0.2	< 0.2
5	< 5.0	< 5.0	< 5.0	< 5.0	< 1.25	< 5.0	< 0.2	< 0.2
6	< 5.0	< 5.0	< 5.0	< 5.0	< 1.25	< 5.0	< 0.2	< 0.2
8	< 5.0	< 5.0	< 5.0	< 5.0	< 1.25	< 5.0	< 0.2	< 0.2
9	< 5.0	< 5.0	< 5.0	< 5.0	< 1.25	< 5.0	< 0.2	< 0.2
12	< 5.0	< 5.0	< 5.0	< 5.0	< 1.25	< 5.0	< 0.2	< 0.2

<0.2, <1.25, and <5.0: concentration of probe drug or metabolite were below the detectable limits of the assay.
0Hr: zero hour, serum and urine samples were collected from participants prior to receiving the probe drug cocktail

Appendix B

Clinical protocol

Exploring the Effects of Obesity-Related Inflammation and Exercise on Drug Metabolism in Cancer Patients

An Exploratory Study to Assess the Impact of Obesity-Related Inflammatory Markers on Breast Cancer Drug Metabolism in Response to Regular Moderate Exercise during Chemotherapy

Principle Investigator:
Dr Matthew Strother

Co-Investigators:
Dr Margaret Currie (UOC)
Professor Bridget Robinson (UOC/CDHB)
Associate Professor Matthew Doogue (UOC)
Associate Professor Gabi Dachs (UOC)
Associate Professor Nuala Helsby (University of Auckland)
Dr Lynnette Jones (UO)
Rebekah Crake (PhD Student)

Schema

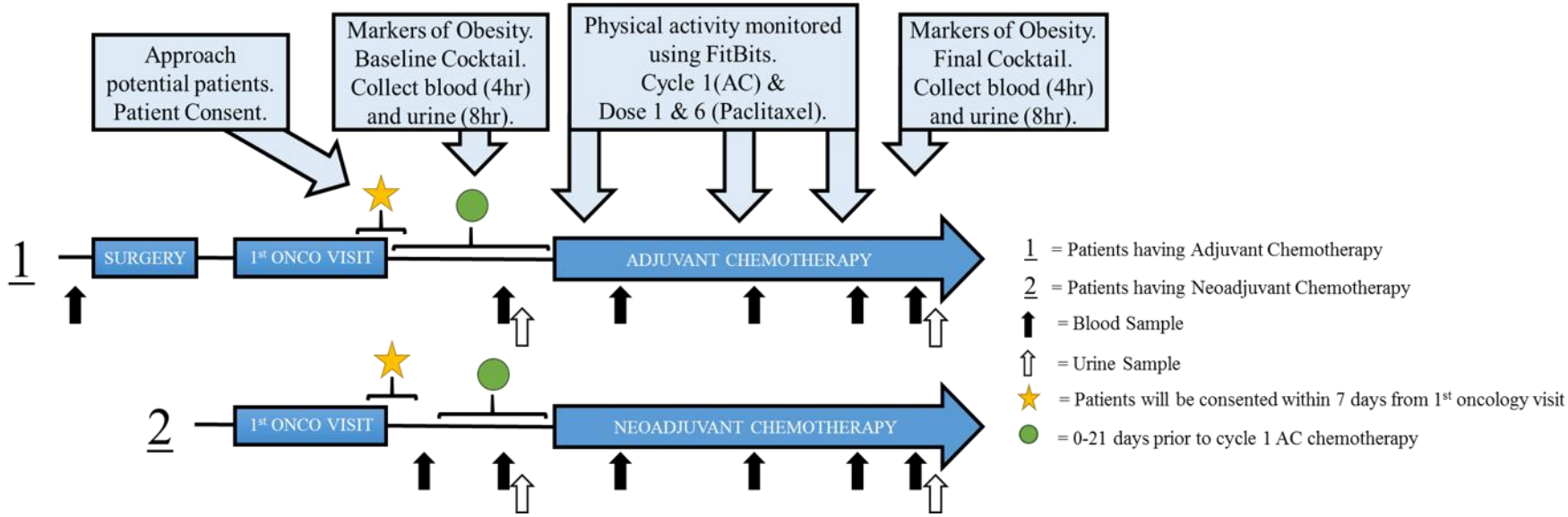

Schema. Initial blood sample collected by The Cancer Society Tissue Bank at the pre-admission visit (up to a week prior to beginning neoadjuvant chemotherapy OR up to a week prior to surgery for adjuvant chemotherapy patients). Patients will be approached during their first oncology visit, then given up to a week to consent. Following consent, and within the 21 days preceding cycle 1 AC (AC is the combination of doxorubicin and cyclophosphamide chemotherapy used together to treat breast cancer) neoadjuvant or adjuvant chemotherapy, patients will have body morphometry measured and be given the baseline cocktail (with pharmacokinetic sampling). Expected timeframe between neoadjuvant or adjuvant chemotherapy cycles is as follows: AC, 21 ± 2 days; Paclitaxel, 7 ± 2 days. FitBits will be expected to be worn after specified neoadjuvant or adjuvant chemotherapy cycles/doses for these timeframes (AC, 21 ± 2 days; Paclitaxel, 7 ± 2 days). After 'FitBit wearing' periods blood samples will be taken. The final cocktail will be administered 21 ± 7 days after Dose 6 of paclitaxel is given (with pharmacokinetic sampling).

1. Objectives

1.1 Primary Objectives

1. To determine if cytochrome p450 3A4-mediated midazolam metabolism is different in obese cancer patients as compared to age-matched normal weight cohort.

2. To examine the relationship between physical activity levels and cytochrome p450 3A4 activity in patients treated for breast cancer; as measured by midazolam metabolism.

1.2 Secondary Objectives

1. To compare the concentrations of inflammatory cytokines in blood samples collected from obese and age-matched normal weight breast cancer patients at stipulated time-points during neoadjuvant or adjuvant chemotherapy treatment.
2. To examine the relationship between body composition and cytochrome p450 3A4 metabolism in patients treated for breast cancer.
3. To explore the patterns of activity in obese and normal weight breast cancer patients over cycle one of AC (AC is the combination of doxorubicin and cyclophosphamide chemotherapy used together to treat breast cancer; see Appendix 11.3) chemotherapy and dose one & six of weekly paclitaxel (including patients on 3 weekly trastuzumab; see Appendix 11.4 and 11.5 for example charts) by objectively measuring physical activity using FitBit One® accelerometers.
4. To examine the relationship between chemotherapy dosing and obesity, physical activity, drug metabolism, and measurements of systemic inflammation.

1.3 Exploratory Objectives

1. Collect blood samples for later analysis to determine if there is differential impact on the activity of other cytochrome P450 enzymes in obese and non-obese cancer patients.
2. Perform secondary analysis of laboratory complete blood counts of neutrophil to lymphocyte ratio, measured under routine clinical practice to monitor saftey.

2. Background

2.1 Breast Cancer: Obesity and Inflammation

Obesity is prevalent worldwide and New Zealand (NZ) is not an exception, as one in three NZ adults are obese and a further 35% are overweight but not obese[1,2]. Epidemiologic studies strongly link obesity with increased risk of breast cancer as well an increased risk of breast cancer-associated mortality[3,4]. Obese women with breast cancer present with more advanced disease at diagnosis, have a higher rate of recurrence and have shorter survival times, when compared to normal weight patients[4,5]. Collectively, these observations suggest that obesity promotes breast cancer metastasis, and that chemotherapy may be less effective in obese patients. However, the reasons for this remain unclear. It is established that obese subjects have higher levels of circulating inflammatory markers[6,7] and that this inflammation is a hallmark of cancer[8]. Thus, one possible hypothesis suggests that obesity-associated chronic, low-grade, systemic inflammation has a negative impact on patient's responsiveness to chemotherapy. Research suggests that obese women with breast cancer have increased levels of circulating obesity-related inflammatory cytokines (e.g. CRP, IL-6 and TNF-alpha), and such increases promote breast cancer development and mortality[9,10,11].

2.2 Breast Cancer: Obesity, Exercise and Inflammation

Patient obesity is generally concurrent with other characteristics associated with risk of mortality, such as decreased physical activity. A sedentary lifestyle pre-diagnosis has been associated with an increased risk of recurrence in oestrogen receptor(ER)/progesterone receptor(PR) negative breast tumours[12]. Similarly, reduced physical activity is an independent predictor of cancer-specific mortality, particularly in breast and colon cancers[13,14,15]. The literature suggests that aerobic and resistance exercise implemented during adjuvant chemotherapy displays a trend toward improved treatment responses and thus breast cancer outcomes, particularly for women who were overweight or obese[16]. Furthermore, breast cancer patients performing high doses of approximately 50-60 minutes of either aerobic, or aerobic and resistance training combined has been proven to be both achievable during treatment, and harmless for the patient and their rate of chemotherapy completion[17]. The mechanisms by which increased physical activity improves breast cancer outcome are not fully understood, yet one hypothesis includes the alleviation of obesity

associated systemic chronic low-grade inflammation by promoting anti-inflammatory environments.

Two related systematic reviews analysed the relationship between exercise and biomarkers important in breast cancer, including inflammatory cytokines. They concluded that there is biological relevance in the association between exercise and breast cancer outcome as physical activity can positively alter levels of circulating inflammatory cytokines as well as other cancer-related biomarkers[18],[19]. Since these reviews, additional research suggests that after chemotherapy, exercise and calorie restriction in a group of early stage breast cancer survivors resulted in modest body weight and waist-to-hip reduction and that these body compositional changes were positively correlated with markers of inflammation[20]. A more recent systematic review, with meta-analysis, further supports the positive influence of exercise in improving serum concentrations of chronic, low-grade inflammatory markers[21]. Conversely however, some studies have not seen the same level of change in circulating inflammatory markers as a response to exercise[22],[23].

When measuring physical activity in cancer patients undergoing, or after, chemotherapy many studies include survey and/or questionnaire based assessments. However, as they are now more readily available, it has become possible to include objective measures of physical activity through the use of pedometers, accelerometers, or global positioning satellite (GPS) data. Objective measures of physical activity offer several advantages over the traditional survey- or questionnaire-based assessments including reduction of recall bias, continuous physical activity data, and objective measurement of adherence. Several commercially available accelerometers have been used in clinical studies (RT3, activePAL, Actigraph, Qstartz, Yamax) to determine free range physical activity in both children and adults, with and without the addition of global positioning satellite data[24,25,26]. Accelerometer data has been validated as a measure of PA in studies using PA questionas as well as objective validation against observed activity, such as treadmill walking[27]. Preliminary studies have validated the use of accelerometers in cancer patients, during and following treatment[28,29]. Finally, a pilot study in 16 cancer patients provided feasibility in the use of Fitbit One® to measure exercise during chemotherapy (Unpublished Data; Matthew Strother, 2015). Furthermore, the same pilot study provided evidence that patients naturally separated themselves into more physically active and less physically active cohorts without any intervention in place (Fig 1). Several studies have validated products

manufactured by FitBit (San Francisco, USA), a consumer-oriented accelerometer commercially available in New Zealand[27,30].

2.3 Cytochrome P450 Enzymes in Breast Cancer: Inflammation and Chemotherapy Drug Metabolism

Cytochrome (CYP) P450 enzymes are a family of mixed-function oxidases which can modify functional groups and contribute to a significant proportion of drug metabolism in the body[31]. CYP enzymes are predominantly localised to the liver, although they can be found in various tissues in the human body such as kidney, lung and gut. CYP enzymes are substrate specific- with CYP1A2, CYP2C9, CYP2C19, CYP2D6 and CYP3A4/5 contributing considerably to the metabolism of breast cancer chemotherapy agents, including tamoxifen, cyclophosphamide, dexamethasone, doxorubicin and paclitaxel[32]. Clinical impact in terms of drug toxicity and efficacy can vary between patients due to variability in CYP activity. Interpatient variability in CYP activity stems from differences in genetic makeup, environmental exposures and/or epigenetic events. Similarly, drug metabolising enzyme polymorphisms can alter drug toxicity

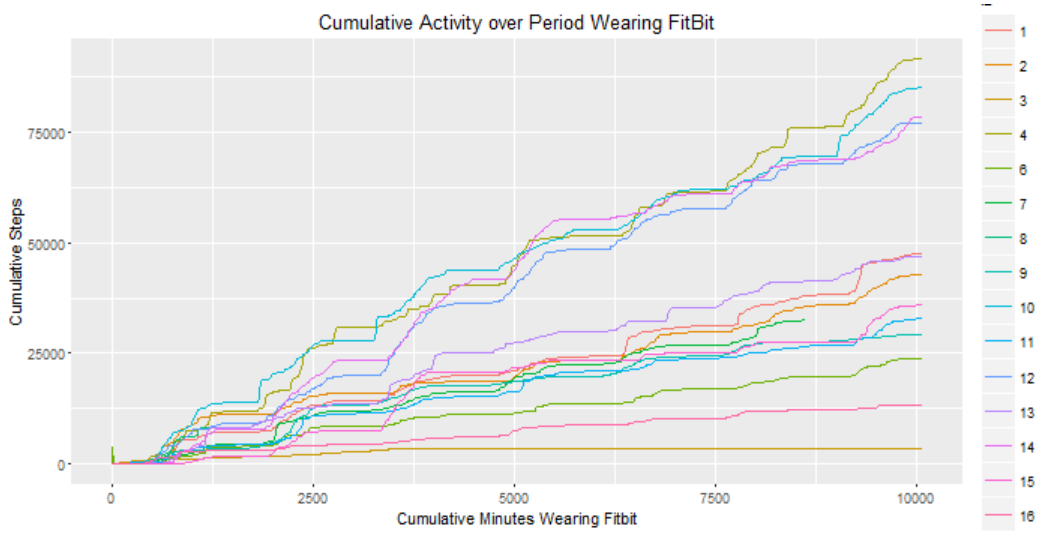

Figure 1. A pilot study showed that it is possible to measure physical activity (cumulative steps) in breast cancer patients during chemotherapy using FitBit One® devices.

and efficacy within an individual. Recently however, it has been established that although an individual may be classed as an extensive drug metaboliser because of their drug metabolising genotype, this genotype does not always reflect or accurately predict the observed drug metabolising phenotype[33]. In cytochrome P450 enzymes this phenomena has been extensively reviewed by Shah and Smith, who have termed this event 'phenoconversion', and suggest that it can result from co-administration of medications inhibiting the functional quality of certain CYP enzymes[34]. Furthermore, Shah and Smith present evidence from non-clinical research over the last 20 years that shows elevated levels of pro-inflammatory cytokines can inhibit gene expression of P450 enzymes causing a transient down-regulation in their numbers and therefore drug metabolising capacity[35]. One clinical study of 16 cancer patients found evidence suggestive of a genotype-phenotype mismatch in CYP2C19 and ruled out interference by other drugs[36], yet inflammatory cytokine involvement was not investigated. In the literature, analysis of circulating inflammatory cytokines has linked systemic inflammation with adverse breast cancer prognosis[37]. This link may be explained, at least in part, by the transient phenoconversion of CYP P450 enzymes by circulating inflammatory cytokines, hindering breast cancer drug metabolism.

Whether in whole animal models or human subjects, CYPs activity is studied through use of probe drugs. Probe drugs are medications that have been determined to be predominantly metabolized by one CYP, thus allowing the clinical scientist to gain insight into the activity of that CYP *in vivo*[38]. An example of this is use of midazolam and its metabolites to study CYP3A4 – through administration of this drug and subsequent sampling from the systemic circulation to measure the parent compound (midazolam) and metabolites (4-OH midazolam), it is possible to phenotype the activity of CYP3A4. The probe drug methodology can be used to study specific CYPs in relative isolation, or through combinations of multiple probe drugs (frequently called "cocktails") the phenotype of multiple CYPs can be assessed concurrently.

The cocktail approach to CYP phenotyping is well-established in academia and the pharmaceutical industry. Phenotyping cocktails are designed to limit the potential for interactions between components, exhibit adequate specificity of agents to allow accurate CYP phenotyping, and minimize observable clinical effects[39]. Specifically, with regards to the latter point, many probe drugs have either been selected because of limited potential for harm at standard dosing (even in the setting of intentional increased exposure such as in

CYP-inhibition studies), or reduction in dosing to subtherapeutic ranges. Examples of CYP phenotyping cocktails include the "Pittsburgh" cocktail[40], the "Basel" cocktail[41], and the "Inje" cocktail[42]: their respective constituent components and sampling schedules are presented in Table 1.

Table 1. Examples of Phenotyping Cocktails

Cocktail	Components (Enzymes/Transporters Assessed)	Sampling Schedule
Pittsburgh	Caffeine (CYP1A2) Chlorzoxazone (CYP2E1) Phenytoin (CYP2C19) Debrisoquin (CYP2D6) Dapsone (CYP3A4)	Plasma sample at baseline, 4 and 8 hours Urine sample 0-8 hours (inclusive)
Basel	Caffeine (CYP1A2) Efavirenz (CYP2B6) Omeprazole (CYP2C19) Metoprolol (CYP2D6) Losartan (CYP2C9) Midazolam (CYP3A4)	Plasma samples at 0.25, 0.5, 0.75, 1, 2,3, 4, 6, 8, 12, 24, 48, and 72 hours
Inje	Caffeine (CYP1A2) Omeprazole (CYP2C19) Dextromethorphan (CYP2D6) Losartan (CYP2C9) Midazolam (CYP3A4)	Plasma sample at 4 hours Urine sample at 8 hours

2.4 Summary of Published Data

Low grade, systemic inflammation is a well-established characteristic of chronic obesity and has been linked to the increased risk of and mortality from breast cancer. Based on previous research it could be speculated that obese breast cancer patients have worse outcomes after chemotherapy due to increased levels of circulating inflammatory cytokines inhibiting liver CYP enzymes, and thus, less effective metabolism of breast cancer chemotherapy drugs. It is therefore hypothesized that 1) clinical inflammation in obese breast cancer patients induces transient 'phenoconversion' and inhibits functional activity of liver CYP enzymes and 2) regular moderate exercise reduces obesity-related inflammation and improves chemotherapy outcome. We propose to elucidate the impact of exercise on breast cancer

chemotherapy drug metabolism via liver CYPs, and investigate the role that circulating inflammatory cytokines play in this process.

3. Patient Selection

3.1 Inclusion Criteria

- Women of age ≥ 18.
- Obese (BMI >30 kg/m^2) or normal weight (18.5≤BMI≤24.9 kg/m^2) at diagnosis, according to BMI scoring.
- Ability to understand and give written informed consent.
- Ability to take oral medications.
- Clinically defined stage II or III breast cancer.
- Planned neoadjuvant or adjuvant chemotherapy with AC-T (cyclophosphamide, doxorubicin, paclitaxel).
- Willing to wear FitBit One® throughout the selected cycles/doses of chemotherapy.
- Willing to take probe drug cocktail and provide subsequent blood/urine samples.
- No known sensitivity or contraindications to any of the cocktail components, including: midazolam, losartan, caffeine, omeprazole and dextromethorphan.
- Have adequate end-organ function, as measured by:

Creatinine	≤ 2x Upper Limit of Normal (ULN)
Haemoglobin	> 90 g/L
Systolic Blood Pressure	> 90 mmHg
AST	≤ 3x ULN
ALT	≤ 3x ULN
Bilirubin	≤ 2x ULN

3.2 Exclusion Criteria

- Enrollment in any conflicting clinical trials.
- Uncontrolled intercurrent illness including, but not limited to, on-going or active infection and psychiatric illness/social situations that would limit compliance with study requirements.
- Patients that suffer from ongoing urinary incontinence and/or current use of a urinary catheter.
- Cirrhosis as documented by liver biopsy, fibroscan, or a clinical history laboratory findings consistent with cirrhosis.
- Impaired mobility due to disability or medical illness. For example:

    - Amputation of either or both lower extremities
    - Restricted to a wheelchair
- Are known to have active infection with a viral hepatitis (e.g. Hepatitis B or C).
- Unwilling to comply with requirements for recording times when the FitBit One® is not worn.
- Any abnormal laboratory value or medical condition that would, in the investigators' judgement, make the patient a poor candidate for the study.
- Use of concurrent medications known to be inhibitors or inducers of the cytochrome P450 enzymes being studied. Weak inducers or inhibitors will be acceptable for inclusion. Table 2, below, is derived from the FDA recommendations regarding in vivo CYP probes, inducers, and inhibitors[43]. This list is non-comprehensive, but covers the prototypical strong inhibitors and inducers. This exclusion is specifically referencing chronic medications that cannot be stopped during period preceding cocktail administration, by at least 7 days. This does not reference medications taken intermittently, especially those during chemotherapy. An example of this is aprepitant, which is administered as part of the standard anti-emetic regimen for AC – however, the use of this medication is separated from any cocktail administration by > 7 days. See Appendix 11.1 and 11.2 for a more comprehensive FDA derived guideline on strong inducers and inhibitors.

Table 2. Prototypical Inducers and Inhibitors Prohibited by Study

CYP	Inducer	Inhibitor
1A2	Smoker	Fluvoxamine
2B6	Rifampin	
2C9	Rifampin	Fluconazole, amiodarone
2C19	Rifampin	Omeprazole, fluvoxamine, moclobemide
2D6		Paroxetine, quinidine, fluoxetine
2E1	Ethanol	Disulfiram
3A4/5	Rifampin, carbamazepine	Atazanavir, clarithromycin, indinavir, itraconazole, ketoconazole, nefazodone, nelfinavir, ritonavir, saquinavir, telithromycin

3.3 Accrual Targets

This study strives to include a total of 40 breast cancer patients having neoadjuvant or adjuvant chemotherapy after breast cancer surgery. Potential patients will be approached during their first oncology visit and subsequently consented, prior to beginning neoadjuvant or adjuvant chemotherapy. Patients will be preferentially recruited to include obese (n=20; BMI >30 kg/m^2) and age-matched normal (n=20; BMI 18.5-24.9 kg/m^2) subjects. Time for recruitment is predicted to be 12 months, judging from current hospital data.

4 Clinical and Laboratory Evaluations

4.1 Baseline Clinical and Laboratory Evaluations

4.1.1 Baseline Clinical Examination

Complete patient history will be taken, and a physical examination will be performed at first oncology appointment.

Measurements of patients' body morphometry (ie height, weight, BMI, waist circumference, triceps skin-fold and body composition analysis) will be taken within 21 days prior to starting cycle 1 of AC neoadjuvant or adjuvant chemotherapy or on the day of baseline cocktail administration (see Section 4.1.4).

The Cancer Society Tissue Bank (CSTB) Christchurch will collect pre-administration (baseline) blood samples (5 mL) from all consenting cancer patients and records all tumour pathology data from each patient, and these will be available to this study to explore patients' circulating inflammatory cytokines.

4.1.2 Baseline Laboratory Evaluations

All baseline laboratory evaluations will be performed either, prior to beginning neoadjuvant chemotherapy or, after breast cancer surgery prior to beginning cycle 1 of AC adjuvant chemotherapy. Baseline laboratory evaluations will be as per standard of care and will be comprised of complete blood count (including neutrophil to lymphocyte ratio) and full liver, electrolytes and renal function tests.

4.1.3 Baseline Concomitant Medications

All concomitant medications in the pre-chemotherapy period (and post-operative period for patients receiving adjuvant chemotherapy) will be recorded on the Concomitant Medications Form by study nurses. This list will be inclusive of medications administered or taken within the preceding 24 hours of cocktail drug administration, along with estimated time of administration.

4.1.4 Baseline Cocktail Drug Administration

The ability of patients to take oral medications and blood pressure will be assessed. To proceed with planned phenotyping cocktail administration, subjects must be able to take oral medications, and must have a minimum systolic blood pressure of 90 mmHg without

vasopressor support. If the subjects do not meet these requirements, but are expected to clinically improve, patients may be reassessed within 7 days to meet these requirements.

2 to 21 days prior to cycle 1 of neoadjuvant or adjuvant chemotherapy patients will be administered a low dose 'Inje' probe drug cocktail (see Section 5.2).

4.2 Recurrent Clinical and Laboratory Evaluations

4.2.1 Passive Dose Assessment

This study will monitor patient chemotherapy prescribing, doses administered and dose reductions and delays, to exclude 'dose capping' as a cause for poor chemotherapy outcome in these patients.

4.2.2 FitBit One® Data Collection and Inflammatory Markers Blood Sampling

Patients will be allocated FitBit One® devices on the day of AC cycle 1 and paclitaxel dose 1 and 6 administration (neoadjuvant or adjuvant chemotherapy). After three weeks (21 ± 2) (AC cycle 1) and one week (7 ± 2 days) (paclitaxel Dose 1 and 6) patients will be asked to return to clinic to allow "syncing" of physical activity data from the device, to return the device until next allocation, hand in the 'FitBit One® and Physical Activity' journal (see below) and give a blood sample. Three 5 mL EDTA tubes of blood will be collected. One will be frozen as whole blood; the other two will be spun down and frozen as serum. Both will be stored at -80°C until analysis.

Throughout the designated time points of FitBit wearing participants will be asked to record a journal of when, for how long, and what occurred during events of FitBit One® removal and record any physical activity within 24 hours of blood sampling.

At the end of the exercise monitoring period participants will be required to have body morphometry measured (i.e height, weight, BMI, waist circumference, triceps skin-fold and body composition analysis).

4.2.3 Final Cytochrome P450 Phenotyping Cocktail Administration

After finishing dose 6 of paclitaxel, neoadjuvant or adjuvant chemotherapy patients will be administered with the second low dose of 'Inje' probe drug cocktail. See Section 5.2 for probe drug cocktail administration and sampling procedure.

On day of final phenotyping cocktail administration, a comprehensive assessment of all concomitant medications will be documented. This list will be inclusive of medications administered or taken within the preceding 24 hours, along with time of administration.

Laboratory results performed within 24 hours prior to planned administration of phenotyping cocktail administration will be reviewed. Repeat laboratory studies will be as per standard of care, and will be comprised of: complete blood count with differential; an electrolyte panel, including a serum creatinine; and liver function tests. The minimum requirements for laboratory values that will be used to determine if cocktail administration should proceed are presented in Table 3.

Table 3. Minimum Laboratory Values Required Prior to Cocktail Administration

Laboratory Measurement	Minimum Requirement to Proceed with Phenotyping Cocktail Administration
Systolic Blood Pressure	> 90 mmHg
AST	≤ 3x ULN
ALT	≤ 3x ULN
Bilirubin	≤ 2x ULN

If the subjects do not meet these requirements, but are expected to clinically improve, patients may be reassessed within 7 days until these requirements are met.

5. Administration of Fitbits and Probe Drug Cocktail

5.1 Administration of FitBit One® and Inflammatory Markers Blood Sampling

The current protocol does not include an exercise intervention, but patients will wear Fitbits to monitor physical activity during cycle 1 of AC and during dose 1 and 6 of paclitaxel. Potential participants will be identified from the CDHB Oncology Clinics.

5.1.1 FitBit One® Syncing

Participants will be asked to wear the FitBit One® for three weeks following cycle 1 of AC chemotherapy and for one week each after dose 1 and 6 of paclitaxel. Patients will be asked to return to the clinic with the device three weeks (21 ± 2 days) after cycle 1 of AC

chemotherapy and one week (7 ± 2 days) after dose 1 and 6 of paclitaxel. During the return visit any recent physical activity (within the last 24 hours) carried out by the patient will be recorded (physical activity journal) and the device will be "synched" with the desktop software. During the last FitBit "syncing" visit (one week after dose 6 of paclitaxel) participants will be asked to return the device.

5.1.2 Blood Sampling

The evaluation of the patient's physical activity and circulating inflammatory levels will entail collection and analysis of FitBit One® data received during neoadjuvant or adjuvant chemotherapy along with overlapping blood draws for comparison. Pre-administration blood samples (5 mL) are routinely collected from all cancer patients undergoing surgery in Christchurch Hospital via the Cancer Society Tissue Bank Christchurch, and these will be available to this study for analysis of obesity-related inflammatory biomarkers in patient serum prior to surgery. Additional blood samples will be collected from patients at their first oncology appointment prior to starting cycle 1 (AC) of chemotherapy, and three weeks (21 ± 2 days) following cycle 1 of AC chemotherapy and one week (7 ± 2 days) after dose 1 and 6 of paclitaxel (two 5 mL EDTA tubes of blood will be collected at each visit; 10 mL/per visit; 45 mL total). Blood samples will be, (a) as per standard of care, immediately analysed for routine clinical Complete Blood Counts (including markers of inflammation such as neutrophil and lymphocyte counts), and (b) prepared and stored as per CSTB Christchurch standard operating procedures (SOP) for batched analysis of circulating inflammatory adipokines using commercially available immunoassays (as per manufactures' instructions).

5.2 Administration of Cytochrome P450 Phenotyping Cocktail

5.2.1 Cocktail Administration

The phenotyping cocktail used in this study is a modification of the "Inje" cocktail. It is comprised of the following medications, assessing the following CYPs, respectively: caffeine, CYP1A2; losartan, CYP2C9; omeprazole, CYP2C19; dextromethorphan, CYP2D6; and midazolam, CYP3A4. The probe medications administered as the cocktail will consist of standard tablets of 100 mg caffeine, 25 mg losartan and 20 mg omeprazole. Additionally, 30 mg of dextromethorphan syrup diluted in 50 mL plain water, and 1 mg midazolam in 50 mL plain water. In order to ensure whole midazolam and

dextromethorphan dose is administered, the used cup/s will be rinsed and rinsing water swallowed. This cocktail has been selected because these drugs, at these low doses, have minimal risk of causing clinical effect, even in the context of significantly delayed clearance of drugs.

5.2.2 Pharmacokinetic Sampling

Patients will be requested to fast on the day of cocktail administration. Subjects will be asked to restrain from caffeine-containing beverages for 24 prior to dosing. Blood sampling will be taken at baseline (prior to administration of cocktail) and 4 hours post-administration of cocktail to assay midazolam, caffeine, and omeprazole metabolites. Once the vacutainer has ceased filling, the sample will be immediately placed on ice. All samples will be centrifuged for 10 min at 3,000 rpm at 4°C, and plasma will be removed. Plasma will then be processed, using ethanol precipitation, then stored at -80°C until time of pharmacokinetic analysis. A random urine sample (at least 50 mL) will be collected at baseline, followed by administration of the cocktail medications. Total urine will be collected over 0-8 hours, to assay losartan and dextromethorphan metabolites. Following recording of the urine volume, a 50 mL aliquot will be taken and stored at -80°C until time of pharmacokinetic analysis.

Please refer to Table 5 for the schedule of pharmacokinetic sampling.

5.2.3 Schedule for Cocktail Administration

The baseline phenotyping cocktail will be administered either, before the patient begins neoadjuvant chemotherapy or, after the patient's breast cancer surgery and within three weeks of starting AC adjuvant chemotherapy. The final phenotyping cocktail will be administered after cessation of neoadjuvant or adjuvant chemotherapy.

5.2.4 Pharmaceutical Information

- **Caffeine**
  - Storage Conditions
    Foil-wrapped tablets should be stored at or below 30°C.
  - How Provided
    Tablets of over the counter caffeine citrate contain 100 mg caffeine. They are provided in an aluminium foil packet.
  - Stability
    48 months stored at or below 30°C.
  - Administration Information
    One tablet, containing 100 mg caffeine, will be administered with 100 mL plain water.
  - Availability
    Caffeine will be sourced from Christchurch Hospital Pharmacy.
- **Losartan**

- Storage Conditions
  Losartan potassium tablets are stored in an aluminium blister pack at or below 25°C.
- How Provided
  Blister packs containing 30 or 90 tablets. Individual tablets contain 25 mg of losartan.
- Stability
  24 months stored at or below 25°C.
- Administration Information
  Administration of one 25 mg tablet with 100 mL plain water.
- Availability
  Losartan will be sourced from Christchurch Hospital Pharmacy.

- **Omeprazole**
  - Storage Conditions
    Omeprazole modified release tablets are stored in an aluminium blister pack at or below 25°C.
  - How Provided
    Blister packs containing 30 or 90 tablets. Individual tablets contain 20 mg of omeprazole.
  - Stability
    24 months stored at or below 25°C.
  - Administration Information
    Administration of one 20 mg tablet with 100 mL plain water.
  - Availability
    Omeprazole will be sourced from Christchurch Hospital Pharmacy.
- **Dextromethorphan**
  - Storage Conditions
    Dextromethorphan hydrobromide monohydrate is liquid, and should be stored at or below 25°C.
  - How Provided
    Dextromethorphan hydrobromide monohydrate liquid at 1 mg/mL is provided in a 200 mL bottle. For dosing, 30 mL (30 mg) will be withdrawn with a syringe.
  - Stability
    Stable at ≤ 25°C until expiry date shown on the pack.
  - Administration Information
    30 mL of 1 mg/mL dextromethorphan hydrobromide monohydrate should be added to 50 mL of plain water. The syringe used to draw up 30 mL should be washed three times with the water solution.
  - Availability
    Dextromethorphan will be sourced from Christchurch Hospital Pharmacy.
- **Midazolam**
  - Storage Conditions
    Ampoules should be stored below 30°C, out of direct sunlight. Ampoules are single-use only. Ampoules should not be frozen.
  - How Provided
    Midazolam is available as a 5mg/5mL ampoule.
  - Stability
    Stable at < 30°C until expiry date shown on the pack. It should not be diluted with macrodex 6% in dextrose.
  - Administration Information
    Ampoules will be broken open, and 1 mL of liquid will be removed using a 5 mL syringe. This will placed in 50 mL plain water, and 5 mL will be withdrawn and flushed into the container three times.
  - Availability
    Midazolam will be sourced from Christchurch Hospital Pharmacy.

5.3 Passive Dose Assessment

Information regarding laboratory values, chemotherapy dosing, adverse events, and any additional hospital contacts will be derived passively from the health record.

6. Laboratory and Data Analysis Plan

6.1 Laboratory Analysis of Circulating Inflammatory Adipokines

All patient serum and whole blood samples will be stored at -80 °C until they are required for analysis. Analysis will utilise commercially available immunoassays. Laboratory analysis will be performed in the Mackenzie Cancer Research Group laboratory, Pathology, University of Otago, Christchurch (UOC).

6.2 Laboratory Analysis of Phenotyping Cocktail Medications

All patient samples (plasma and urine) will be stored at -80 °C until they are required for analysis. Analysis will utilise a validated laboratory developed assay, on high pressure liquid chromatography using mass spectroscopy detection (HPLC-MS/MS), based on prior published assays. This assay will determine concentrations of the parent compounds, as well as metabolites as appropriate (i.e. midazolam/4-OH midazolam; losartan/E-3174; caffeine/paraxanthine; omeprazole/5-hydroxyomeprazole; dextromethorphan/dextrorphan). This will be performed in Clinical Pharmacology, University of Otago, Christchurch (UOC). Quality assurance/quality control (QA/QC) will be performed as per routine including determination of intra- and inter-day variability, stability, and exploration of other sources of assay variability.

7. Study Calendar

Table 4. Schedule of Events

Events	1st Onco Visit	+7 days	Baseline Cocktail	AC (Cycle 1)	21 ± 2 days from AC (1)	Paclitaxel (Dose 1)	7 ± 2 days from (Dose 1)	Paclitaxel (Dose 6)	7 ± 2 days from (Dose 6)	Final cocktail
Distribute Patient Information Sheet	X									
Informed Written Consent	X									
Exercise Monitoring										
Distribution of FitBit One®				X		X		X		
FitBit One® "Syncing"*					X		X		X	
Blood Sampling					X		X		X	
'FitBit One® and Physical Activity' Journal				X		X		X		
Collection of FitBit One®					X		X		X	
Probe Drug Intervention										
Safety Lab**	X		X							X
Clinical Assessment***	X		X							X
Concomitant Medications***			X							X
Cocktail Administration			X							X
Pharmacokinetic Sampling****			X							X

***** Fit Bit "Syncing" will require the participant and FitBit One® to present at clinic for data to be retrieved using desktop software. "Syncing" will be performed following the designated chemotherapy cycles/doses.
****** Safety lab will consist of comprehensive liver metabolic profile (inclusive of AST/ALT and bilirubin). This will be performed within 24 hours of cocktail administration.
******* Clinical assessment and concomitant medications will be assessed at baseline and on day of cocktail administration (See Section 4.).
******** Please refer to Table 5. for pharmacokinetic sampling procedure.

Table 5. Pharmacokinetic Sampling****

	0 hrs	4 hrs	8 hrs
Cocktail Administration	X		
Blood Sampling		X	
Urine Sampling	Total Urine Collection; Collect 50 mL aliquot at 8 hours		

8. Data Reporting/Regulatory Concerns

Storage of data will follow a double-lock arrangement, being protected by password on a computer that is in a securely locked room. All data will be de-identified and results will be available by publication in scientific, clinical and/or medical journals, and/or during conference and project presentations.

9. Statistical Considerations

Data generated by this study will include: patient demographics; objective measures of physical activity over three pre-selected weeks of neoadjuvant or adjuvant chemotherapy; laboratory measures of inflammation at baseline, during chemotherapy and post-chemotherapy; and time-concentration data for probe drugs and metabolites at baseline and post-chemotherapy.
All calculations will be performed in MS-Excel (Microsoft Corporation) or in R (R Foundation for Statistical Computing, Vienna, Austria).

Physical activity analysis will be exploratory and therefore there is not a power calculation to determine sample size. Data from the FitBit One® device will be extracted from the desktop software using the R (**http://www.R-project.org/**) package FitBitScraper (**https://github.com/corynissen/FitBitScraper**). Descriptive statistics (mean, median, confidence intervals) as well as temporal trends in FitBit One® data will be explored. These data will then be compared within and across patients to measures of inflammation using paired and unpaired t-test's, respectively, for significance ($p<0.05$). The PAS will be scored as per the instrument's scoring criteria, which converts responses to a metabolic equivalent time (MET)[44]. Relationship between PAS reported METs and FitBit One® data will be explored. Relationship between FitBit temporal trends and timing of chemotherapy, adverse events, and other comorbidities and laboratory abnormalities during the periods in question will be explored.

Pharmacokinetic analysis will be performed to determine the metabolite to probe drug ratio. These data will then be compared within-subject by a paired t-test for significance ($p<0.05$) baseline and post exercise monitoring.

Exploratory analyses will be performed to examine the correlation between amount of physical activity and change in circulating inflammatory adipokine concentrations from

stored serum samples. Additionally, serum inflammatory adipokines will be correlated to probe drug/metabolite ratios.

10. References

1. Marie, N. G. *et al.* Global, regional, and national prevalence of overweight and obesity in children and adults during 1980–2013: a systematic analysis for the Global Burden of Disease Study 2013. *Lancet* **384,** 766–781 (2014).
2. New Zealand Ministry of Health. Annual Update of Key Results 2014/15: New Zealand Health Survey. Available at: http://www.health.govt.nz/system/files/documents/publications/annual-update-key-results-2014-15-nzhs-dec15-1.pdf.
3. Jemal, A. *et al.* Global cancer statistics. *CA Cancer J Clin* **61,** 69–90 (2011).
4. Protani, M., Coory, M. & Martin, J. H. Effect of obesity on survival of women with breast cancer: Systematic review and meta-Analysis. *Breast Cancer Res. Treat.* **123,** 627–635 (2010).
5. Ewertz, M., Jensen, M. & Gunnarsdóttir, K. Effect of obesity on prognosis after early-stage breast cancer. *J. Clin.* (2011).
6. Visser, M. *et al.* Elevated C-Reactive Protein Levels in Overweight and Obese Adults. *JAMA* **282,** 2131 (1999).
7. Maachi, M. *et al.* Systemic low-grade inflammation is related to both circulating and adipose tissue TNFα, leptin and IL-6 levels in obese women. *Int. J. Obes.* **28,** 993–997 (2004).
8. Balkwill, F. R. & Mantovani, A. Cancer-related inflammation: common themes and therapeutic opportunities. in *Seminars in cancer biology* **22,** 33–40 (Elsevier, 2012).
9. Pierce, B. L. *et al.* Elevated biomarkers of inflammation are associated with reduced survival among breast cancer patients. *J. Clin. Oncol.* **27,** 3437–3444 (2009).
10. Van Kruijsdijk, R. C. M., Van Der Wall, E. & Visseren, F. L. J. Obesity and cancer: The role of dysfunctional adipose tissue. *Cancer Epidemiol. Biomarkers Prev.* **18,** 2569–2578 (2009).
11. Gunter, M., Wang, T. & Cushman, M. Circulating adipokines and inflammatory markers and postmenopausal breast cancer risk. *J.* (2015).
12. Schmidt, M. E. *et al.* Association of pre-diagnosis physical activity with recurrence and mortality among women with breast cancer. *Int. J. Cancer* **133,** 1431–1440 (2013).
13. Vrieling, A. & Kampman, E. The role of body mass index, physical activity, and diet in colorectal cancer recurrence and survival: a review of the literature. *Am. J. Clin. Nutr.* **92,** 471–490 (2010).
14. Demark-Wahnefried, W. *et al.* Practical clinical interventions for diet, physical activity, and weight control in cancer survivors. *CA Cancer J Clin* **65,** 167–189 (2015).
15. Wu, C.-Y. *et al.* The association of physical activity with all-cause, cardiovascular, and cancer mortalities among older adults. *Prev. Med. (Baltim).* **72,** 23–29 (2015).
16. Courneya, K., Segal, R., McKenzie, D. & Dong, H. Effects of exercise during adjuvant chemotherapy on breast cancer outcomes. *Med Sci Sport.* (2014).
17. Courneya, K. S. *et al.* Effects of exercise dose and type during breast cancer chemotherapy: multicenter randomized trial. *J. Natl. Cancer Inst.* **105,** 1821–32 (2013).
18. Ballard-Barbash, R. *et al.* Physical activity, biomarkers, and disease outcomes in cancer survivors: a systematic review. *J. Natl. Cancer Inst.* **104,** 815–40 (2012).
19. Löf, M., Bergström, K. & Weiderpass, E. Physical activity and biomarkers in breast cancer survivors: A systematic review. *Maturitas* **73,** 134–142 (2012).
20. Scott, E. *et al.* Effects of an exercise and hypocaloric healthy eating program on biomarkers associated with long-term prognosis after early-stage breast cancer: a randomized controlled trial. *Cancer Causes Control* **24,** 181–191 (2013).
21. Meneses-Echavez, J. F. *et al.* The effect of exercise training on mediators of inflammation in breast cancer survivors: a systematic review with meta-analysis. *Cancer Epidemiol. Biomarkers Prev.* (2016). doi:10.1158/1055-9965.EPI-15-1061
22. Jones, S. B. *et al.* Effect of Exercise on Markers of Inflammation in Breast Cancer Survivors: The Yale Exercise and Survivorship Study. *Cancer Prev. Res.* **6,** 109–118 (2013).
23. Swisher, A. K. *et al.* Exercise and dietary advice intervention for survivors of triple-negative breast cancer: effects on body fat, physical function, quality of life, and adipokine profile. *Support. Care Cancer* **23,** 2995–3003 (2015).
24. Klinker, C., Schipperijn, J. & Christian, H. Using accelerometers and global positioning system devices

to assess gender and age differences in children's school, transport, leisure and home based. *Int J Behav Nutr* (2014).
25. Webber, S. & Porter, M. Monitoring mobility in older adults using global positioning system (GPS) watches and accelerometers: a feasibility study. *J Aging Phys Act* (2009).
26. Rodriguez, D., Brown, A. & Troped, P. Portable global positioning units to complement accelerometry-based physical activity monitors. *Med. Sci. Sport.* (2005).
27. Takacs, J. *et al.* Validation of the Fitbit One activity monitor device during treadmill walking. *J. Sci. Med. Sport* **17,** 496–500 (2014).
28. Broderick, J., Hussey, J. & Kennedy, M. Testing the 'teachable moment'premise: does physical activity increase in the early survivorship phase? *Support. Care* (2014).
29. Ferriolli, E., Skipworth, R., Hendry, P. & Scott, A. Physical activity monitoring: a responsive and meaningful patient-centered outcome for surgery, chemotherapy, or radiotherapy? *J. pain* (2012).
30. Tully, M. A., McBride, C., Heron, L. & Hunter, R. F. The validation of Fibit Zip™ physical activity monitor as a measure of free-living physical activity. *BMC Res. Notes* **7,** 952 (2014).
31. Evans, W. & Relling, M. Pharmacogenomics: translating functional genomics into rational therapeutics. *Science (80-.).* (1999).
32. Harmsen, S., Meijerman, I. & Beijnen, J. The role of nuclear receptors in pharmacokinetic drug–drug interactions in oncology. *Cancer Treat.* (2007).
33. Gressier, F., Verstuyft, C., Hardy, P. & Becquemont, L. Response to CYP2D6 substrate antidepressants is predicted by a CYP2D6 composite phenotype based on genotype and comedications with CYP2D6 inhibitors. *J. Neural* (2015).
34. Shah, R. & Smith, R. Addressing phenoconversion: the Achilles' heel of personalized medicine. *Br. J. Clin. Pharmacol.* (2015).
35. Shah, R. & Smith, R. Inflammation-induced phenoconversion of polymorphic drug metabolizing enzymes: hypothesis with implications for personalized medicine. *Drug Metab. Dispos.* (2015).
36. Williams, M., Bhargava, P. & Cherrouk, I. A discordance of the cytochrome P450 2C19 genotype and phenotype in patients with advanced cancer. *Br. J.* (2000).
37. Grivennikov, S. & Karin, M. Inflammatory cytokines in cancer: tumour necrosis factor and interleukin 6 take the stage. *Ann. Rheum. Dis.* (2011).
38. Streetman, D., Bleakley, J. & Kim, J. Combined phenotypic assessment of CYP1A2, CYP2C19, CYP2D6, CYP3A, N-acetyltransferase-2, and xanthine oxidase with the 'Cooperstown cocktail'. *Clinical* (2000).
39. Fuhr, U., Jetter, A. & Kirchheiner, J. Appropriate phenotyping procedures for drug metabolizing enzymes and transporters in humans and their simultaneous use in the 'cocktail' approach. *Clin. Pharmacol.* (2007).
40. Frye, R. F., Matzke, G. R., Adedoyin, A., Porter, J. A. & Branch, R. A. Validation of the five-drug 'Pittsburgh cocktail' approach for assessment of selective regulation of drug-metabolizing enzymes. *Clinical* (1997).
41. Derungs, A., Donzelli, M., Berger, B. & Noppen, C. Effects of Cytochrome P450 Inhibition and Induction on the Phenotyping Metrics of the Basel Cocktail: A Randomized Crossover Study. *Clinical* (2016).
42. Ryu, J., Song, I., Sunwoo, Y. & Shon, J. Development of the 'Inje Cocktail' for High-throughput Evaluation of Five Human Cytochrome P450 Isoforms in vivo. *Clinical* (2007).
43. Research. C. for D. E. and. Drug Interactions & Labeling - Drug Development and Drug Interactions: Table of Substrates, Inhibitors and Inducers. Available at: http://www.fda.gov/Drugs/DevelopmentApprovalProcess/DevelopmentResources/DrugInteractionsLabeling/ucm093664.htm.
44. Aadahl, M. & Jørgensen, T. Validation of a new self-report instrument for measuring physical activity. *Med. Sci. Sports Exerc.* **35,** 1196–202 (2003).

11. Appendices

11.1 FDA guideline on strong inhibitors

CYP Enzymes	Strong Inhibitors[2] ≥ 5-fold increase in AUC or > 80% decrease in CL	Moderate inhibitors[3] ≥ 2 but < 5-fold increase in AUC or 50-80% decrease in CL	Weak inhibitors[4] ≥ 1.25 but < 2-fold increase in AUC or 20-50% decrease in CL
CYP1A2	Ciprofloxacin, enoxacin, fluvoxamine	Methoxsalen, mexiletine, oral contraceptives, phenylpropanolamine, thiabendazole, vemurafenib, zileuton	Acyclovir, allopurinol, caffeine, cimetidine, Daidzein,[5], disulfiram, Echinacea[5] famotidine, norfloxacin, propafenone, propranolol, terbinafine, ticlopidine, verapamil
CYP2B6			Clopidogrel, ticlopidine prasugrel
CYP2C8	Gemfibrozil[6]		Fluvoxamine, ketoconazole, trimethoprim
CYP2C9		Amiodarone, fluconazole, miconazole, oxandrolone	Capecitabine, cotrimoxazole, etravirine, fluvastatin, fluvoxamine, metronidazole, sulfinpyrazone, tigecycline, voriconazole, zafirlukast
CYP2C19	Fluconazole,[7] fluvoxamine,[8] ticlopidine[9]	Esomeprazole, fluoxetine, moclobemide, omeprazole, voriconazole	Allicin (garlic derivative), armodafinil, carbamazepine, cimetidine, etravirine, human growth hormone (rhGH), felbamate, ketoconazole, oral contraceptives[10]
CYP3A	Boceprevir, clarithromycin, conivaptan, grapefruit juice,[11] indinavir, itraconazole,	Amprenavir, aprepitant, atazanavir, ciprofloxacin, crizotinib, darunavir/ritonavir, diltiazem, erythromycin, fluconazole,	Alprazolam, amiodarone, amlodipine, atorvastatin, bicalutamide, cilostazol, cimetidine, cyclosporine, fluoxetine, fluvoxamine, ginkgo,[5]

11.2. FDA guideline on strong inducers

CYP Enzymes	**Strong Inducers** ≥ 80% decrease in AUC	**Moderate Inducers** 50-80% decrease in AUC	**Weak Inducers** 20-50% decrease in AUC
CYP1A2		Montelukast, phenytoin, smokers versus non-smokers[2]	Moricizine, omeprazole, phenobarbital,
CYP2B6		Efavirenz, rifampin	Nevirapine
CYP2C8		Rifampin	
CYP2C9		Carbamazepine, rifampin	Aprepitant, bosentan, phenobarbital, St. John's wort[3,4]
CYP2C19		Rifampin	Artemisinin
CYP3A	Avasimibe,[5] carbamazepine, phenytoin, rifampin, St. John's wort[3]	Bosentan, efavirenz, etravirine, modafinil, nafcillin	Amprenavir, aprepitant, armodafinil, clobazamechinacea,[4] pioglitazone, prednisone, rufinamide, vemurafenib
CYP2D6	None known	None known	None known

11.3. Breast cancer adjuvant chemotherapy: AC (doxorubicin-cyclophosphamide)

Christchurch Oncology Service Chemotherapy Chart

Regimen: AC

Disease: Breast Cancer

Intent: Palliative/Adjuvant

Height	cm
Weight	kg
BSA	m^2

Patient Label

Cycle length:	21 days
Cycle N^{o}:	of
Destination	Day Ward
	Ward 27
	Timaru
	Ashburton

CBC	Day 1	Limits
Date		
Hb		80 g l^{-1}
WCC		3 x 10^{9} l^{-1}
Neuts		1.5 x 10^{9} l^{-1}
Plats		100 x 10^{9} l^{-1}

Biochemistry	Day 1	Limits
Date		
Bilirubin		21umol l^{-1}

Cardiac	Cycle 1	Limits
Date		
LVEF		50%
FS		28%

Agent	Dose	Round	Modification
DOXORUBICIN D1	60 mg m^{-2}	5mg	
CYCLOPHOSPHAMIDE D1	600 mg m^{-2}	50mg	

DOXORUBICIN (prior cumulative) mg m^{-2}

Date	Day	Agent	Dose		Instructions	Doctor	Time up	Time down	Nurse	Check
	1	0.9S			500ml (for flushing) IV					
	1	ONDANSETRON	16	mg	Pre-chemo PO/IV					
	1	APREPITANT	125	mg	Pre chemo PO					
	1	DEXAMETHASONE	8	mg	Pre-chemo PO/Bolus or in 100ml 0.9S over 5 min IV					
	1	**DOXORUBICIN**		mg	Slow bolus (sidearm) over 3 to 5 min IV					
	1	**CYCLOPHOSPHAMIDE**		mg	Added to 100mL 0.9S over 15-30 min IV					

Note: Calculate cumulative anthracycline dose before each cycle. Check LVEF after 4 cycles for curative regimens

Prescribe:	
Ondansetron 16mg pre-chemo (Rx 8 x 8mg tabs)	
Aprepitant 125mg pre-chemo, 80mg D2,3 (Rx 4 packs)	
Dexamethasone 8mg pre-chemo, 8mg mane D2-4, (+/-4mg day 5 prn) (Rx 36 x 4mg tabs)	
Domperidone 10-20mg qid prn or metoclopramide 10mg qid prn	

SPECIAL AUTHORITY: Aprepitant

Patient Category: **OSP Group:** **Consultant:**

YJAPO13Z **1234567** **MCRN:**

CDHB Division: Oncology Authorised by:D Gibbs Reference: J Clin Oncol **20**(14): 3114-21 Expiry date: July 2012 Page 1 of 1

11.4. Breast cancer adjuvant chemotherapy: Weekly paclitaxel

Christchurch Oncology Service Chemotherapy Chart

Regimen: Weekly paclitaxel

Disease: Breast cancer, adjuvant

Intent: Curative

Height	cm
Weight	kg
BSA	m^2

Patient Label

Cycle length:	9-12 weeks
Destination	Day Ward
	Ward 27
	Timaru
	Greymouth
	Ashburton

CBC	Week 1	Week 2	Limits
Date			
Hb			80 g l^{-1}
Neuts			1.0 x 10^9 l^{-1}
Plats			100 x 10^9

Biochemistry	Week 1	Limits
Date		
Bilirubin		21 umol l^{-1}

Agent	Dose	Round	Modification
PACLITAXEL weekly	80mg m^{-2}	15mg	

Date	Day	Agent	Dose		Instructions	Doctor	Time up	Time down	Nurse	Check
	Week 1	0.9S			500ml IV (for flushing)					
		CETIRIZINE	10	mg	PO 1 hour before treatment					
		OR CHLORPHENIRAMINE	10	mg	IV 30 mins before treatment					
		RANITIDINE	150	mg	PO 1 hr before treatment or 50mg bolus in 100ml 0.9S over 5 min IV					
		DEXAMETHASONE	8	mg	PO at least 1 hour prior to chemo or in 100ml 0.9S over 5 min IV					
		PACLITAXEL		mg	Added to 250ml 0.9S over 1 hour IV					
	Week 2	0.9S			500ml IV (for flushing)					
		CETIRIZINE	10	mg	PO 1 hour before treatment					
		OR CHLORPHENIRAMINE	10	mg	IV 30 mins before treatment					
		RANITIDINE	150	mg	PO 1 hr before treatment or 50mg bolus in 100ml 0.9S over 5 min IV					
		DEXAMETHASONE	8	mg	PO at least 1 hour prior to chemo or in 100ml 0.9S over 5 min IV					
		PACLITAXEL		mg	Added to 250ml 0.9S over 1 hour IV					

Prescribe:	
Dexamethasone 8mg PO 1 hour prior to chemo (Rx 4mg 4 tabs)	
Ranitidine 150mg PO 1 hour prior to chemo Rx 3	
Cetirizine 10mg 1 hour prior to chemo Rx 4	
Domperidone 10-20mg qid pm or metoclopramide 10mg qid prn	

Patient Category: **OSP Group:** **Consultant:**
Y J A P O 1 3 Z **1 2 3 4 5 6 7** **MCRN:**

CDHB Division: Oncology Authorised by:D Gibbs Reference: Sparano *NEJM* 2008;358:1663-71 Expiry date:Dec 2013 Page 1 of 6

11.5. Breast cancer adjuvant chemotherapy: Weekly paclitaxel, 3 Weekly Trastuzumab

Christchurch Oncology Service Chemotherapy Chart

Regimen: Weekly paclitaxel, 3 weekly trastuzumab

Disease: Breast cancer, adjuvant

Intent: Curative

Height	cm
Weight	kg
BSA	m^2

Patient Label

Cycle length:	9-12 weeks
Destination	Day Ward
	Timaru
	Greymouth
Ward 26	Ashburton

CBC	Week 1	Week 2	Limits
Date			
Hb			80 g l^{-1}
Neuts			1.0 x 10^9 l^{-1}
Plats			100 x 10^9

Biochemistry	Week 1	Limits
Date		
Bilirubin		21 umol l^{-1}

Agent	Dose	Round	Modification
PACLITAXEL weekly	80mg m^{-2}	15mg	
TRASTUZUMAB, day 1	8mg kg^{-1}	10mg	
TRASTUZUMAB, other	6mg kg^{-1}	10mg	

Date	Day	Agent	Dose		Instructions	Doctor	Time up	Time down	Nurse	Check
	Week 1	0.9S			500ml IV (for flushing)					
		CETIRIZINE	10	mg	PO 1 hour before treatment					
		OR CHLORPHENIRAMINE	10	mg	IV 30 mins before treatment					
		RANITIDINE	150	mg	PO 1 hr before treatment or 50mg bolus in 100ml 0.9S over 5 min IV					
		DEXAMETHASONE	8	mg	PO at least 1 hour prior to chemo or in 100ml 0.9S over 5 min IV					
		PACLITAXEL		mg	Added to 250ml 0.9S over 1 hour IV					
		TRASTUZUMAB		mg	Added to 250ml 0.9S over 60min IV					
	Week 2	0.9S			500ml IV (for flushing)					
		CETIRIZINE	10	mg	PO 1 hour before treatment					
		OR CHLORPHENIRAMINE	10	mg	IV 30 mins before treatment					
		RANITIDINE	150	mg	PO 1 hr before treatment or 50mg bolus in 100ml 0.9S over 5 min IV					
		DEXAMETHASONE	8	mg	PO at least 1 hour prior to chemo or in 100ml 0.9S over 5 min IV					
		PACLITAXEL		mg	Added to 250ml 0.9S over 1 hour IV					

Prescribe:	
Dexamethasone 8mg PO 1 hour prior to chemo (Rx 4mg 4 tabs)	
Ranitidine 150mg PO 1 hour prior to chemo Rx 3	
Cetirizine 10mg 1 hour prior to chemo Rx 4	
Domperidone 10-20mg qid prn or metoclopramide 10mg qid prn	

Patient Category: Y J A P O 1 3 Z **OSP Group:** 1 2 3 4 5 6 7 **Special authority:** **Consultant:** **MCRN:** **Trastuzumab**

CDHB Division: Oncology Authorised by:D Gibbs Reference: Sparano *NEJM* 2008;358:1663-71 Expiry date:Jul 2014 Page 1 of 7

Appendix C

Patient information sheet and consent form

Canterbury DHB
District Health Board
Te Poari Hauora ō Waitaha

Participant Information Sheet

Title: An Exploratory Study to Assess the Impact of Inflammatory Markers on Breast Cancer Drug Metabolism in Response to Physical Activity during Chemotherapy

Principal Investigator: Dr Matthew Strother

1. Introduction

You are being invited to take part in this study because you are undergoing chemotherapy for breast cancer. The research you are being asked to participate in is not studying chemotherapy. It is studying if physical activity during chemotherapy changes your body's level of inflammation. This study will compare subjects that have a BMI > 30 to subjects that have a BMI ranging between 18.5 and 24.9. Inflammation is your body's response to stress or injury. Swelling of an ankle, or a fever, is a common sign of inflammation. People that have a BMI > 30 have been shown to have higher levels of markers of inflammation in their bloodstream. The level of inflammation recorded in blood samples from overweight subjects is still lower than the levels of inflammation experienced in an acute response. However, this type of low level inflammation is sustained over prolonged periods of time and may impact your body's ability to process medications. Many medications are processed in your body by enzymes in the liver. The chemical messengers in your body that cause inflammation can change the function of these liver enzymes and decrease the ability of your body to process medications.

It is not known at this time whether physical activity during chemotherapy affects inflammation or the function of these liver enzymes. This participant information sheet contains detailed information about the research study, which is seeking to determine if patients undergoing chemotherapy have differences in their body's ability to process prescribed medications, and if the amount of physical activity they engage in impacts this process. The purpose of this information sheet is to explain to you as openly and as clearly as possible all the procedures involved in the study before you decide whether to take part in it.

Please take time to read the following information carefully and, if you wish, discuss it with friends and Whanau and your GP.

You may choose not to take part in the study without giving a reason and there will be no disadvantage to you of any kind.

2. What is the purpose of the study?

This study will be observing two things. First, physical activity will be measured at specified times using a FitBit One® device. This will allow us to determine how chemotherapy impacts your activity level. Second, this study will measure your body's ability to process prescribed medications at fixed times during chemotherapy. This will be done by administering a combination of oral medications at two points in relation to your chemotherapy: within one to three weeks prior to beginning chemotherapy and again within two to three weeks after chemotherapy is finished. If this feasibility study indicates that physical activity levels are associated with altered liver enzyme function, we hope to propose a further study where patients are given an exercise intervention programme to follow.

The chemotherapy itself is not being tested- this is being administered to you because your doctors have determined it to be a needed step to improve your health. This study is only studying your routine activity during chemotherapy and the way your liver enzymes are processing the medications.

3. Study procedures

If you agree to join the study you will be asked to sign the consent form.

You will have body measurements recorded at two different time points: before you start chemotherapy and after you finish chemotherapy. Additional information will be collected from your medical record, including your height, weight, cancer diagnosis, chemotherapy regimen, and laboratory values.

This study will require you to wear a FitBit One® device over several weeks during your chemotherapy. This device will be distributed to you. During these times you will be asked to wear the device as much as possible, but it could be removed for sleeping and bathing, or other activities in which it would be disruptive. Additionally, we will ask you to fill out a diary of when you remove the FitBit One®, recording the date of removal, the estimated time it is taken off and the activity for which the FitBit was removed. The FitBit One® will be collected from you upon your return to clinic for your next scheduled chemotherapy appointment and re-distributed when required. At this time a blood sample will be taken for analysis to measure inflammation and the way your liver enzymes are functioning. You will have to wear the FitBit One® for a total of approximately five (5) weeks; split into a three (3) week, and two (2) one (1) week periods. You will not be expected to engage in any amount or form of physical activity other than what you personally choose to do.

The second part of this study will measure your liver's activity with regards to processing medications. To do this, you will be asked to take a combination of medications administered by mouth, followed by removal of blood and urine collection to determine the concentration of these medications in the bloodstream. This procedure will occur at

two separate time-points – prior to you beginning chemotherapy and after you have completed chemotherapy. You will be asked to both fast on the day of, and restrain from caffeine containing beverages for 24 hours prior to, the planned liver activity assessment. Each time-point will have the following procedures done:

- Within 24 hours of the planned assessment day, blood will be taken to ensure that it is safe to proceed with the study medications. Two (2) 5mL tubes of blood (about 1 teaspoon with each tube) will be removed for assessments of your liver function.
- On the planned assessment day you will undergo a medical review and physical examination to ensure that it is safe for you to continue on the study.
- Two (2) 5mL tubes of blood (about 1 teaspoon with each tube) will be taken.
- You will then be asked to take five (5) medications, either as pills or as a liquid. These are specifically listed below. The effects of these medications and risks in taking them are presented later in this information sheet.
    - Midazolam liquid in plain water.
    - Caffeine tablet with plain water.
    - Losartan tablet with plain water.
    - Omeprazole tablet with plain water.
    - Dextromethorphan liquid with plain water.
- Following administration of these medications you will be observed by a study nurse.
- Over the following 8 hours, all of your urine will be collected and you will have two (2) 5mL (about 1 teaspoon) blood sample taken.

The medications being administered as part of this study are all routine medications given to patients for treatment of medical conditions. These drugs have been specifically selected because they allow the doctors to look at specific paths of medication elimination in the liver. The combination of these medications and the doses have been selected because they have been shown in many prior studies to have minimal to no effect on how your feel, or your health. However, each medication has some potential risks associated with taking them, which are listed:

- Midazolam: This is a drug used to make people sleepy and to remove anxiety. It can cause sleepiness or sedation. You will be observed by a study team member during this period to ensure your safety. A reversal agent is available if you have sleepiness beyond the expectation of this study.
- Caffeine: This drug is used to increase wakefulness. It can cause excitability or wakefulness. At higher doses, some people experience tremors, anxiety, and/or palpitations. The dose administered in this study would not be expected to produce these adverse effects.
- Losartan: This is a drug used to lower peoples' blood pressure. It can cause low blood pressure. Again, you will undergo routine observation and monitoring as part of this study, and the dose being administered is not expected to cause change in blood pressure.
- Omeprazole: This is a medication used to treat acid indigestion and is not associated with common side effects.
- Dextromethorphan: This is a medication used to treat coughs. It may be associated with either sleepiness or excitability in some people, although this is uncommon, and would be very uncommon at the dose used in this study.

Study procedures

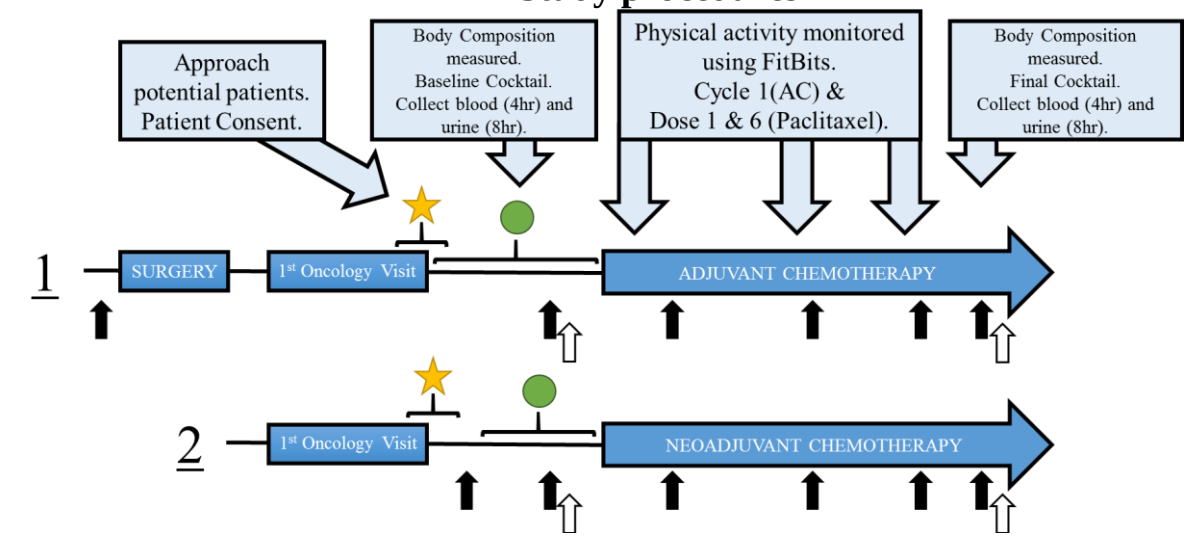

1 = Patients having Adjuvant Chemotherapy

2 = Patients having Neoadjuvant Chemotherapy

⬆ = Blood Sample

⇧ = Urine Sample

★ = Patient Consent

● = 0-21 days prior to cycle 1 chemotherapy

4. What are the possible risks?

Most of the risks associated with this study are related to the medications administered. However, as noted above, the dose being administered as part of this study has a small likelihood of causing symptoms. The two risks for which the study team will be primarily assessing after the dose will be, sleepiness and low blood pressure. If either of these develop, a study doctor will be informed, will assess you, and make appropriate recommendations to minimize risk of these events.
Additional risks include:

- The risks of blood tests, which include fainting and/or pain, bruising, swelling, or rarely infection where the needle is inserted.
- A risk of loss of confidentiality. If participating in this study, some information about you will be stored in study records. Every effort will be made to prevent any risk of loss of this information.

5. What are the potential benefits?

You will not receive any direct benefit from taking part in this study. By taking part in this study, you will contribute to our understanding of how liver enzyme functioning is

influenced by levels of inflammation and what impact physical activity has on this association. This information may benefit other patients having chemotherapy in the future.

What Data or Information will be collected and what use will be made of it?

All information collected from you will be confidential and securely stored in such a way that only individuals involved in the study will be able to gain access. The data will not be linked directly to your name, as you will be assigned a unique study identification number to keep your information as confidential as possible. The clinical data collected will relate to your chemotherapy doses, the standard laboratory and clinical assessments carried out before and during chemotherapy, and laboratory assessments carried out prior to your administration of the combination of medications to measure liver enzyme activity. Additionally we will collect information regarding any other medications and your physical health at the time of assessments.

The data will be used to determine if physical activity is associated with a reduction in inflammation, and an increase in liver enzyme activity.

At the end of the project any personal information or raw data on which the results of the project depend, will be retained in secure storage for ten years, after which time it will be destroyed. Blood samples will be disposed of by standard disposal methods. You may choose to have your sample(s) disposed of with the appropriate karakia (blessing) performed by Chaplains in the Christchurch Hospital Chapel. Blood will be stored within Canterbury Health Laboratories, and any remaining samples will be disposed of after five years.

After completion of this study, aggregate results abstract or paper form will be available to any participant should they wish to have a copy.

Costs

You will not be charged for taking part in this study. You will not be paid for taking part in this study.

Compensation

If you were injured in this study, which is unlikely, you would be eligible for compensation from ACC just as you would be if you were injured in an accident at work or at home. This does not mean that your claim will automatically be accepted. You will

have to lodge a claim with ACC, which may take some time to assess. If your claim is accepted, you will receive funding to assist in your recovery.

If you have private health or life insurance, you may wish to check with your insurer that taking part in this study won't affect your cover.

Voluntary participation and early withdrawal

Taking part in this research study is voluntary. You may decide not to take part or you may stop participating in the study at any time without having to give a reason. The study doctor may remove you from the study at any time for medical reasons or if you fail to follow the instructions given to you. If you do not wish to take part, leave or are asked to leave the study early you will not lose any benefits that you would otherwise have and your present or future medical care will not be affected.

If you have any questions about our project, either now or in the future, please feel free to contact either:-

Dr Matthew Strother or Dr Margaret Currie

Phone 03 364 0230 Phone 03 364 0544

If you want to talk to someone who isn't involved with the study, you can contact an independent health and disability advocate on:
Phone: 0800 555 050
Fax: 0800 2 SUPPORT (0800 2787 7678)
Email: advocacy@hdc.org.nz
For Maori health support, or to discuss any concerns or issues regarding this study, please contact Theona Ireton (Maori Health team),
Email: Theona.Ireton@cdhb.health.nz
Maori Health Team- Phone: 03 364 0160
You can also contact the health and disability ethics committee (HDEC) that approved this study on:
Phone: 0800 4 ETHICS
Email: hdecs@moh.govt.nz

Canterbury DHB
District Health Board
Te Poari Hauora ō Waitaha

Participant Consent Form

Title: Measurement of Physical Activity and Liver CYP Activity
Principal Investigator: Dr Matthew Strother

REQUEST FOR INTERPRETER

English	I wish to have an interpreter.	Yes	No
Maori	E hiahia ana ahau ki tetahi kaiwhakamaori/kaiwhaka pakeha korero.	Ae	Kao
Samoan	Ou te mana'o ia i ai se fa'amatala upu.	Ioe	Leai
Tongan	Oku ou fiema'u ha fakatonulea.	Io	Ikai
Cook Island	Ka inangaro au i tetai tangata uri reo.	Ae	Kare
Niuean	Fia manako au ke fakaaoga e taha tagata fakahokohoko kupu.	E	Nakai

1. I have read the attached Participant Information Sheet Version 1 dated 5/3/16 outlining the nature and purpose of the research study and I understand what I am being asked to do.
2. I have discussed my participation in this study with members of the study team. I have had the opportunity to ask questions and I am satisfied with the answers I have received
3. I have been informed about the possible risks of taking part in this study.
4. I consent to medical practitioners, other health professionals, hospitals or laboratories outside this institution releasing information concerning my condition and treatment which is needed for this study and understand that such information will remain confidential.
5. I understand that my participation is voluntary and that I am free to withdraw at any time during the study without affecting my future health care.
6. I consent to the storage and use of blood taken from me for use, as described in the relevant section of the Participant Information Sheet for research.
7. I am happy for my GP to be informed of my participation in this study
   YES / NO
8. I request that any remaining tissue sample(s) at the end of a study be disposed of with *karakia* (blessing). YES / NO

Name of Participant	Signature of Participant	Date

Name of Investigator	Signature of Investigator	Date

Participant will be provided with a copy of the Participant Information Sheet and this Consent Form

All parties signing the Consent Form must date their own signature